PRODUCTION OF CURCUMIN FORMULATIONS BY SUPERCRITICAL FLUID-ASSISTED COATING AND COPRECIPITATION PROCESSES

by

RAVENNA LESSA MATOS

A thesis submitted to the University of Birmingham for the degree of

DOCTOR OF PHILOSOPHY

Department of Chemical Engineering

College of Engineering and Physical Sciences

University of Birmingham

January 2020

ABSTRACT

Particle size reduction and solid dispersions are common strategies used to improve the solubility of active pharmaceutical ingredients (APIs). The Supercritical Antisolvent (SAS) process has been proved to be advantageous over conventional micronization techniques however, due to the high surface energy of fine particles, handling and post-processing of the micronized material remains an issue. The combination of the SAS process with fluidized bed is an alternative to allow simultaneous precipitation of the API and coating onto the surface of larger particles, so the release and flow properties of the formulation can be improved in a single step. The aim of this project is to extend the understanding and applicability of SAS in conjunction with fluidized bed and produce formulations of curcumin, a model compound with poor water solubility. SAS-FB was initially used to precipitate curcumin onto lactose particles (125 μm), producing a free-flowing powder. As the size reduction of curcumin achieved was insufficient to significantly enhance its solubility, curcumin was coprecipitated with a hydrophilic polymer, poly (vinyl pyrrolidone) (PVP). Finally, simultaneous coprecipitation and coating onto several particles (MCC, 175 μm; corn starch, 15 μm and lactose, < 5 μm) was performed for combined flow and dissolution enhancement.

To my family

ACKNOWLEDGMENTS

I would like to thank the National Council of Technological and Scientific Development (CNPq) for providing financial support through the Science Without Borders Program.

The support and encouragement received from my supervisors Dr Andrew Ingram and Prof Gary Leeke are also very much appreciated. Thank you so much for being friendly and accessible, and for trusting and allowing me to be independent to make decisions about the directions of this project. I am sure this has given me unique research skills and contributed towards my personal development.

I want to express my gratitude to Dr Tiejun Lu for answering to all my questions about the experimental rig, and for being happy to help me dealing with problems in the rig and to adapt it whenever necessary. I also would like to thank Dr Valentina Prosapio for the rich discussions and good suggestions, Dr Christopher McConville for giving me access to the School of Pharmacy, the instruments there available, and for helping me with some initial analytical measurements, and all staff and fellow postgrads in the Chemical Engineering department, especially my friends Dr Laís Speranza and Dr Leslie Labarre.

Others, far away from Brazil, have also given important contributions. Prof Silvio A.B. Vieira de Melo, thank you for making the initial connection between me and my supervisors in Birmingham, for providing recommendations of my work and for giving me valuable support and guidance especially in the first year of this project. Thanks, Prof Elaine C.M. Cabral Albuquerque, for recommending my work and for contributing in the discussions, together with Prof Silvio, which helped me to elaborate the proposal of this PhD project. Many thanks to my good friends Dr Verônica Pereira and Ane Borges (soon Dr Ane Borges), for being supportive and for sharing with me the highs and lows of PhD life.

Finally, I want to thank my husband, David Góes, for always encouraging me and supporting my carrier development, even when that would mean to be living 5000 miles apart. To my family, I want to say thank you for the unconditional support that I have always received.

Mãe, pai e Manu, obrigada pelo apoio e por sempre acreditarem em mim.

CONTENTS LISTING

LIST OF PUBLICATIONS AND PRESENTATIONS

Published papers:

1. **R.L. Matos**, T. Lu, C. McConville, G. Leeke, A. Ingram, Analysis of curcumin precipitation and coating on lactose by the integrated supercritical antisolvent-fluidized bed process. *The Journal of Supercritical Fluids*, 141 (2018), 143–156. (Chapter 3)
2. **R.L. Matos**, T. Lu, V. Prosapio, C. McConville, G. Leeke, A. Ingram, Coprecipitation of curcumin/PVP with enhanced dissolution properties by the supercritical antisolvent process. *Journal of CO2 Utilization*, 30 (2019), 48–62. (Chapter 4)
3. **R.L. Matos**, S.A.B. Vieira de Melo, E.C.M. Cabral Albuquerque, N.R. Foster, Dense CO_2 technology: Overview of recent applications for drug processing/formulation /delivery. *Chemical Engineering and Processing: Process Intensification*, 140 (2019), 64–77. (Chapter 2)
4. **R.L. Matos**, T. Lu, V. Prosapio, C. McConville, G. Leeke, A. Ingram, Single-step coprecipitation and coating to prepare curcumin formulations by supercritical fluid technology. *The Journal of Supercritical Fluids*, 159 (2020). (Chapter 5)

Oral presentations

1. 22nd International Symposium on Microencapsulation (ISM), 2019 – Brazil (Salvador)
2. The European Summer School in High Pressure Technology (ESS-HPT), 2018 – Maribor (Slovenia) and Graz (Austria). The extended abstract (DOI: 10.3217/978-3-85125-619-2) can be found in the following link: http://diglib.tugraz.at/book-of-abstracts-ess-hpt-2018-2018

3. 12th International Symposium on Supercritical Fluids (ISSF), 2018 – Antibes (France). The published proceedings can be found in the following link: http://supflu2018.fr/pdf/OD08.pdf
4. X Association of Brazilian Graduate Students and Researchers in the United Kingdom (ABEP-UK), 2018 – London (UK). The published abstract can be found in the following link: https://sites.google.com/view/xabepukconference/abstracts
5. ChemEngDayUK, 2017 – Birmingham (UK). The published abstract can be found in the following link: https://static1.squarespace.com/static/565c30ace4b06b23bf33cffd/t/58d3d91f1b10e32d5850071f/1490278702390/ChemEngDay+UK+2017+Book+of+Abstracts+final+21-3-17.pdf
6. VIII Association of Brazilian Graduate Students and Researchers in the United Kingdom (ABEP-UK), 2016 - London (UK). The published abstract can be found in the following link: https://drive.google.com/file/d/1LN4fkIzP9KewsPnnnfagd4XXl4NzsGvW/view

Poster presentations

1. 16th European Meeting on Supercritical Fluids (EMSF), 2017 – Lisbon (Portugal)
2. UK Particle Technology Forum – Birmingham (UK), 2017

TABLE OF CONTENTS

LIST OF FIGURES

LIST OF TABLES

LIST OF APPENDICES

Chapter 1 -

GENERAL INTRODUCTION

1.1. Motivation

Curcumin is a polyphenolic hydrophobic compound with several therapeutic properties such as anticancer, antioxidant, anti-microbial and anti-inflammatory [1,2]. However, the use of curcumin in pharmaceutical formulations is limited by its very low water solubility and consequent poor bioavailability.

Common approaches to improve the dissolution properties of active pharmaceutical ingredients (APIs) include: modifying its crystalline structure; preparing composites with hydrophilic excipients; and/or increasing the surface area of the material by decreasing its size [3]. Traditional particle size reduction techniques (micronization) are usually divided into two main categories, top-down and bottom-up. In the former, mechanical means are used to break large particles, usually requiring high energy input and resulting in unstable and cohesive powders with wide particle size distribution [4–6]. While in the latter, particles are precipitated from solution so usually high temperatures are required in the drying step and often a low precipitation yield is obtained [7–9].

Particle engineering using supercritical carbon dioxide (sc-CO_2) is advantageous over conventional micronization techniques since the mild critical conditions of CO_2 enable the processing of thermo-sensitive compounds and the production of formulations with low or no residual organic solvent content, avoiding product degradation and the need for further drying, which is especially important for the processing of pharmaceuticals. Moreover, by the manipulation of the process operating conditions (such as pressure and temperature), the fluid density and solvation power can be adjusted, allowing the control of the solute supersaturation and precipitation [10]. Thus, particle properties can be tuned and narrow particle size distribution with high precipitation yield can be achieved [11–13].

In the supercritical antisolvent (SAS) process, sc-CO_2 acts as an antisolvent for the material to be micronized. This technique has been employed for several years to precipitate a wide variety of APIs alone or in conjunction with excipients [14,15]; however, due to the high surface energy of fine particles, handling and post-processing of the micronized material remains an issue, especially in the case of nanometric particles.

The combination of the SAS process and fluidized beds has been proposed more recently as an alternative [16]. In this way, APIs can be simultaneous precipitated and coated onto the surface of carrier particles in a single step, addressing the aforementioned issues of poor solubility and flowability. Such process integration also reduces the number of processing steps and the need for transfer of the product between equipment, lowering the risk of workers' exposure to nanoparticles. Moreover, high-pressure fluidization with sc-CO_2 avoids the agglomeration of the bed particles, since no liquid bridges are formed between them, and eliminates the possibility of forming explosive vapour phase mixtures, as is the case when air and organic solvents are employed as fluidizing medium [17,18].

1.2. Thesis Aims and Outline

This work aims to employ different formulation strategies to improve the dissolution and flow properties of curcumin, exploring the advantages offered by supercritical fluid (SCF)-based precipitation in conjunction with fluidized beds, while extending the applicability and understanding of such techniques. In order to do that, the study was divided into steps, which are covered in the objectives of Chapters 3-5 described later in this section.

This thesis has an alternative format in which publication-style chapters are integrated in the body of the text. In Chapter 1, the motivation, aims and overview of the work are given, together with some theoretical background information, to facilitate the understanding of the

following chapters, and basic principles and limitations of the analytical techniques used. Then, four publication-style chapters are presented (Chapter 2-5). Chapter 6 closes the study with a general discussion about the work, showing the main findings and recommendations for future work. A more detailed description of the content of each publication-style chapter and how they are connected is provided below. Visual representation of the thesis structure and main objectives of each chapter is shown in **Figure 1-1**.

Chapter 2

The applicability of SCFs to prepare a wide variety of pharmaceutical formulations is presented in Chapter 2. The fundamentals of well-known SCF-based processing techniques are discussed and recently developed processes are classified, and their differences and similarities discussed. Strategies to improve dissolution and flow properties of API formulations are also presented, giving insights into the selection of the most suitable formulation and processing method.

Chapter 3

In this chapter, simultaneous curcumin precipitation and coating on carrier particles (lactose, 125 μm) is performed via SAS-FB (SAS integrated with a fluidized bed) aiming to improve the dissolution and flowability properties of the formulation. The characteristics of curcumin precipitation by SAS and SAS-FB are evaluated and the effect of several process parameters are investigated, with focus on correlating the morphology of the curcumin crystals obtained with the position of the operational point in the binary vapour-liquid equilibrium phase diagram of the system solvent-CO_2. Pulmonary delivery is the proposed route of administration of the formulation.

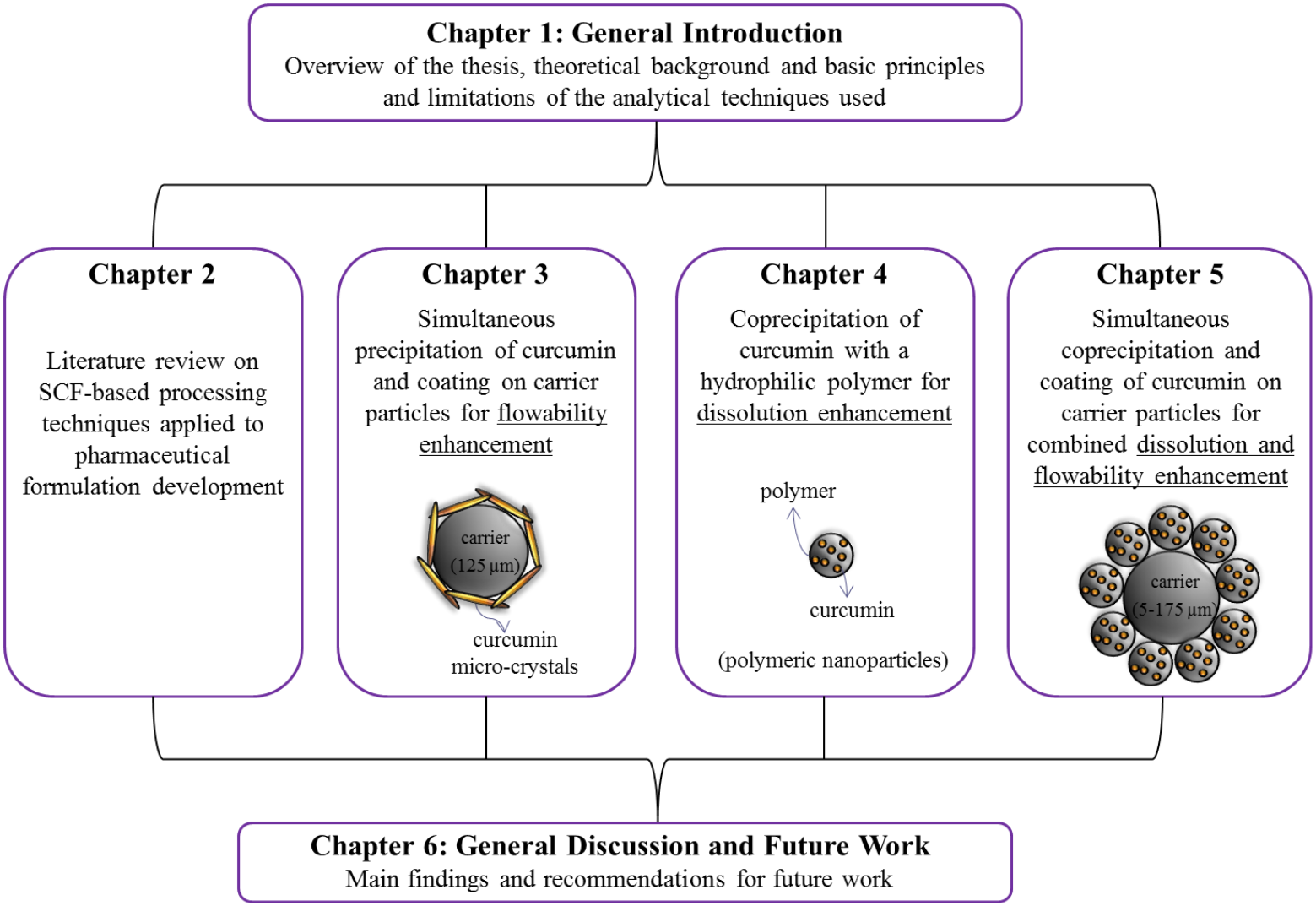

Figure 1-1. Visual representation of thesis outline and objectives of each chapter (particle size of the formulations are not in scale).

Chapter 4

Further development of the work showed that the size reduction achieved by SAS and SAS-FB in the previous chapter was not enough to significantly improve the aqueous solubility of curcumin. Therefore, Chapter 4 focuses on improving the solubility of curcumin by coprecipitation with a hydrophilic polymer, poly (vinyl pyrrolidone) (PVP), by SAS. Several operating conditions are tested and different solvent mixtures are employed to understand their effect on particle size and product recovery.

Chapter 5

Although successful in enhancing curcumin dissolution properties, the particles produced in Chapter 4 are aggregated due to their small size (327-51 nm). For this reason, Chapter 5 aims to combine improved dissolution and flow properties in the same formulation, which was the ultimate objective of this project. SAS-FB was used to coat free-flowing carrier particles (MCC, 175 µm) with curcumin/PVP coprecipitates in a single step and then the experimental rig was adapted to allow the coating of finer particles (corn starch, 15 µm and lactose, < 5 µm) in a stirred vessel. The properties of fluidization in tapered beds and stirred vessels are discussed and, depending on the particle size of the carrier particles, oral or pulmonary delivery administration routes would be suitable.

Although the published articles are the result of collaborative work, it is important to clarify that Ravenna Lessa Matos was responsible for designing and performing all experiments and analyses, interpreting the data, writing and editing the manuscripts in full. Tiejun Lu helped with adapting the experimental rig, interpreting the data and revising the manuscripts, Valentina Prosapio, Christopher McConville, Gary Leeke and Andrew Ingram helped with interpreting the data and revising the manuscripts (Chapters 3-5). Silvio A. B. Vieira de Melo,

Elaine C. M. Cabral Albuquerque and Neil R. Foster helped with revising the manuscript (Chapter 2).

1.3. Theoretical Background

1.3.1. Supercritical Fluid Technology

1.3.1.1. Properties of SCFs

The phase diagram of pure CO_2 is given in **Figure 1-2**a, showing the solid, liquid, gas and supercritical regions, depending on the pressure and temperature. The equilibrium between two phases is observed on the saturation curves and, at the triple point, solid, liquid and vapour coexist. The supercritical region is found at the end of the vaporization curve, above the critical pressure (P_c) and critical temperature (T_c), where the liquid and vapour phases became identical. Therefore, a fluid is said to be supercritical when it is compressed beyond its P_c and heated beyond its T_c [10] (**Figure 1-2**a).

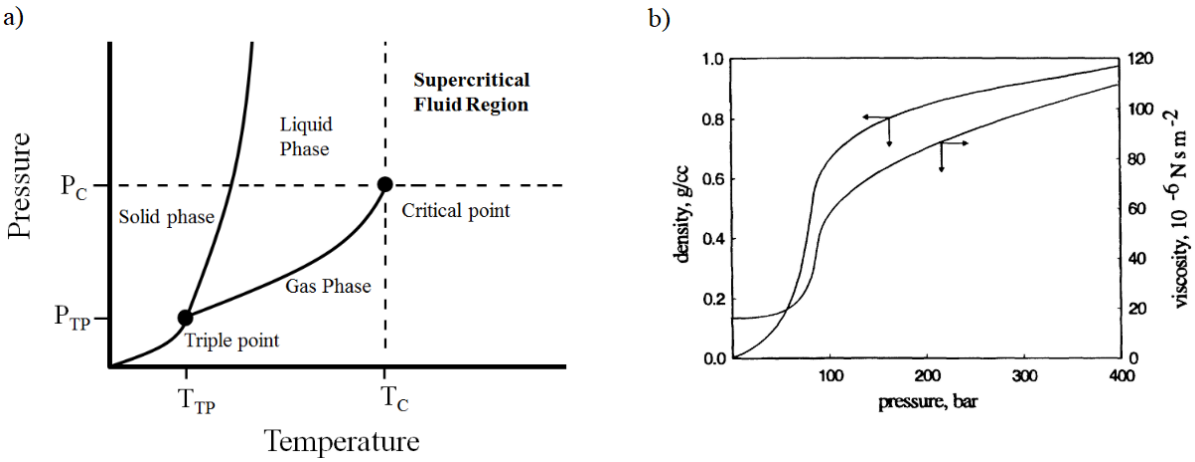

Figure 1-2. a) P-T diagram of CO_2 (adapted from [19]); b) variation in density and viscosity of CO_2 with pressure at 310K (adapted from [20]).

In the supercritical region, unique properties are observed, including liquid-like density, gas-like viscosity and diffusivity (**Table 1-1**) and zero surface tension. In the proximity of the critical point, small changes in pressure and temperature lead to significant variations in the

fluid density and viscosity, as exemplified in **Figure 1-2**b. These properties can be easily tuned by adjusting pressure and/or temperature, giving process flexibility to obtain products with varied characteristics.

Table 1-1. Comparison of the order of magnitude of different thermo-physical properties of fluids in different states (adapted from [21]).

State	Density (kg/m^3)	Viscosity (Pa.s)	Diffusion coefficient (m^2/s)	Thermal conductivity (W/m.K)
gas	1 - 100	10^{-5} - 10^{-4}	10^{-5} - 10^{-4}	2.10^{-5} - 5.10^{-4}
supercritical	250 - 800	10^{-4} - 10^{-3}	10^{-8} - 10^{-7}	5.10^{-2} - 10^{-1}
liquid	800 - 1200	10^{-3} - 10^{-2}	10^{-9} - 10^{-8}	$\approx 10^{-1}$

The critical properties of commonly used SCFs are given in **Table 1-2**. The most used is CO_2 since it has moderate critical pressure (7.39 MPa) and low critical temperature (31.1°C); it is non-toxic, non-flammable, inexpensive and considered environmental-friendly if compared with organic solvents. It can also be easily separated from the final product and recovered in the end of the process just by reducing the pressure to atmospheric conditions.

Table 1-2. Critical properties of frequently used SCFs (adapted from [22]).

Fluid	Molecular weight (g/mol)	Critical temperature (°C)	Critical pressure (Mpa)
carbon dioxide	44.0	31.0	7.4
water	18.0	374.2	22.1
methane	16.0	-82.8	4.6
ethane	30.1	32.2	4.9
propane	44.1	96.7	4.3
ethylene	28.1	9.3	5.0
propylene	42.1	91.8	4.6
methanol	32.0	239.5	8.1
ethanol	46.1	240.8	6.1
acetone	58.1	235.0	4.7
ammonia	17.0	132.5	11.3

1.3.1.2. Supercritical Antisolvent (SAS) Process

Antisolvent methods are based on the high solubility and diffusivity of sc-CO_2 in organic solvents. In a typical Supercritical Antisolvent (SAS) process (**Figure 1-3**), the solute is dissolved in an organic solvent and then sprayed into a high pressure vessel through which sc-CO_2 is passed continuously. The instantaneous mixing of the phases leads to the supersaturation of the liquid solution and consequent precipitation of the solute, which is collected on a filter (detailed description of the experimental setup and procedure are given in Chapters 3 - 5). In a supersaturated solution, the solute concentration exceeds that of the saturated one. The degree of supersaturation is defined as the ratio between the concentration of the refered solutions (supersaturated/saturated), which is the driving force for crystallization/precipitation (rapid crystallization). Therefore, it is the most important factor affecting the rate of precipitation and the characteristics of the final particles [23–25]. Within this thesis, the words crystallization and precipitation are used interchangeably.

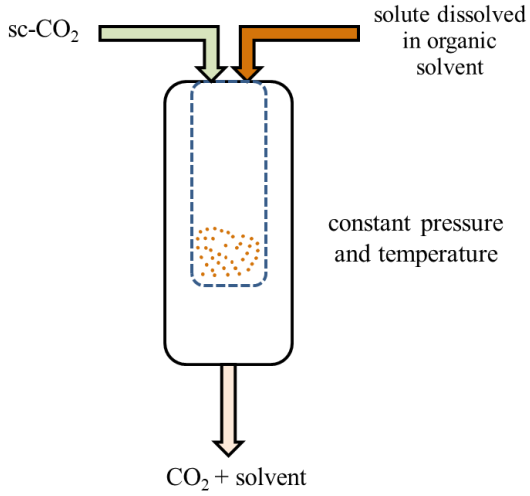

Figure 1-3. Simplified diagram of the SAS process.

The SAS process is affected by a number of variables including, pressure, temperature, solution flow rate, solution initial concentration, CO_2 flow rate, duration of the precipitation step, type of organic solvent and type of the solution injection device. In order to achieve a

successful precipitation by SAS, two basic requirements must be met: complete miscibility between solvent and antisolvent (sc-CO_2) at the operating conditions and insolubility of the solute in the solvent/antisolvent mixture.

1.3.1.2.1. Selection of operating conditions

The knowledge of the phase diagram of the components involved is crucial for understanding the precipitation mechanisms and appropriate selection of operating conditions. As experimental high-pressure phase equilibria data of ternary systems (solid-organic solvent-CO_2) of interest for SAS are scarce, usually the binary vapour-liquid equilibrium (VLE) diagram of solvent and CO_2 is used to analyse the ternary system and select the operating point. Insignificant effect of solute is expected in the solvent-CO_2 VLE diagram when the initial concentration of the liquid solution is very low or the solute is considered insoluble in the supercritical phase, which is not always true.

Mixtures of CO_2 and organic solvents usually have a typical VLE diagram, classified as type I by Van Konynenburg and Scott [26]. The shape of the curve showing pressure versus the molar fraction of CO_2 (P-X_{CO2}) at a fixed temperature is shown in **Figure 1-4**, where the saturated liquid and saturated vapour lines meet at the mixture critical point (MCP). The different regions of the diagram are presented in **Figure 1-4**a, for the system CO_2-DMSO at 329K [27], while **Figure 1-4**b presents the VLE of ethanol-CO_2 [20], showing how the MCP of the system varies with temperature: at higher temperature, P_c increases and X_c decreases. In order to benefit from the previously mentioned properties of SCFs, the operating point is usually chosen in the supercritical region, that is, above the critical point of the mixture solvent-CO_2 ($P > P_c$ and $X > X_c$ for a given temperature).

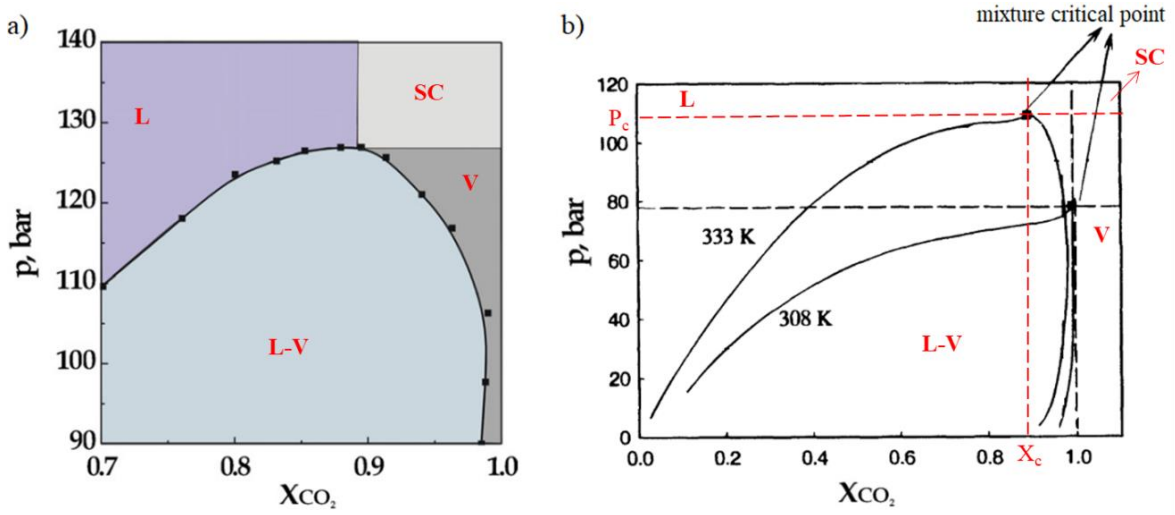

Figure 1-4. Binary vapour-liquid equilibrium of a) CO_2-DMSO at 329K (adapted from [28], equilibrium data from [27]); b) CO_2-ethanol at two different temperatures: 308K and 333K (adapted from [20]).

Once P, T and X_{CO2} have been selected, the flow rate of the organic solution needs to be chosen. Usually a capillary tube is employed to disperse the solution inside the vessel and liquid jet atomization can happen depending on the velocity of the jet and position of the operating point [14]. In the proximity of the solvent-CO_2 MCP, atomization can occur because the time required for the jet break-up to happen is shorter than the time taken for complete vanishing of the liquid surface tension (multi-phase mixing) [29]. Near above the MCP, jet velocities of 0.33-0.42 m/s (critical atomization velocity) were found to be enough to promote the atomization of different solvents in sc-CO_2 [30]. On the other hand, at completely developed supercritical conditions, the surface tension vanishes before the jet break-up so no droplets are formed and the jet spreads as an expanding gas plume (single-phase mixing) [29].

There have been attempts to correlate the morphology of particles precipitated by SAS with the position of the operating point in the solvent-CO_2 VLE phase diagram and the fluid dynamics of the solution jet when injected into CO_2. It has been reported that nanoparticles are usually obtained in completely developed supercritical conditions (far above the MCP),

microparticles are precipitated near above the MCP, expanded microparticles (EMP) are produced in the subcritical vapour region, while crystals are formed when the solute has very fast crystallization kinetics or the operating point is within the biphasic region [28]. Other authors, on the other hand, believe that the level of supersaturation achieved determines if the solute precipitates (as amorphous particles) or crystallizes: moderate solution supersaturation would lead to crystallization, while high supersaturation would lead to precipitation [31,32].

Figure 1-5 summarizes the two possible mechanisms of amorphous particle formation proposed by Reverchon and De Marco [28]. In the proximity of the MCP, particles are formed by drying of the atomized jet (mass transfer in and out of each droplet), so particles keep the spherical shape of the initial droplets. Far above the MCP, as no droplets are formed, the very fast mixing of the fluids (single-phase mixing) leads to a very high supersaturation and formation of a large number of nuclei which will develop into nanoparticles [28]. Other researches have proved that such morphologies can also be obtained by the manipulation of the initial concentration of the liquid solution since at higher concentrations the time required for the liquid surface tension to vanish increases, leading to an increase in particle size [32].

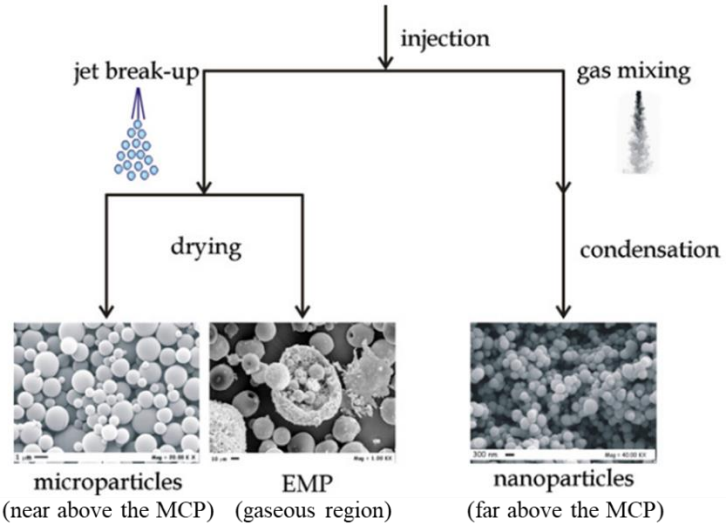

Figure 1-5. Possible mechanisms of amorphous particles precipitation (adapted from [28]).

Besides considering the MCP of the binary system to select the operating point based on the intended morphology, it also important to know that the properties of the solvent (viscosity and surface tension) will determine the required increment in pressure to move from the transition region (near above the MCP) to completely developed supercritical conditions (far above the MCP). Ethanol and acetone, for example, present a narrower pressure transition range than DMSO [33].

In the SAS process, particle growth happens mostly by condensation (deposition of molecules onto particles) and in minor extent by coagulation (collision of particles) [34]. Due to the interactions of many physical phenomena (thermodynamics, fluid dynamics, mass transfer and precipitation kinetics) and the number of operating parameters involved, prediction of particle characteristics remains a difficult task [34,35]. In order to demonstrate the complexity of the process, possible effects of changing some of the operating parameters are summarized in **Figure 1-6**, where an increase in the nucleation rate is associated with a decrease in particle size, and vice versa (deeper discussion is provided in Chapters 3 and 4). As it can be seen, variations in any of the parameters has at least two opposite effects on supersaturation and nucleation rate. Therefore, experimental work remains a very important part of the research involving particle engineering by SAS, owing to its compound-dependent characteristic.

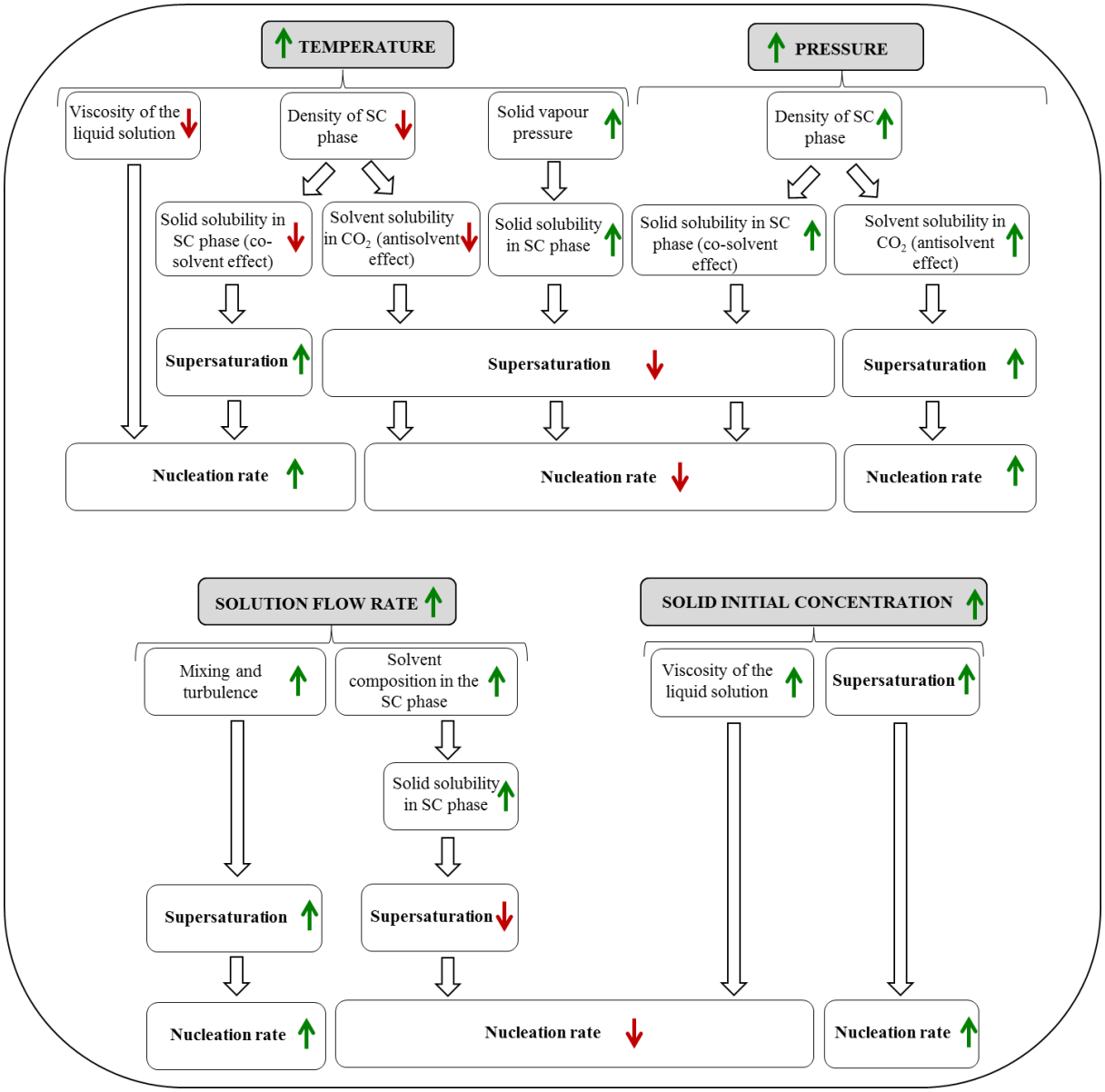

Figure 1-6. Effect of changing SAS operating parameters in the solution supersaturation and nucleation rate.

1.3.2. Curcumin – problems and promises

Curcumin is an orange-yellow polyphenolic compound traditionally used as a spice and food additive. It is extracted from the rhizome of turmeric (*Curcuma longa*) in association with smaller quantities of other compounds (curcuminoids), namely: demethoxycurcumin, bis-demethoxycurcumin and cyclocurcumin (**Figure 1-7**).

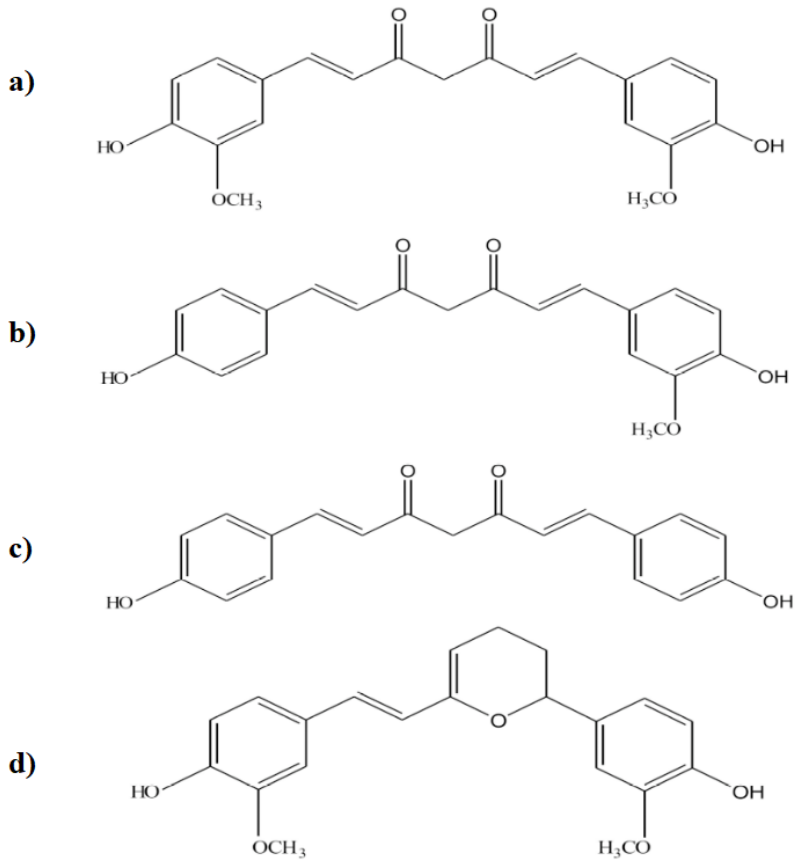

Figure 1-7. Chemical structures of curcuminoids: a) curcumin, b) demethoxycurcumin, c) bis-demethoxycurcumin, d) cyclocurcumin (adapted from [36]).

Curcumin is an attractive compound for the pharmaceutical industry since it has a wide range of biological activity, including anti-inflammatory, antioxidant, antibacterial, antiviral, antiarthritic, antifungal and anticancer so potentially it could be used to treat numerous diseases [1,2].

However, the bioavailability of curcumin is limited by its poor solubility in aqueous media, low absorption and fast intestinal metabolism [37]. In addition, curcumin undergoes degradation when exposed to light, heat and alkaline pH [38,39]. For those reasons, extensive research in the past years has focused on finding appropriate processing methods and delivery systems to overcome these issues [40–42].

1.3.3. Pulmonary delivery formulations

Pulmonary delivery is one of the proposed routes for the administration of curcumin formulations. Besides being a non-invasive route, other advantages of lung delivery for the treatment of systemic diseases are: rapid onset of therapeutic action due to the enormous alveoli surface area, thin epithelial barrier and high blood supply, enabling a great mass transfer between air and blood and avoidance of first-pass metabolism which can increase drug bioavailability [43].

Developing formulations for inhalation is challenging due to the specific flowability requirements. It is generally accepted that in order to reach the lungs, particles should have an aerodynamic diameter between 1-5 μm. In order to avoid particle aggregation and improve the handling of the material, active pharmaceutical ingredients (APIs) are usually combined with larger excipient or carrier particles [44–46], as shown in **Figure 1-8**. By the inspiratory airflow force, drug and carrier should dissociate, small drug particles travel towards the lungs, while coarse carrier particles are deposited in the upper airways [47,48]. This is the formulation strategy used in Chapter 3.

A more innovative approach consists of preparing nano-on-micron formulations by coating fine drug particles (1-5 μm) with nanoparticles of excipients, as reviewed elsewhere [49]. In this case, the nanoparticles work as spacers between the microparticles, improving their flow properties [49]. In Chapter 5, the same concept (nano-on-micron) is employed however the excipient/carrier is in the form of microparticles while the drug is dispersed within nanoparticles (**Figure 1-8**).

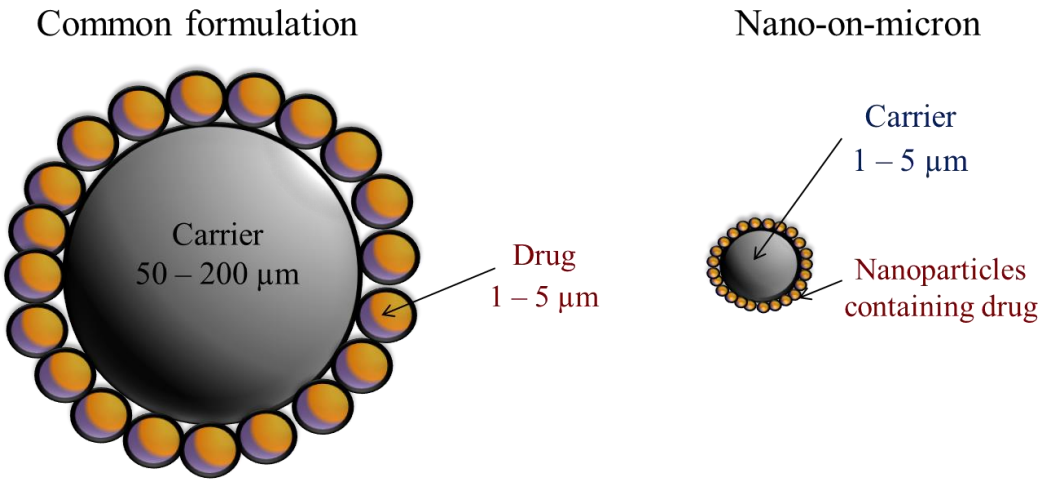

Figure 1-8. Examples of formulation strategies for pulmonary delivery [49].

1.4.Fundamentals and limitations of analytical techniques

In this section the fundamentals and limitations of the analytical techniques used to characterize the formulations produced are briefly discussed. Detailed methodology was covered in each chapter where appropriate references for each method were given.

1.4.1. Scanning electron microscopy (SEM) and particle size measurements

Scanning electron microscopy (SEM) was employed to observe the morphology of the particles produced. In brief, the SEM works by delivering a beam of electrons to scan the sample and registering the pattern created by them when bounced off from the surface of the material. The signal obtained from the scattered electrons is then converted into a magnified picture.

The common limitations of the SEM are the difficulty in observing a representative sample of the material since only small amounts can be analysed at a time and the fact that the images taken can be subject to the user's intentions. Samples were usually unchanged by the measurements however damage of the particle structure by the electron beam was noticed on

a few occasions (some curcumin crystals being removed from the surface of lactose and damage of the surface of uncoated corn starch at high magnification).

Particle size distribution was assessed using Image J analysis software with particles being measured one by one, manually. Automatic measurements using techniques based on laser diffraction, for instance, were not possible due to the difficulties in finding a proper dispersing medium for the samples. In the case of Chapter 3 where the samples were composed of fine curcumin crystals and lactose, water was tested as a dispersing medium which would dissolve the lactose and allow the measurements of curcumin size by Mastersizer 2000. However, due to the poor wetting of the curcumin crystals, most of them ended up floating and aggregating on the surface of the liquid, making accurate measurements impossible. Surfactants were also added to the medium as an attempt to improve the wetting and dispersion of the samples, but then the crystals were solubilized. Coprecipitates of curcumin and PVP are soluble in water and most known organic solvents so particle size was also only assessed by measuring their diameters from SEM pictures.

1.4.2. UV-visible spectrophotometry

UV-visible spectrophotometry is a simple and fast method to obtain the concentration of a solute in solution by measuring the variation of intensity of a light beam when passing through it. This variation is related to the solution absorbance, which is directly proportional to the solute concentration (Beer-Lambert Law). A calibration curve is hence necessary to correlate absorbance and concentration of a certain material at fixed wavelength. The calibration curve used to obtain the concentration of curcumin in 50% (v/v) water-acetone solution is given below in **Figure 1-9**a.

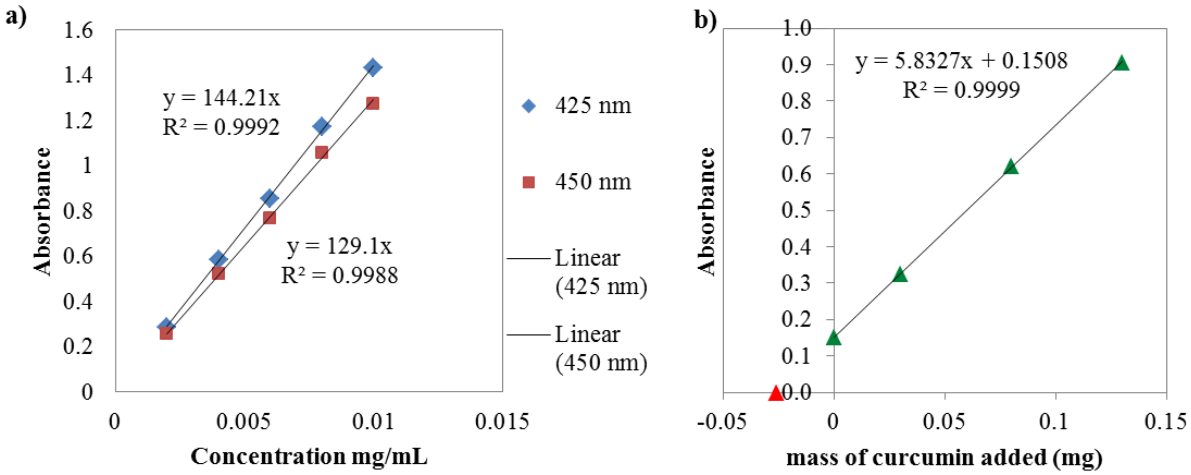

Figure 1-9. a) Calibration curve to quantify curcumin in 50% (v/v) water-acetone by UV-vis; b) standard addition method to determine the mass of curcumin added to a solution of CURC/PVP in water + 0.25% SDS (red triangle).

It is important to notice that the linear relationship between absorbance and concentration is valid when the dissolved molecules do not interact with each other, which should be the case of low concentrated solutions. Another fact limiting the range of concentrations to be used is the detection limits (upper and lower) of the instrument. Proper determination of the solute concentration can only be done when the solution concentration is within the range used in the calibration curve. Therefore, sometimes multiple dilutions of the sample prior to analysis are required, which can introduce errors in the measurements.

When more than one solute is present in solution, interferences in the absorbance might occur (matrix effects). The standard addition method [50,51] was then employed to check for interferences caused by PVP and SDS on the measurement of curcumin absorbance (since the medium used in the dissolution rate measurements was water + 0.25% SDS). The method is represented in **Figure 1-10**. It basically works by preparing a standard solution of curcumin in 50% water-acetone (known curcumin concentration) and another solution of CURC/PVP coprecipitate in water + 0.25% SDS (unknown curcumin concentration). The latter solution is divided into four vials and then three of them are spiked with different volumes (3, 8 and 13

ml) of the standard solution. The unspiked and spiked solutions are diluted to the same final volume (25 ml) with water + 0.25 SDS and their absorbances are determined.

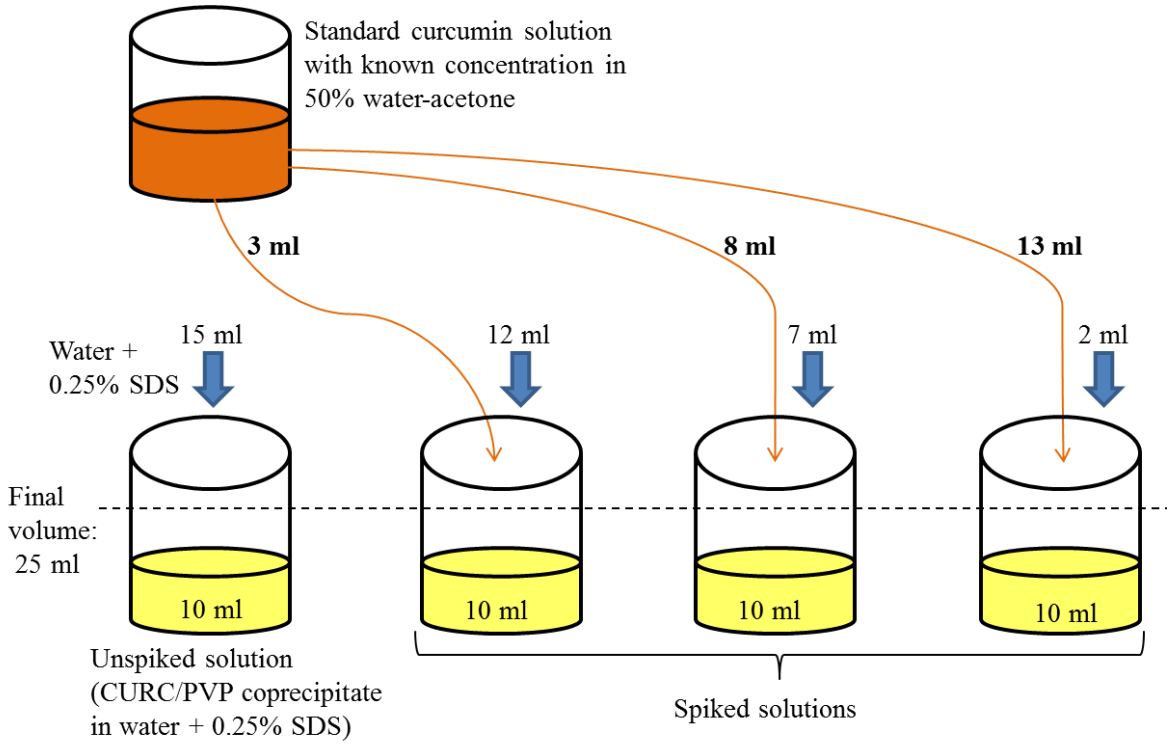

Figure 1-10. Schematic representation of the standard addition method.

When the values of absorbance are plotted as a function of the mass of curcumin added (or volume of the standard solution added), it is possible to determine the mass of curcumin present in the unspiked sample, as shown in **Figure 1-9**b, by extrapolating the curve to the point on the x-axis at which y = 0 (red triangle in **Figure 1-9**b). The mass of curcumin was also determined using the calibration curve of curcumin in 50% water-acetone (**Figure 1-9**a) for comparison. The relative difference between the values obtained from **Figure 1-9**a and **Figure 1-9**b was below 1%, showing that SDS and PVP do not interfere in the absorbance of curcumin at 425 nm.

1.4.3. High Performance Liquid Chromatography (HPLC)

High Performance Liquid Chromatography (HPLC) is a more robust and sensitive technique capable of determining the concentration of several solutes in solution based on the time required (retention time) for the molecules to move throughout a column filled with an adsorbent (stationary phase). High pressure is employed in on side of the column to force the movement of the sample (dispersed in a mobile phase) to the other side, in which a detector (such as UV, infrared, refractive index, etc.) identifies each substance. Due to the different interactions between the molecules of distinct materials and the stationary phase, different retention times can be obtained but method development is usually an arduous task, involving the adjustment of several parameters.

HPLC was used to quantify curcumin in coprecipitated samples and verify if the proportion between curcumin and other curcuminoids varies after processing due to curcumin degradation (Chapter 4). The calibration curve is given in **Figure 1-11**.

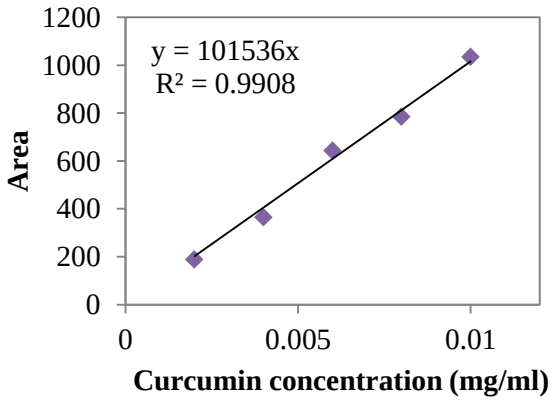

Figure 1-11. Calibration curve to quantify curcumin by HPLC.

1.4.4. Fourier Transform Infrared spectroscopy (FTIR)

Fourier transform infrared spectroscopy (FTIR) is a simple and fast technique employed to identify functional groups in a material. When the sample is exposed to infrared light,

different wavelengths are absorbed, corresponding to the frequencies in which the bonds between the atoms constituting the molecules vibrate [52]. A mathematical technique (Fourier Transform) is then applied by the computer to convert the raw absorbance signal captured by the detector in an absorbance spectrum (absorbance/transmittance versus wavenumber). The Attenuated Total Reflectance (ATR) is an accessory used to enable the direct analysis of solid or liquid samples in their original state [53].

FTIR-ATR was used in this work as a qualitative tool to check for the generation of molecular interactions between the components of the formulation and solvents used during processing.

1.4.5. Differential Scanning Calorimetry (DSC)

Differential Scanning Calorimetry (DSC) is a technique largely employed in the pharmaceutical industry to identify physical and chemical events in a sample by analysing variations in its enthalpy or heat capacity [54]. It works by employing two identical sensors to measure the difference in the amount of heat required (absorbed or released) to change the temperature of the sample and reference at the same rate.

Identification of thermal transitions can sometimes be difficult when more than one thermal event is happening at the same temperature. Therefore, deciding on a suitable operating mode and developing an appropriate method can be challenging. Although a destructive technique, a great advantage of DSC is the requirement of only small amounts of sample (few milligrams).

1.4.6. X-ray diffraction (XRD)

X-ray diffraction (XRD) is a technique used to characterize the crystal lattice of solid samples. The material is exposed to a beam of X-rays which interacts with the atoms of a crystal (different planes of the crystal diffract the beam at different angles). Hence, this

technique enables the identification of a material and its polymorphic forms by comparison with reference spectra and the assessment of its degree of crystallinity [55].

XRD was used in this work as an additional method to distinguish between amorphous and crystalline samples (qualitative analysis). It is advantageous over DSC since it is a non-destructive technique (no heating required) with straight-forward interpretation of the spectra; however a much greater amount of powder is needed.

1.5. References

[1] S.C. Gupta, S. Patchva, B.B. Aggarwal, Therapeutic Roles of Curcumin: Lessons Learned from Clinical Trials, Am. Assoc. Pharm. Sci. J. 15 (2013) 195–218. doi:10.1208/s12248-012-9432-8.

[2] O. Naksuriya, S. Okonogi, R.M. Schiffelers, W.E. Hennink, Curcumin nanoformulations: A review of pharmaceutical properties and preclinical studies and clinical data related to cancer treatment, Biomaterials. 35 (2014) 3365–3383. doi:10.1016/j.biomaterials.2013.12.090.

[3] S. Jain, N. Patel, S. Lin, Solubility and dissolution enhancement strategies: current understanding and recent trends, Drug Dev. Indusrial Pharm. 41 (2015) 875–887. doi:10.3109/03639045.2014.971027.

[4] J. Zhang, L. Wu, H.K. Chan, W. Watanabe, Formation, characterization, and fate of inhaled drug nanoparticles, Adv. Drug Deliv. Rev. 63 (2011) 441–455. doi:10.1016/j.addr.2010.11.002.

[5] M. D. Ticehurst, P. A. Basford, C. I. Dallman, T. M. Lukas, P. V. Marshall, G. Nichols, D. Smith, Characterisation of the influence of micronisation on the crystallinity and physical stability of revatropate hydrobromide, Int. J. Pharm. 193 (2000) 247–259. doi:10.1016/S0378-5173(99)00347-6.

[6] N. Rasenack, B.W. Müller, Micron-Size Drug Particles: Common and Novel Micronization Techniques, Pharm. Dev. Technol. 9 (2004) 1–13. doi:10.1081/PDT-120027417.

[7] R. Kaur, T. Garg, B. Malik, U.D. Gupta, P. Gupta, G. Rath, A.K. Goyal, Development and characterization of spray-dried porous nanoaggregates for pulmonary delivery of anti-tubercular drugs, Drug Deliv. 23 (2016) 882–887. doi:10.3109/10717544.2014.920428.

[8] D.F. Bain, D.L. Munday, A. Smith, Solvent influence on spray-dried biodegradable microspheres, J. Microencapsul. 16 (1999) 453–474. doi:10.1080/026520499288915.

[9] C. Bosquillon, C. Lombry, V. Préat, R. Vanbever, Influence of formulation excipients and physical characteristics of inhalation dry powders on their aerosolization performance, J. Control. Release. 70 (2001) 329–339. doi:10.1016/S0168-3659(00)00362-X.

[10] R.B. Gupta, Supercritical fluid technology for particle engineering, in: R.B. Gupta, U.B. Kompella (Eds.), Nanoparticle Technol. Drug Deliv., 1st ed., Taylor and Francis Group, New York, 2006: pp. 53–84.

[11] R.L. Matos, T. Lu, C. McConville, G. Leeke, A. Ingram, Analysis of curcumin precipitation and coating on lactose by the integrated supercritical antisolvent-fluidized bed process, J. Supercrit. Fluids. 141 (2018) 143–156. doi:10.1016/j.supflu.2017.12.013.

[12] R.L. Matos, T. Lu, V. Prosapio, C. McConville, G. Leeke, A. Ingram, Coprecipitation of curcumin/PVP with enhanced dissolution properties by the supercritical antisolvent process, J. CO2 Util. 30 (2019) 48–62. doi:10.1016/j.jcou.2019.01.005.

[13] A. Tandya, H.Q. Zhuang, R. Mammucari, N.R. Foster, Supercritical fluid micronization techniques for gastroresistant insulin formulations, J. Supercrit. Fluids. 107 (2016) 9–16. doi:10.1016/j.supflu.2015.08.009.

[14] E. Badens, Y. Masmoudi, A. Mouahid, C. Crampon, Current situation and perspectives in drug formulation by using supercritical fluid technology, J. Supercrit. Fluids. 134 (2018) 274–283. doi:10.1016/j.supflu.2017.12.038.

[15] V. Prosapio, I. De Marco, E. Reverchon, Supercritical antisolvent coprecipitation mechanisms, J. Supercrit. Fluids. 138 (2018) 247–258. doi:10.1016/j.supflu.2018.04.021.

[16] Q. Li, D. Huang, T. Lu, J.P.K. Seville, L. Xing, G.A. Leeke, Supercritical fluid coating

of API on excipient enhances drug release, Chem. Eng. J. 313 (2017) 317–327. doi:10.1016/j.cej.2016.12.066.

[17] F. Niu, J. Haslam, R. Rajewski, B. Subramaniam, A fluidized-bed coating technology using near-critical carbon dioxide as fluidizing and drying medium, J. Supercrit. Fluids. 66 (2012) 315–320. doi:10.1016/j.supflu.2011.11.007.

[18] S. Rodríguez-Rojo, J. Marienfeld, M.J. Cocero, RESS process in coating applications in a high pressure fluidized bed environment: Bottom and top spray experiments, Chem. Eng. J. 144 (2008) 531–539. doi:10.1016/j.cej.2008.07.054.

[19] I. Pasquali, R. Bettini, Are pharmaceutics really going supercritical?, Int. J. Pharm. 364 (2008) 176–187. doi:10.1016/j.ijpharm.2008.05.014.

[20] S. Palakodaty, P. York, Phase behavioral effects on particle formation processes using supercritical fluids., Pharm. Res. 16 (1999) 976–985. doi:10.1023/A:1011957512347.

[21] S.I. de M. Antunes, Micronização Supercrítica do β-Caroteno, Universidade Técnica de Lisboa, 2007.

[22] M. Selvamuthukumaran, J. Shi, Recent advances in extraction of antioxidants from plant by-products processing industries, Food Qual. Saf. 1 (2017) 61–81. doi:10.1093/fqsafe/fyx004.

[23] S. Bristow, T. Shekunov, B.Y. Shekunov, P. York, Analysis of the supersaturation and precipitation process with supercritical CO2, J. Supercrit. Fluids. 21 (2001) 257–271. doi:10.1016/S0896-8446(01)00100-0.

[24] P. York;, U.B. Kompella;, B.Y. Shekunov, eds., Supercritical Fluid Technology for Drug Product Develoament, Marcel Dekker, Inc., New York, 2004.

[25] P. York, U.B. Kompella, B.Y. Shekunov, Supercritical fluid technology for drug product development, 2004. doi:10.1201/9780203021378.

[26] P.H. Van Konynenburg, R.L. Scott, Critical Lines and Phase Equilibria in Binary Van Der Waals Mixtures, 298 (1980) 495–540. doi:10.1098/rsta.1948.0007.

[27] H.M.L. S.C. Chang, M.J. Lee, The influence of phase behavior on the morphology of protein a-chymotrypsin prepared via a supercritical antisolvent process, in: Proc. 8th Int. Symp. Supercrit. Fluids, Kioto, Japan, 2006: p. paper PB-1-41.

[28] E. Reverchon, I. De Marco, Mechanisms controlling supercritical antisolvent precipitate morphology, Chem. Eng. J. 169 (2011) 358–370. doi:10.1016/j.cej.2011.02.064.

[29] C.S. Lengsfeld, J.P. Delplanque, V.H. Barocas, T.W. Randolph, Mechanism Governing Microparticle Morphology during Precipitation by a Compressed Antisolvent: Atomization vs Nucleation and Growth, J. Phys. Chem. B. 104 (2000) 2725–2735. doi:10.1021/jp9931511.

[30] T. Petit-Gas, O. Boutin, I. Raspo, E. Badens, Role of hydrodynamics in supercritical antisolvent processes, J. Supercrit. Fluids. 51 (2009) 248–255. doi:10.1016/j.supflu.2009.07.013.

[31] M. Kind, Colloidal aspects of precipitation processes, Chem. Eng. Sci. 57 (2002) 4287–4293. doi:10.1016/S0009-2509(02)00345-7.

[32] M. Rossmann, A. Braeuer, S. Dowy, T.G. Gallinger, A. Leipertz, E. Schluecker, Solute solubility as criterion for the appearance of amorphous particle precipitation or crystallization in the supercritical antisolvent (SAS) process, J. Supercrit. Fluids. 66 (2012) 350–358. doi:10.1016/j.supflu.2011.11.023.

[33] I. De Marco, O. Knauer, F. Cice, A. Braeuer, E. Reverchon, Interactions of phase equilibria, jet fluid dynamics and mass transfer during supercritical antisolvent micronization: The influence of solvents, Chem. Eng. J. 203 (2012) 71–80. doi:10.1016/j.cej.2012.06.129.

[34] A. Martín, M.J. Cocero, Numerical modeling of jet hydrodynamics, mass transfer, and crystallization kinetics in the supercritical antisolvent (SAS) process, J. Supercrit. Fluids. 32 (2004) 203–219. doi:10.1016/j.supflu.2004.02.009.

[35] A. Martín, M.J. Cocero, Micronization processes with supercritical fluids: Fundamentals and mechanisms, Adv. Drug Deliv. Rev. 60 (2008) 339–350. doi:10.1016/j.addr.2007.06.019.

[36] C.L. Lin, J.K. Lin, Curcumin: A potential cancer chemopreventive agent through suppressing NF-κB signaling, J. Cancer Mol. 4 (2008) 11–16. doi:10.29685/JCM.200804.0002.

[37] P. Anand, A.B. Kunnumakkara, R.A. Newman, B.B. Aggarwal, Bioavailability of

curcumin: Problems and promises, Mol. Pharm. 4 (2007) 807–818. doi:10.1021/mp700113r.

[38] R.I. Mahran, M.M. Hagras, D. Sun, D.E. Brenner, Bringing Curcumin to the Clinic in Cancer Prevention: a Review of Strategies to Enhance Bioavailability and Efficacy, AAPS J. 19 (2017) 54–81. doi:10.1208/s12248-016-0003-2.

[39] L.P. Cunico, M.C. Acosta, C. Turner, Experimental measurements and modeling of curcumin solubility in CO2-expanded ethanol, J. Supercrit. Fluids. (2017) 1–8. doi:10.1016/j.supflu.2017.06.018.

[40] R. Jamwal, Bioavailable curcumin formulations: A review of pharmacokinetic studies in healthy volunteers, J. Integr. Med. 16 (2018) 367–374. doi:10.1016/j.joim.2018.07.001.

[41] A. Umerska, C. Gaucher, F. Oyarzun-Ampuero, I. Fries-Raeth, F. Colin, M.G. Villamizar-Sarmiento, P. Maincent, A. Sapin-Minet, Polymeric nanoparticles for increasing oral bioavailability of Curcumin, Antioxidants. 7 (2018) 1–18. doi:10.3390/antiox7040046.

[42] Z. Hussain, H. Ei, M. Wahab, F. Hussain, T.A. Ahmed, S. Khan, Exploring recent developments to improve antioxidant , anti-inflammatory and antimicrobial efficacy of curcumin : A review of new trends and future perspectives, Mater. Sci. Eng. C. 77 (2017) 1316–1326. doi:10.1016/j.msec.2017.03.226.

[43] H.M. Mansour, Y.S. Rhee, X. Wu, Nanomedicine in pulmonary delivery, Int. J. Nanomedicine. 4 (2009) 299–319. doi:10.2147/IJN.S4937.

[44] D.I. Daniher, J. Zhu, Dry powder platform for pulmonary drug delivery, Particuology. 6 (2008) 225–238. doi:10.1016/j.partic.2008.04.004.

[45] H. Larhrib, G.P. Martin, C. Marriott, D. Prime, The influence of carrier and drug morphology on drug delivery from dry powder formulations, Int. J. Pharm. 257 (2003) 283–296. doi:10.1016/S0378-5173(03)00156-X.

[46] N. Islam, M.J. Cleary, Developing an efficient and reliable dry powder inhaler for pulmonary drug delivery - A review for multidisciplinary researchers, Med. Eng. Phys. 34 (2012) 409–427. doi:10.1016/j.medengphy.2011.12.025.

[47] A.S. Silva, M.T. Tavares, A. Aguiar-Ricardo, Sustainable strategies for nano-in-micro particle engineering for pulmonary delivery, J. Nanoparticle Res. 16 (2014) 1–17. doi:10.1007/s11051-014-2602-0.

[48] M.J. Telko, A.J. Hickey, Dry powder inhaler formulation., Respir. Care. 50 (2005) 1209–1227. doi:10.2165/00128413-200615470-00016.

[49] P.G. Rogueda, D. Traini, The nanoscale in pulmonary delivery. Part 2: formulation platforms, Expert Opin. Drug Deliv. 4 (2007) 595–606. doi:10.1517/17425247.4.6.595.

[50] L. CUADROS RODRIGUEZ, A. GARCIA CAMPANA, F. BARRERO, C. JIMENEZ LINARES, M. ROMAN CEBA, Validation of an Analytical Instrumental Method by Standard Addition Methodology, J. AOAC Int. 78 (1995) 471.

[51] E. Bertozzini, L. Galluzzi, A. Penna, M. Magnani, Application of the standard addition method for the absolute quantification of neutral lipids in microalgae using Nile red, J. Microbiol. Methods. 87 (2011) 17–23. doi:10.1016/j.mimet.2011.06.018.

[52] W.M. Doyle, Principles and applications of fourier transform infrared (FTIR) process analysis, Process Control Qual. 2 (1992) 11–41.

[53] M.M. Beasley, E.J. Bartelink, L. Taylor, R.M. Miller, Comparison of transmission FTIR, ATR, and DRIFT spectra: Implications for assessment of bone bioapatite diagenesis, J. Archaeol. Sci. 46 (2014) 16–22. doi:10.1016/j.jas.2014.03.008.

[54] I. Journal, D.Q.M. Craig, Modulated Temperature Differential Scanning Calorimetry:a Novel Approach To Pharmaceutical Thermal Analysis, Int. J. Pharm. 135 (1996) 13–29.

[55] X. Zhang, M. Cresswell, Materials Characterization of Inorganic Controlled Release, 2016. doi:10.1016/b978-0-08-099991-3.00003-x.

Chapter 2 -

DENSE CO_2 TECHNOLOGY: OVERVIEW OF RECENT APPLICATIONS FOR DRUG PROCESSING/FORMULATION/DELIVERY

Published article:

Chemical Engineering & Processing: Process Intensification 140 (2019) 64‑77

2.1. Abstract

Graphical Abstract

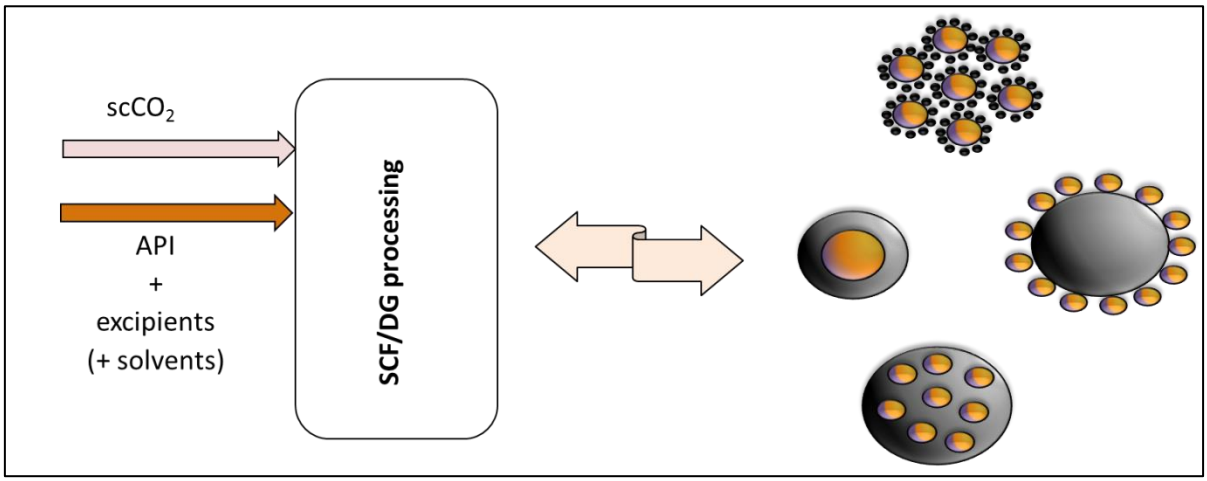

Dense carbon dioxide technology is promising for the processing of drug compounds and development of varied pharmaceutical formulations through micronization, coprecipitation, encapsulation and coating techniques. The main advantages of this technology are the possibility to process thermo-sensitive compounds at low temperatures and using no/low amounts of organic solvents. Many processes have been developed and modified throughout the years to allow the production of composite materials with the desired characteristics. In this review, various processing methods using dense CO_2 and recent process modifications are classified, and their differences and similarities are discussed. Formulation strategies to improve dissolution and flow properties of active compounds are also presented, giving insights into the selection of the most suitable formulation strategy and processing method.

Keywords: drug processing; formulation development; drug delivery; dense CO_2; supercritical fluids

2.2. Introduction

Drug formulation development is a challenging field. Depending on the delivery route and target site of action, specific requirements of particle size, morphology, density and surface properties can pose a great challenge in the development of the formulation. The selection of the most suitable formulation strategy requires an understanding of the physico-chemical properties of the active pharmaceutical ingredients (API) and their interaction within the body. This information will also be the input for the selection of the processing method, which should ensure the preservation of the chemical structure of the API and the acquisition of the desired features.

Traditionally used techniques for drug processing such as spray drying, solvent evaporation and jet milling usually require the use of large amounts of solvent, and time/energy-consuming processing steps to remove residual solvent from the product. Additional issues are the use of high temperatures and the difficult control of particle size and particle size distribution. Supercritical fluid (SCF) or dense gas (DG) technology is an emerging and promising field in the development of pharmaceuticals. In the near-critical region, i.e. relatively close to the critical point of the system, liquid-like properties, such as high density, and gas-like properties such as low viscosity and high diffusivity, coexist. These properties can be easily tuned by adjusting pressure and temperature, giving process flexibility to obtain products with varied characteristics. Supercritical carbon dioxide ($scCO_2$) is selected in most applications due to its relatively low critical conditions (T_c = 31.1C° and p_c = 73.9 bar). It is also non-toxic, non-flammable and inexpensive. These properties make $scCO_2$ especially attractive in the pharmaceutical field because the processing of labile compounds can be done at low temperatures and in many cases without the aid of organic solvents, which can be easily removed from the formulation when their use is necessary. The applicability of SCFs to

produce lipid-based formulations [1,2], polymeric composites [3], and also to sterilize biomaterials [4–6] has been reviewed in the past years. SCF-based processing techniques, such as extrusion [7], coprecipitation [8] and encapsulation [9,10] have also been investigated.

This review aims to classify existing techniques for drug processing by DGs/SCFs, exploring the most recent developments in the field rather than discussing the selection of operation conditions. Insights on the selection of the processing method are provided from a formulation point of view.

2.3. Formulation strategies for drug delivery

Many reviews have focused on describing different formulation strategies for drug delivery [11–13], some of them represented in **Figure 2-1**. The association of active pharmaceutical ingredients (APIs) with excipients and/or additives can improve the API release kinetics and flow properties, and provide stability and protection against external conditions. In the following sections, an overview of SCF-based techniques for producing such formulations is presented.

2.4. Principles of well-known SCF-based techniques for pharmaceutical processing

A short description of the principles and common modifications of the most used SCF-based processes is shown in this section while detailed information regarding their operation can be found elsewhere [14–17]. **Table 2-1** summarizes the main characteristics of the processes.

2.4.1 SCF as solvents

The **Rapid Expansion of Supercritical Solutions (RESS)** explores the significant modification of the solvent power of SCFs with changes in pressure. It operates in a batch mode following two steps: first, dissolution of the solute in $scCO_2$; second, sudden

depressurization of the solution through a heated nozzle/capillary, as shown in **Figure 2-2**a. The solvent power of $scCO_2$ is reduced, leading to supersaturation of the solution and instantaneous precipitation of the solute in small particles [18]. The main advantages of the RESS process are its simplicity and the absence of organic solvents. However, its use and scaling up are restricted by the mandatory solubility of the API in $scCO_2$ (> 10^{-3} $kg/kgCO_2$ [14]), nozzle clogging during depressurization and particle agglomeration [19].

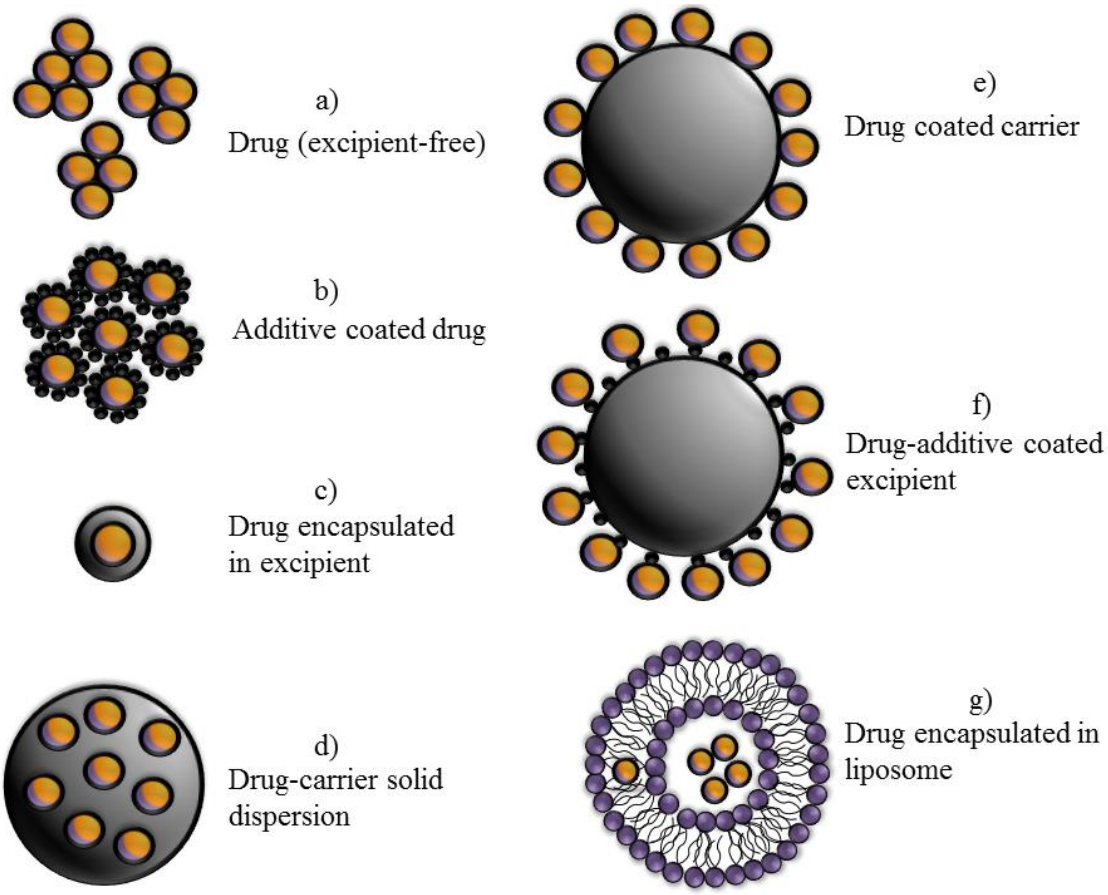

Figure 2-1. Formulation strategies for drug delivery. Drug particles are represented in orange, excipients in grey, additives in black and phospholipids in purple [11–13]**.**

Table 2-1. Characteristics of SCF-based processes

Process	Main role of $scCO_2$	Operation mode	High-pressure stage	Low-pressure stage	Main characteristics
RESS	solvent	batch	saturation	precipitation	Solute-CO_2 solution is depressurized; solvent-free; might require large amounts of CO_2 [18].
RESOLV	solvent	batch	saturation	precipitation	Solute-CO_2 solution is depressurized into a liquid solvent; particle agglomeration and growth is avoided; extra step required to dry the suspension [20,21].
RESAS	solvent	batch	saturation	precipitation	Solute-CO_2 solution is depressurized into a water-surfactant solution; particle agglomeration and growth is avoided; extra step required to dry the suspension [22,23].
RESS-N	solvent	batch	saturation	precipitation	A co-solvent is added to improve solute solubility in $scCO_2$; extra step required to remove the co-solvent [24].
RESS-SC	solvent	batch	saturation	precipitation	Use of a solid co-solvent to improve solute solubility in sc CO_2; particle agglomeration and growth is avoided [25,26].
GAS	antisolvent	batch	atomization; precipitation	-	$scCO_2$ is added to a organic solution. Difficult removal of residual solvent from the powder [27].
SAS /ASES / PCA	antisolvent	semi-continuous	atomization; precipitation	-	Solution is sprayed into $scCO_2$, improving the mass transfer compared to GAS [28–30].
SEDS	antisolvent	semi-continuous	atomization; precipitation	-	Use of a co-axial three-component nozzle, improving the mass transfer compared to SAS [31].

Process	Main role of $scCO_2$	Operation mode	High-pressure stage	Low-pressure stage	Main characteristics
SAS-EM	antisolvent	semi-continuous	atomization; precipitation	-	Use of an ultrasonic vibrating surface, improving the mass transfer compared to SAS [32].
PGSS	solute; plasticizer	batch/continuous	mixing	atomization; precipitation	Depressurization of a melted material containing $scCO_2$ leads to cooling and particle formation; easy scale-up; solvent-free [33–35].
DELOS	co-solvent	batch	saturation (ELS)*	atomization; precipitation	An ELS ($scCO_2$ + solvent + solute) is depressurized; high temperature needed to remove the solvent at ambient pressure [39].
PPRGEL	co-solvent	batch	saturation (ELS)*	atomization; precipitation	An ELS ($scCO_2$ + solvent + solute) is generated using sub-critical CO_2 to avoid the use of high pressure pumps; high temperature needed to remove the solvent at ambient pressure [40,41].
SAA	co-solvent	semi-continuous	saturation (ELS)*	atomization; precipitation	An ELS ($scCO_2$ + solvent + solute) is generated in a packed tower and then depressurized; N_2 is used to induce solvent evaporation; high temperature needed to remove the solvent at ambient pressure [42].
CAN-BD	nebulization agent	semi-continuous	mixing	atomization; nebulization; precipitation	An emulsion containing the solute and $scCO_2$ contact in T forming microbubbles and microdroplets; N_2 is used to induce solvent evaporation [44–46].
SFEE / SEE-C	extractor	continuous	atomization; precipitation	-	Organic solution-water emulsion contact $scCO_2$ in counter-current; particle agglomeration and growth is avoided; extra step required to dry the suspension [47–50].

Process	Main role of $scCO_2$	Operation mode	High-pressure stage	Low-pressure stage	Main characteristics
CTAR	antisolvent	semi-continuous	atomization; precipitation	-	The pecipitator is a small tube (cheaper than large vessels); improved local fluid mixing; easy scale-up; difficult sample collection [53,54].
IJT	antisolvent	semi-continuous	atomization; precipitation	-	The jets of $scCO_2$ and solution impinge inside the precipitator, improving mass transfer [55].
ELAS	antisolvent	semi-continuous	atomization; precipitation	-	Addition of a polar organic solvent to act as co-antisolvent for aqueous solutions; facilitate the processing of hydrosoluble compounds; more energy consuming [59].
RESS-C	co-solvent	continuous	atomization; precipitation	atomization; precipitation	Integration of SEDS and RESS processes; continuous operation. Facillitates the processing of compounds with partial solubility in $scCO_2$ [63].
SEA	co-solvent	semi-continuous	mixing	atomization; precipitation	The fluids are pre-mixed to improve the liquid jet breakup [66,67].
ASAIS	antisolvent	semi-continuous	mixing; precipitation	atomization	The fluids are pre-mixed and precipitation happens before atomization; the precipitator is a small tube (cheaper than large vessels; particles are recovered in cyclones [68].
Vacuum-SAA	co-solvent	semi-continuous	saturation (ELS)*	atomization; precipitation	The precipitator is operated below atmospheric pressure enabling the processing of thermos labile compounds at low temperature [71].
SAS-EM encapsulation	antisolvent and fluidizing medium	semi-continuous	atomization; precipitation	-	A ultrasound device is placed inside of the high-pressure precipitator to fluidize preloaded particles; the SAS jet is delivered inside the fluidized bed [74].

Process	Main role of $scCO_2$	Operation mode	High-pressure stage	Low-pressure stage	Main characteristics
ARISE	antisolvent	batch	atomization; precipitation	-	The atomization is promoted by pressure difference; nozzles are not required; Easier scale-up [77].
SAA-HCM	co-solvent	semi-continuous	saturation (ELS)*	atomization; precipitation	Introduction of a hydrodynamic cavitation mixer to improve the mass transfer between the fluids [83].
SAILA	co-solvent	semi-continuous	saturation (ELS)*	atomization; precipitation	The ELS is sprayed into water (act as antisolvent). particle agglomeration and growth is avoided; extra step required to dry the suspension [89].
SpEDS	antisolvent	semi-continuous	atomization; precipitation	-	Introduction of an injector to allow the delivery of a suspension [99].
SAS-Wurster	antisolvent and fluidizing medium	semi-continuous	atomization; precipitation	-	A Wurster coater is placed inside of the high-pressure precipitator to receive the SAS jet [97].
RESS-WTS	solvent	semi-continuous	saturation	precipitation	The RESS jet is depressurized inside a Wurster coater preloaded with the material to be coated [101].
RESS-BFB	solvent and fluidizing medium	semi-continuous	saturation	precipitation	The RESS jet is depressurized inside a fluidized bed preloaded with the material to be coated [101].
SAS-FB	antisolvent and fluidizing medium	semi-continuous	atomization; precipitation	-	A fluidized bed is placed inside of the high-pressure precipitator to receive the SAS jet [102].

Process	Main role of $scCO_2$	Operation mode	High-pressure stage	Low-pressure stage	Main characteristics
SAS-DEM	antisolvent and fluidizing medium	semi-continuous	atomization; precipitation	-	A stirrer is placed inside of the high-pressure precipitator to fluidize preloaded particles; the SAS jet is delivered inside of the fluidized bed. Small particles can be fluidized [104].

*ELS = Expanded Liquid Solution.

Some of these limitations have been addressed by other similar processes. In **RESOLV (Rapid Expansion of a Supercritical Solution into a Liquid Solvent)**, the supercritical solution is expanded into a liquid solvent, instead of air, to prevent particle agglomeration [20,21]. Similarly, in **RESAS (Rapid Expansion from Supercritical Solution to Aqueous Solution)**, a water-surfactant solution receives the supercritical jet and stabilizes the particles preventing their aggregation and growth [22,23]. **RESS-N (Rapid Expansion from Supercritical Solution with a Non-solvent)** uses a compound that improves the solute solubility at supercritical conditions but acts as a non-solvent at atmospheric conditions [24]. In these processes a suspension is formed. Therefore, the solute must not be soluble in the liquid used**.** In **RESS-SC (Rapid Expansion of Supercritical Solutions with a Solid Co-solvent)**, the addition of a solid co-solvent, which can be removed from the system by sublimation, improves the solute solubility and inhibits particle growth by coagulation [25,26]. Although the modifications cited can be useful for certain applications, these processes can no longer be characterized as solvent-free.

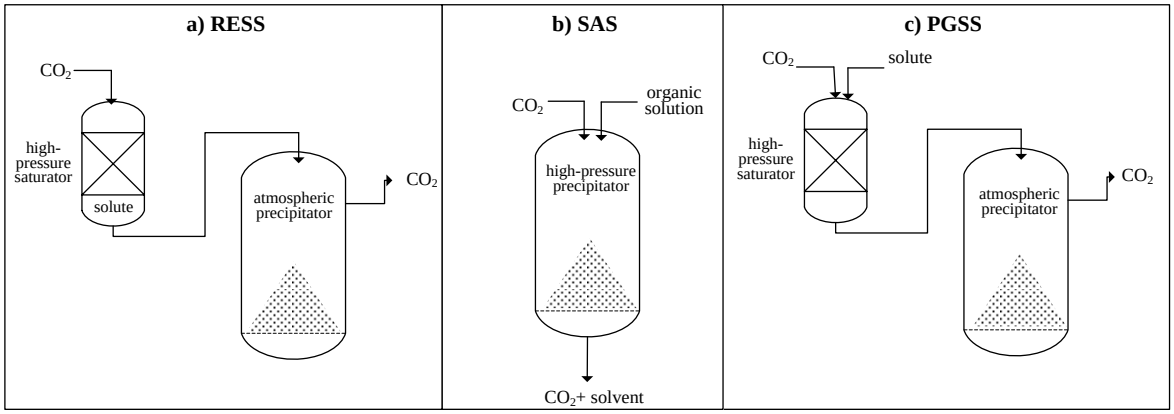

Figure 2-2. Process diagram of main SCF-based techniques: a) RESS, b) SAS and c) PGSS.

2.4.2 SCF as antisolvent

Antisolvent methods are based on the high solubility and diffusivity of SCFs in organic solvents. The solute is usually dissolved in an organic solvent and then the solution is put in

contact with the $scCO_2$. The diffusion of $scCO_2$ into the liquid phase decreases the solvation power of the organic solvent, leading to the precipitation of the solute. A final washing step with pure $scCO_2$ needs to be carried out to remove residual solvent from the powder. Therefore, the basic requirements to allow precipitation via antisolvent techniques are: complete miscibility between solvent and antisolvent (CO_2) at the operating conditions and the mixture solvent/antisolvent must not solubilize the solute.

Different antisolvent processes follow the same principles but with distinct ways of mixing the organic solution and the supercritical fluid. In the **Gas Antisolvent (GAS)** process [27], first the solution is loaded in the precipitation vessel and then the $scCO_2$ is added to reach the operating pressure. In **Supercritical Antisolvent (SAS)** (**Figure 2-2**b), the $scCO_2$ is pumped into the precipitation vessel until the operational pressure is reached, after which the solution enters the vessel through a nozzle. This process is also known as **Aerosol Solvent Extraction System (ASES)** [28] or **Precipitation by Compressed Antisolvent (PCA)** [29,30]. **Solution Enhanced Dispersion by Supercritical Fluids (SEDS)** uses a co-axial three-component nozzle that enables a turbulent flow and better mixture before the components enter the precipitation vessel [31]. In **Supercritical Antisolvent Precipitation with Enhanced Mass Transfer (SAS-EM)**, the solution atomization is improved by contacting an ultrasonic vibrating surface [32].

2.4.3 SCF as solute/plasticizer/co-solvent/atomizing or nebulizing agent

Supercritical or dense CO_2 can play other roles in particle generation including co-solute, co-solvent, dispersing agent and plasticizer. In **Particles from Gas Saturated Solutions (PGSS)**, $scCO_2$ is dissolved in a substance (or mixture of substances) at high pressure, acting as a plasticizer. The viscosity and melting point (or glass transition temperature) of the material is decreased, allowing it to be sprayed into ambient conditions. Upon

depressurization, the gas evaporates, and the system is cooled drown (Joule-Thomson effect) below the melting point of the material, leading to the solidification of the droplets and formation of fine particles [33–35]. PGSS can be operated in batch mode or continuously feeding the materials into the precipitator through a static mixer (**Figure 2-2**c) [36]. Variations of PGSS are: **Continuous Powder Coating Spraying Process (CPCSP)** applied for the manufacture of powder coatings [37] and **Gas Assisted Melting Atomization (GAMA)** which uses air to improve the atomization [38].

In other processes organic solvents and $scCO_2$ are used to generate expanded liquid solutions. In **Depressurization of an Expanded Liquid Organic Solution (DELOS)**, the material to be micronized is dissolved in an organic solvent, and then the solution is mixed with $scCO_2$ to form an expanded liquid solution. Undesirable particles possibly formed at this stage (GAS process) are collected in a filter and finally, the pressure is decreased to ambient leading to the cooling of the solution and particle precipitation [39]. The **Precipitation by Pressure Reduction of Gas-expanded Liquids (PPRGEL)** follows the same steps as the DELOS process, however, ambient temperature and sub-critical CO_2 are employed, avoiding the use of high pressure pumps [40,41]. While DELOS and PRRGEL operate in a batch mode, in **Supercritical-Assisted Atomization (SAA)** the organic solution and $scCO_2$ are mixed in a packed tower, forming an expanded liquid which is then atomized near atmospheric pressure in a semi-continuous operation. Nitrogen is also delivered to the vessel to induce liquid evaporation [42]. Still, high temperatures in the precipitator are usually applied to dry the particles.

Other PGSS-based processes are used to dry solutions in which the solvent has low solubility in $scCO_2$, such as aqueous solutions. In **PGSS-drying**, the solution to be dried and $scCO_2$ contact in a static mixer at high pressure and temperature following depressurization in a

spray tower (no nitrogen used). The post-expansion temperature have to be carefully selected (above the dew point of the solvent-CO_2 mixture) in order to obtain a dry powder [43]. In **Carbon Dioxide-Assisted Nebulization with a Bubble Dryer® (CAN-BD)** the contact of near-critical or supercritical CO_2 with aqueous or aqueous-organic solution is promoted in a low volume tee. The emulsion generated is then expanded, forming microbubbles and micro-droplets dried by hot N_2 [44–46]. In these processes $scCO_2$ acts as a co-solute and nebulization agent.

2.4.4 Miscellaneous

In **Supercritical Fluid Extraction of Emulsion (SFEE)** [47,48] and **Continuous Supercritical Emulsions Extraction (SEE-C)** [49,50] the solute is dissolved in an organic solvent, and then an emulsion in water is prepared. The emulsion is atomized in counter-current with $scCO_2$, so that the organic phase is extracted generating a suspension in water. SFEE/SEE-C is said to offer more flexibility to tune particle characteristics, enhanced reduction in particle size compared to SAS and the ability to avoid particle agglomeration due to the presence of water, however, drying of the product needs to be carried out afterwards. In **Supercritical Reverse Phase Evaporation (scRPE),** $scCO_2$ is mixed with an organic solution containing a phospholipid and then an aqueous solution is introduced in the resulting homogeneous mixture to generate liposomes in a batch mode [51]. Later, the same group developed the **Improved Supercritical Reverse Phase Evaporation (IscRPE),** a completely solvent-free method in which the liposomes are formed by first mixing the water solution and phospholipid with posterior introduction of $scCO_2$ [52].

2.5. SCF-based processes for drug formulations development

In this section, novel/modified processes developed by using SCFs or DGs are analysed. The type of formulation produced and some examples of compounds processed are summarized in **Table 2-2**.

2.5.1. Micronization of single compounds

Drug only formulations (excipient-free) (**Figure 2-1**a) can be advantageous in the delivery of APIs that require high dosage while avoiding the possible side effects of excipients. The applicability of recently developed/modified processes is usually demonstrated by the processing of single compounds, such as APIs or polymers. This section discusses the features of these processes and their use to micronize materials of interest for the pharmaceutical industry.

In SAS-type processes, the mixing of the fluids is of great importance to achieve high supersaturation and produce small and uniform particles. Recently, two different injection systems have been tested by the same research group. The **Concentric Tube Antisolvent Reactor (CTAR)** is simpler, and hence easier to scale up than the typical SAS process, as the reactor is composed of a small tube to which the $scCO_2$ is delivered, and a capillary for the atomization of the organic solution (**Figure 2-3**). The authors propose an industrial scale setup made of several injection systems with the same size as the lab scale to control turbulences locally, avoiding poor fluid mixing which can happen when several solution jets are sprayed into the same bulk CO_2. L-PLA was used as model compound and the micronization results were similar or superior to the conventional SAS process. However, difficulties in collecting the powder deposited in the annular part of the reactor, plugging and the rapid filling of the powder recovery system are some of the issues reported [53,54]. Years

later, **Impinging Jets Technology (IJT)** was associated with the SAS process. In this configuration, jets of organic solution and $scCO_2$ collide face to face improving the mass transfer (**Figure 2-3**). Griseofulvin [55] and sulfathiazole [56] have been processed using this technique. A comparison between these injection devices on the processing of L-PLA and griseofulvin reveals that the IJT can be more efficient in decreasing the particle size of the API, while CTAR is simpler and provided better results in terms of process intensification [57]. In all the systems evaluated, IJT and CTAR produced smaller particles compared to the classical SAS process, but usually larger than those obtained by more complex processes such as SAA and SAS-EM. Modelling of the crystallization process was later proposed [58].

Table 2-2. SCF-based processes and examples of drug formulations recently developed.

Process	Purpose	API	Excipient	Reference
CTAR, IJT	micronization	-	L-PLA	[53,57]
	micronization	griseofulvin	-	[55,57]
IJT	micronization	sulfathiazole	-	[56]
ELAS	micronization	yttrium acetate, BSA	-	[59]
	micronization	BSA	-	[60]
	micronization	lysozyme	-	[61]
	micronization	-	sodium alginate and PVA	[62]
RESS-C	micronization	-	PLA–PEG–PLA	[63]
	micronization	lonidamine	-	[64]
SEA	micronization	lysozyme	-	[65]
	coprecipitation	indomethacin, theophylline, caffeine, sulfamethazine, aspirin, carbamazepine	saccharin (cocrystal former)	[66,67]
ASAIS	micronization	theophylline	-	[68]

Process	Purpose	API	Excipient	Reference
Vacuum-SAA	micronization	-	PLLA, BSA	[69]
	micronization	-	PEG	[70]
	micronization	-	PLA–PEG copolymer	[71]
	coprecipitation	rotenone	PEG, PVP and sodium alginate	[72]
	coprecipitation	lincomycin hydrochloride	BSA	[73]
Modified SAS-EM	coprecipitation	curcumin	PLGA	[74]
ARISE	micronization	levothyroxine sodium	-	[75]
	micronization	curcumin	-	[76]
	micronization	para-coumaric acid (PCA)	HP-β-CD	[77]
	coprecipitation	curcumin	HP-β-CD and PVP	[78,79]
	coprecipitation	insulin	HPMCP	[80]
	coprecipitation	curcumin	methyl-b-cyclodextrin	[81]
SAS with swirl mixer	coprecipitation	curcumin	PVP	[82]
SAA-HCM	micronization	BSA	-	[83]
	micronization	lysozyme	-	[84]
	micronization	levofloxacin hydrochloride	-	[85]
	micronization	-	chitosan	[86]
	coprecipitation	trypsin	chitosan	[87]
	coprecipitation	insulin	N-trimethyl chitosan	[88]
SAILA	micronization	-	Polycaprolactone	[89]
	micronization	-	PMMA	[90]

Process	Purpose	API	Excipient	Reference
	micronization	-	PLGA, PLA	[91]
	coprecipitation	piroxicam, diclofenac, indomethacin	PLGA	[92]
Modified PGSS	coprecipitation	coenzyme Q10	PEG6000	[93]
	coprecipitation	ibuprofen	PEG6000	[94]
	coprecipitation	curcumin	tristearin and soy phosphatidylcholine	[95]
	coprecipitation	vitamin B2	fully hydrogenated canola oil and sodium lauryl sulfate	[96]
SAS-Wurster	encapsulation	caffeine	MCC, ethyl cellulose, Eudragit®, poly(DL-lactide-co-glycolide)	[97]
Modified SAS-EM	encapsulation	curcumin	PLGA	[98]
SpEDS	encapsulation	methotrexate	Fe_3O_4, PLLA-PEG-PLLA	[99]
	encapsulation	methotrexate	PLLA-PEG-PLLA	[100]
RESS-WTS and RESS-BFB	coating	benzoic acid, adamantane, ferrocene, phenanthrene, stearic acid and vitamin K3	MCC	[101]
SAS-FB	coating	naringin	MCC	[102]
	coating	curcumin	lactose	[103]
SAS-DEM	coating	nevirapine	lactose and MCC	[104]
	coating	itraconazole	lactose	[105]
	coating	rifampicin	lactose	[106]

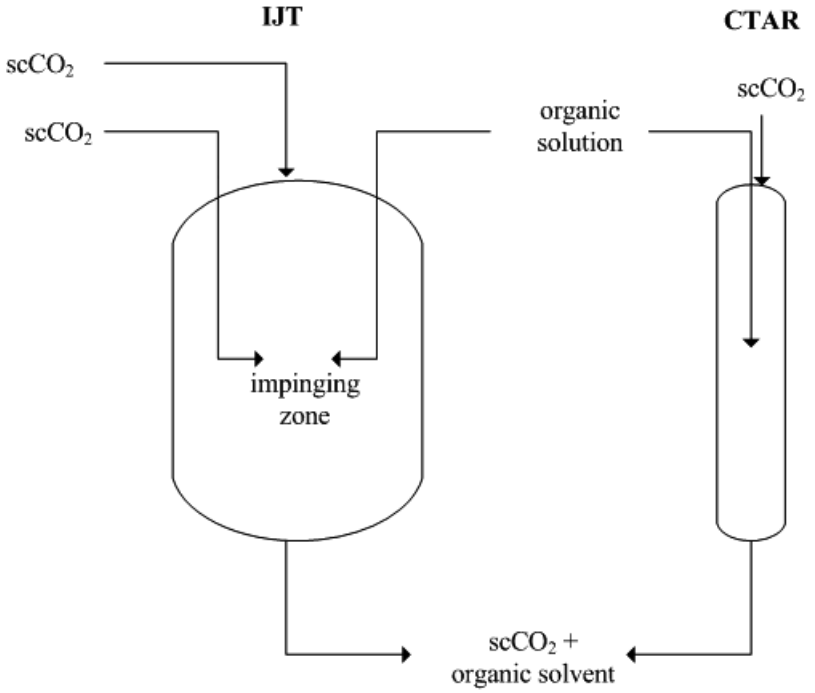

Figure 2-3. Injection systems for CTAR and IJT processes [58].

Another modification of the SAS process consists of using a supercritical mixture of a polar organic solvent and CO_2 as the antisolvent to precipitate hydrosoluble compounds from aqueous solutions. This technique was called **Expanded Liquid Antisolvent (ELAS)** by Reverchon's group in 2012 [59], although other researchers had already used the same technique for many years [107–110]. The ELAS process is more complex than the SAS process as it requires an understanding of multiple components phase diagrams. It is also more energy intensive because an extra pump is required for the delivery of the organic solvent (co-antisolvent), which is premixed with $scCO_2$ before entering the precipitator (**Figure 2-4**a), and an additional washing step with the antisolvent mixture needs to be carried out to remove residual water from the system followed by the washing with pure $scCO_2$. Different materials have been processed by ELAS, including yttrium acetate and bovine serum albumin [59,60], lysozyme [61], sodium alginate and polyvinyl alcohol (PVA) [62].

The precipitation of composite materials is challenging due to the number of compounds possibly affecting the phase equilibrium.

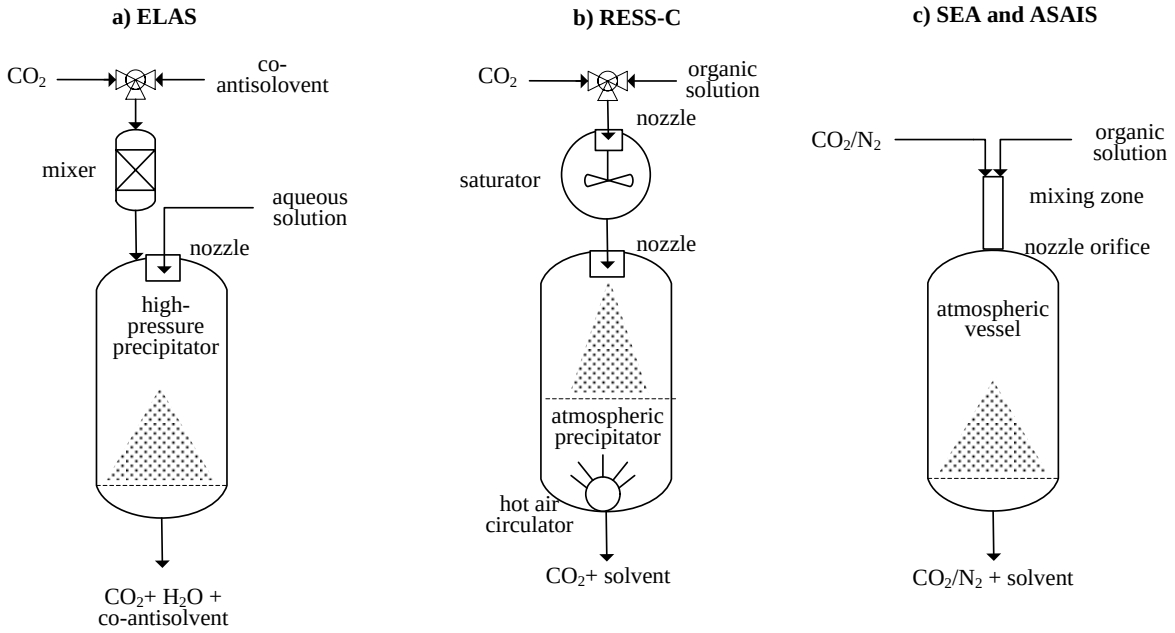

Figure 2-4. Principles of micronization by: a) ELAS, b) RESS-S, c) SEA and ASAIS [61,63,64,68].

For compounds with partial solubilitity in $scCO_2$, the precipitation yield by either RESS or SAS is usually low, therefore **Continuous Rapid Expansion of Supercritical Solution (RESS-C)** was proposed (**Figure 2-4**b), consisting of a combination of the SEDS and RESS processes, operating in a continuous mode. Here the organic solution and $scCO_2$ are sprayed together in a high pressure vessel using a coaxial nozzle and then the resulting mixture is sprayed into ambient conditions. This setup was used to produce microparticles of polylactide–poly(ethylene glycol)–polylactide (PLA–PEG–PLA) at 12 MPa and with the temperature of extraction and expansion vessels controlled by a gas bath at 33°C. When processed by SEDS and RESS in similar conditions, particles could not be obtained [63]. Further improvements in the rig, such as the addition of a mechanical stirrer in the extraction vessel to ensure solubilization of the solute in $scCO_2$ and carefully designed expansion vessel to control the temperature and avoid particle agglomeration and redissolution have been

recently proposed as illustrated in **Figure 2-4**b. In this last work, nanoparticles of lonidamine were produced at 20 MPa and 55°C with the expansion vessel being kept at 50°C by a water bath [64]. RESS-C configuration is similar to SAA, differing on the internal structure of the extraction vessel/saturator and also no nitrogen flow is used for RESS-C.

By combining the concepts of antisolvent precipitation and atomization due to depressurization, Azevedo and co-workers developed the **Supercritical Enhanced Atomization (SEA)** process [67], also named **Atomization and Anti-solvent (AAS)** [66], and the **Atomization of Supercritical Antisolvent Induced Suspensions (ASAIS)** process [68]. In the SEA process, CO_2 and the organic solution are mixed in a coaxial nozzle before atomization in order to improve the liquid jet breakup that will then happen in the next stage at near-atmospheric conditions (**Figure 2-4**c). This process has been employed to precipitate lysozyme from water-ethanol solutions by using either supercritical CO_2 (antisolvent and atomizing agent) or N_2 (atomizing agent) between 8 MPa and 25 MPa and 40-60°C to study the precipitation mechanisms governing the process. It was found that spherical particles were formed when the precipitation happened after atomization by spray-drying mechanism. On the other hand, when the antisolvent effect was high enough, antisolvent crystallization happened in the mixer before atomization, leading to the formation of fibres and compromising the enzyme activity [65]. The applicability of the SEA process to produce cocrystals of APIs (indomethacin, theophylline, caffeine, sulfamethazine, aspirin, carbamazepine) with saccharin (cocrystal former) has also been investigated [66,67]. The ASAIS process differs from the SEA process in the way the fluids are mixed before the nozzle orifice and on the mechanism of particle separation after precipitation: SEA uses an in-line filter and ASAIS uses a cyclone. In ASAIS, the conditions are selected in order to achieve precipitation in the small in-line mixer and then the suspension is spray dried in an

atmospheric vessel to remove the solvent (**Figure 2-4**c). This reduces the cost of the high-pressure vessel, which is a small tube (similar to the CTAR). Microparticles of theophylline have been produced using this technique with $scCO_2$ and N_2 at 5-10 MPa and 45°C and computational fluid dynamics (CFD) simulations were carried out to determine the distribution of the solute concentration in the high pressure vessel [68].

2.5.2. Coprecipitation (matrix systems)

Coprecipitates are composite materials usually obtained by the simultaneous precipitation of drug and excipient from the same solution. Ideally, drug molecules should be well dispersed in a matrix of excipient (**Figure 2-1**d), usually a polymer or a lipid. This configuration can deliver the API to a specific target with controlled release, avoiding its degradation and also improving the handling and flowability of the formulation when a larger structure containing the API is produced. When a hydrophilic polymer is used, molecular interactions between the compounds during precipitation might change the solid state of the drug, improving its solubility and dissolution properties in aqueous media. However, successful coprecipitation is not always achieved due to the formation of two distinct phases prior to precipitation (polymer-rich and drug-rich) so the compounds precipitate separately.

Even though the solubility of the API and excipient in the selected solvent is a preliminary requirement, the final drug loading will depend on the process conditions rather than on the initial solution composition. Coprecipitates of several materials can be obtained by employing SCF-based processes. Recently developed experimental setups which have been used to coprecipitate drug and excipient using SCF technology are discussed below.

Atomised Rapid Injection for Solvent Extraction (ARISE) is an antisolvent batch process developed by Foster and Sih [111,112] to overcome the common issues associated with

nozzle blockage which hinders process scale-up. In this process, the precipitation chamber is filled with $scCO_2$, and then the organic solution is loaded in the injection chamber and pressurized by an inert gas (nitrogen/argon) with a pressure higher than the one in the precipitation chamber (**Figure 2-5**a). After equilibration, the valve connecting the vessels is opened and the pressure difference promotes rapid atomization of the solution and effective mixing between the fluids. The ARISE process has been applied to micronize APIs such as levothyroxine sodium [75] and curcumin [76]. Composite materials combining curcumin, polyvinylpyrrolidone (PVP) and hydroxypropyl-beta-cyclodextrin (HP-β-CD) for pulmonary delivery have also been obtained through coprecipitation [78,79] and the improvement in curcumin dissolution properties has been demonstrated [81]. Coprecipitates of insulin and hydroxypropyl methyl cellulose phthalate (HPMCP) were also produced and a comparative study with other antisolvent precipitation methods showed that ARISE usually leads to higher recovery (84.4%) than GAS (50.9%) and ASES (72.6%) processes [80]. Recently, a study of the scale-up of the ARISE process and an economic evaluation demonstrated its viability to produce pharmaceutical formulations [77].

In 2014, Zabihi et al.[74] modified the operational procedure of SAS-EM to produce curcumin-PLGA nanoparticles (20 - 808 nm). In this procedure, the precipitator is initially loaded with $scCO_2$, then the inlet and outlet valves are closed at the desired pressure. The ultrasound starts to operate, and a certain amount of solution is pumped into the precipitator. After some time of mixing, fresh $scCO_2$ flushes the vessel to remove the solvent. Fresh solution can be pumped several times into the precipitator and the mixing and washing steps are repeated (**Figure 2-6**). The authors claim that the sequential replacement of $scCO_2$ increased the supersaturation of the organic phase leading to high yield (23 - 96%) and loading (9 - 48%).

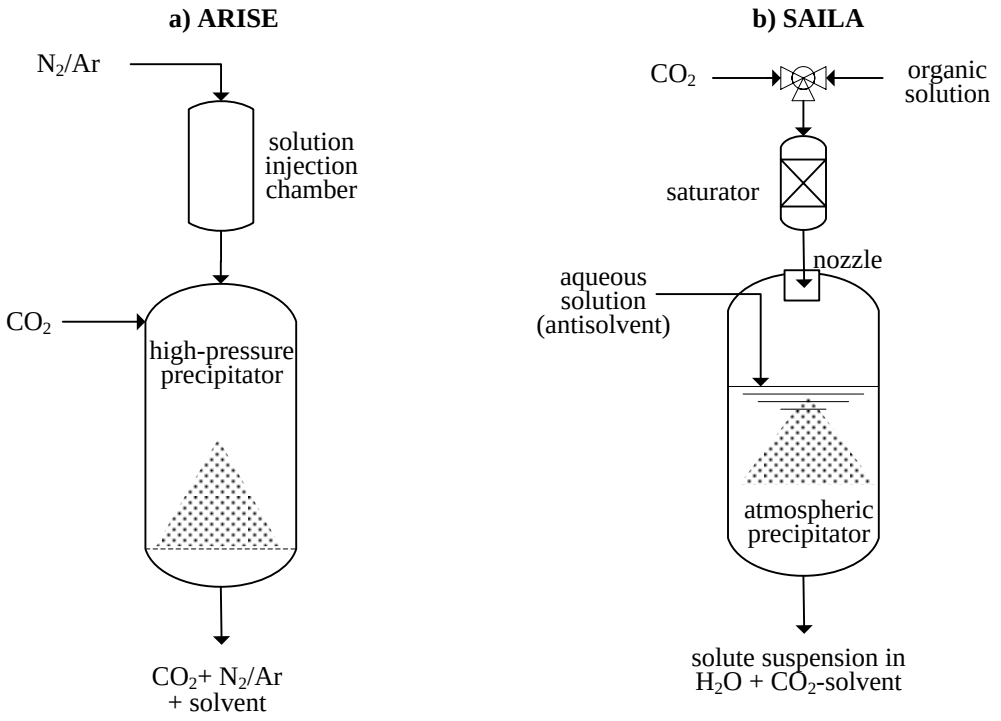

Figure 2-5. Principles of coprecipitation by: a) ARISE and b) SAILA [89,111].

In order to improve the mixing and mass transfer between the fluids, Chhouk et al. [113] prepared coprecipitates of curcumin and PVP by the SAS process using a micro swirl mixer device. Although sub-microparticles and nanoparticles (25-342 nm) were obtained, the material was highly coalescing and a comparison of the particle size obtained by using a typical capillary or nozzle was not provided.

The use of mixing devices has also been reported for the SAA process to improve the mass transfer between the liquid solution and $scCO_2$. In **SAA-HCM**, a hydrodynamic cavitation mixer was used. Levofloxacin hydrochloride was first micronized with the aid of the mixer and the use of a vacuum pump to keep the precipitator below atmospheric pressure was reported [85]. In further works, BSA [83], lysozyme [84], chitosan [86] were micronized. Recently, the authors studied the coprecipitation of trypsin with chitosan [87] and insulin with N-trimethyl chitosan [88]. The typical SAA process has been applied to coprecipitate a variety of active compounds with different kinds of excipients [73,114–120]. However, this

technique is not suitable for the processing of thermo labile compounds due to the high temperature required in the precipitator to dry the particles. The operation of the precipitator below atmospheric pressure allows the precipitation at lower temperatures as confirmed by Adami et al. [69] through the micronization of PLLA and BSA using pressures of 0.5 - 0.87 bar and temperatures as low as 30°C. The vacuum system was also employed to micronize PEG [70], PLA–PEG copolymer [71] and to produce coprecipitates of rotenone with PEG, PVP and sodium alginate [72] and lincomycin hydrochloride dispersed in BSA [73].

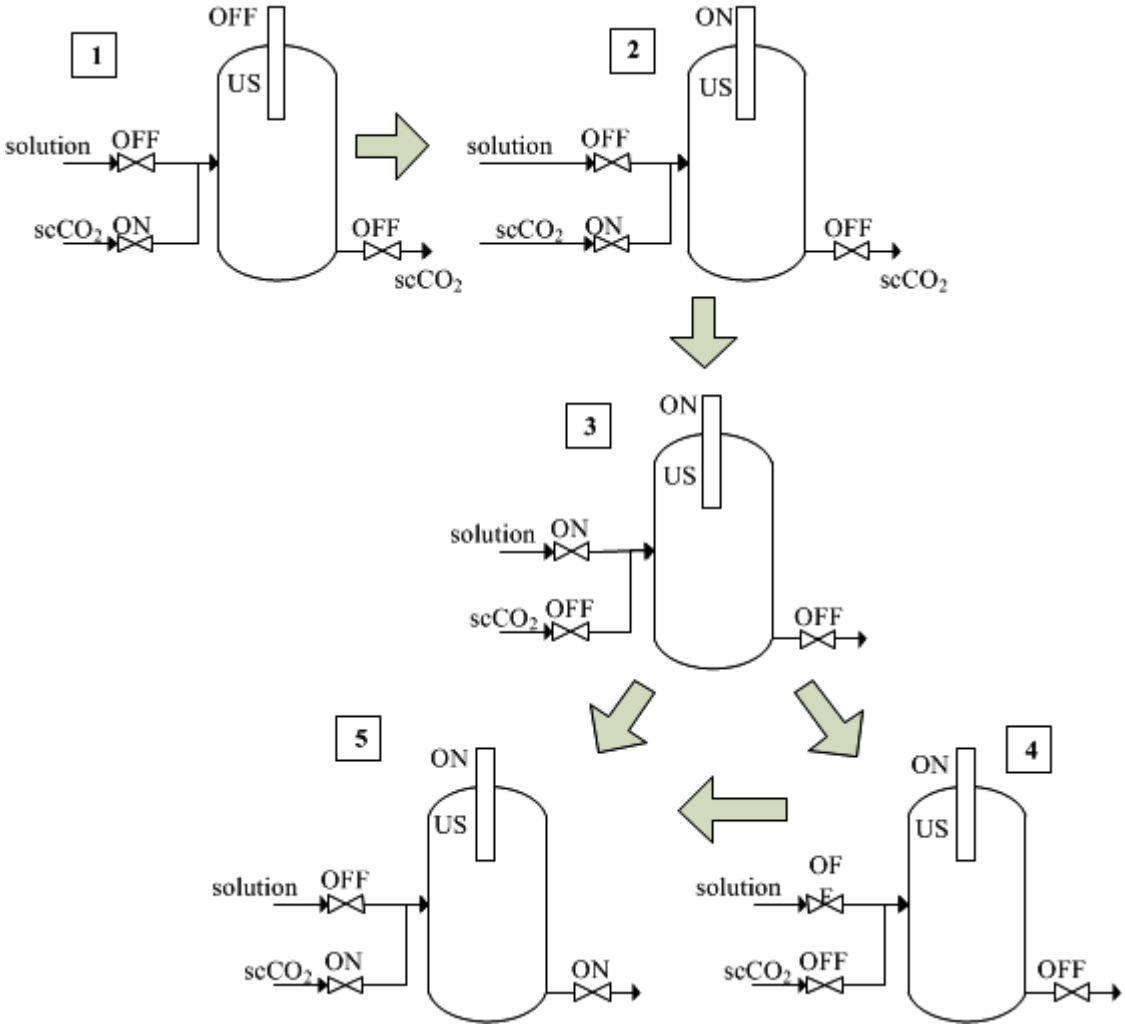

Figure 2-6. Modified operating procedure for SAS-EM encapsulation [74].

The configuration of **Supercritical Assisted Injection in a Liquid Antisolvent (SAILA)** is similar to the SAA process; however, the expanded solution obtained by contacting the organic solution and $scCO_2$ is sprayed into water (possibly containing a surfactant) rather than air. The water acts as an antisolvent leading to the precipitation of the solute, generating a suspension (**Figure 2-5**b). Naturally, the organic solvent and water must be miscible while the solute must be insoluble in water. The authors claim that the use of expanded liquids would improve the mixing and produce smaller particles compared to a typical antisolvent precipitation using ordinary liquids. This process can be advantageous to avoid particle coalescence (in a similar way to RESOLV and RESAS), nevertheless, a post-processing step is required to separate the organic solvent from the suspension. Polymeric particles of polycaprolactone [89], Polymethylmethacrylate (PMMA) [90], PLGA and PLA [91] have been produced using this technique. The production of composite materials for controlled release purposes has also been reported for the coprecipitation of PLGA with some anti-inflammatory drugs. Successful coprecipitation was achieved only for a very low drug/polymer ratio (1/20) while the encapsulation efficiency varied between 50 and 97% [92]. High temperatures in the saturator (60-100°C) were used in the previously reported works, limiting the application of SAILA for the processing of thermo-sensitive compounds.

Although largely used to produce a variety of composite materials, adaptations in the experimental setup of the PGSS process have been reported, such as the introduction of a coaxial nozzle for the delivery of the gas-saturated solution (inner side) and CO_2 (outer side) to prevent the blockage of the nozzle by solid particles; and addition of a high pressure pump after the mixer to control the flow rate of the solution into the precipitation vessel [93]. In the reported work, the coprecipitation of coenzyme Q10 with PEG6000 (a water-soluble dispersant) was carried out to avoid the coagulation of the coenzyme, which is slowly

solidified when precipitated alone. Then, PEG6000 was dissolved in water to obtain the intended nanoparticles of coenzyme Q10 in a suspension, following centrifugation and freeze-drying to separate the aqueous solution from the nanoparticles. In another work, the authors used the same approach to prepare ibuprofen nanoparticles [94]. More recently, São Pedro et al. [95] used a coaxial nozzle to deliver nitrogen together with a gas-saturated lipid solution into the precipitator, also to avoid particle coalescence and agglomeration. Curcumin-loaded solid lipid nanoparticles containing tristearin and soy phosphatidylcholine (PC) were produced. Another modification of the PGSS process consisted in depressurizing the gas-expanded solution of the materials to be micronized in counter-current with an aqueous PEG solution stream, as an attempt to decrease the size of the particles. This process was used to encapsulate vitamin B2 in solid lipid nanoparticles of fully hydrogenated canola oil (FHCO), using sodium lauryl sulfate (SLS) as surfactant [96]. Other PGSS-based techniques have been used to produce varied formulations, such as metal loaded lipid microparticles [121], hollow [122] and oil-loaded hollow solid lipid particles [123,124].

2.5.3. Encapsulation (film-on-particle)

The encapsulation of active ingredients is widely applied in the pharmaceutical industry for different purposes, such as to protect the API against humidity, light and oxidation, to improve appearance and/or taste of formulations, to tailor the surface properties and particle size, to avoid caking during transportation and storage and to develop delayed or controlled release systems [125]. A film of the coating material is usually precipitated onto the surface of previously existing API particles (**Figure 2-1**c). Therefore, if a specific particle size of the API is required, a previous micronization step needs to be carried out, increasing the overall operational costs. The dissolution properties of hydrophobic APIs can be improved by changing their surface wettability, however, more significant improvement can be obtained by

coprecipitation since the API is well dispersed in an excipient matrix. The solvent used should be able to dissolve only the coating material, keeping the API particles unchanged. Supercritical fluid technology has been used to encapsulate APIs under mild temperature conditions. Recently developed SCF-based encapsulation processes and formulations are discussed in this section.

The combination of fluidized bed coating and supercritical fluid-based precipitation has been reported for many years. In 1995, Tsutsumi et. al. [126] precipitated paraffin by RESS onto the surface of microspheroidal catalyst particles (56μm) in a circulating fluidized bed. The coating rate was found to be constant and particle agglomeration was avoided due to the absence of liquid droplets. Other core materials such as glass beds, ceramic beads, plastic granules and proteins have also been coated with paraffin or wax by similar processes [127–131].

In the previous year, Benoit et al. [132] had developed a simple batch process to coat microparticles of APIs with lipids or polymers soluble in $scCO_2$. Initially, the coating material and API are loaded in a high pressure mixed chamber which is then pressurized with CO_2. After some time, when the $scCO_2$ has solubilized the coating material, depressurization leads to its precipitation and coating onto the surface of the suspended API particles. This process was used to encapsulate a model protein, bovine serum albumin (BSA), within two different lipids: trimyristin and Gelucire® 50-02. While trimyristin was crystalized producing a discontinuous coating and burst release of BSA, Gelucire® 50-02 precipitated as a film and hence, a sustained release was observed [133]. Later, other aspects of this technique were further discussed [134–136].

It is important to notice that for a successful encapsulation, the SCF should be able to dissolve the coating material but not the core particles. This limits its use. If the coating material is not

soluble in $scCO_2$, an antisolvent method can be employed. Niu et al. [97] used a Wurster-type coater (**Figure 2-7**a) to encapsulate glass beads (1-2 mm), stents (< 20 mm long) and caffeine-loaded MCC beads (1-1.4 mm) and tables (3.2-7.9 mm) within polymer films using near-critical CO_2 (52-66 bar) as antisolvent and fluidizing medium. After coating with ethyl cellulose, the initial burst release of caffeine from MCC beads was delayed, and the release rate decreased. Slower release could be achieved by increasing the coating time, demonstrating the applicability of process in preparing controlled-release formulations. The mild conditions used and the safety of the process compared to conventional coating techniques is highlighted by the authors; because air is replaced by dense CO_2, a flame retardant, the formation of explosive mixtures with organic solvents is avoided.

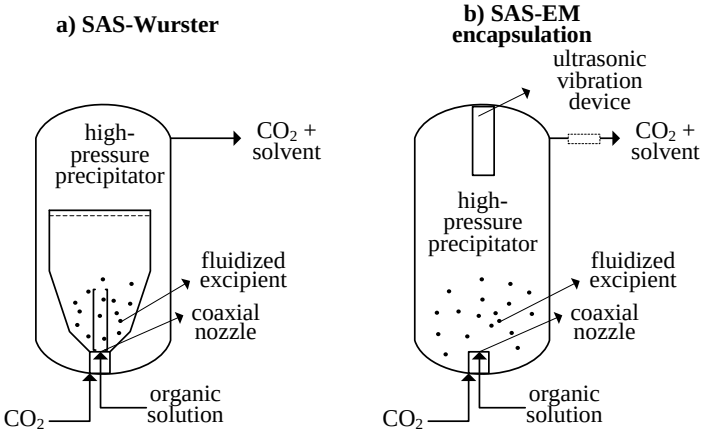

Figure 2-7. Principles of encapsulation by: a) SAS-Wurster and b) SAS-EM [97,98].

A similar process, based on SAS-EM, was used to encapsulate nanoparticles of curcumin in PLGA. Previously precipitated by SAS-EM, curcumin nanoparticles were fluidized in batch mode for 15 seconds by an ultrasonic vibration probe placed on the top of the precipitator (**Figure 2-7**b). The PLGA solution was then sprayed onto the fluidized nano-curcumin. The ultrasonic power (100-350 W) could be adjusted to enhance drug loading (4-38%), however, the precipitation yield was still very low (12-51%). Based on the sustained release profile of curcumin (without initial burst release), the authors suggested that PLGA particles were

initially formed and then attached to each other to form a porous structure around curcumin particles [98]. As the mean size of the final formulation increased up to 84 times compared to the size of the initial curcumin particles, PLGA probably encapsulated curcumin agglomerates, rather than individual nanoparticles. It is also important to note that, although the removal of the organic solvent by $scCO_2$ is fast, some curcumin could have been solubilized by the organic solvents used (ethanol and ethyl acetate).

In order to increase the loading efficiency of microencapsulation, a modification of the SEDS process, named **Suspension-Enhanced Dispersion by Supercritical Fluid (SpEDS)**, has been developed. It consists of introducing an injector to allow the delivery of a suspension to the precipitator, instead of a solution. The setup was tested to produce magnetic microspheres by microencapsulation and coprecipitation processes. For the microencapsulation, nanoparticles of Fe_3O_4 were suspended in an organic solution containing the API (methotrexate) and then sprayed into $scCO_2$ to precipitate the API encapsulating the Fe_3O_4. The resulting material (API-loaded Fe_3O_4) was suspended in an organic polymeric (PLLA–PEG–PLLA) solution and then sprayed again into $scCO_2$ generating a second layer of microencapsulation. Unlike the previously cited encapsulation processes, in SpEDS, there is no need to preload the material to be coated in the precipitator. For the coprecipitation, the Fe_3O_4 was suspended in an API-polymer organic solution and then sprayed into $scCO_2$. In the same operational conditions, the microencapsulation was able to produce microspheres with higher drug load (8.9%) and loading efficiency (60.8%) than the coprecipitation and improved release kinetics for sustained release of methotrexate [99]. In another work, the coprecipitation and microencapsulation of methotrexate by PLLA-PEG-PLLA using SpDES was also analysed [100]. The same concept had been used years before by Wang et al. [137]

to encapsulate silica nanoparticles with Eudarit. The polymer solution contacting suspended silica nanoparticles was sprayed into $scCO_2$ (SAS process).

APIs can also be encapsulated in liposomes (**Figure 2-1**g) in a more complex structure as already reviewed elsewhere [1,2]. Recently, a continuous process to produce liposomes has been reported [138–140].

2.5.4. Coating (particle-on-particle)

Powder flowability is an important parameter in pharmaceutical processing. Micronization, often required to improve the dissolution properties of APIs, usually generates aggregates due to the intense inter-particle attraction force existing between fine particles. To improve the stability, handling and flowability of powder formulations, APIs are combined with larger carrier/excipient particles. However, drug content uniformity and further aggregation in downstream processing steps remain a concern [141].

The simultaneous precipitation of fine API particles and coating onto the surface of larger excipient particles can be an alternative to avoid such issues. When supercritical fluid-based micronization is used, the API particle size and morphology can be tuned for the intended application. In addition, the association with a hydrophilic excipient can improve the dissolution properties of poorly water-soluble APIs, by increasing its wettability, while enhancing its flow properties. However, the type of formulation produced (**Figure 2-1**e,f) is not ideal for applications in which prolonged/controlled release and protection of the API are required since the drug particles are exposed to the environment. In general, coating processes are limited by the fact that the solvent used must not solubilize the excipient particles, which should keep their original size and morphology, not affecting the prevailing phase equilibria.

This section illustrates examples of novel SCF-based techniques for particle-on-particle coating in which the API is the coating material.

Taking advantage of the solvent properties of $scCO_2$, Leeke et al. [101] adapted the RESS process for coating purposes using two different configurations: Wurster coater (**RESS-WTS**) and fluidized bed (**RESS-BFB**), as demonstrated in **Figure 2-8**a,b. In both solvent-free processes, the jet of $scCO_2$ saturated with the API is expanded upwards in a bed of excipient particles. For RESS-WTS the fluidization is aided by the flow of hot air passing through a gas distributor. Nanoparticles of six different APIs (< 30 nm) were precipitated onto the surface of microcrystalline cellulose (MCC, 300 μm) close to their point of origin, inhibiting further particle growth and agglomeration. Therefore, the flowability and handling of the final formulations were improved while keeping the advantageous features of nanoparticles. The drug content, however, was very low (0.01-0.54 wt% for 10 minutes coating time) with process yield varying from 14-74%.

As the main limitation of the RESS process is the mandatory solubility of the API in $scCO_2$, recently, the same group integrated the SAS process with a fluidized bed (FB) under pressure (**SAS-FB**) to process APIs with low solubility in $scCO_2$. In this single-step process, the fluidized bed is placed inside the precipitator and the jet of drug solution is sprayed from the bottom into a bed of excipient particles fluidized by the upward flow of $scCO_2$ delivered through a gas distributor (**Figure 2-8**c). Nanoparticles of narigin (< 200 nm) were coated onto MCC particles (175-444 μm) and a faster drug release rate was obtained when compared with a formulation of the same materials prepared by a conventional fluidized bed coating process. The authors claim that the formulation could be directly administered orally since the drug content was around 2.5 wt% [102]. The same rig was used by Matos et al. [103] to coat lactose particles (125-145 μm) with curcumin. Several operational parameters were analysed

and formulations potentially suitable for pulmonary delivery were produced with a curcumin content of around 1-6 wt% and drug yield between 71-93%. Due to the improved mixing and collection of particles close to their origin, SAS-FB produced smaller and less aggregated curcumin particles than SAS under the same operational conditions.

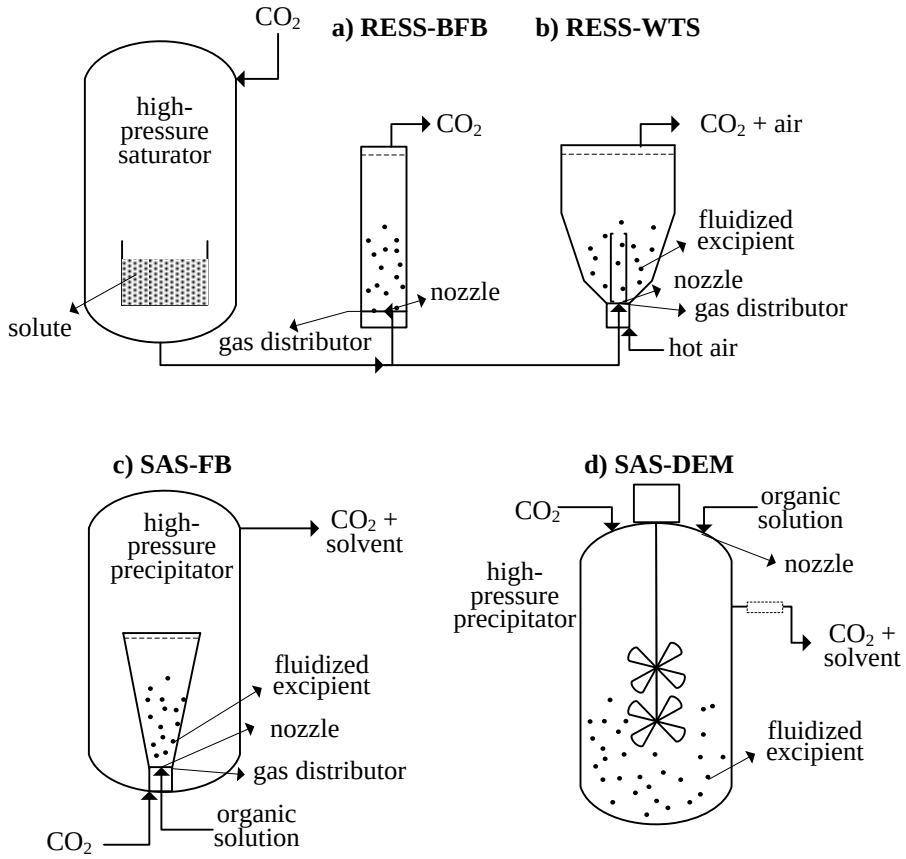

Figure 2-8. Scheme of coating by: a) RESS-BFB, b) RESS-WTS, c) SAS-FB and d) SAS-DEM [102,101,104].

As the fluidization occurs inside the precipitator, the CO_2 flowrate selected for SAS-FB processing should be high enough to ensure particles are fluidized and precipitation happens under supercritical conditions. High-pressure fluidization can be used to investigate different fluidization patterns with small changes in pressure [142] while taking advantage of the high

degree of mixing and high rates of heat and mass transfer, typical of fluidized beds, to achieve uniform coatings.

A common weakness of conventional fluidized beds is the difficulty of fluidizing small particles (< 30 μm, group C) [143]. Therefore, the bed material must be composed of large particles, which limits the surface area available for particle deposition and, consequently, the amount of drug that can be loaded in the formulation. Consequently, RESS-WTS, RESS-BFB and SAS-FB are more useful in the preparation of formulations of highly potent drugs that require low dosages.

If fine excipient particles are desired, a possible solution is to mix them with surfactants (additives), known as force control agents [144], in a previous processing step to decrease the attraction force between excipient particles, hence improving their flowability. Then a drug-additive-excipient formulation (**Figure 2-1**f) can be obtained, however, the administration route restricts the number of additives. Additives are also used to improve the bulk density and flow properties of the formulation by changing the API surface properties (**Figure 2-1**b). This allows direct tablet compaction without the need for prior granulation [141,145].

In the **Supercritical Antisolvent-Drug Excipient Mixing (SAS-DEM)** process, a stirrer placed in the high-pressure precipitator provides the extra energy source needed to allow the fluidization of fine particles (**Figure 2-8**d). This process has been used to coat lactose (100 μm) and MCC particles (50 μm) with nevirapine (10-54 wt% loading). It was found that by increasing the drug loading, the API particle size increased and the configuration of the API-excipient mixture changed from ordered to ordered-random [104]. In another work, SAS-DEM was used to precipitate itraconazole (6-50 wt% loading) onto lactose (100 μm) in the presence of two surfactants, sodium dodecyl sulfate and polaxamer 407, to improve the deaggregation of flaky API particles [105]. Although sub-microparticles and microparticles of

the drug were obtained in both works, sometimes with a similar surface area to a SAS-processed drug, improved dissolution properties were attributed to the efficient deagglomeration and wetting of drug particles in the presence of the excipients. Ober et al. [106] prepared pulmonary delivery formulations of micro-sized rifampicin particles onto lactose microfine (< 10 μm) with drug loading between 1.2–25.7%. As the particle size of the precipitated API is similar to the lactose, the formulation resembles more a solid mixture rather than a coated material. It is worth noting that, depending on the characteristics of the core particles, their attrition with the impeller and walls of the vessel might lead to undesired particle breakage when specific size and morphology are required. Additionally, the extra energy input might increase operational costs.

For the mixing of nanoparticles, the rapid expansion of high pressure or supercritical suspensions (REHPS) can be used. This simple technique consists of suspending insoluble compounds in $scCO_2$ and then depressurizing the suspension through a nozzle. REHPS has been initially used to mix different species of nanoparticles and several analytical techniques have demonstrated its improved efficacy when compared with conventional mixing techniques, especially for compounds with similar densities [146]. The effective break up of particle agglomerates was attributed to the shear stress in the nozzle and the posterior collision of the agglomerates with the mach disc [147]. The efficiency of this process was later demonstrated by deagglomeration and mixing of alumina and titania nano-powders [148]. This technique can potentially be applied to mix/coat pharmaceutical compounds and excipients, although no reports of such application have been found so far.

2.6. Conclusions

This review has demonstrated the applicability of SCF/DGs to prepare a wide variety of pharmaceutical formulations. Due to their attractive properties, including rapid variation of

density with pressure and/or temperature and low viscosity, the processing of thermo-labile compounds is possible while keeping their molecular integrity. Additionally, they are considered environmentally friendly technologies since the use of large amounts of organic solvents is avoided. Many modifications in previously existing processes have been developed in recent years, showing the interest in the improvement of these techniques to bring them to an industrial scale. Insights into the selection of the most appropriate processing technique have also been provided considering different types of formulation strategies.

2.7. Declarations of interest

None.

2.8. Acknowledgements

The authors would like to thank the Brazilian National Council for Scientific and Technological Development (CNPq) for their financial support through the program Science Without Borders.

2.9. References

[1] C.C. Beh, R. Mammucari, N.R. Foster, Lipids-based drug carrier systems by dense gas technology: A review, Chem. Eng. J. 188 (2012) 1–14. doi:10.1016/j.cej.2012.01.129.

[2] I.E. Santo, A.S. Pedro, R. Fialho, E. Cabral-Albuquerque, Characteristics of lipid micro- and nanoparticles based on supercritical formation for potential pharmaceutical application., Nanoscale Res. Lett. 8 (2013) 386. doi:10.1186/1556-276X-8-386.

[3] A. Tandya, R. Mammucari, F. Dehghani, N.R. Foster, Dense gas processing of polymeric controlled release formulations, 328 (2007) 1–11. doi:10.1016/j.ijpharm.2006.08.016.

[4] N. Foster, R. Mammucari, F. Dehghani, A. Barrett, K. Bezanehtak, E. Coen, G. Combes, L. Meure, A. Ng, H.L. Regtop, A. Tandya, Processing Pharmaceutical Compounds Using Dense Gas Technology, Ind. Eng. Chem. Res. 42 (2003) 6476–

6493. doi:10.1021/ie030219x.

[5] S.S. Karajanagi, R. Yoganathan, R. Mammucari, H. Park, J. Cox, S.M. Zeitels, R. Langer, N.R. Foster, Application of a dense gas technique for sterilizing soft biomaterials, Biotechnol. Bioeng. 108 (2011) 1716–1725. doi:10.1002/bit.23105.

[6] M. Perrut, Sterilization and virus inactivation by supercritical fluids (a review), J. Supercrit. Fluids. 66 (2012) 359–371. doi:10.1016/j.supflu.2011.07.007.

[7] M. Chauvet, M. Sauceau, J. Fages, Extrusion assisted by supercritical CO2: A review on its application to biopolymers, J. Supercrit. Fluids. 120 (2017) 408–420. doi:10.1016/j.supflu.2016.05.043.

[8] V. Prosapio, I. De Marco, E. Reverchon, Supercritical antisolvent coprecipitation mechanisms, J. Supercrit. Fluids. 138 (2018) 247–258. doi:10.1016/j.supflu.2018.04.021.

[9] M.J. Cocero, Á. Martín, F. Mattea, S. Varona, Encapsulation and co-precipitation processes with supercritical fluids: Fundamentals and applications, J. Supercrit. Fluids. 47 (2009) 546–555. doi:10.1016/j.supflu.2008.08.015.

[10] M. Kalani, R. Yunus, Application of supercritical antisolvent method in drug encapsulation: a review., Int. J. Nanomedicine. 6 (2011) 1429–1442. doi:10.2147/IJN.S19021.

[11] D.I. Daniher, J. Zhu, Dry powder platform for pulmonary drug delivery, Particuology. 6 (2008) 225–238. doi:10.1016/j.partic.2008.04.004.

[12] A.S. Silva, M.T. Tavares, A. Aguiar-Ricardo, Sustainable strategies for nano-in-micro particle engineering for pulmonary delivery, J. Nanoparticle Res. 16 (2014) 1–17. doi:10.1007/s11051-014-2602-0.

[13] P.G. Rogueda, D. Traini, The nanoscale in pulmonary delivery. Part 2: formulation platforms, Expert Opin. Drug Deliv. 4 (2007) 607–620. doi:10.1517/17425247.4.6.607.

[14] E. Badens, Y. Masmoudi, A. Mouahid, C. Crampon, Current situation and perspectives in drug formulation by using supercritical fluid technology, J. Supercrit. Fluids. 134 (2018) 274–283. doi:10.1016/j.supflu.2017.12.038.

[15] T.K. Fahim, I.S.M. Zaidul, M.R. Abu Bakar, U.M. Salim, M.B. Awang, F. Sahena,

K.C.A. Jalal, K.M. Sharif, M.H. Sohrab, Particle formation and micronization using non-conventional techniques- review, Chem. Eng. Process. Process Intensif. 86 (2014) 47–52. doi:10.1016/j.cep.2014.10.009.

[16] Y. Sun, Supercritical Fluid Particle Design for Poorly Water-soluble Drugs (Review)., Curr. Pharm. Des. 20 (2014) 349–68. doi:10.2174/13816128113199990404.

[17] V. Miwa, H. Yoshida, V. Manuel, C. Figueiredo, M. Maria, D.C. Vila, J. Martins, O. Júnior, N. Aranha, M.P. Daflon, M.V. Chaud, Supercritical fluid and pharmaceutical applications. Part I : Process classification, African J. Pharm. Pharmacol. 10 (2016) 132–144. doi:10.5897/AJPP2014.4259.

[18] M. Türk, Manufacture of submicron drug particles with enhanced dissolution behaviour by rapid expansion processes, J. Supercrit. Fluids. 47 (2009) 537–545. doi:10.1016/j.supflu.2008.09.008.

[19] N.R. Foster, R. Mammucari, L.T. Danh, W.H. Teoh, Particle Engineering by Dense Gas Technologies Applied to Pharmaceuticals, in: M.O. Balaban, G. Ferrentino (Eds.), Dense Phase Carbon Dioxide Food Pharm. Appl., 1st ed., Blackwell Publishing, 2012: pp. 199–226. doi:10.1002/9781118243350.ch10.

[20] P. Pathak, M.J. Meziani, T. Desai, Y.P. Sun, Nanosizing drug particles in supercritical fluid processing, J. Am. Chem. Soc. 126 (2004) 10842–10843. doi:10.1021/ja046914t.

[21] M.J. Meziani, P. Pathak, F. Beacham, L.F. Allard, Y.P. Sun, Nanoparticle formation in rapid expansion of water-in-supercritical carbon dioxide microemulsion into liquid solution, J. Supercrit. Fluids. 34 (2005) 91–97. doi:10.1016/j.supflu.2004.10.005.

[22] T.J. Young, S. Mawson, K.P. Johnston, I.B. Henriksen, G.W. Pace, A.K. Mishra, Rapid expansion from supercritical to aqueous solution to produce submicron suspensions of water-insoluble drugs, Biotechnol. Prog. 16 (2000) 402–407. doi:10.1021/bp000032q.

[23] M. Türk, D. Bolten, Formation of submicron poorly water-soluble drugs by rapid expansion of supercritical solution (RESS): Results for Naproxen, J. Supercrit. Fluids. 55 (2010) 778–785. doi:10.1016/j.supflu.2010.09.023.

[24] K. Mishima, K. Matsuyama, D. Tanabe, S. Yamauchi, T.J. Young, K.P. Johnston, Microencapsulation of proteins by rapid expansion of supercritical solution with a

nonsolvent, AIChE J. 46 (2000) 857–865. doi:10.1002/aic.690460418.

[25] C. Domingo, F.E. Wubbolts, R. Rodriguez-Clemente, G.M. van Rosmalen, Solid crystallization by rapid expansion of supercritical ternary mixtures, J. Cryst. Growth. 198–199 (1999) 760–766. http://www.sciencedirect.com/science/article/B6TJ6-3X23HR7-4W/2/af5c4cc82ffa0bf73241bdb2da0adc43.

[26] R. Thakur, R.B. Gupta, Rapid expansion of supercritical solution with solid cosolvent (RESS-SC) process: Formation of griseofulvin nanoparticles, Ind. Eng. Chem. Res. 44 (2005) 7380–7387. doi:10.1021/ie050417j.

[27] S.D. Yeo, G.B. Lim, P.G. Debenedetti, H. Bernstein, Formation of microparticulate protein powders using a supercritical fluid antisolvent, Biotechnol. Bioeng. 41 (1993) 341–346. doi:10.1002/bit.260410308.

[28] J. Bleich, B.W. Müller, W. Waßmus, Aerosol solvent extraction system - a new microparticle production technique, Int. J. Pharm. 97 (1993) 111–117. doi:10.1016/0378-5173(93)90131-X.

[29] D.J. Dixon, K.P. Johnston, Formation of microporous polymer fibers and oriented fibrils by precipitation with a compressed fluid antisolvent, J. Appl. Polym. Sci. 50 (1993) 1929. doi:https://doi.org/10.1002/app.1993.070501110.

[30] S. Mawson, M.Z. Yates, M.L. O'Neil, K.P. Johnston, Stabilized Polymer Microparticles by Precipitation with a Compressed Fluid Antisolvent. 2. Poly(propylene oxide)- and Poly(butylene oxide)-Based Copolymers, Langmuir. 13 (1997) 1519–1528. doi:10.1021/la961017r.

[31] M. Hanna, P. York, Method and apparatus for the formation of particles, US 5851453 A, 1998.

[32] P. Chattopadhyay, R.B. Gupta, Production of griseofulvin nanoparticles using supercritical CO2 antisolvent with enhanced mass transfer, Int. J. Pharm. 228 (2001) 19–31. doi:10.1021/ie010040r.

[33] E. Weidner, Z. Knez, Z. Novak, Process for preparing particles or powders, EP0744992B1, 1994.

[34] E. Weidner, Z. Knez, Z. Novak, Process for preparing particles or powders,

US6056791A, 1994.

[35] E. Weidner, Z. Knez, Z. Novak, Process for preparing particles or powders, JP3510262B2, 1994.

[36] Ž. Knez, M. Škerget, M. Knez Hrnčič, D. Čuček, Chapter 2 - Particle Formation Using Sub- and Supercritical Fluids, 2014. doi:http://dx.doi.org/10.1016/B978-0-444-62696-7.00002-2.

[37] E. Weidner, M. Petermann, K. Blatter, V. Rekowski, Manufacture of powder coatings by spraying of gas-enriched melts, Chem. Eng. Technol. 24 (2001) 529–533. doi:10.1002/1521-4125(200105)24:5<529::AID-CEAT529>3.0.CO;2-L.

[38] S. Salmaso, N. Elvassore, A. Bertucco, P. Caliceti, Production of Solid Lipid Submicron Particles for Protein Delivery Using a Novel Supercritical Gas-Assisted Melting Atomization Process, J. Pharm. Sci. 98 (2009) 640–650. doi:10.1002/jps.

[39] N. Ventosa, S. Sala, J. Veciana, J. Torres, J. Llibre, Depressurization of an Expanded Liquid Organic Solution (DELOS): A New Procedure for Obtaining Submicron- Or Micron-Sized Crystalline Particles, Cryst. Growth Des. 1 (2001) 299–303. doi:10.1021/cg0155090.

[40] S. V. Dalvi, M. Mukhopadhyay, Large and Rapid Temperature Reduction of Organic Solutions with Subcritical CO2, AIChE J. 53 (2007) 2814–2823. doi:10.1002/aic.

[41] S. V. Dalvi, M. Mukhopadhyay, A novel process for precipitation of ultra-fine particles using sub-critical CO2, Powder Technol. 195 (2009) 190–195. doi:10.1016/j.powtec.2009.05.029.

[42] E. Reverchon, Supercritical-assisted atomization to produce micro- and/or nanoparticles of controlled size and distribution, Ind. Eng. Chem. Res. 41 (2002) 2405–2411. doi:10.1021/ie010943k.

[43] D. Meterc, M. Petermann, E. Weidner, Drying of aqueous green tea extracts using a supercritical fluid spray process, J. Supercrit. Fluids. 45 (2008) 253–259. doi:10.1016/j.supflu.2008.02.001.

[44] R.E. Sievers, E.T.S. Huang, J.A. Villa, J.K. Kawamoto, M.M. Evans, P.R. Brauer, Low-temperature manufacturing of fine pharmaceutical powders with supercritical

fluid aerosolization in a Bubble Dryer®, Pure Appl. Chem. 73 (2001) 1299–1303. doi:10.1351/pac200173081299.

[45] R.E. Sieversa, E.T.S. Huang, J.A. Villa, G. Engling, P.R. Brauer, Micronization of water-soluble or alcohol-soluble pharmaceuticals and model compounds with a low-temperature Bubble Dryer®, J. Supercrit. Fluids. 26 (2003) 9–16. doi:10.1016/S0896-8446(02)00188-2.

[46] R.E. Sievers, B.P. Quinn, S.P. Cape, J.A. Searles, C.S. Braun, P. Bhagwat, L.G. Rebits, D.H. McAdams, J.L. Burger, J.A. Best, L. Lindsay, M.T. Hernandez, K.O. Kisich, T. Iacovangelo, D. Kristensen, D. Chen, Near-critical fluid micronization of stabilized vaccines, antibiotics and anti-virals, J. Supercrit. Fluids. 42 (2007) 385–391. doi:10.1016/j.supflu.2007.03.001.

[47] P. Chattopadhyay, B.Y. Shekunov, J.S. Seitzinger, Method and apparatus for continuous particle prodution using supercritical fluid, US7083748B2, 2003.

[48] B.Y. Shekunov, P. Chattopadhyay, J. Seitzinger, R. Huff, Nanoparticles of poorly water-soluble drugs prepared by supercritical fluid extraction of emulsions, Pharm. Res. 23 (2006) 196–204. doi:10.1007/s11095-005-8635-4.

[49] G. Della Porta, N. Falco, E. Reverchon, Continuous supercritical emulsions extraction: A new technology for biopolymer microparticles production, Biotechnol. Bioeng. 108 (2011) 676–686. doi:10.1002/bit.22972.

[50] G. Della Porta, R. Campardelli, E. Reverchon, Monodisperse biopolymer nanoparticles by Continuous Supercritical Emulsion Extraction, J. Supercrit. Fluids. 76 (2013) 67–73. doi:10.1016/j.supflu.2013.01.009.

[51] K. Otake, T. Imura, H. Sakai, M. Abe, Development of a New Preparation Method of Liposomes Using Supercritical Carbon Dioxide, Langmuir. 17 (2001) 3898–3901. doi:10.1021/la010122k.

[52] K. Otake, T. Shimomura, T. Goto, T. Imura, T. Furuya, S. Yoda, Y. Takebayashi, H. Sakai, M. Abe, Preparation of liposomes using an improved supercritical reverse phase evaporation method, Langmuir. 22 (2006) 2543–2550. doi:10.1021/la051654u.

[53] O. Boutin, C. Maruejouls, G. Charbit, A new system for particle formation using the principle of the SAS process : The Concentric Tube Antisolvent Reactor (CTAR), J.

Supercrit. Fluids. 40 (2007) 443–451. doi:10.1016/j.supflu.2006.07.012.

[54] O. Boutin, Apparatus for forming particles of a target substance, US20090056080A1, 2007.

[55] B. Calvignac, O. Boutin, The impinging jets technology: A contacting device using a SAS process type, Powder Technol. 191 (2009) 200–205. doi:10.1016/j.powtec.2008.10.009.

[56] S. Careno, O. Boutin, E. Badens, Drug recrystallization using supercritical anti-solvent (SAS) process with impinging jets: Effect of process parameters, J. Cryst. Growth. 342 (2012) 34–41. doi:10.1016/j.jcrysgro.2011.06.059.

[57] O. Boutin, T. Petit-Gas, E. Badens, Powder Micronization using a CO2 supercritical antisolvent type process: Comparison of different introduction devices, Ind. Eng. Chem. Res. 48 (2009) 5671–5678. doi:10.1021/ie8017803.

[58] O. Boutin, Influence of introduction devices on crystallisation kinetic parameters in a supercritical antisolvent process, J. Cryst. Growth. 342 (2012) 13–20. doi:10.1016/j.jcrysgro.2010.11.099.

[59] I. De Marco, E. Reverchon, Supercritical carbon dioxide+ethanol mixtures for the antisolvent micronization of hydrosoluble materials, Chem. Eng. J. 187 (2012) 401–409. doi:10.1016/j.cej.2012.01.135.

[60] V. Prosapio, E. Reverchon, I. De Marco, Antisolvent micronization of BSA using supercritical mixtures carbon dioxide + organic solvent, J. Supercrit. Fluids. 94 (2014) 189–197. doi:10.1016/j.supflu.2014.07.012.

[61] V. Prosapio, E. Reverchon, I. De Marco, Production of lysozyme microparticles to be used in functional foods, using an expanded liquid antisolvent process, J. Supercrit. Fluids. 107 (2016) 106–113. doi:10.1016/j.supflu.2015.09.001.

[62] V. Prosapio, E. Reverchon, I. De Marco, Polymers' ultrafine particles for drug delivery systems precipitated by supercritical carbon dioxide + organic solvent mixtures, Powder Technol. 292 (2016) 140–148. doi:10.1016/j.powtec.2016.01.033.

[63] A.Z. Chen, Z. Zhao, S. Bin Wang, Y. Li, C. Zhao, Y.G. Liu, A continuous RESS process to prepare PLA-PEG-PLA microparticles, J. Supercrit. Fluids. 59 (2011) 92–

97. doi:10.1016/j.supflu.2011.08.012.

[64] B.Q. Chen, R.K. Kankala, S. Bin Wang, A.Z. Chen, Continuous nanonization of lonidamine by modified-rapid expansion of supercritical solution process, J. Supercrit. Fluids. 133 (2018) 486–493. doi:10.1016/j.supflu.2017.11.016.

[65] M.A. Rodrigues, J. Li, L. Padrela, A. Almeida, H.A. Matos, E.G. de Azevedo, Anti-solvent effect in the production of lysozyme nanoparticles by supercritical fluid-assisted atomization processes, J. Supercrit. Fluids. 48 (2009) 253–260. doi:10.1016/j.supflu.2008.06.006.

[66] L. Padrela, M.A. Rodrigues, S.P. Velaga, H.A. Matos, E.G. de Azevedo, Formation of indomethacin-saccharin cocrystals using supercritical fluid technology, Eur. J. Pharm. Sci. 38 (2009) 9–17. doi:10.1016/j.ejps.2009.05.010.

[67] L. Padrela, M.A. Rodrigues, S.P. Velaga, A.C. Fernandes, H.A. Matos, E.G. de Azevedo, Screening for pharmaceutical cocrystals using the supercritical fluid enhanced atomization process, J. Supercrit. Fluids. 53 (2010) 156–164. doi:10.1016/j.supflu.2010.01.010.

[68] M.A. Rodrigues, L. Padrela, V. Geraldes, J. Santos, H.A. Matos, E.G. Azevedo, Theophylline polymorphs by atomization of supercritical antisolvent induced suspensions, J. Supercrit. Fluids. 58 (2011) 303–312. doi:10.1016/j.supflu.2011.05.012.

[69] R. Adami, S. Liparoti, E. Reverchon, A new supercritical assisted atomization configuration, for the micronization of thermolabile compounds, Chem. Eng. J. 173 (2011) 55–61. doi:10.1016/j.cej.2011.07.036.

[70] S. Liparoti, R. Adami, E. Reverchon, PEG micronization by supercritical assisted atomization , operated under reduced pressure, J. Supercrit. Fluids. 72 (2012) 46–51. doi:10.1016/j.supflu.2012.08.009.

[71] R. Adami, S. Liparoti, L. Izzo, D. Pappalardo, E. Reverchon, PLA – PEG copolymers micronization by supercritical assisted atomization, J. Supercrit. Fluids. 72 (2012) 15–21. doi:10.1016/j.supflu.2012.06.019.

[72] L. Martin, S. Liparoti, G. Della Porta, R. Adami, J.L. Marqués, J.S. Urieta, A.M. Mainar, E. Reverchon, Rotenone coprecipitation with biodegradable polymers by supercritical assisted atomization, J. Supercrit. Fluids. 81 (2013) 48–54.

doi:10.1016/j.supflu.2013.03.032.

[73] R. Adami, S. Liparoti, G. Della Porta, P. Del Gaudio, E. Reverchon, Lincomycin hydrochloride loaded albumin microspheres for controlled drug release, produced by Supercritical Assisted Atomization, J. Supercrit. Fluids. 119 (2017) 203–210. doi:10.1016/j.supflu.2016.09.017.

[74] F. Zabihi, N. Xin, J. Jia, T. Chen, Y. Zhao, High Yield and High Loading Preparation of Curcumin–PLGA Nanoparticles Using a Modified Supercritical Antisolvent Technique, Ind. Eng. Chem. Res. 53 (2014) 6569–6574. doi:10.1021/ie404215h.

[75] S.A.B.V. De Melo, L.T. Danh, R. Mammucari, N.R. Foster, Dense CO2 antisolvent precipitation of levothyroxine sodium: A comparative study of GAS and ARISE techniques based on morphology and particle size distributions, J. Supercrit. Fluids. 93 (2014) 112–120. doi:10.1016/j.supflu.2013.11.019.

[76] F. Kurniawansyah, R. Mammucari, N.R. Foster, Polymorphism of curcumin from dense gas antisolvent precipitation, Powder Technol. 305 (2017) 748–756. doi:10.1016/j.powtec.2016.10.067.

[77] F. Kurniawansyah, R. Mammucari, A. Tandya, N.R. Foster, Scale − Up and economic evaluation of the atomized rapid injection solvent extraction process, J. Supercrit. Fluids. 127 (2017) 208–216. doi:10.1016/j.supflu.2017.03.006.

[78] F. Kurniawansyah, R. Mammucari, N.R. Foster, Inhalable curcumin formulations by supercritical technology, Powder Technol. 284 (2015) 289–298. doi:10.1016/j.powtec.2015.04.083.

[79] F. Kurniawansyah, H.T.T. Duong, T.D. Luu, R. Mammucari, O. Vittorio, C. Boyer, N. Foster, Inhalable curcumin formulations: Micronization and bioassay, Chem. Eng. J. 279 (2015) 799–808. doi:10.1016/j.cej.2015.05.087.

[80] A. Tandya, H.Q. Zhuang, R. Mammucari, N.R. Foster, Supercritical fluid micronization techniques for gastroresistant insulin formulations, J. Supercrit. Fluids. 107 (2016) 9–16. doi:10.1016/j.supflu.2015.08.009.

[81] F. Kurniawansyah, L. Quachie, R. Mammucari, N.R. Foster, Improving the dissolution properties of curcumin using dense gas antisolvent technology, Int. J. Pharm. 521 (2017) 239–248. doi:10.1016/j.ijpharm.2017.02.018.

[82] K. Chhouk, Wahyudiono, H. Kanda, S.I. Kawasaki, M. Goto, Micronization of curcumin with biodegradable polymer by supercritical anti-solvent using micro swirl mixer, Front. Chem. Sci. Eng. (2017) 1–10. doi:10.1007/s11705-017-1678-3.

[83] Q. Wang, Y.X. Guan, S.J. Yao, Z.Q. Zhu, Controllable preparation and formation mechanism of BSA microparticles using supercritical assisted atomization with an enhanced mixer, J. Supercrit. Fluids. 56 (2011) 97–104. doi:10.1016/j.supflu.2010.12.002.

[84] Z. Du, Y.X. Guan, S.J. Yao, Z.Q. Zhu, Supercritical fluid assisted atomization introduced by an enhanced mixer for micronization of lysozyme: Particle morphology, size and protein stability, Int. J. Pharm. 421 (2011) 258–268. doi:10.1016/j.ijpharm.2011.10.002.

[85] M.-Q. Cai, Y.-X. Guan, S.-J. Yao, Z.-Q. Zhu, Supercritical fluid assisted atomization introduced by hydrodynamic cavitation mixer (SAA-HCM) for micronization of levofloxacin hydrochloride, J. Supercrit. Fluids. 43 (2008) 524–534. doi:10.1016/j.supflu.2007.07.008.

[86] Y. Bin Shen, Z. Du, Q. Wang, Y.X. Guan, S.J. Yao, Preparation of chitosan microparticles with diverse molecular weights using supercritical fluid assisted atomization introduced by hydrodynamic cavitation mixer, Powder Technol. 254 (2014) 416–424. doi:10.1016/j.powtec.2014.01.054.

[87] Y. Bin Shen, Y.X. Guan, S.J. Yao, Supercritical fluid assisted production of micrometric powders of the labile trypsin and chitosan/trypsin composite microparticles, Int. J. Pharm. 489 (2015) 226–236. doi:10.1016/j.ijpharm.2015.05.004.

[88] Y. Bin Shen, Z. Du, C. Tang, Y.X. Guan, S.J. Yao, Formulation of insulin-loaded N-trimethyl chitosan microparticles with improved efficacy for inhalation by supercritical fluid assisted atomization, Int. J. Pharm. 505 (2016) 223–233. doi:10.1016/j.ijpharm.2016.03.053.

[89] R. Campardelli, R. Adami, E. Reverchon, Nanoparticle precipitation by Supercritical Assisted Injection in a Liquid Antisolvent, Procedia Eng. 192 (2012) 246–251. doi:10.1016/j.proeng.2012.07.542.

[90] R. Campardelli, E. Oleandro, R. Adami, E. Reverchon, Polymethylmethacrylate

(PMMA) sub-microparticles produced by Supercritical Assisted Injection in a Liquid Antisolvent, J. Supercrit. Fluids. 92 (2014) 93–99. doi:10.1016/j.supflu.2014.05.012.

[91] R. Campardelli, E. Oleandro, E. Reverchon, Supercritical assisted injection in a liquid antisolvent for PLGA and PLA microparticle production, Powder Technol. 287 (2016) 12–19. doi:10.1016/j.powtec.2015.09.035.

[92] R. Campardelli, E. Reverchon, Instantaneous coprecipitation of polymer/drug microparticles using the supercritical assisted injection in a liquid antisolvent, J. Supercrit. Fluids. 120 (2017) 151–160. doi:10.1016/j.supflu.2016.11.005.

[93] X. Hu, Y. Guo, L. Wang, D. Hua, Y. Hong, J. Li, Coenzyme Q 10 nanoparticles prepared by a supercritical fluid-based method, J. Supercrit. Fluids. 57 (2011) 66–72. doi:10.1016/j.supflu.2011.01.007.

[94] W. Chen, X. Hu, Y. Hong, Y. Su, H. Wang, J. Li, Ibuprofen nanoparticles prepared by a PGSS ™ -based method, Powder Technol. 245 (2013) 241–250. doi:10.1016/j.powtec.2013.04.042.

[95] A. Sao Pedro, S.D. Villa, P. Caliceti, S.A.B.V. De Melo, E.C. Albuquerque, A. Bertucco, S. Salmaso, Curcumin-loaded solid lipid particles by PGSS technology, J. Supercrit. Fluids. 107 (2016) 534–541. doi:10.1016/j.supflu.2015.07.010.

[96] R. Couto, V. Alvarez, F. Temelli, Encapsulation of Vitamin B2 in solid lipid nanoparticles using supercritical CO2, J. Supercrit. Fluids. 120 (2017) 432–442. doi:10.1016/j.supflu.2016.05.036.

[97] F. Niu, J. Haslam, R. Rajewski, B. Subramaniam, A fluidized-bed coating technology using near-critical carbon dioxide as fluidizing and drying medium, J. Supercrit. Fluids. 66 (2012) 315–320. doi:10.1016/j.supflu.2011.11.007.

[98] F. Zabihi, N. Xin, S. Li, J. Jia, T. Cheng, Y. Zhao, Polymeric coating of fluidizing nano-curcumin via anti-solvent supercritical method for sustained release, J. Supercrit. Fluids. 89 (2014) 99–105. doi:10.1016/j.supflu.2014.02.021.

[99] A.Z. Chen, L. Li, S. Bin Wang, X.F. Lin, Y.G. Liu, C. Zhao, G.Y. Wang, Z. Zhao, Study of Fe 3O 4-PLLA-PEG-PLLA magnetic microspheres based on supercritical CO 2: Preparation, physicochemical characterization, and drug loading investigation, J. Supercrit. Fluids. 67 (2012) 139–148. doi:10.1016/j.supflu.2012.04.009.

[100] A.Z. Chen, G.Y. Wang, S. Bin Wang, L. Li, Y.G. Liu, C. Zhao, Formation of methotrexate-PLLA-PEG-PLLA composite microspheres by microencapsulation through a process of suspension-enhanced dispersion by supercritical CO2, Int. J. Nanomedicine. 7 (2012) 3013–3022. doi:10.2147/IJN.S32662.

[101] G.A. Leeke, T. Lu, R.H. Bridson, J.P.K. Seville, Application of nano-particle coatings to carrier particles using an integrated fluidized bed supercritical fluid precipitation process, J. Supercrit. Fluids. 91 (2014) 7–14. doi:10.1016/j.supflu.2014.03.012.

[102] Q. Li, D. Huang, T. Lu, J.P.K. Seville, L. Xing, G.A. Leeke, Supercritical fluid coating of API on excipient enhances drug release, Chem. Eng. J. 313 (2017) 317–327. doi:10.1016/j.cej.2016.12.066.

[103] R.L. Matos, T. Lu, C. McConville, G. Leeke, A. Ingram, Analysis of curcumin precipitation and coating on lactose by the integrated supercritical antisolvent-fluidized bed process, J. Supercrit. Fluids. In press. (n.d.). doi:10.1016/j.supflu.2017.12.013.

[104] G.P. Sanganwar, S. Sathigari, R.J. Babu, R.B. Gupta, Simultaneous production and co-mixing of microparticles of nevirapine with excipients by supercritical antisolvent method for dissolution enhancement, Eur. J. Pharm. Sci. 39 (2010) 164–174. doi:10.1016/j.ejps.2009.11.011.

[105] S.K. Sathigari, C.A. Ober, G.P. Sanganwar, R.B. Gupta, R.J. Babu, Single-Step Preparation and Deagglomeration of Itraconazole Microflakes by Supercritical Antisolvent Method for Dissolution Enhancement, J. Pharm. Sci. 100 (2011) 2952–2965. doi:10.1002/jps.22524.

[106] C.A. Ober, L. Kalombo, H. Swai, R.B. Gupta, Preparation of rifampicin/lactose microparticle composites by a supercritical antisolvent-drug excipient mixing technique for inhalation delivery, Powder Technol. 236 (2013) 132–138. doi:10.1016/j.powtec.2012.04.057.

[107] R.T. Bustami, H.-K. Chan, F. Dehghani, N.R. Foster, Generation of micro-particles of proteins for aerosol delivery using high pressure modified carbon dioxide, Pharm. Res. 17 (2000) 1360–1366.

[108] R.T. Bustami, H.K. Chan, T. Sweeney, F. Dehghani, N.R. Foster, Generation of Fine Powders of Recombinant Human Deoxyribonuclease Using the Aerosol Solvent

Extraction System, Pharm. Res. 20 (2003) 2028–2035. doi:10.1023/B:PHAM.0000008053.69903.c1.

[109] A. Bouchard, N. Jovanović, W. Jiskoot, E. Mendes, G.J. Witkamp, D.J.A. Crommelin, G.W. Hofland, Lysozyme particle formation during supercritical fluid drying: Particle morphology and molecular integrity, J. Supercrit. Fluids. 40 (2007) 293–307. doi:10.1016/j.supflu.2006.07.005.

[110] A. Bouchard, N. Jovanović, Á. Martín, G.W. Hofland, D.J.A. Crommelin, W. Jiskoot, G.J. Witkamp, Effect of the modifier on the particle formation and crystallisation behaviour during precipitation from aqueous solutions, J. Supercrit. Fluids. 44 (2008) 409–421. doi:10.1016/j.supflu.2007.09.015.

[111] R.P.T. Sih, New process development of dense gas technology for the processing of pharmaceuticals, The University of New South Wales, 2008.

[112] N.R. Foster, R.P.T. Sih, Process for producing particles via atomized rapid injection for solvent extraction, US8389013B2, 2006.

[113] K. Chhouk, W. Diono, H. Kanda, S.I. Kawasaki, M. Goto, Micronization of curcumin with biodegradable polymer by supercritical anti-solvent using micro swirl mixer, Front. Chem. Sci. Eng. 12 (2018) 184–193. doi:10.1007/s11705-017-1678-3.

[114] G. Della Porta, R. Adami, P. Del Gaudio, L. Prota, R. Aquino, E. Reverchon, Albumin/Gentamicin Microspheres Produced by Supercritical Assisted Atomization: Optimization of Size, Drug Loading and Release, J. Pharm. Sci. 99 (2010) 4720–4729. doi:10.1002/jps.

[115] R.P. Aquino, G. Auriemma, T. Mencherini, P. Russo, A. Porta, R. Adami, S. Liparoti, G. Della Porta, E. Reverchon, P. Del Gaudio, Design and production of gentamicin/dextrans microparticles by supercritical assisted atomisation for the treatment of wound bacterial infections, Int. J. Pharm. 440 (2013) 188–194. doi:10.1016/j.ijpharm.2012.07.074.

[116] F. De Cicco, E. Reverchon, R. Adami, G. Auriemma, P. Russo, E.C. Calabrese, A. Porta, R.P. Aquino, P. Del Gaudio, In situ forming antibacterial dextran blend hydrogel for wound dressing: SAA technology vs. spray drying, Carbohydr. Polym. 101 (2014) 1216–1224. doi:10.1016/j.carbpol.2013.10.067.

[117] H.T. Wu, C.P. Yang, S.C. Huang, Dissolution enhancement of indomethacin-chitosan hydrochloride composite particles produced using supercritical assisted atomization, J. Taiwan Inst. Chem. Eng. 67 (2016) 98–105. doi:10.1016/j.jtice.2016.08.012.

[118] R. Adami, A. Di Capua, E. Reverchon, Supercritical Assisted Atomization for the production of curcumin-biopolymer microspheres, Powder Technol. 305 (2017) 455–461. doi:10.1016/j.powtec.2016.10.020.

[119] A. Di Capua, R. Adami, E. Reverchon, Production of Luteolin/Biopolymer Microspheres by Supercritical Assisted Atomization, Ind. Eng. Chem. Res. 56 (2017) 4334–4340. doi:10.1021/acs.iecr.7b00211.

[120] A. Di Capua, R. Adami, Luteolin / dextran-FITC fl uorescent microspheres produced by supercritical assisted atomization, J. Supercrit. Fluids. 130 (2017) 97–104.

[121] V. Martín, V. Gonçalves, S. Rodríguez-rojo, D. Nunes, E. Fortunato, R. Martins, M. José, C. Duarte, Production of copper loaded lipid microparticles by PGSS ® (particles from gas satured solutions) process, J. Supercrit. Fluids. 131 (2018) 124–129. doi:10.1016/j.supflu.2017.09.001.

[122] J. Yang, O.N. Ciftci, Formation of hollow solid lipid micro- and nanoparticles using supercritical carbon dioxide, Food Bioprod. Process. 98 (2016) 151–160. doi:10.1016/j.fbp.2016.01.004.

[123] J. Yang, O.N. Ciftci, Development of free- flowing peppermint essential oil-loaded hollow solid lipid micro- and nanoparticles via atomization with carbon dioxide, Food Res. Int. J. 87 (2016) 83–91. doi:10.1016/j.foodres.2016.06.022.

[124] J. Yang, O.N. Ciftci, Encapsulation of fish oil into hollow solid lipid micro- and nanoparticles using carbon dioxide, Food Chem. 231 (2017) 105–113. doi:10.1016/j.foodchem.2017.03.109.

[125] K. Saleh, P. Guigon, Coating and Encapsulation Processes in Powder Technology, in: Handb. Powder Technol. - Granulation, 2006: pp. 323–375.

[126] A. Tsutsumi, S. Nakamoto, T. Mineo, K. Yoshida, A novel fluidized-bed coating of fine particles by rapid expansion of supercritical fluid solutions, Powder Technol. 85 (1995) 275–278. doi:10.1016/0032-5910(95)03021-X.

[127] S. Rodríguez-Rojo, J. Marienfeld, M.J. Cocero, RESS process in coating applications in a high pressure fluidized bed environment: Bottom and top spray experiments, Chem. Eng. J. 144 (2008) 531–539. doi:10.1016/j.cej.2008.07.054.

[128] T.J. Wang, A. Tsutsumi, H. Hasegawa, T. Mineo, Mechanism of particle coating granulation with RESS process in a fluidized bed, Powder Technol. 118 (2001) 229–235. doi:10.1016/S0032-5910(00)00400-9.

[129] R. Schreiber, C. Vogt, J. Werther, G. Brunner, Fluidized bed coating at supercritical fluid conditions, J. Supercrit. Fluids. 24 (2002) 137–151. doi:10.1016/S0896-8446(02)00029-3.

[130] R. Schreiber, B. Reinke, C. Vogt, J. Werther, G. Brunner, High-pressure fluidized bed coating utilizing supercritical carbon dioxide, Powder Technol. 138 (2003) 31–38. doi:10.1016/j.powtec.2003.08.044.

[131] K. Rosenkranz, M.M.M. Kasper, J. Werther, G. Brunner, Encapsulation of irregularly shaped solid forms of proteins in a high-pressure fluidized bed, J. Supercrit. Fluids. 46 (2008) 351–357. doi:10.1016/j.supflu.2007.11.012.

[132] J. Benoit, H. Rolland, C. Thies, V. Vande Velde, Method of coating particles and coated spherical particles, US6087003A, 1994.

[133] I. Ribeiro Dos Santos, J. Richard, B. Pech, C. Thies, J.P. Benoit, Microencapsulation of protein particles within lipids using a novel supercritical fluid process, Int. J. Pharm. 242 (2002) 69–78. doi:10.1016/S0378-5173(02)00149-7.

[134] C. Thies, I. Ribeiro dos Santos, J. Richards, V. Vandevelde, H. Rolland, J.P. Benoit, A supercritical fluid-based coating technology 1: Process considerations, J. Microencapsul. 20 (2003) 87–96. doi:10.1080/02652040210162649.

[135] I. Ribeiro dos Santos, C. Thies, J. Richards, D. Le Meurlay, V. Gajan, V. Vandevelde, J.P. Benoit, A supercritical fluid-based coating technology. 2: Solubility considerations, J. Microencapsul. 20 (2003) 97–109. doi:10.1080/02652040210162649.

[136] I. Ribeiro dos Santos, J. Richard, C. Thies, B. Pech, J.P. Benoit, A supercritical fluid-based coating technology. 3: Preparation and characterization of bovine serum albumin particles coated with lipids, J. Microencapsul. 20 (2003) 110–128. doi:10.1080/02652040210162630.

[137] Y. Wang, R.N. Dave, R. Pfeffer, Polymer coating/encapsulation of nanoparticles using a supercritical anti-solvent process, J. Supercrit. Fluids. 28 (2004) 85–99. doi:10.1016/S0896-8446(03)00011-1.

[138] I.E. Santo, R. Campardelli, E.C. Albuquerque, S.V. de Melo, G. Della Porta, E. Reverchon, Liposomes preparation using a supercritical fluid assisted continuous process, Chem. Eng. J. 249 (2014) 153–159. doi:10.1016/j.cej.2014.03.099.

[139] R. Campardelli, I. Espirito Santo, E.C. Albuquerque, S.V. De Melo, G. Della Porta, E. Reverchon, Efficient encapsulation of proteins in submicro liposomes using a supercritical fluid assisted continuous process, J. Supercrit. Fluids. 107 (2016) 163–169. doi:10.1016/j.supflu.2015.09.007.

[140] C.C. Beh, R. Mammucari, N.R. Foster, Process intensification : Nano-carrier formation by a continuous dense gas process, Chem. Eng. J. 266 (2015) 320–328. doi:10.1016/j.cej.2014.12.072.

[141] X. Han, C. Ghoroi, R. Davé, Dry coating of micronized API powders for improved dissolution of directly compacted tablets with high drug loading, Int. J. Pharm. 442 (2013) 74–85. doi:10.1016/j.ijpharm.2012.08.004.

[142] A. Marzocchella, P. Salatino, Fluidization of solids with CO2 at pressures from ambient to supercritical, AIChE J. 46 (2000) 901–910. doi:10.1002/aic.690460505.

[143] D. Geldart, Types of gas fluidization, Powder Technol. 7 (1973) 285–292. doi:10.1016/0032-5910(73)80037-3.

[144] Q.T. Zhou, D. a V Morton, Drug-lactose binding aspects in adhesive mixtures: Controlling performance in dry powder inhaler formulations by altering lactose carrier surfaces, Adv. Drug Deliv. Rev. 64 (2012) 275–284. doi:10.1016/j.addr.2011.07.002.

[145] L. Qu, Q. Zhou, J.A. Denman, P.J. Stewart, K.P. Hapgood, D.A. V Morton, Influence of coating material on the flowability and dissolution of dry-coated fine ibuprofen powders, Eur. J. Pharm. Sci. 78 (2015) 264–272. doi:10.1016/j.ejps.2015.07.016.

[146] J. Yang;, Y. Wang;, R.N. Dave, R. Pfeffer, Mixing of nano-particles by rapid expansion of high-pressure suspensions, Adv. Powder Technol. 14 (2003) 471–493.

[147] D. To, R. Dave, X. Yin, S. Sundaresan, Deagglomeration of Nanoparticle Aggregates

via Rapid Expansion of Supercritical or High-Pressure Suspensions, Am. Inst. Chem. Eng. 55 (2009) 2807–2826. doi:10.1002/aic.11887.

[148] C. Ghoroi, X. Han, D. To, L. Jallo, L. Gurumurthy, R.N. Davé, Dispersion of fine and ultrafine powders through surface modification and rapid expansion, Chem. Eng. Sci. 85 (2013) 11–24. doi:10.1016/j.ces.2012.02.038.

Chapter 3 -

ANALYSIS OF CURCUMIN PRECIPITATION AND COATING ON LACTOSE BY THE INTEGRATED SUPERCRITICAL ANTISOLVENT-FLUIDIZED BED PROCESS

Published article:

The Journal of Supercritical Fluids 141 (2018) 143–156

3.1. Abstract

Graphical Abstract

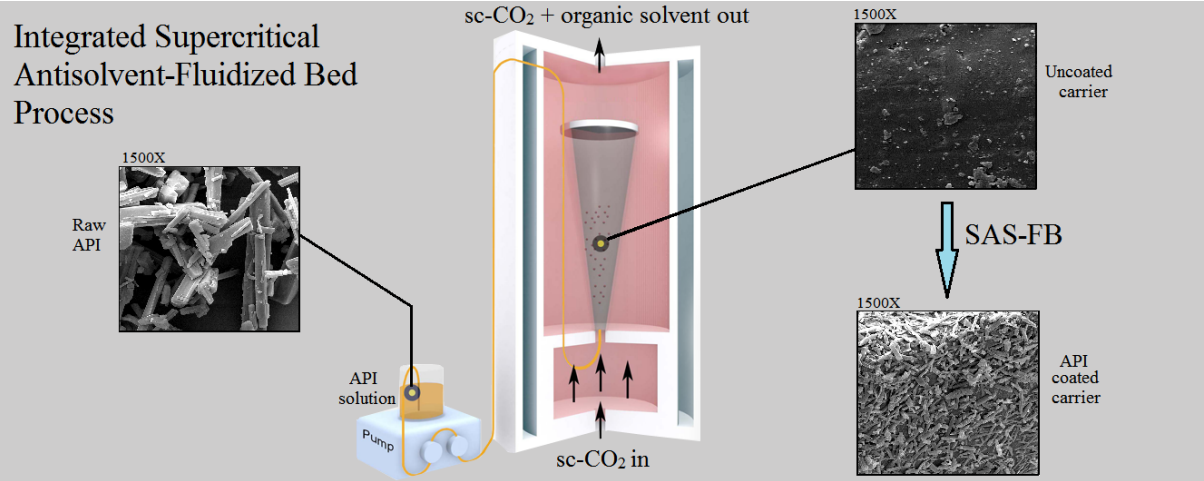

Dry powder formulations with potential application in pulmonary drug delivery were produced by integrating the Supercritical Antisolvent (SAS) process with a fluidized bed (FB) under pressure. The simultaneous precipitation and coating of curcumin on lactose was performed in a single step combining the advantages of both processes. Ethanol and acetone were used as solvents. The effects of operating parameters: pressure, temperature, drug-lactose mass ratio, solution flow rate and solution concentration on the drug size, morphology and yield were investigated. Due to the high degree of mixing in the fluidized bed, a uniform coating of curcumin onto lactose was achieved with drug yield varying from 71.0 to 93.3% and curcumin crystals with length between 0.41 – 12.08 µm. The formulations produced were solvent-free and the crystallinity of curcumin was reduced.

Keywords: supercritical antisolvent, fluidized bed, coating, curcumin, lactose, pulmonary delivery

3.2. Highlights

- Single-step precipitation and coating was performed via SAS-FB.
- SAS-FB particles are smaller and less aggregated than SAS particles.
- Solvent-free formulations with very good flow properties were produced.
- The location of the operational point affects particle size distribution.

3.3. Introduction

In the recent decades, there has been a considerable investigation of the potential use of the lungs as a non-invasive drug delivery route. The large surface area of the alveolar region, high blood supply, thin epithelial barrier and lack of first pass metabolism contributes to a rapid onset of therapeutic action and enhances drug bioavailability [1]. The main factor controlling the efficiency of particle deposition in the lungs is the aerodynamic diameter which should be between 1-5 μm [2]. However, due to the high Van der Waals interactions, particles within this size range tend to be aggregated causing poor flowability, irregular dispersion and formulation instability. For those reasons, active pharmaceutical ingredients (APIs) are usually combined with larger excipient or carrier particles improving drug flow properties, handling and metering [3–5]. By the inspiratory airflow force, drug and carrier dissociate. While small particles of drug travel towards the lungs, coarse carrier particles are deposited and cleared in the upper airways [6,7].

There are several traditional methods for micronizing APIs such as: wet milling, high pressure homogenization and spray drying [8]. Particle engineering using supercritical fluid (SCF) technology has demonstrated advantages over conventional micronization processes as control of particle morphology, size and particle size distribution can be easily achieved with changes in pressure, temperature or other operational parameters [9,10]. Furthermore, heat

sensitive compounds can be processed at mild temperatures and formulations with low or no residual solvent can be obtained. The Supercritical Antisolvent (SAS) process is widely used to produce a variety of materials with different morphologies [11–15]. In a typical SAS process, the API is dissolved in an organic solvent, which is highly miscible with the SCF, and this solution is sprayed inside a high-pressure vessel (HPV) through which the SCF flows continuously. Upon contact, the SCF diffuses into the liquid phase, decreasing the solvation power of the organic solvent and leading to the precipitation of the API.

To generate particles in the size range required for deep lung deposition while avoiding agglomeration issues, single-step SAS precipitation and coating in a fluidized bed (FB) under pressure was employed. In SAS-FB, the particles of the API precipitated by SAS process are simultaneously coated on the surface of carrier particles which comprise the fluidized bed material. Due to the high degree of mixing in the fluidized bed, a uniform coating of fine drug particles onto the excipient surface can be achieved while preventing aggregation of the drug precipitate, hence leading to a high drug dissolution rate and bioavailability [16]. Curcumin was selected as a model API for pulmonary delivery. Known for a long time as a spice and food additive, it also has many therapeutic properties including antioxidant, antimicrobial, anticancer and anti-inflammatory. However, the use of curcumin in drug formulations is limited by its poor water solubility, fast intestinal metabolism and low bioavailability after oral administration [17]. Therefore, pulmonary delivery is proposed as a non-invasive route for improving curcumin absorption in the body. Lactose was chosen as the carrier for being stable, inexpensive, available in several sizes and morphologies and approved by the Food and Drug Administration (FDA) [6].

The combination of supercritical precipitation and fluidized bed coating has been reported previously using supercritical carbon dioxide (sc-CO_2) as fluidizing medium and solvent in

the Rapid Expansion of a Supercritical Solution process (RESS) [18–24]. The association of fluidized bed with supercritical antisolvent processes is more recent. Previous work of Li et al. [16] successfully coated nano-sized naringin onto microcrystalline cellulose via SAS-FB and the effects of several operational parameters on subsequent drug release were analysed. A similar rig was used to coat nanoparticle agglomerates of titanium dioxide with polymer Pluronic F-127 [25]. In this case, the coating material is deposited as a film rather than individual particles. Niu et al. [26], also precipitating polymer films, coated several materials using dense CO_2 as antisolvent and fluidizing medium in a Wurster coater. Other researchers encapsulated nano-curcumin on PLGA by using ultrasonic vibration to fluidize the agglomerates [27]. The supercritical antisolvent-drug excipient mixing process uses a stirred vessel to fluidize and coat drug particles produced by SAS on excipients [28–30]. However, none of the previously reported works aimed to precipitate and coat curcumin on lactose by SAS-FB to prepare pulmonary drug delivery formulations.

This work also attempts to understand how SAS-FB operational conditions affect the characteristics of the final drug formulation including curcumin morphology, particle size and drug yield. The operational parameters analysed were: pressure, temperature, drug-carrier mass ratio, curcumin solution flow rate and solution concentration. The effect of solvent was investigated by comparing the use of ethanol and acetone.

3.4. Materials and Methods

3.4.1. Materials

All materials were used as-received from the suppliers without additional purification. Curcumin (purity ≥ 90%) was purchased from Cayman Chemical, UK, α-lactose monohydrate (Lactohale® 100) with mean particle size between 125 - 145 μm was kindly provided by DFE

Pharma, Germany, ethanol (HPLC grade > 99.8%) and acetone (purity > 99.8%) were purchased from Scharlau and Sigma-Aldrich Company Ltd., UK, respectively. Carbon dioxide (purity ≥ 99.8%) was purchased from BOC, UK.

3.4.2. SAS and SAS-FB Experimental Procedure

SAS-FB process, using the sc-CO_2 flow and the solution jet of SAS to fluidize lactose particles, instantly precipitates and coats nano/micro-sized curcumin particles onto the lactose. A complete description of SAS-FB apparatus was previously done by Li et al. [16]. A schematic flowsheet of the process is shown in **Figure 3-1**. For a typical SAS-FB experiment, the conical fluidized bed is initially preloaded with 1 g of lactose and placed inside the 0.5 litre high pressure vessel (HPV). The system is pressurized via the top port (not shown in figure; shown in **Appendix I**) with CO_2 until the desired pressure is reached. Then the CO_2 feed is switched to the bottom of the high pressure vessel (HPV), to fluidize the preloaded lactose. A filter cap on the top of the fluidized bed prevents the loss of particles. In order to obtain quasi-steady state composition of solvent and CO_2, pure solvent is pumped through a nozzle (127 μm) located at the bottom centre of the fluidized bed for 10 minutes (see **Appendix III**). Following this, the pump feed is switched from solvent to drug solution to start SAS-FB precipitation and coating. When the solution injection is completed, the pump is switched back to pure solvent to purge the pipe lines and guarantee the designed amount of drug was delivered to the HPV. Pure CO_2 then flushes the system to remove any remaining solvent dissolved in the supercritical phase (see **Appendix III**). Finally, the pressure is gradually decreased and the sample collected. For the SAS experiment the same procedure was used, except that no lactose was loaded into the bed.

3.4.3. SAS and SAS-FB Operational Conditions

In this study, the simultaneous precipitation and coating of curcumin on lactose generating a formulation with potential application for pulmonary drug delivery is presented. The final formulation is obtained with no further drying or mixing steps. The organic solvents were chosen due to their ability to solubilize curcumin, their high miscibility with sc-CO_2 in the range of conditions studied, and their safety toward pharmaceutical applications. In addition, the solvents should not dissolve the lactose in the fluidized bed, and therefore, ethanol was selected as the standard solvent, although some experiments with acetone were also performed.

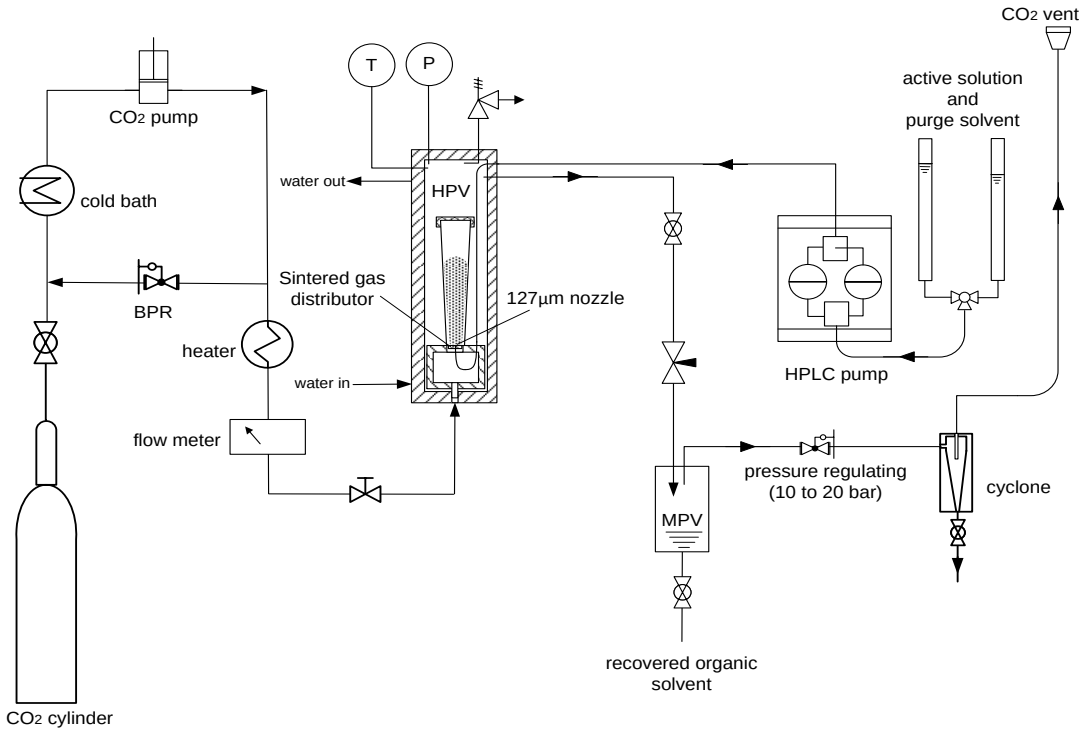

Figure 3-1. SAS-FB experimental apparatus [16]. HPV = high pressure vessel, MPV = middle pressure vessel, BPR = back pressure regulator.

Considering that at low concentrations the presence of curcumin does not significantly change the ethanol-CO_2 vapour-liquid equilibrium (VLE) [31], this was used to predict the phase

behaviour of the ternary system (ethanol-CO_2-curcumin). **Figure 3-2** shows the region of interest of the VLE for ethanol-CO_2 at 40°C obtained from Joung et al. [32]. The figure also includes the location of different SAS-FB experiments performed at the same temperature. In the literature, it has been observed that microparticles are generally produced if the operational pressure is located in the proximity of the mixture critical point of solvent-CO_2 [10,12]. Once the aim of this work is to precipitate microparticles suitable for inhalation, a pressure of 9.0 MPa was selected for the standard experiment, as it is slightly higher than the critical pressure of the system ethanol-CO_2 at 40°C (pc = 8.16 MPa; $x\mathrm{c}_{CO2}$ = 0.963 [32]). The standard operational conditions are then fixed at: temperature T = 40°C, pressure p = 9.0 MPa, initial solution concentration C = 2 mg/ml, solution flow rate f = 1 ml/min and CO_2 mass flow rate fCO_2 = 40 g/min, giving a CO_2 molar fraction of x_{CO2} = 0.981 to ensure the precipitation happens in the supercritical region (**Figure 3-2**). The mass flow rate of CO_2 was kept constant at 40 g/min for all experiments, thus the CO_2 molar fraction was varied by changing the organic solution flow rate only. For the SAS-FB experiments 1 g of lactose was loaded in the bed and a curcumin-lactose mass ratio of MR = 2% was set as standard, while in the SAS experiments no lactose was loaded in the bed. A 127 µm ID capillary was used as the nozzle in all experiments.

3.4.4. Fluidized Bed Behaviour

Tapered beds are employed in several processes and applications preventing some problems of conventional cylindrical beds such as slugging, entrainment of particles and channelling. Due to the increase in the cross-section area with bed height, the fluid velocity decreases gradually, improving the mixing and enabling the fluidization of materials with a wide particle size distribution [33,34].

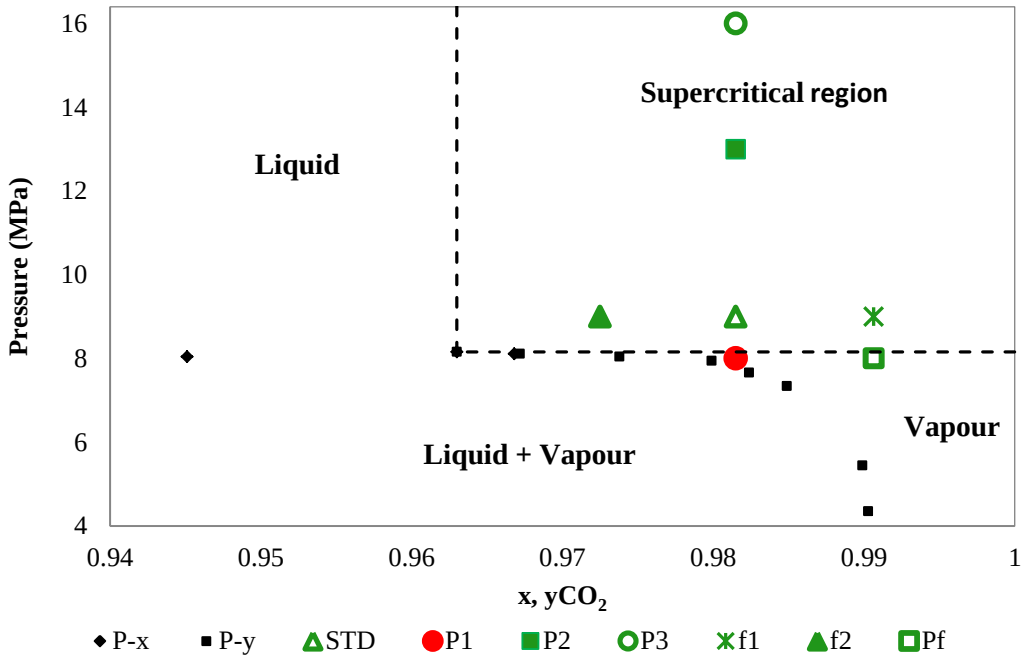

Figure 3-2. Vapor-liquid equilibrium of ethanol-CO_2 at 40°C obtained from Joung et al. [32] and operational points. Experiments that produced one population of particles are shown in green while the experiment with two populations is in red.

A conical fluidized bed with base diameter of 5.9 mm was used in this work. The selected CO_2 mass flow rate of 40 g/min resulted in a CO_2 velocity ranging between 2.4 cm/s (at 16 MPa) - 6.9 cm/s (at 8 MPa) calculated considering the base diameter. A precise determination of the minimum fluidization velocity by observation of the bed behaviour through the sapphire window on the HPV was difficult since the top of the bed at minimum fluidization flow rate was not high enough to be completely seen. However, observations of the bed behaviour during fluidization showed that the CO_2 velocities used are high enough to fluidize the lactose particles, but not so high that particles are blown out of the bed. This was true also in the presence of the jet of solvent. For all conditions tested, a fully fluidized bed was obtained, characterized by the upward movement of particles in the centre and downward movement of particles with lower speed outside of the core [35]. Although there are operational points in the vapour, liquid and supercritical regions (**Figure 3-2**, **Figure 3-7**), no

significant difference on the fluidization was noticed probably because the fluid velocities used are much higher than the minimum fluidization velocities in each condition.

3.4.5. Preparation of the Physical Mixture

For comparison with the standard SAS-FB experiment, the physical mixture of curcumin and lactose was prepared with the same curcumin-lactose mass ratio (2%). The sample was hand-mixed by shaking the powder in a sealed vial for 5 minutes.

3.4.6. Analyses and Observations

3.4.6.1. Scanning Electron Microscopy (SEM) and Particle Size Measurements

The morphology of particles was accessed by Scanning Electron Microscopy (SEM) model Philips XL-30 FEG at 10 kV and 10 mA. Samples were placed on a double-sided adhesive carbon tape and sputter coated with platinum at 25 mA for 3 min in an Emscope SC500 coating machine prior to the analysis. For the calculation of particle size distribution, at least 300 particles of different SEM images were measured for each sample using Image J analysis software. Due to the elongated nature of the particles, measurements of length and width were taken. The results are expressed as mean length ± standard deviation and the aspect ratio (mean length/mean width) was also calculated.

3.4.6.2. Drug Yield and Formulation Uniformity

Drug yield (Y) is defined as the percentage ratio of the mass of drug precipitated to the mass of drug introduced. The mass of precipitated drug was determined using an ultraviolet (UV)–visible spectrophotometer (Jenway, Genova Plus) at $\lambda = 450$ nm. The absorbance of lactose at this wavelength can be neglected. A known mass of sample (circa 1 mg) was dissolved in 10 ml 50% water-acetone solution and the corresponding curcumin concentration was obtained using a calibration curve ($R^2 = 0.9988$, **Figure 1-9**a). Each sample was analysed 3-4 times and

the mean values are shown. The uniformity of the formulation was investigated by calculating the relative standard deviation (RSD) of drug content in each batch.

3.4.6.3. Solubility Measurements

Equilibrium solubility of curcumin in the solvents used at the temperatures of the experiments were determined. Tests were carried out at 35°C and 50°C for ethanol and at 40°C for ethanol and acetone. Excess amount of curcumin was added in vials containing the solvent and kept in a water bath at the desired temperature until equilibrium was reached. The supernatants were filtered through a 0.22 μm pore size membrane filter and diluted to be further analysed via an ultraviolet (UV)-visible spectrophotometer (Thermo Scientific Orion AquaMate).

3.4.6.4. Thermogravimetric Analysis (TGA)

Solvent residue was analysed by Thermogravimetric Analysis (TGA, Exstar 6000, Seiko Instruments Inc, UK, coupled with a 1G/DTA6300). Fresh made samples of approximately 5 mg were heated from 20°C to 120°C at a rate of 2°C/min. Nitrogen was used as a purge gas with a flow rate of 20 ml/min.

3.4.6.5. Fourier Transform Infrared Spectroscopy (FT-IR)

The infrared spectra of the samples and raw compounds were taken with a Fourier Transform Infrared (FT-IR Jasco-6300) Spectrometer in a range of 800-4000 cm^{-1}. The spectra are composed of 64 scans with a resolution of 4 cm^{-1}.

3.4.6.6. X-Ray Diffraction (XRD)

XRD patterns of processed and unprocessed curcumin were obtained using a powder diffractometer (Bruker D8, UK) to investigate the crystallinity of the samples. Powder samples were packed in the sample holder and characterized with a beam angle from 5° to 40° with step size of 0.02°. The beam generation was set at 40 KVand 30 mA.

3.5. Results and Discussion

3.5.1. Scanning Electron Microscopy (SEM)

A summary of the operational conditions tested and the results obtained is shown in **Table 3-1**. In the preliminary experiments, curcumin was precipitated via SAS from an ethanol solution (experiment SAS-Et) at standard conditions (i.e. p = 9.0 MPa, T = 40°C, C = 2 mg/ml, f = 1 ml/min and fCO_2 = 40 g/min). SEM images of SAS-Et can be seen in **Figure 3-3**c, while raw curcumin, as-received from the supplier, is illustrated in **Figure 3-3**a. It is clear that after SAS processing at standard conditions curcumin morphology changed from a rod-like shape with a wide size distribution (18 ± 11 μm) to a filament/dendritic-like structure. Acetone was also tested as solvent (experiment SAS-Ac) in the same conditions and a similar morphology was obtained (**Figure 3-3**d). The formation of dendritic structures might be the result of non-uniform supersaturation and uncontrolled nucleation and particle growth [36]. The interconnected nature of the filaments of SAS processed samples made the particle size distribution measurements from the SEM images unfeasible. In the literature, curcumin has been previously processed by SAS using dichloromethane [37] and acetone, acetonitrile, and methanol [38] as solvents. The morphologies obtained are highly dependent on the operational conditions used, varying from irregular, rod, needle and spherical with sizes from 90 nm to 8.3 μm.

The agglomerated drug particles produced by SAS are too cohesive for pulmonary delivery hence their combination with larger excipient or carrier particles to improve drug flow properties, handling and metering is required. SAS-FB process is proposed to allow simultaneous drug precipitation and coating on an excipient, avoiding an additional mixing step of SAS particles with excipients.

Table 3-1. Operational conditions and results. L/W = aspect ratio; Y = drug yield; RSD = relative standard deviation.

Exp. ID	P (MPa)	T (°C)	f (ml/min)	C (mg/ml)	MR (%)	Solvent	Length ± SD (µm)	L/W	Y (%)	RSD (%)	Size distribution	Morphology
SAS-Et	9.0	40	1.0	2.0	2	ethanol	-	-	-	-	unimodal	filament/ dendritic
SAS-Ac	9.0	40	1.0	2.0	2	acetone	-	-	-	-	unimodal	filament/ dendritic
STD	9.0	40	1.0	2.0	2	ethanol	4 ± 1	5.8	89.2	4.6	unimodal	rectangular, needle
P1	8.0	40	1.0	2.0	2	ethanol	0.4 ± 0.2 -	3.3 -	90.0	2.9	bimodal	irregular
P2	13.0	40	1.0	2.0	2	ethanol	12 ± 5	7.3	76.6	2.4	unimodal	rectangular, needle
P3	16.0	40	1.0	2.0	2	ethanol	11 ± 5	8.2	80.4	4.2	unimodal	rectangular, needle
Pf	8.0	40	0.5	2.0	2	ethanol	4 ± 2	6.3	85.3	4.6	unimodal	rectangular, needle
T1	9.0	35	1.0	2.0	2	ethanol	5 ± 3 0.5 ± 0.2	6.5 4.9	71.0	3.5	bimodal	needle
T2	9.0	50	1.0	2.0	2	ethanol	6 ± 2; 0.8 ± 0.2	5.7 4.9	82.3	3.4	bimodal	rectangular, needle, comma

Exp. ID	P (MPa)	T (°C)	f (ml/min)	C (mg/ml)	MR (%)	Solvent	Length ± SD (µm)	L/W	Y (%)	RSD (%)	Size distribution	Morphology
Tf	9.0	35	0.5	2.0	2	ethanol	3 ± 2	3.7	87.1	2.4	unimodal	rectangular, needle
MR1	9.0	40	1.0	2.0	1	ethanol	3 ± 1	4.7	83.4	4.7	unimodal	rectangular, needle
MR6	9.0	40	1.0	2.0	6	ethanol	6 ± 2	5.3	86.4	4.7	unimodal	rectangular, needle
f1	9.0	40	0.5	2.0	2	ethanol	4 ± 1	5.7	91.5	2.8	unimodal	rectangular, needle
f2	9.0	40	1.5	2.0	2	ethanol	6 ± 2	5.7	82.7	4.1	unimodal	rectangular, needle
S1	9.0	40	1.0	2.0	2	acetone	5 ± 2	4.7	85.2	3.0	unimodal	rectangular, needle
C1	9.0	40	1.0	8.0	2	acetone	4 ± 2	3.7	93.3	3.3	unimodal	rectangular, needle
C2	9.0	40	1.0	20.0	2	acetone	2 ± 1	2.6	86.0	3.6	unimodal	irregular, agglomerated

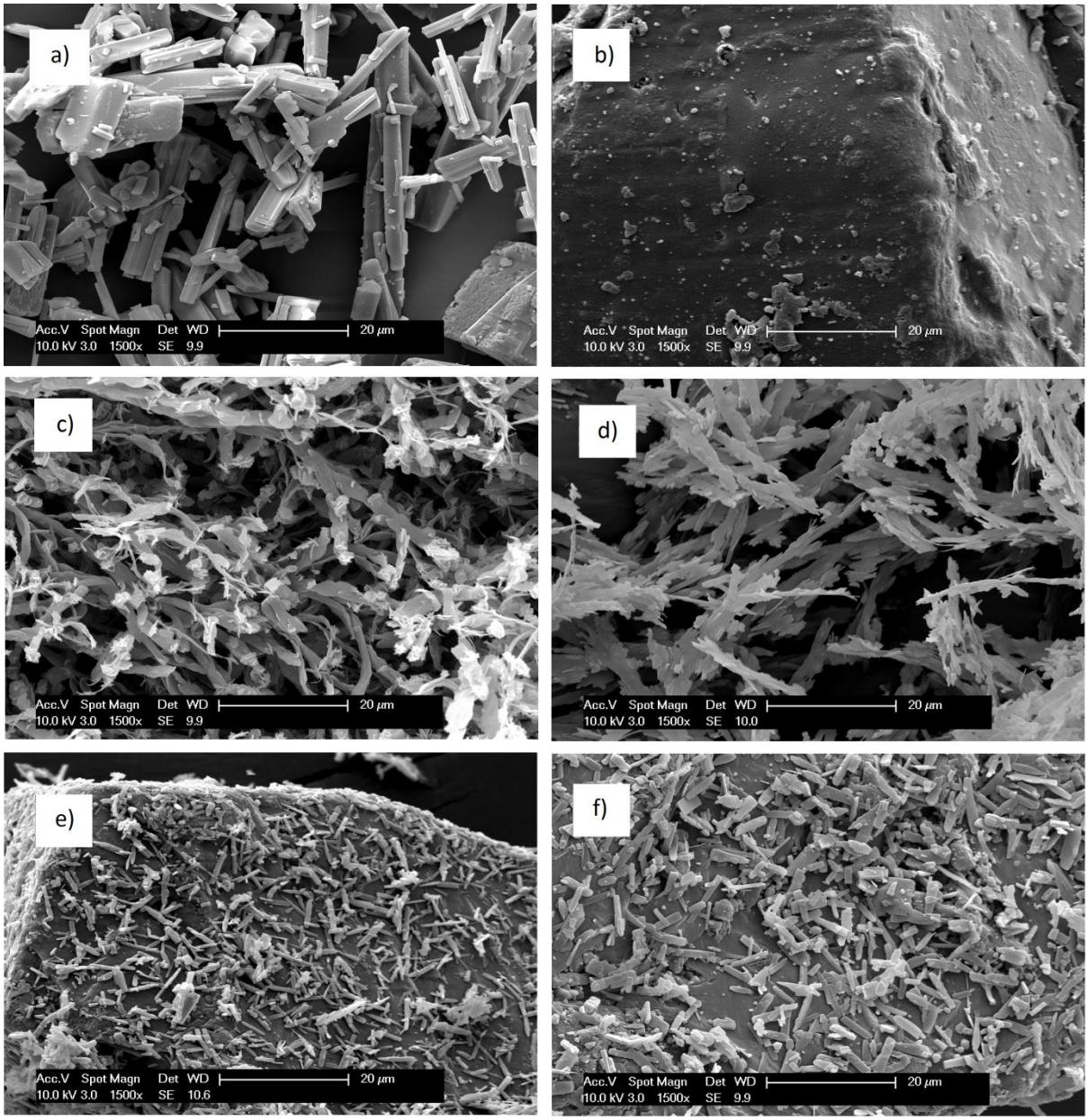

Figure 3-3. a) Raw curcumin; b) uncoated lactose; c) Ethanol processed curcumin (SAS-Et); d) Acetone processed curcumin (SAS-Ac); e) curcumin coated lactose from ethanol (STD); f) curcumin coated lactose from acetone (S1) . The experiment ID and conditions used are listed in **Table 3-1**.

Curcumin was then processed by SAS-FB under the standard conditions, as used in SAS-Et above, with lactose (125-145 µm) being fluidized inside the HPV (experiment STD). For comparison, the uncoated lactose surface, as-received from the supplier is shown in **Figure 3-3**b. After SAS-FB processing, it is clear the deposition of curcumin particles on the lactose surface in a much smaller and less aggregated state (**Figure 3-3**e) than SAS-Et particles

(**Figure 3-3**c). There was also a change in morphology from the filament/dendritic-like structure in SAS-Et to a rectangular and needle shape in STD. Similarly, curcumin processed by SAS-FB using acetone (experiment S1) also at standard conditions yielded smaller and less agregated particles (**Figure 3-3**f) than SAS-Ac (**Figure 3-3**d). It is believed that the collection of curcumin particles onto lactose close to their point of origin inhibited further particle growth and aggregation [16]. The smaller particle size in the SAS-FB compared to the SAS may be attributed to the movement of lactose particles inside the fluidized bed, improving the mixing and turbulance which caused higher degree of supersaturation, and hence higher nucleation rate. Another benefit of SAS-FB is to facilitate the removal of curcumin particles from the HPV as it was observed that most of the particles attached on the free-flowing lactose. This clearly shows the advantages of SAS-FB at improving the handling of the product.

3.5.2. Effect of Process Parameters

In antisolvent processes, particle size is strongly related with the degree of supersaturation promoted by sc-CO_2 in the liquid solution. The supersaturation levels may vary with the density of the fluid phase, which determines the equilibrium solubility of the drug in the fluid phase, the initial solution concentration, and the solvent molar fraction in the fluid mixture. In the case of drug yield, it is determined by the amount of drug that stays dissolved in the fluid phase [39,40]. The effect of operational parameters on particle size, morphology and drug yield were analysed by changing the conditions from the standard SAS-FB experiment (STD). It can be seen in **Table 3-1** that three levels of pressure (experiments P1, P2 and P3) and two levels of temperature (experiments T1 and T2), curcumin-lactose mass ratio (experiments MR1 and MR6) and solution flow rate (experiments f1 and f2) were tested. The effect of solution concentration was analysed only for acetone (experiments S1, C1 and C2) because

curcumin concentration in ethanol in STD (2 mg/ml) was already close to its saturated solution [41]. The combined effect of pressure and solution flow rate was analysed in the experiment Pf, while the effect of temperature and solution flow rate was tested in Tf keeping all the other operational parameters as standard. Process recovery was calculated as a percentage of the final mass recovered compared to the total mass introduced in the vessel (curcumin and lactose) and ranged between 93% and 97% for the entire set of experiments. Small amount of sample was clearly lost attached to the walls of the bed and gas distributor.

3.5.2.1. Effect of Pressure

To investigate the effect of pressure on the final formulation, three different experiments were run and compared with STD performed at 9.0 MPa. The following pressure values were used: 8.0 MPa (P1), 13.0 MPa (P2) and 16.0 MPa (P3), while all the other operational parameters were fixed at standard conditions (i.e. T = 40°C, C = 2 mg/ml, f = 1 ml/min, fCO_2 = 40 g/min and MR = 2%). The effect of pressure on the length of curcumin particles is shown in **Figure 3-4**a.

Pressure has a high impact on the CO_2 density and consequently on the density of the fluid phase formed by the mixture ethanol-CO_2 once it contains around 98% (in mole) of CO_2. At 8.0 MPa (P1) a complete coverage of lactose surface is observed in **Figure 3-5**a,b due to the formation of a large amount of irregular small particles (0.4 ± 0.2 µm). A few large particles were also formed, however, due to their low number, reliable particle size distribution measurements could not be taken.

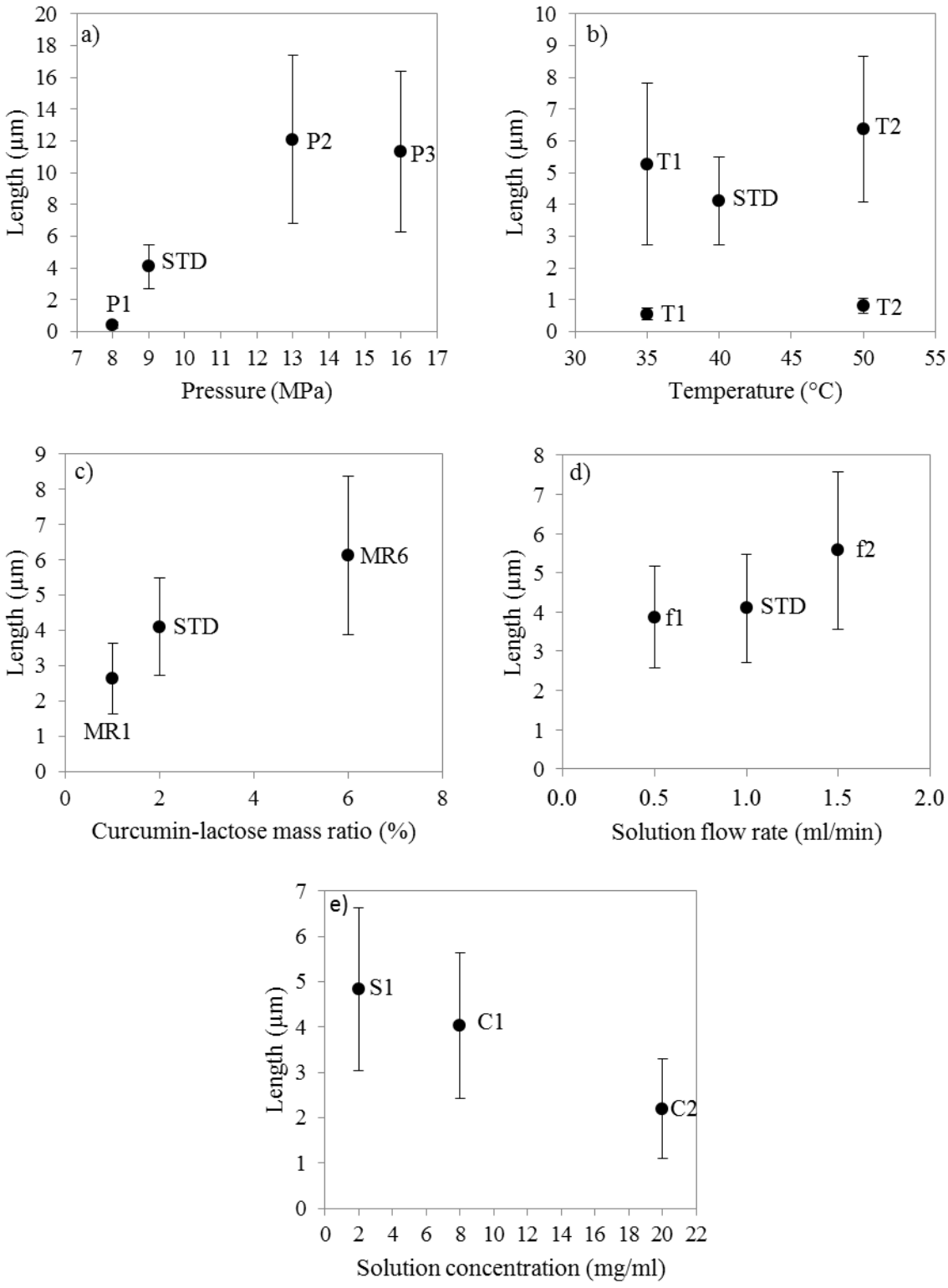

Figure 3-4. Variations of curcumin length compared to the experiment STD (p = 9 MPa, T = 40°C, C = 2 mg/ml, f = 1 ml/min, fCO2 = 40 g/min and MR = 2%) at different: a) pressures - P1 (8 MPa), P2 (13 MPa), P3 (16 MPa); b) temperatures - T1 (35°C), T2 (50°C); c) curcumin-lactose mass ratios - MR1 (1%), MR6 (6%); d) solution flow rates - f1 (0.5 ml/min), f2 (1.5 ml/min); e) solution concentrations - S1 (2 mg/ml), C1 (8 mg/ml), C2 (20 mg/ml).

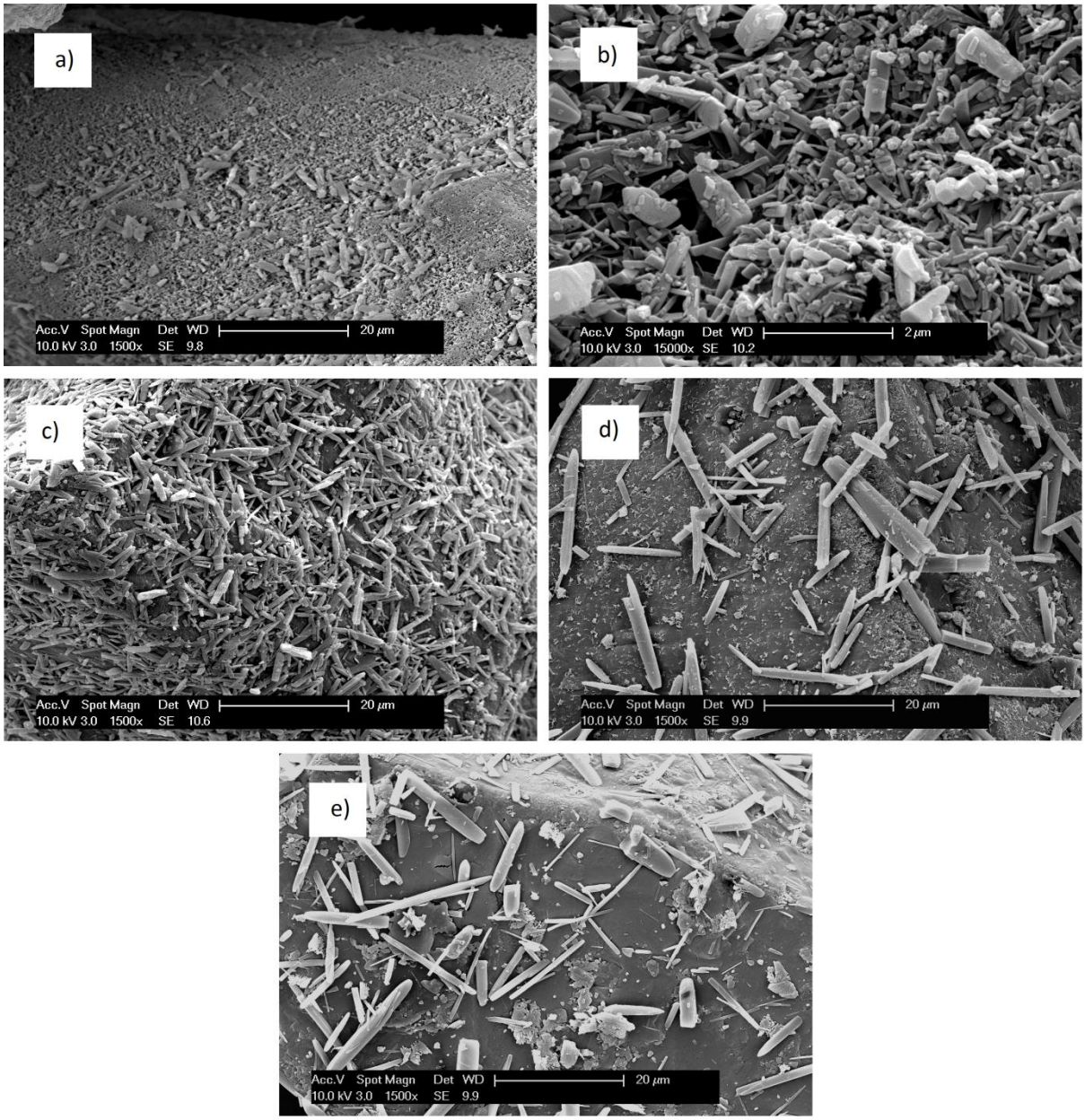

Figure 3-5. SEM images of curcumin coated lactose via SAS-FB at different pressures and solution flow rates: a) P1 (8 MPa, 1 ml/min), Mag 1500; b) P1, Mag 15000; c) Pf (8 MPa, 0.5 ml/min), Mag 1500; d) P2 (13 MPa, 1 ml/min), Mag 1500; e) P3 (16 MPa, 1 ml/min), Mag 1500.

In this experiment (P1), the operational point of the system is presumably located below the supercritical region on the boundary between the vapour and liquid-vapour regions of the ethanol-CO_2 VLE diagram (see P1 in **Figure 3-2**). The ethanol-rich phase, capable of solubilizing more curcumin, would form a solution with low supersaturation, and consequently, large particles originate. On the other hand, the CO_2-rich phase with high

supersaturation, due to the low solubility of curcumin in CO_2, generates submicron particles [42]. To verify this hypothesis, another experiment (Pf) was performed away from the boundary of liquid-vapour region at the same pressure but with higher CO_2 molar fraction (0.991), by decreasing the solution flow rate to 0.5 ml/min and keeping fixed the CO_2 flow rate in 40 g/min. The operational point is now located in the vapour region (see Pf in **Figure 3-2**) and a uniform distribution of particles was produced as demonstrated in **Figure 3-5**c. Therefore, one can attribute the formation of two different populations of particles in P1 to the existence of two phases. By having an increment of 1.0 MPa in pressure, at 9.0 MPa (STD) the CO_2 density becomes 75% higher [43] and the mean particle length is around 10 times higher than at P1. When the pressure increases to 13.0 MPa (P2), the CO_2 density is 53% higher than that at 9.0 MPa [43] and particle length increases further to 12 ± 5 μm. A small number of rectangular and needle-like particles with a wide size distribution were formed (**Figure 3-5**d). Finally, at 16.0 MPa (P3, **Figure 3-5**e) the CO_2 density is only 7% higher than at 13.0 MPa [43]. The particles measure 11 ± 5 μm, and therefore, no further increase in length was observed. As with STD, only one population of particles was detected in P2 and P3 as the operational points are far away from the biphasic region (**Figure 3-2**). The aspect ratio (L/W = length/width) increased with pressure with values equal to 3.3, 5.8, 7.3 and 8.2 in P1, STD, P2 and P3, respectively. It has been demonstrated that particles with high aspect ratio have improved aerodynamic properties, favouring drug detachment from the carrier`s surface and deep lung deposition [4]. Therefore, the formulation originated in P3 should have the best properties for pulmonary delivery.

The results of increasing the operational pressure on particle size can be explained by the competition of two opposite effects caused by the rise in CO_2 density: i) the ability of CO_2 to solubilize the solvent (antisolvent effect) is increased, improving the supersaturation of the

liquid solution which causes a high nucleation rate and fast particle grow. This leads to the formation of a large number of small particles [39,44] and, ii) the ability of ethanol-CO_2 to solubilize the solute (cosolvent effect) is increased, diminishing the solution supersaturation and consequently the nucleation rate. The higher the concentration of ethanol in the fluid phase, more significant is the increase in drug solubility with pressure [45]. If the fluid phase is still supersaturated after nucleation, the solute may continuously migrate to the solid phase, leading to particle growth [39]. The increase in particle size observed (**Figure 3-4**a) when the pressure increased from 8.0 to 13.0 MPa leads to the conclusion that the cosolvent behaviour of CO_2 is favoured at higher pressures. Two recent papers [45,46] support this conclusion through the measurement of curcumin solubility in ethanol-CO_2 mixtures. They found out that for a given temperature and ethanol composition, the solubility of curcumin in the fluid phase increases with pressure. At 16.0 MPa, the antisolvent effect would probably start to compensate the cosolvent effect as no further increase in length occurred. Similar effect of pressure was observed by Jia et al. [37] in the precipitation of curcumin from a dichloromethane solution: at 8.0 MPa irregular and rod morphology was observed, whereas at 12.0 MPa much larger rod and needle-like particles were produced. These results evidence that the supersaturation of the dichloromethane solution decreased with pressure, likewise the ethanol solution studied here, although quantitative measurements of particle size were not shown. Conversely, Anwar et al. [38] noticed a decrease in the mean particle size of curcumin processed by SAS with methanol, acetonitrile and acetone when the pressure was increased. Curcumin processed with acetone by SEDS (Solution Enhanced Dispersion by Supercritical Fluids) also showed a decrease in particle size with pressure [47].

With respect to drug yield, negligible change was observed from 8.0 MPa (Y = 90.0%) to 9.0 MPa (Y = 89.2%). At 13.0 MPa, one of the lowest values for drug yield (Y = 76.6%) was

obtained probably due to the high drug solubility in the fluid phase (cosolvent effect), as discussed before. At 16.0 MPa, as the CO_2 density change became not significant with the change of pressure, the cosolvent effect intensity was weaker, giving a yield of 80.4%. In general, in the range of CO_2 density distinctly affected by pressure, for the curcumin-ethanol-CO_2 system, the cosolvent effect probably dominated the competition with the antisolvent effect, leading to large particle size and low yield at high pressures.

3.5.2.2. Effect of Temperature

Tests of curcumin coating lactose using SAS-FB process at temperatures 35°C (T1) and 50°C (T2) with all other conditions constant (i.e. p = 9.0 MPa, C = 2 mg/ml, f = 1 ml/min, fCO_2 = 40 g/min and MR = 2%) were carried out to be compared with STD performed at 40°C. SEM images of curcumin coated lactose at 35°C and 50°C are shown in **Figure 3-6**a,b and **Figure 3-6**c,d, respectively. Two populations of particles were obtained in both tests with lengths shown in **Figure 3-4**b.

Considering the VLE of ethanol-CO_2 at 35°C obtained from Tanaka and Kato [48], T1 was probably performed in the liquid region (**Figure 3-7**a). The lower diffusivity of liquids compared with supercritical fluids may have caused a non-uniform mixing and supersaturation which lead to the formation of two populations of particles. To understand the influence of the fluid phase behaviour on the morphology of curcumin particles, another experiment (Tf) was performed at the same temperature but with higher CO_2 molar fraction (0.991) by decreasing the solution flow rate to 0.5 ml/min and keeping the CO_2 flow rate at 40 g/min. In Tf (**Figure 3-7**a), the operational point is located in the border of the supercritical region (xc_{CO2} = 0.994, [48]) and only one population of particles was observed (**Figure 3-6**e,f). In this case, the higher concentration of CO_2 might have increased the diffusivity of the fluid leading to a faster and more uniform mixing and supersaturation.

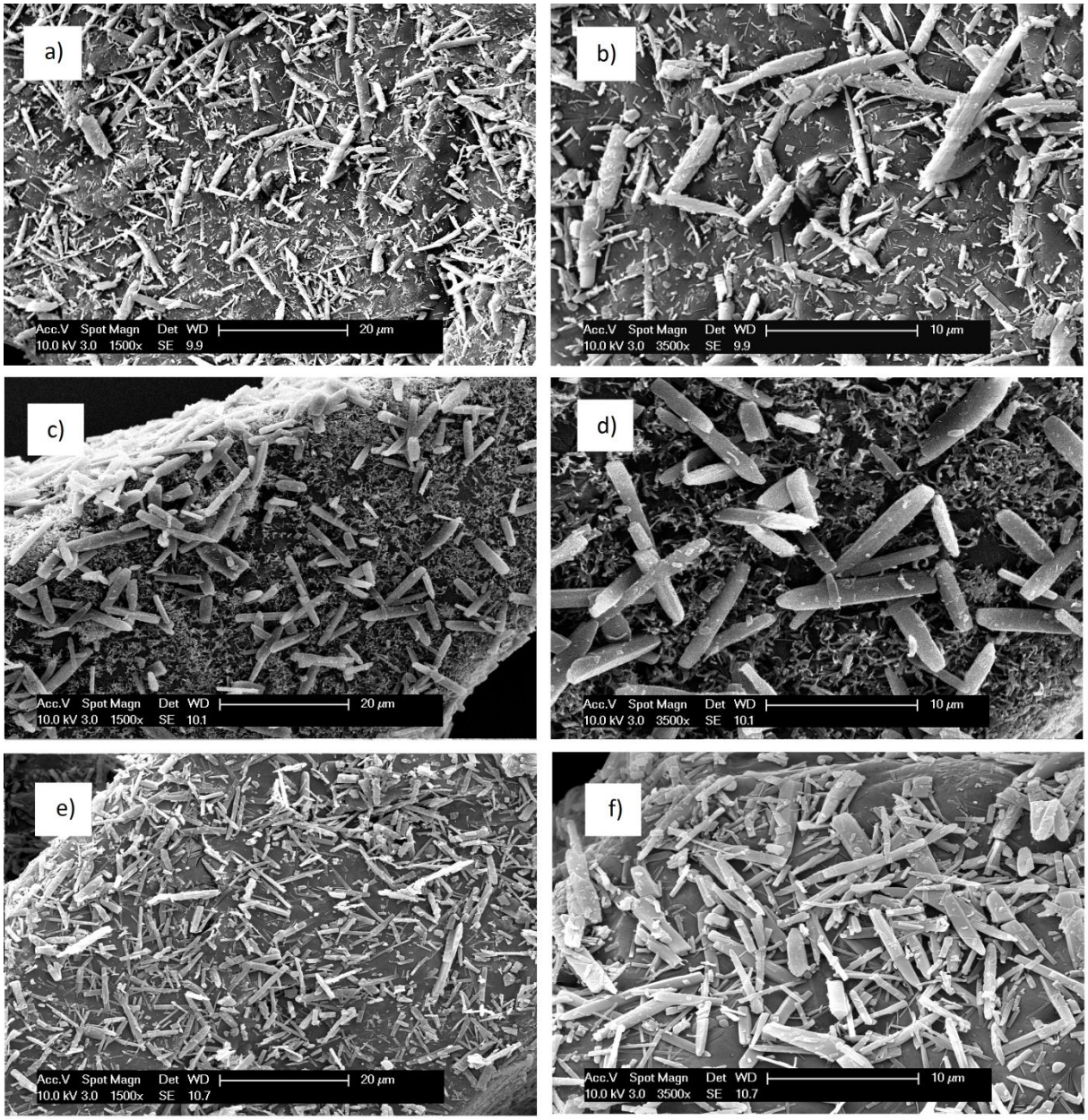

Figure 3-6. SAS-FB results of curcumin coated lactose at different temperatures and flow rates: a) T1 (35°C, 1 ml/min), Mag 1500; b) T1, Mag 3500; c) T2 (50°C, 1 ml/min), Mag 1500; d) T2, Mag 3500; e) Tf (35°C, 0.5 ml/min), Mag 1500; f) Tf, Mag 3500.

At 50°C (T2), taking the VLE data from Joung et al. [32] as reference, the operational point should be located in the vapour region (**Figure 3-7**b), albeit very close to the boundaries of the biphasic region where liquid and vapour can be found. Thereby, small oscillations on the process conditions could easily lead to precipitation in the biphasic region. The large particles would likely to be formed from a liquid phase originated when small fluctuations in CO_2 flow

rate occurred. At immiscible conditions, the mechanisms of supersaturation are more complex than in miscible systems so they cannot describe properly the precipitation process [39].

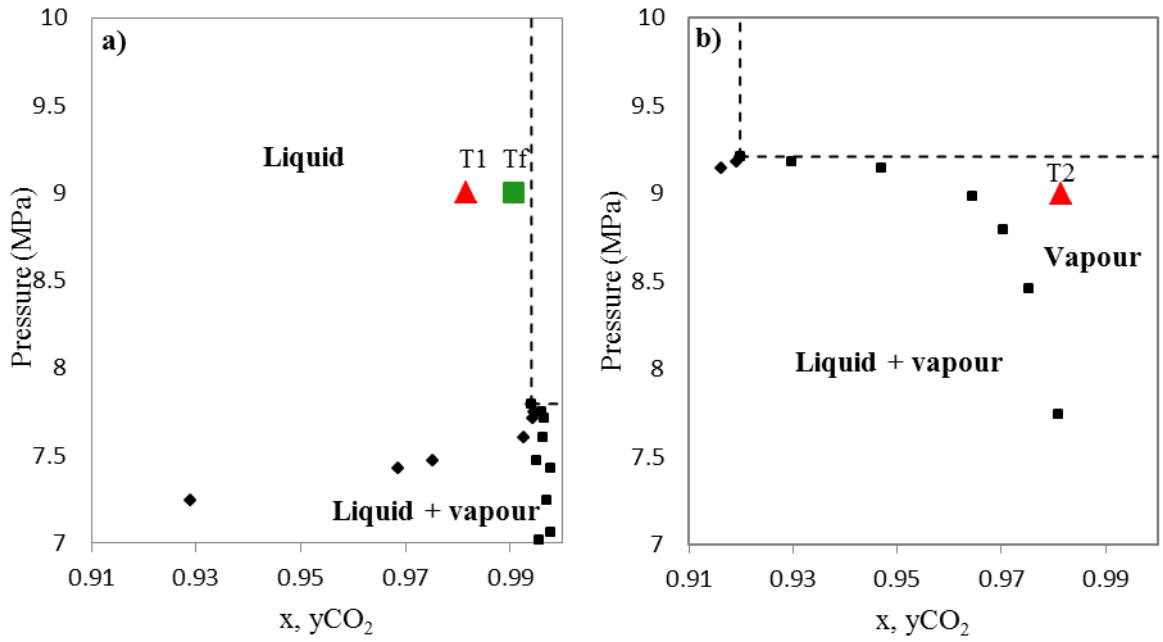

Figure 3-7. a) Vapor-liquid equilibrium of ethanol-CO2 at 35°C obtained from Tanaka and Kato [48]; b) vapor-liquid equilibrium of ethanol-CO2 at 49.4°C obtained from Joung et al. [32]. The dashed lines limit the supercritical region. The experiment that produced one population of particles is shown in green while the experiments with two populations are in red.

The temperature affects the SAS precipitation process in different ways: it changes the vapour pressure of the drug and densities of CO_2 and solvent which influence the solid solubility in the fluid phase and, ultimately, the degree of supersaturation; the viscosity of the liquid solution can also change which influences the nucleation rate. The most significant impact on drug yield was observed at 35°C (T1), where the fluid density is the highest among the three temperatures tested. As discussed previously in Section 3.5.2.1, high ethanol-CO_2 density enhances drug solubility in the fluid phase (cosolvent effect), decreasing the supersaturation. Cunico et al. [46] observed that the effect of temperature on the solubility of curcumin in ethanol-CO_2 is substantially higher than the effect of pressure and this might explain why at 35°C the lowest drug yield (Y = 71.0%) was observed in this work. Other authors have

concluded that high temperature improves curcumin recovery from ethanol and ethanol-acetone solutions processed by Gas Antisolvent (GAS) and Atomized Rapid Injection of Solvent Extraction (ARISE) [36]. At 50°C, the yield (Y = 82.3%) was not higher than at 40°C (Y = 89.2%), despite the decrease in the fluid density. In this case, the increase in the vapour pressure of the drug might have compensated the effect of density. Also, the equilibrium solubility of curcumin in ethanol increased from 7.5 mg/ml to 10.4 mg/ml when the temperature changed from 40°C to 50°C which could decrease the supersaturation of the liquid solution.

3.5.2.3. Effect of Drug-Carrier Mass Ratio

In order to analyse the surface area available for drug deposition two tests were performed: the first at 1% curcumin-lactose mass ratio (MR1) and the second at 6% curcumin-lactose mass ratio (MR6), with all the other conditions constant as the experiment STD (i.e. T = 40°C, p = 9.0 MPa, C = 2 mg/ml, f = 1 ml/min and fCO_2 = 40 g/min). The mass of lactose in the bed was kept constant (1 g) so only the amount of drug pumped inside the HPV was varied. **Figure 3-8** shows the lower mass ratio results (MR1) in the lefthand column and the higher mass ratio (MR6) in righthand column.

It is clear that in the lower mass ratio test (MR1) the lactose surface is not completely covered as some free space can be observed. Conversely, increasing the mass ratio to 6% (MR6) resulted in the formation of agglomerated particles and mutiple layered coating with many curcumin particles not attached to the carrier surface. In this case, the relative surface area of lactose particles available is much lower so the chance of forming drug agglomerates is higher. As the solution flow rate and concentration were kept constant, the coating time was varied to reach the desired curcumin-lactose mass ratio. In addition to these changes in morphology, **Figure 3-4**c suggests (cautiously, since the results do not appear statistically

significant) that increasing the drug-carrier mass ratio leads to an increase in the mean size of the curcumin partcles. If true, this may be explained by the increase in residence time of partices in the HPV [39]: in MR1, STD and MR6 the respective coating times were 5, 10 and 30 minutes.

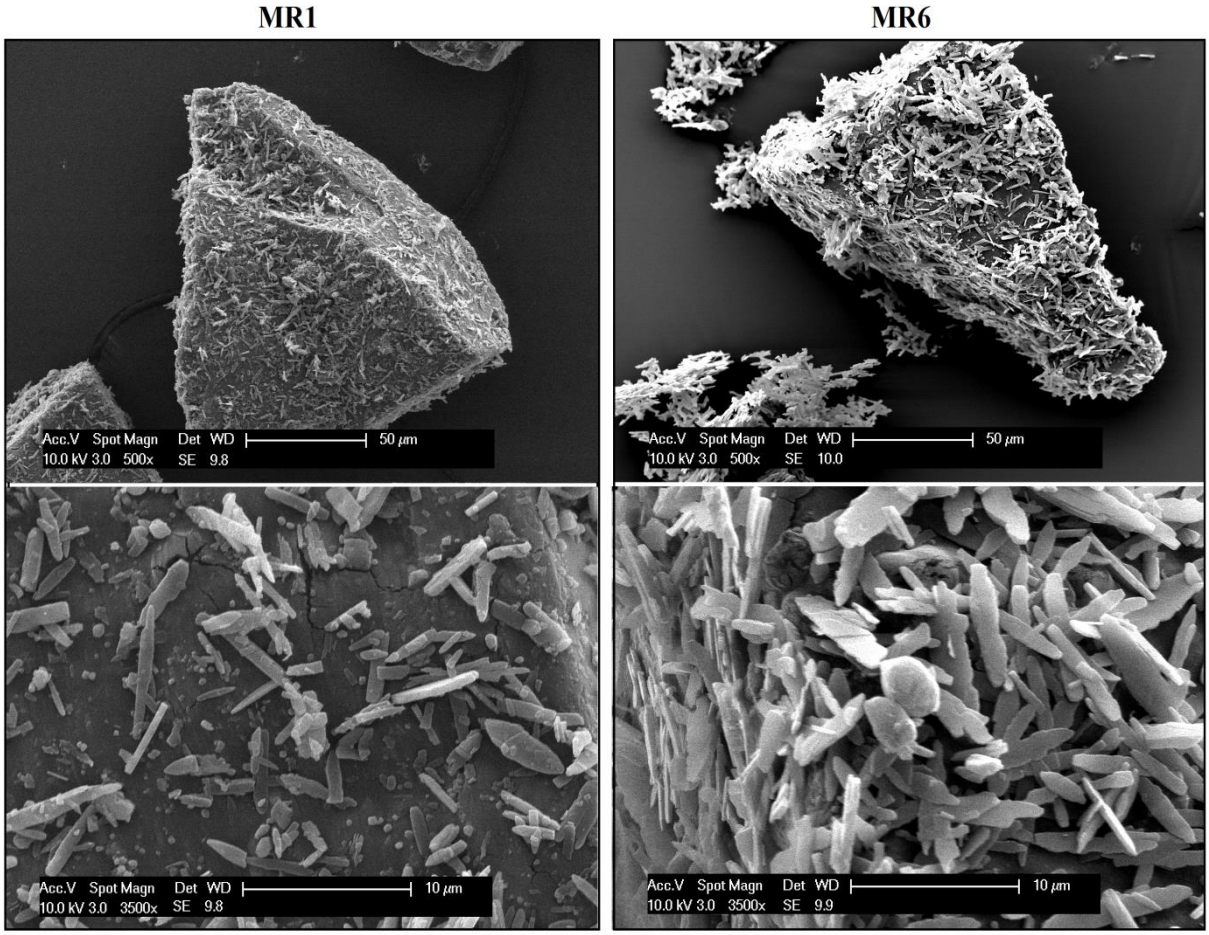

Figure 3-8. SAS-FB results of curcumin coated lactose at different curcumin-lactose mass ratios. Lefthand column: mass ratio of 1% (MR1); righthand column: mass ratio of 6% (MR6).

As expected, no significant changes in drug yield could be observed comparing the STD (Y = 89.2%), MR1 (Y = 83.4%) and MR6 (Y = 86.4%) experiments. Once pressure, temperature, solution initial concentration and flow rate were kept constant, the yields were not substantially influenced by changes in the drug-carrier mass ratio.

3.5.2.4. Effect of Solution Flow Rate

The effect of changing the solution flow rate from the experiment STD (1 ml/min) was analysed for two different values: 0.5 ml/min (f1) and 1.5 ml/min (f2). All the other operational conditions were kept constant (i.e. T = 40°C, *p* = 9.0 MPa, C = 2 mg/ml, fCO_2 = 40 g/min and MR = 2%). There is a suggestion of an increase in curcumin length with the solution flow rate (**Figure 3-4**d), but the data is not statistically significant. In f1, rectangular and needle-like particles were formed (**Figure 3-9**a). As the solution flow rate increased to 1.5 ml/min, the morphology of particles (**Figure 3-9**b) was kept similar to the experiments before, however there may be an increase in the mean particle length. In both experiments (f1 and f2), only one population of particles was obtained as the operational points are located in the supercritical region (see f1 and f2 in **Figure 3-2**).

Drug yield decreased from 91.5% in f1 to 82.7% in f2. The possible reason is that the presence of more solvent enabled more curcumin to be solubilized in the fluid phase [45,46]. Furthermore, there was a small decrease in the contact time between solution and sc-CO_2, thus the solution supersaturation could decrease. Other authors [38,47] have reached the same conclusions regarding flow rate and supersaturation of curcumin solutions, however the opposite effect has been also reported justified by the fact that high solution flow rate improves the mixing [44].

3.5.2.5. Effect of Solvent

The effect of solvent on particle size can be observed by comparing the experiment STD, in which ethanol was used as solvent, to the experiment S1 that used acetone with all the other conditions constant (i.e. T = 40°C, *p* = 9.0 MPa, C = 2 mg/ml, f = 1 ml/min, fCO_2 = 40 g/min and MR = 2%). The length of the particles obtained in S1 (**Figure 3-3**f) was slightly larger

than in STD (**Figure 3-3**e) while the morphology was similar. Therefore, in the case of this work, the choice of organic solvent has little impact on particle size and morphology if the same concentration is used.

There was a small decrease in drug yield from 89.2% in STD to 85.2% in S1. Since the ability of acetone to solubilize curcumin at 40°C is much higher (67.5 mg/mL) than ethanol (7.5 mg/ml), the supersaturation in the ethanol solution was probably higher. To increase the supersaturation of the acetone solution, other tests were performed with acetone at higher concentrations.

3.5.2.6. Effect of Solution Concentration

Acetone solution concentrations of 8 mg/ml (C1) and 20 mg/ml (C2) were tested with all the other conditions fixed as standard (i.e. T = 40°C, p = 9.0 MPa, f = 1 ml/min, fCO_2 = 40 g/min and MR = 2%). Increasing the solution concentration effectively increases the supersaturation of the liquid at the prevailing conditions and would appear to result in smaller curcumin particles (**Figure 3-4**e). The morphology of curcumin particles in C2 was changed to irregular and agglomerated (**Figure 3-9**d) while C1 particles still kept the rectangular shape (**Figure 3-9**c) as S1 (**Figure 3-3**f). The aspect ratio also decreased with concentration, measuring 4.7, 3.7 and 2.6 in S1, C1 and C2, respectively.

Drug yield increased from 85.2% in S1 to 93.3% in C1 due to the higher supersaturation attained. In fact, C1 delivered the highest yield in this work. Increasing the concentration even more, drug yield was equal to 86.0% in C2. No further increase in yield probably resulted from the increase in the viscosity of the liquid solution at the elevated concentration, leading to a poor diffusion between sc-CO_2 and acetone and thus a non-uniform supersaturation [44]. If the experiments using acetone (S1, C1, C2) are compared with the standard experiment

using ethanol (STD), it is possible to see that acetone with an intermediate concentration (8 mg/ml) provides higher drug yield than the standard ethanol solution (2 mg/ml), however the aspect ratio is larger in the latter. These results regarding drug yield are in agreement with the observations of Kurniawansyah et al. [36].

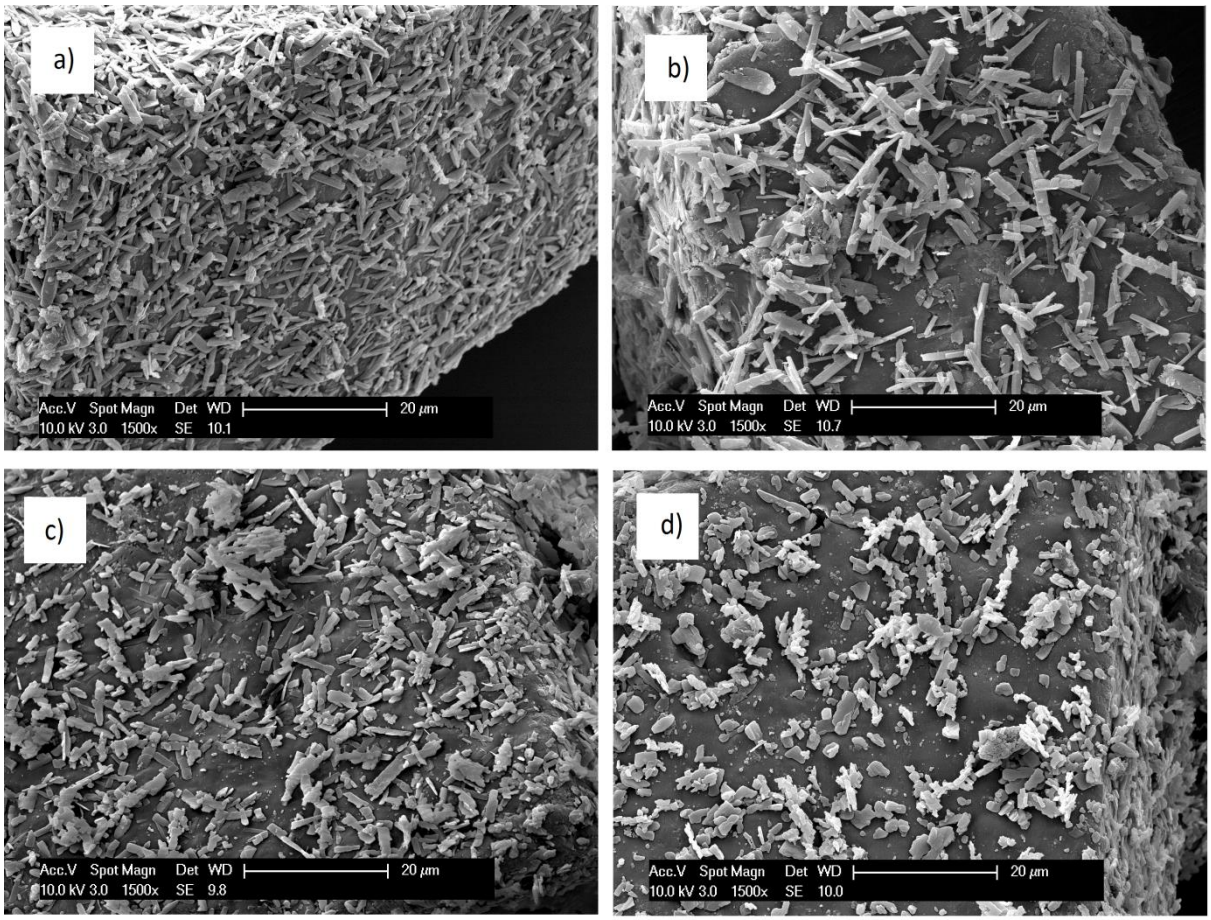

Figure 3-9. SAS-FB results of lactose coated curcumin at different solution flow rates a) f1 (0.5 ml/min); b) f2 (1.5 ml/min) and different solution concentrations c) C1 (8 mg/ml); d) C2 (20 mg/ml).

3.5.3. Formulation Uniformity

An indication of the uniformity of the formulation can be analysed by calculating the relative standard deviation (RSD) of the curcumin yield in each sample based on 3 to 4 measurements. The FDA [49] recommendation is that the RDS should not exceed 6%. Due to the high degree of mixing in the fluidized bed, highly uniform samples were obtained once the RSD varied from 2.4% to 4.7% (**Table 3-1**).

3.5.4. Thermogravimetric Analysis (TGA)

In the pharmaceutical industry, the amount of residual organic solvent existing in the final formulation is critical. Not only are they harmful to the human health, but also high levels of organic solvents can affect the formulation physicochemical properties [50]. According to the USP 467 for residual solvent, ethanol and acetone belong to class 3 and therefore the maximum concentration recommended is 5000 ppm or 0.5%. The sample STD was analysed immediately after processing to investigate possible mass loss due to solvent evaporation. Solvent-free curcumin-lactose physical mixture was also tested as reference for comparison. **Figure 3-10** demonstrates that the thermal behaviour of curcumin-lactose physical mixture and STD have very similar weight loss curves with no significant mass loss (about 0.1%) before 90°C. The boiling point of ethanol is 78°C so it would have started to evaporate below 90°C, leading to the conclusion that there is only trace residual solvent in the samples processed by SAS-FB. As acetone (boiling point = 56°C) is even more volatile than ethanol, it is likely than even lower amounts of residual solvent would be found in SAS-FB samples processed by acetone.

These results show the ability of the process in producing solvent-free formulations without the need for an extra drying step. Proper quantification of residual solvent content can be obtained by employing a headspace sampler coupled to a gas chromatograph with a flame ionization detector [51,52].

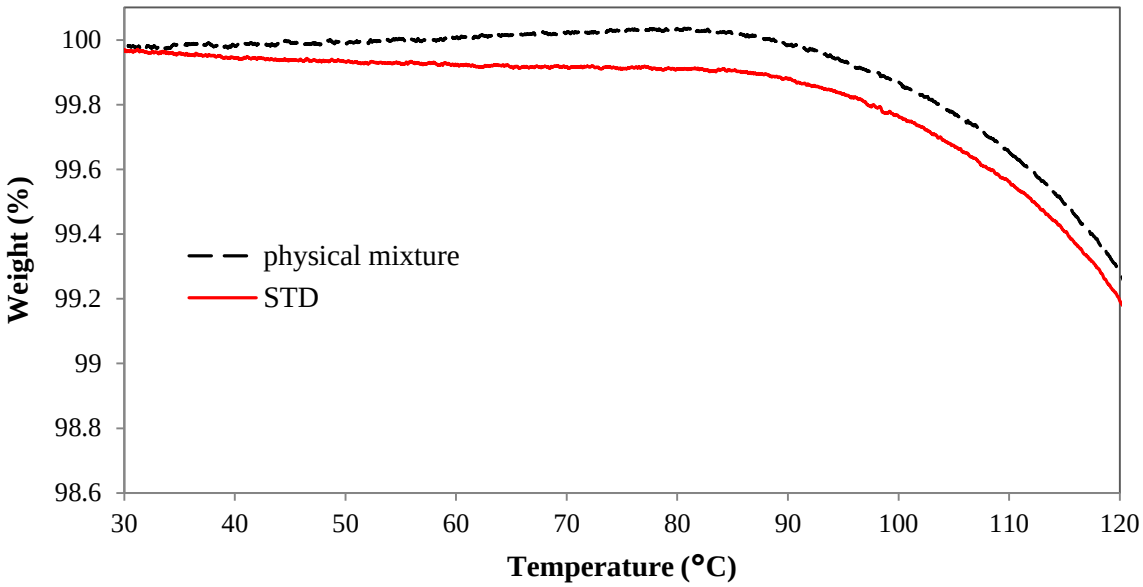

Figure 3-10. TGA thermograms of curcumin coated lactose via SAS-FB (STD) and curcumin-lactose physical mixture.

3.5.5. X-Ray Diffraction (XRD)

The XRD patterns of raw curcumin and curcumin processed by SAS with ethanol (SAS-Et) are shown in **Figure 3-11**. It can be seen that after SAS processing the intensity of the peaks is decreased. This means that there was a reduction in the crystallinity of SAS-Et samples compared with raw curcumin. Moreover, changes on its crystal structure are observed since the peaks appear in different positions, as previously observed after curcumin processing by a similar supercritical antisolvent technique [36].

3.5.6. Fourier Transform Infrared Spectroscopy (FT-IR)

FT-IR was performed to analyse possible chemical interactions among lactose, curcumin, CO_2 and ethanol after SAS and SAS-FB. As can be seen from **Table 3-1**, similar IR spectra were obtained for raw curcumin and SAS-Et. The spectra of STD and lactose also show high similarity once STD contains around 98% of lactose. No new peaks were observed when comparing the processed samples (SAS-Et and STD) with the raw curcumin and lactose,

indicating that there is no chemical interaction among the compounds and their physicochemical properties remained unchanged.

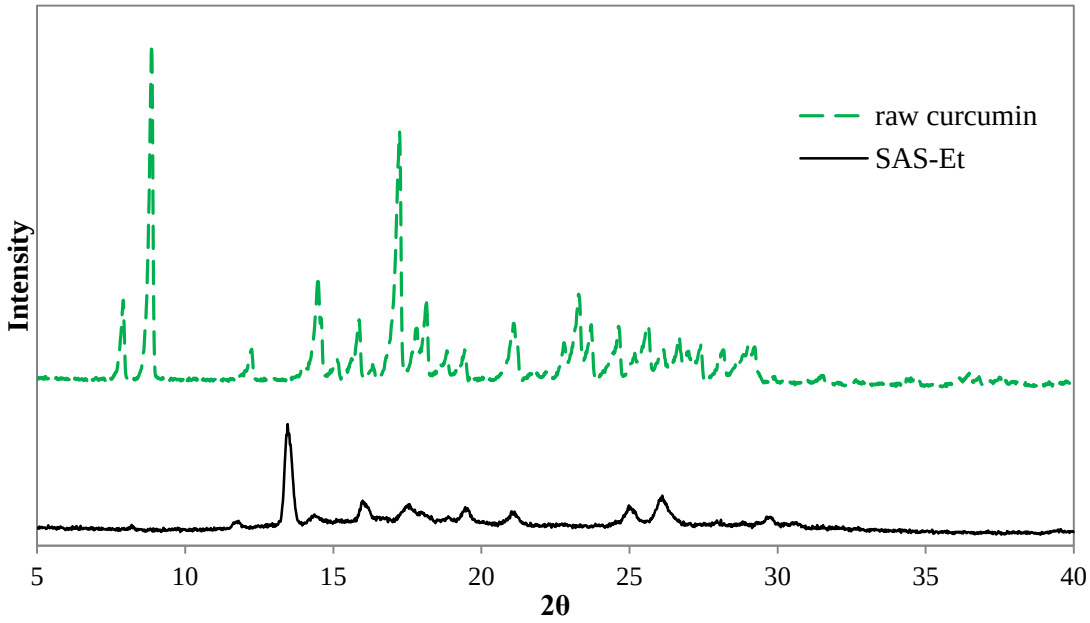

Figure 3-11. XRD patterns of raw curcumin and SAS processed curcumin (SAS-Et).

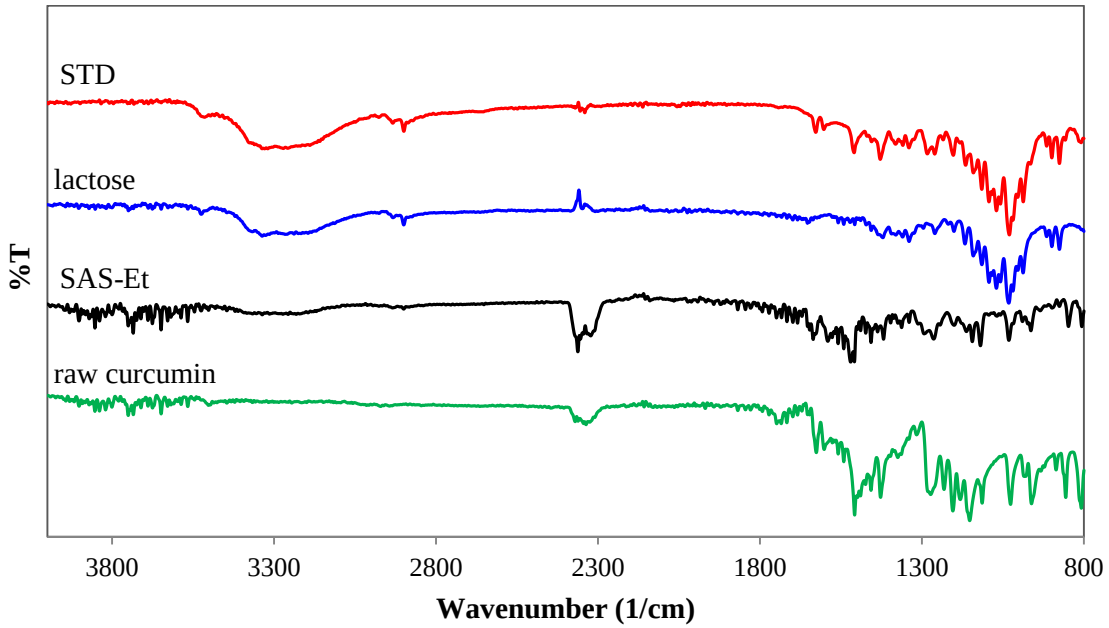

Figure 3-12. IR spectra of processed and raw materials: raw curcumin; SAS processed curcumin (SAS-Et); raw lactose; curcumin coated lactose via SAS-FB (STD).

3.6. Conclusions

SAS-FB process successfully precipitated and coated curcumin particles on the surface of lactose in a single step. Due to the improved mixing and collection of drug particles close to their point of origin in the fluidized bed, SAS-FB precipitates are normally smaller and less aggregated than SAS particles. The coating also gives the formulation better handling properties and flowability with potential application for pulmonary drug delivery. In the range of conditions tested, the operational pressure showed the highest impact on curcumin particle size, which varied between 0.41 and 12.08 μm. Drug yield varied from 71.0 to 93.3% with the highest value obtained when acetone was used as solvent. By careful use of the operational point in the multiple component phase diagram, a bimodal particle distribution could be obtained or avoided.

3.7. Acknowledgements

The authors acknowledge the financial support from National Council for Scientific and Technological Development (CNPQ) through Science Without Borders Program and DFE Pharma for kindly providing the sample of Lactohale® 100. The advice and suggestions of Prof. Silvio Alexandre Beisl Vieira de Melo and Dr. Valentina Prosapio are also much appreciated.

3.8. Competing interests

The authors would like to declare that there are no competing interests.

3.9. References

[1] G. Scheuch, M.J. Kohlhaeufl, P. Brand, R. Siekmeier, Clinical perspectives on pulmonary systemic and macromolecular delivery, Adv. Drug Deliv. Rev. 58 (2006) 996–1008. doi:10.1016/j.addr.2006.07.009.

[2] W. Yang, J.I. Peters, R.O. Williams, Inhaled nanoparticles—A current review, Int. J. Pharm. 356 (2008) 239–247. doi:10.1016/j.ijpharm.2008.02.011.

[3] D.I. Daniher, J. Zhu, Dry powder platform for pulmonary drug delivery, Particuology. 6 (2008) 225–238. doi:10.1016/j.partic.2008.04.004.

[4] H. Larhrib, G.P. Martin, C. Marriott, D. Prime, The influence of carrier and drug morphology on drug delivery from dry powder formulations, Int. J. Pharm. 257 (2003) 283–296. doi:10.1016/S0378-5173(03)00156-X.

[5] N. Islam, M.J. Cleary, Developing an efficient and reliable dry powder inhaler for pulmonary drug delivery - A review for multidisciplinary researchers, Med. Eng. Phys. 34 (2012) 409–427. doi:10.1016/j.medengphy.2011.12.025.

[6] A.S. Silva, M.T. Tavares, A. Aguiar-Ricardo, Sustainable strategies for nano-in-micro particle engineering for pulmonary delivery, J. Nanoparticle Res. 16 (2014) 1–17. doi:10.1007/s11051-014-2602-0.

[7] M.J. Telko, A.J. Hickey, Dry powder inhaler formulation., Respir. Care. 50 (2005) 1209–1227. doi:10.2165/00128413-200615470-00016.

[8] J. Zhang, L. Wu, H.K. Chan, W. Watanabe, Formation, characterization, and fate of inhaled drug nanoparticles, Adv. Drug Deliv. Rev. 63 (2011) 441–455. doi:10.1016/j.addr.2010.11.002.

[9] M.J. Cocero, Á. Martín, F. Mattea, S. Varona, Encapsulation and co-precipitation processes with supercritical fluids: Fundamentals and applications, J. Supercrit. Fluids. 47 (2009) 546–555. doi:10.1016/j.supflu.2008.08.015.

[10] E. Reverchon, I. De Marco, Mechanisms controlling supercritical antisolvent precipitate morphology, Chem. Eng. J. 169 (2011) 358–370. doi:10.1016/j.cej.2011.02.064.

[11] E. Reverchon, I. De Marco, R. Adami, G. Caputo, Expanded micro-particles by supercritical antisolvent precipitation: Interpretation of results, J. Supercrit. Fluids. 44 (2008) 98–108. doi:10.1016/j.supflu.2007.08.008.

[12] E. Reverchon, R. Adami, G. Caputo, I. De Marco, Spherical microparticles production by supercritical antisolvent precipitation: Interpretation of results, J. Supercrit. Fluids.

47 (2008) 70–84. doi:10.1016/j.supflu.2008.06.002.

[13] E. Reverchon, I. De Marco, E. Torino, Nanoparticles production by supercritical antisolvent precipitation: A general interpretation, J. Supercrit. Fluids. 43 (2007) 126–138. doi:10.1016/j.supflu.2007.04.013.

[14] V. Prosapio, E. Reverchon, I. De Marco, Formation of PVP/nimesulide microspheres by supercritical antisolvent coprecipitation, J. Supercrit. Fluids. 118 (2016) 19–26. doi:10.1016/j.supflu.2016.07.023.

[15] V. Prosapio, E. Reverchon, I. De Marco, Polymers' ultrafine particles for drug delivery systems precipitated by supercritical carbon dioxide + organic solvent mixtures, Powder Technol. 292 (2016) 140–148. doi:10.1016/j.powtec.2016.01.033.

[16] Q. Li, D. Huang, T. Lu, J.P.K. Seville, L. Xing, G.A. Leeke, Supercritical fluid coating of API on excipient enhances drug release, Chem. Eng. J. 313 (2017) 317–327. doi:10.1016/j.cej.2016.12.066.

[17] P. Anand, A.B. Kunnumakkara, R.A. Newman, B.B. Aggarwal, Bioavailability of curcumin: Problems and promises, Mol. Pharm. 4 (2007) 807–818. doi:10.1021/mp700113r.

[18] A. Tsutsumi, S. Nakamoto, T. Mineo, K. Yoshida, A novel fluidized-bed coating of fine particles by rapid expansion of supercritical fluid solutions, Powder Technol. 85 (1995) 275–278. doi:10.1016/0032-5910(95)03021-X.

[19] T.J. Wang, A. Tsutsumi, H. Hasegawa, T. Mineo, Mechanism of particle coating granulation with RESS process in a fluidized bed, Powder Technol. 118 (2001) 229–235. doi:10.1016/S0032-5910(00)00400-9.

[20] R. Schreiber, C. Vogt, J. Werther, G. Brunner, Fluidized bed coating at supercritical fluid conditions, J. Supercrit. Fluids. 24 (2002) 137–151. doi:10.1016/S0896-8446(02)00029-3.

[21] R. Schreiber, B. Reinke, C. Vogt, J. Werther, G. Brunner, High-pressure fluidized bed coating utilizing supercritical carbon dioxide, Powder Technol. 138 (2003) 31–38. doi:10.1016/j.powtec.2003.08.044.

[22] S. Rodríguez-Rojo, J. Marienfeld, M.J. Cocero, RESS process in coating applications

in a high pressure fluidized bed environment: Bottom and top spray experiments, Chem. Eng. J. 144 (2008) 531–539. doi:10.1016/j.cej.2008.07.054.

[23] O. Ratcharak, A. Sane, Surface coating with poly (trifluoroethyl methacrylate) through rapid expansion of supercritical CO2 solutions, J. Supercrit. Fluids. 89 (2014) 106–112.

[24] G.A. Leeke, T. Lu, R.H. Bridson, J.P.K. Seville, Application of nano-particle coatings to carrier particles using an integrated fluidized bed supercritical fluid precipitation process, J. Supercrit. Fluids. 91 (2014) 7–14. doi:10.1016/j.supflu.2014.03.012.

[25] V. Martín, R. Romero-Díez, S. Rodríguez-Rojo, M.J. Cocero, Titanium dioxide nanoparticle coating in fluidized bed via supercritical anti-solvent process (SAS), Chem. Eng. J. 279 (2015) 425–432. doi:10.1016/j.cej.2015.05.014.

[26] F. Niu, J. Haslam, R. Rajewski, B. Subramaniam, A fluidized-bed coating technology using near-critical carbon dioxide as fluidizing and drying medium, J. Supercrit. Fluids. 66 (2012) 315–320. doi:10.1016/j.supflu.2011.11.007.

[27] F. Zabihi, N. Xin, S. Li, J. Jia, T. Cheng, Y. Zhao, Polymeric coating of fluidizing nano-curcumin via anti-solvent supercritical method for sustained release, J. Supercrit. Fluids. 89 (2014) 99–105. doi:10.1016/j.supflu.2014.02.021.

[28] G.P. Sanganwar, S. Sathigari, R.J. Babu, R.B. Gupta, Simultaneous production and co-mixing of microparticles of nevirapine with excipients by supercritical antisolvent method for dissolution enhancement, Eur. J. Pharm. Sci. 39 (2010) 164–174. doi:10.1016/j.ejps.2009.11.011.

[29] C.A. Ober, L. Kalombo, H. Swai, R.B. Gupta, Preparation of rifampicin/lactose microparticle composites by a supercritical antisolvent-drug excipient mixing technique for inhalation delivery, Powder Technol. 236 (2013) 132–138. doi:10.1016/j.powtec.2012.04.057.

[30] S.K. Sathigari, C.A. Ober, G.P. Sanganwar, R.B. Gupta, R.J. Babu, Single-Step Preparation and Deagglomeration of Itraconazole Microflakes by Supercritical Antisolvent Method for Dissolution Enhancement, J. Pharm. Sci. 100 (2011) 2952–2965. doi:10.1002/jps.22524.

[31] W.M. Giufrida, R. Favareto, V.F. Cabral, M.A. A.Meireles, L. Cardozo-Filho, M.L.

Corazza, High-Pressure Vapor-Liquid Equilibrium Data for Ternary Systems CO2 + Organic Solvent + Curcumin, Open Chem. Eng. J. 4 (2010) 3–10. doi:10.2174/1874123101004020003.

[32] S.N. Joung, C.W. Yoo, H.Y. Shin, S.Y. Kim, K.P. Yoo, C.S. Lee, W.S. Huh, Measurements and correlation of high-pressure VLE of binary CO2-alcohol systems (methanol, ethanol, 2-methoxyethanol and 2-ethoxyethanol), Fluid Phase Equilib. 185 (2001) 219–230. doi:10.1016/S0378-3812(01)00472-1.

[33] M. Rasteh, F. Farhadi, A. Bahramian, Hydrodynamic characteristics of gas-solid tapered fluidized beds: Experimental studies and empirical models, Powder Technol. 283 (2015) 355–367. doi:10.1016/j.powtec.2015.06.002.

[34] M.H. Khani, Models for prediction of hydrodynamic characteristics of gas-solid tapered and mini-tapered fluidized beds, Powder Technol. 205 (2011) 224–230. doi:10.1016/j.powtec.2010.09.018.

[35] Y. Peng, L.T. Fan, Hydrodynamic characteristics of fluidization in liquid-solid tapered beds, Chem. Eng. Sci. 52 (1997) 2277–2290. doi:10.1016/S0009-2509(97)00061-4.

[36] F. Kurniawansyah, R. Mammucari, N.R. Foster, Polymorphism of curcumin from dense gas antisolvent precipitation, Powder Technol. 305 (2017) 748–756. doi:10.1016/j.powtec.2016.10.067.

[37] J. Jia, W. Wang, Y. Gao, Y. Zhao, Controlled morphology and size of curcumin using ultrasound in supercritical CO2 antisolvent., Ultrason. Sonochem. 27 (2015) 389–94. doi:10.1016/j.ultsonch.2015.06.011.

[38] M. Anwar, I. Ahmad, M.H. Warsi, S. Mohapatra, N. Ahmad, S. Akhter, A. Ali, F.J. Ahmad, Experimental investigation and oral bioavailability enhancement of nano-sized curcumin by using supercritical anti-solvent process, Eur. J. Pharm. Biopharm. 96 (2015) 162–172. doi:10.1016/j.ejpb.2015.07.021.

[39] S. Bristow, T. Shekunov, B.Y. Shekunov, P. York, Analysis of the supersaturation and precipitation process with supercritical CO2, J. Supercrit. Fluids. 21 (2001) 257–271. doi:10.1016/S0896-8446(01)00100-0.

[40] A. Martín, M.J. Cocero, Numerical modeling of jet hydrodynamics, mass transfer, and crystallization kinetics in the supercritical antisolvent (SAS) process, J. Supercrit.

Fluids. 32 (2004) 203–219. doi:10.1016/j.supflu.2004.02.009.

[41] F. Kurniawansyah, R. Mammucari, N.R. Foster, Inhalable curcumin formulations by supercritical technology, Powder Technol. 284 (2015) 289–298. doi:10.1016/j.powtec.2015.04.083.

[42] C.S. Lengsfeld, J.P. Delplanque, V.H. Barocas, T.W. Randolph, Mechanism Governing Microparticle Morphology during Precipitation by a Compressed Antisolvent: Atomization vs Nucleation and Growth, J. Phys. Chem. B. 104 (2000) 2725–2735. doi:10.1021/jp9931511.

[43] NIST Chemistry WebBook, Thermophysical Properties of Carbon dioxide, SRD 69. (2017). http://webbook.nist.gov/cgi/fluid.cgi?ID=C124389&Action=Page (accessed January 1, 2017).

[44] M. Kakran, N.G. Sahoo, I.L. Tan, L. Li, Preparation of nanoparticles of poorly water-soluble antioxidant curcumin by antisolvent precipitation methods, J. Nanoparticle Res. 14 (2012). doi:10.1007/s11051-012-0757-0.

[45] S. and C. of C.S. in S.C.D. Zhan, S. Li, Q. Zhao, W. Wang, J. Wang, Measurement and Correlation of Curcumin Solubility in Supercritical Carbon Dioxide, (2017). doi:10.1021/acs.jced.6b00798.

[46] L.P. Cunico, M.C. Acosta, C. Turner, Experimental measurements and modeling of curcumin solubility in CO2-expanded ethanol, J. Supercrit. Fluids. (2017) 1–8. doi:10.1016/j.supflu.2017.06.018.

[47] Z. Zhao, M. Xie, Y. Li, A. Chen, G. Li, J. Zhang, H. Hu, X. Wang, S. Li, Formation of curcumin nanoparticles via solution-enhanced dispersion by supercritical CO2, Int. J. Nanomedicine. 10 (2015) 3171–3181. doi:10.2147/IJN.S80434.

[48] H. Tanaka, M. Kato, Vapor-Liquid Equilibirum Properties of Carbon Dioxide + Ethanol Mixtures at high Pressures, J. Chem. Eng. Japan. 28 (1995) 263–267.

[49] C.J.S. Brian R. Rohrs, Gregory E. Amidon, Richard H. Meury, Pamela J. Secreast, Harry M. King, Particle Size Limits to Meet USP Content Uniformity Criteria for Tablets and Capsules, J. Pharm. Sci. 95 (2006) 1049–1059. doi:DOI 10.1002/jps.

[50] C.B. Hymer, Residual Solvent Testing : A Review of Gas-Chromatographic and

Alternative Techniques, 20 (2003).

[51] V. Prosapio, E. Reverchon, I. De Marco, Antisolvent micronization of BSA using supercritical mixtures carbon dioxide + organic solvent, J. Supercrit. Fluids. 94 (2014) 189–197. doi:10.1016/j.supflu.2014.07.012.

[52] G. Della Porta, N. Falco, E. Reverchon, Continuous supercritical emulsions extraction: A new technology for biopolymer microparticles production, Biotechnol. Bioeng. 108 (2011) 676–686. doi:10.1002/bit.22972.

Chapter 4 -

COPRECIPITATION OF CURCUMIN/PVP WITH ENHANCED DISSOLUTION PROPERTIES BY THE SUPERCRITICAL ANTISOLVENT PROCESS

Published article:

Journal of CO_2 Utilization 30 (2019) 48–62

4.1. Abstract

The poor solubility of curcumin (CURC) in aqueous media leads to a low bioavailability, which prevents its application in pharmaceutical formulations. In this work, the Supercritical Antisolvent process (SAS) was used to produce coprecipitates of CURC and poly (vinyl pyrrolidone) (PVP) from mixtures of ethanol and acetone. The effects of operating parameters: pressure, temperature, solution concentration, drug/polymer mass ratio and solution flow rate were analysed for a 70-30 (v/v) acetone-ethanol mixture. It was found that the composition of acetone in the solvent mixture is the parameter that affects particle size and curcumin recovery the most. The thermal behaviour, crystallinity, molecular interactions, apparent solubility, release profile of the coprecipitates and possible degradation of curcumin were investigated. The results showed that the SAS process is effective in preparing amorphous formulations of CURC/PVP with an apparent solubility of more than 600 times higher than that of the physical mixture of the raw compounds.

Keywords: coprecipitation; curcumin; PVP; supercritical antisolvent process; dissolution

4.2. Highlights

- Curcumin/PVP coprecipitates were produced from acetone-ethanol mixtures by SAS
- Acetone percentage has great influence on particle size and product recovery
- Nanoparticles (51–96 nm) and sub-microparticles (117–327 nm) were obtained
- Curcumin recovery, crystallinity, release profile and degradation were measured
- The apparent solubility of coprecipitates increased more than 600 times

4.3. Introduction

Curcumin (CURC) is a polyphenolic hydrophobic compound extracted from the roots of *Curcuma longa* and traditionally used as a spice and food additive. It has been demonstrated that curcumin has a wide range of therapeutic properties such as anticancer, antioxidant, antimicrobial and anti-inflammatory [1,2]. However, the use of curcumin in drug formulations is still not approved by the Food and Drug Administration (FDA), limited by several reasons including its low oral bioavailability caused by its poor solubility in aqueous media, low absorption and fast intestinal metabolism. In addition, curcumin undergoes degradation under light, heat and alkaline pH [3,4].

In recent decades, several curcumin formulations have been developed to address these issues including nanoparticles, liposomes, polymeric micelles, dendrimers and hydrogels [5–7]. The coprecipitation of active pharmaceutical ingredients (API) with hydrophilic polymers is advantageous because it can improve the API dissolution properties while protecting it against degradation. Poly(vinyl pyrrolidone) (PVP) was selected in this work because it is a biodegradable polymer approved as an inactive ingredient by the FDA and hence widely used in pharmaceutical applications. Several studies have demonstrated its ability in modifying the crystallisation kinetics of poorly water-soluble compounds by producing amorphous formulations with improved dissolution profile [8–10]. PVP is also expected to inhibit drug recrystallisation in the gastro-intestinal tract after oral administration [11,12], giving time for drug molecules to be absorbed into the systemic circulation, thus increasing its bioavailability [13].

The preparation of solid dispersions of curcumin and PVP with different molecular weights has been reported using conventional micronization techniques, such as spray drying [14] and solvent evaporation [15–17]. These methods have disadvantages such as the use of high

temperature, which causes the degradation of thermo-sensitive compounds, low yields and high residual solvent content in the formulation, often requiring an extra processing step. Moreover, the control of particle morphology, particle size and size distribution is difficult [18–20]. In smaller quantities, PVP has been used as a stabilizer for curcumin nanoparticles prepared via liquid antisolvent methods followed by freeze drying [21–23].

Supercritical fluids (SCFs) are attractive for particle precipitation as they combine liquid-like properties, such as high solvation power, and gas-like properties, including high diffusivity and compressibility. SCF-based micronization has demonstrated advantages over conventional techniques since particle size can be controlled through the manipulation of the operating parameters, the use of relatively low temperatures and formulations with low or no residual solvent can be obtained [24,25]. Carbon dioxide is a usual choice for SCF-based micronization processes since it is inexpensive, non-toxic, non-flammable, environmentally benign and it has a relatively low critical pressure (7.39 MPa) and critical temperature (31.1°C). Depending on the role played by the supercritical carbon dioxide (sc-CO_2) in relation to the solute, it can act as solvent, co-solute, antisolvent, dispersing agent, plasticizer or reaction medium.

In the Supercritical Antisolvent (SAS) process, the solute is typically dissolved in an organic solvent and then sprayed into a high pressure vessel through which sc-CO_2 is passed continuously. The instantaneous diffusion of sc-CO_2 into the liquid solution and, in minor extent, the evaporation of the liquid to the supercritical phase leads to the supersaturation of the liquid solution and precipitation of the solute, which is collected on a filter. Solvent and antisolvent are then separated via simple depressurization in a separator located downstream the precipitation vessel [26]. Although studied for many years, the SAS process is still not widely used in the pharmaceutical industry. A deeper understanding of the phenomena

involved in each step is required to allow the selection of the most appropriate operating conditions and enable process control. Extensive use of SAS at industrial scale to process pharmaceutical and food ingredients is believed likely in the future, especially due to the need of finding more environmentally friendly technologies, as recently discussed [27]. A key feature of SAS is its ability to process a wide variety of compounds to obtain several morphologies and sizes including crystals, nanoparticles, microparticles and expanded microparticles [28–30]. However, the use of SAS to produce coprecipitates has not always been successful. In some works, irregular and coalescing particles with wide particle size distribution [31] and low encapsulation efficiency [32] were obtained and the demonstration of an effective coprecipitation through the improvement of the drug dissolution properties is hardly reported [33].

In our recent work, curcumin was simultaneously precipitated and coated on the surface of lactose particles by the integration of the SAS process with a fluidized bed under pressure (SAS-FB) to improve the flow properties of the formulation [25]. In this work, the aim is to improve also the dissolution properties of curcumin through its coprecipitation with PVP by SAS, which is a suitable technique to treat thermo- and light-sensitive compounds, since low temperatures can be used and the experiments are carried out away from light.

Other SCF-assisted processes have been used to produce CURC/PVP coprecipitates. Adami et al. [34] obtained spherical and collapsed particles with mean size ranging from 220 - 380 nm by the supercritical assisted atomization (SAA), using ethanol as solvent. The issue here is the use of high temperature (80 °C) since curcumin degradation is known to be intensified above 60˚C [4,35]. The quantification of product recovery and possible degradation of curcumin were not presented by the authors. The atomized rapid injection solvent extraction (ARISE) method has also been applied for the coprecipitation of curcumin in ternary composites with

PVP and cyclodextrins, with very few experiments being carried out with the binary CURC/PVP. As the intended application was pulmonary delivery, microparticles were produced and in some of the images presented it was possible to distinguish curcumin crystals in a porous structure, which indicate that the materials precipitated separately [36–38]. Although there are similarities between the SAS and ARISE processes in terms of the role of sc-CO_2, differences between the mixing mechanism can lead to different results. The use of SAS process to produce CURC/PVP coprecipitates for pharmaceutical application has been reported once by Chhouk et al. [39]. They used a micro-swirl mixer, a patented device, to process curcumin and PVP from a 90-10 acetone-ethanol mixture. Highly coalescing nanoparticles (25 - 342 nm) were obtained while very relevant information such as total product recovery, curcumin recovery and drug dissolution kinetics was not presented. Only samples with low curcumin content (3-9%) were produced and no explanation was given for the selection of the solvent mixture used.

Therefore, it is clear that a deeper study and understanding of the coprecipitation of curcumin and PVP by SAS is necessary, which is the aim of this work. It is also the intention of this work to test if it is possible to obtain non-coalescing nanoparticles of the composite material, with high curcumin content (up to 25%) and improved dissolution properties, without the aid of a complex mixing device, as reported in the aforementioned work [39]. For the first time, different organic solvent mixtures were studied to understand how adjusting the solvent properties (solvation power) can modulate particle size and recovery of CURC/PVP coprecipitates. The effects of operating parameters, pressure, temperature, initial solution concentration, drug/polymer ratio and solution flow rate, were also investigated.

4.4. Experimental

4.4.1. Materials

Curcumin (CURC, purity ≥ 90%) was purchased from Cayman Chemical and poly (vinyl pyrrolidone) (PVP, Mw = 10 kg/mol), sodium dodecyl sulphate (SDS) and acetic acid (glacial class 8, purity ≥ 99%) were purchased from Sigma Aldrich, UK and Ireland. Ethanol (EtOH, purity = 99.97%) and carbon dioxide (purity ≥ 99.8%) were purchased from VWR Chemicals and BOC, UK, respectively. Acetone (Ac, purity = 99.99%) and acetonitrile (purity = 99.99%) were purchased from Fisher Chemical, UK. All materials were used as-received.

4.4.2. SAS equipment

Figure 4-1 shows the diagram of the SAS process. CO_2 is delivered to the precipitator or high pressure vessel (HPV) by an air driven pump (PowerStar 4; Model: P464, Sprague). Before entering the pump, the CO_2 line passes through a cold bath (Grant C1G) operated below 0°C to promote the condensation of CO_2 and avoid pump cavitation. After the pump, the CO_2 is heated in a hot water bath (Tecam open bath TECAM1 + Grant Type ZA Grant bridge control unit) to achieve the desired operating temperature and then it enters the precipitation vessel via a tube of 1/4 inch OD. The solvent/solution is delivered by an HPLC pump (Waters M-6000). Detail of the precipitation vessel and injection device can be seen in the supplementary material. A stainless steel capillary with internal diameter of 100 µm, external diameter of 1/32 in and 20 cm in length (Thames Restek UK), placed concentric with the CO_2 delivery tube, is used as a nozzle to promote the atomization of the solvent/solution. The nozzle end, where the solution is sprayed out, is placed 2.4 mm lower than the end of CO_2 inlet tube to avoid the partial blockage of the CO_2 tube with polymer as observed in some preliminary experiments.

The high pressure vessel (HPV) used as precipitator is a 500 ml cylindrical jacketed autoclave (Baskerville Scientific, UK) containing three saphire windows. Hot water is continuously supplied to the heating jacket to keep the HPV at the desired operating temperature by the same heat exchanger used to heat up the CO_2 line. The precise reading of the temperature and pressure inside the vessel is enabled by a thermocouple (RS PRO Type K) and pressure transducer (GE Druck PTX 1400) displayed in a digital process indicator (GE Druck DPI 282). The HPV is protected against overpressure by a safety valve (Swagelok SS-4R3A). Precipitated particles are collected by a cellulose thimble (43 mm x 123 mm, Whatman) installed inside the HPV, allowing the flow of CO_2 + organic solvent mixture. The chamber pressure is controlled by a pressure regulator (Tescom 26-1752-24) located in the by-pass of the CO_2 pump. A middle pressure vessel (MPV) of approximately 300 ml (Swagelok double-ended sample cylinder, 316L-HDF4-300-PD) is connected to the precipitator through a micrommetric valve (MMV) (Hoke 1335G4Y), which enables the manual control of the CO_2 flow rate, which is displyed by a mass flow transmitter (Rheonik RHE08) placed in the CO_2 inlet to the HPV. The MPV pressure is controlled by a pressure reducing regulator (GO BP3-1A11I5J114) at around 1 MPa. It is also protected against overpressure by a safety valve (Swagelok SS-4R3A). Due to the pressure drop, the MPV enables the separation of the phases: the organic solution is condensed and collected in bottom of the vessel, while gaseous CO_2 flows out from the top. The CO_2 then passes through the pressure reducing regulator, decreases its pressure to ambient, enters a cyclone to remove fine droplets of solution possibly entrained in the gas phase and is finally directed to vent. A third heat exchanger and pump (Tecam circulator C-400) supply hot water through a flexible pipe which surrounds the MMV and MPV to avoid their freezing due to depressurization. Additional manometers (Budenberg

966GP) are placed in the outlet of the CO_2 cylinder, outlet of the CO_2 pump, inlet of the precipitation vessel and inlet of the MPV.

4.4.3. SAS experimental procedure

Firstly, the precipitator is pressurized with CO_2 until the desired pressure is achieved. At this point, the outlet micrometric valve (MMV) is opened to give a constant flow of sc-CO_2 (40 g/min for all experiments), whilst maintaining pressure (**Figure 4-1**).

Solvent is then pumped into the precipitator through the 100 µm capillary nozzle for enough time to reach quasi-steady state composition of solvent and CO_2, before the pump is switched to a solution of curcumin, PVP or curcumin and PVP. As the precipitation happens inside of the cellulose thimble and glass connector (dimensions shown in the supplementary material), rather than in the whole volume of the vessel, the mean residence time of the materials varies between 2 and 5 minutes, being close to 3 minutes at 40°C and 9.0 MPa (see **Appendix III**), which is the condition used in most experiments. Assuming the behaviour of an ideal stirred tank, at least three residence times of CO_2 and solvent were allowed to flow before the drug solution was injected so the CO_2/solvent ratio in the vessel was at least 95% of the inlet composition.

After the desired amount of curcumin and/or PVP has been injected into the precipitator (usually 400 mg of solute in 40 ml of solution), the pump is reverted to solvent to purge the line (10 ml) and assure all the solution inside the dead volume has been delivered. Then the solvent pump is stopped and fresh CO_2 runs through the system to remove any residual solvent. Finally, the pressure is gradually decreased to ambient, the thimble is removed from inside the high pressure vessel and then the powder is collected with a spatula. Some material remains entrapped in the pores of the thimble and therefore most, but not all, precipitated

powder can be collected. No powder is found outside the thimble or inside the vessel, however possible loss of nanoparticles might occur in the first minutes of particle generation but it should stop as soon as the particles build up a filter cake.

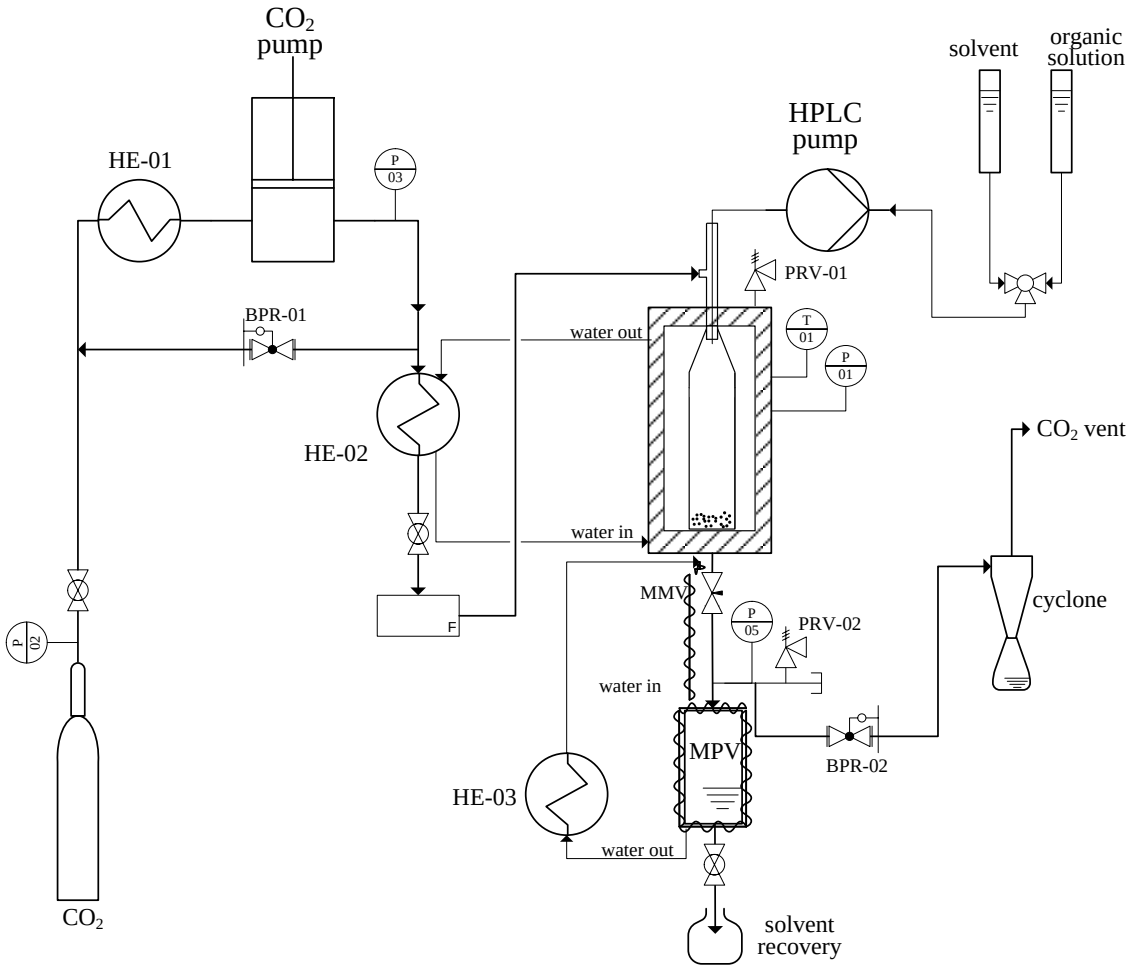

Figure 4-1. SAS experimental setup.

4.4.4. Preparation of the physical mixture

Physical mixtures (PM) of curcumin (CURC) and PVP, obtained by shaking the powders in sealed vials for 5 minutes, were prepared with mass ratios of 1:3 and 1:10 CURC/PVP for comparison with equivalent SAS coprecipitated samples.

4.4.5. Analyses

4.4.5.1. Scanning Electron Microscopy (SEM) and Particle Size Measurements

Scanning Electron Microscopy (SEM - model Philips XL-30 FEG) was used to observe the morphology and particle size of raw materials and coprecipitates at 10 kV and 10 mA. Samples were initially fixed on a double-sided adhesive carbon tape and sputter coated (Polaron SC 7640) with gold for 3 min at 25 mA. Image J analysis software was used to measure particle size and size distribution. Usually 500 particles of each sample in SEM images with different magnifications were accounted. The results are presented as mean diameter ± arithmetic standard deviation.

4.4.5.2. Total product recovery

The total product recovery (Rec.) is an important parameter to assess the efficiency of a process. It was defined as the percentage ratio of the final mass of precipitates collected to the initial mass delivered to the precipitator, as shown below:

$$Rec. = \frac{mass\ (CURC + PVP)\ collected}{mass\ (CURC + PVP) feed} \times 100\%$$

4.4.5.3. Curcumin content and recovery

Accurately weighed samples were dissolved in 50% v/v water-acetone solution and curcumin concentration was determined using an ultraviolet (UV)–visible spectrophotometer (Thermo Scientific Orion AquaMate) to measure the solution absorbance at λ = 425 nm. At this wavelength the absorbance of PVP is negligible (as reported in the supplementary material), while that of curcumin is proportional to its concentration (R^2 = 0.999). All the measurements were taken within few minutes of sample dissolution so the effect of curcumin degradation in contact with water can be considered negligible. Each sample was analysed 3-5 times and the

mean values are reported. Curcumin content (Cont.) was obtained by dividing the mass of curcumin in the analysed sample by the total sample mass, as follows:

$$Cont. = \frac{CURC\ mass\ in\ sample}{total\ sample\ mass} \times 100\%$$

Curcumin recovery (CURC Rec.) was calculated as shown below:

$$CURC\ Rec. = \frac{Rec. \times Cont.}{CURC\ content\ in\ feed}$$

The use of the cellulose thimble described here very conveniently facilitates the recovery of the powder without requiring the precipitator to be completely disassembled from the rig and cleaned after each run. The amount of curcumin retained in the pores of the cellulose thimble (filter) was quantified by washing each filter with a known volume of 50% v/v water-acetone and analysing the resulting solution by (UV)–visible spectrophotometer.

4.4.5.4. High Performance Liquid Chromatography (HPLC)

Raw curcumin and processed samples were analysed by HPLC to investigate possible degradation of curcumin after processing. A gradient elution was employed using an Accucore C18 column (30 mm x 2.1 mm, 2.6 µm, Thermo Scientific) starting with a mobile phase containing acetonitrile and 2% acetic acid initially at 10:90 (v/v). The proportion of the materials was gradually changed to 50:50 by 10 minutes with each run lasting 16 minutes in total. A flow rate of 0.85 ml/min, a column temperature of 30°C, a detection wavelength of 425 nm and an injection volume of 20 µl were employed [40]. Sample solutions were prepared in 50:50 acetonitrile-2% acetic acid and filtered with a 0.22 µm PTFE syringe filter prior to analyses.

4.4.5.5. X-ray diffraction (XRD)

Raw materials and coprecipitates were analysed by X-ray diffraction (XRD, Bruker D8, UK) at 40 kV and 30 mA to determine the degree of crystallinity before and after processing. Patterns were obtained with a beam angle varying from 5° to 40° and a step size of 0.023°.

4.4.5.6. Differential Scanning Calorimetry (DSC)

The thermal behaviour of the samples and unprocessed compounds were assessed by Differential Scanning Calorimetry (Discovery DSC 25, TA Instruments) working with a nitrogen purge of 50 ml/min. A heat-cool-heat cycle was employed to eliminate possible interference of moisture and relieve stress allowing a proper determination of the glass transition temperature (T_g) of the materials [41–43]. First, the samples were placed in aluminium pans and accurately weighed. A hole was made on each lid, allowing the removal of moisture with the purge gas. They were then heated from 50°C to 160°C (above the glass transition of PVP and below the melting point of curcumin) at 20°C/min and after that quench cooled (100°C/min) to the initial temperature. Finally, they were heated to 250°C at 20°C/min. The results presented correspond to the final heating stage in which the glass transition temperature, melting point and enthalpy of fusion were measured. TA Instruments Universal Analysis Software was used to estimate the glass transition temperature (T_g, midpoint of the change in heat capacity) and melting point (T_m, onset temperature) of the samples.

4.4.5.7. Fourier transform infrared spectroscopy (FTIR)

Fourier transform infrared spectroscopy (FTIR, Jasco-6300) equipped with an attenuated total reflectance (ATR) accessory was used to analyse the chemical structure of coprecipitates and

possible molecular interactions generated after processing. 64 scans were taken in a range of 800-4000 cm^{-1} with a resolution of 4 cm^{-1} [44,45].

4.4.5.8. Drug apparent solubility

The apparent solubility of the materials was analysed by adding excess sample to 2 ml of distilled water and then sonicating the suspension at 25°C for 15 minutes. Then the suspension was filtered with a 0.22 µm PTFE syringe filter. Curcumin concentration was determined via UV–visible spectrophotometer. Experiments were performed in triplicates and the mean values are shown.

4.4.5.9. In vitro dissolution studies

In vitro dissolution studies were performed using a USP 2 dissolution apparatus (rotating paddles). Samples were accurately weighed with equivalent amount of curcumin (5 ppm) and incubated at 37 ± 0.5°C in 200 ml of water and 0.25% w/v sodium dodecyl sulphate (SDS). The rotation of the paddles was set to 100 rpm. 2 ml of the solution was withdrawn at different time intervals and replaced with the same volume of fresh medium. Curcumin concentration was then analysed by UV–visible spectrophotometer. Curcumin release was calculated as follows:

$$Release\ (\%) = \frac{m_t}{m_{100\%}} \times 100\%$$

where m_t represents the mass of curcumin released at time t and $m_{100\%}$ is the mass of curcumin at complete dissolution. The tests were performed in triplicates and the mean values are reported.

4.5. Results and discussion

In the SAS process, the selection of the operational conditions is crucial in the success of the precipitation [46,47]. Knowledge of thermodynamics, jet hydrodynamics, mass transfer and crystallization kinetics is required to properly understand the results. Supersaturation is the driving force for precipitation and can be defined as the ratio between the solute concentration in the solvent-CO_2 system and the equilibrium concentration (solubility). Particle size is dependent on the degree of solution supersaturation achieved. High initial solution concentration and low equilibrium concentration of the solute in the fluid phase leads to high supersaturation. Additionally, the supersaturation can be affected by the flow rate of the materials used, responsible for the turbulence and mixing between the phases. The yield of precipitation is especially influenced by the concentration of solute present in the effluent solution [48–50].

For most experiments, pressure, temperature and CO_2 flow rate were kept constant at 40°C, 9.0 MPa and 40 g/min, giving a CO_2 molar fraction (X_{CO2}) between 0.98 - 0.99. According to the literature [51], these conditions would ensure that the precipitation happens in the supercritical region of the mixed solvent-CO_2.

4.5.1. Precipitation of single compounds

Prior to coprecipitation experiments, the compounds were processed separately to compare with their precipitation behaviour (morphology and size) when processed at the same conditions of the coprecipitates. This information is useful to evaluate the success of the coprecipitation and any possible changes in morphology that can occur when the two compounds are processed simultaneously.

PVP is a biocompatible polymer commonly used in drug delivery applications and has been previously precipitated by SAS [24,52,53]. In this work, the experiments were carried out initially using ethanol as solvent, solution concentration of 10 mg/ml and solution flow rate of 1 ml/min, resulting in a CO_2 molar ratio of $X_{CO2} = 0.98$.

Table 4-1 summarises the operational conditions and the results obtained. In run #1 a negligible amount of powder was recovered. Since PVP is highly soluble in ethanol [24], the concentration used might have not been high enough to achieve the minimum supersaturation required for particle generation. In an attempt to increase the supersaturation, in run #2, the solution concentration was increased to 20 mg/ml and the other parameters were kept constant; however this concentration was still not enough and the precipitation was again unsuccessful.

Another way to affect the supersaturation, while keeping the initial solution concentration constant, is by changing the solubility (equilibrium concentration) of the solute in the fluid phase. As the solubility of PVP in ethanol is much higher than in acetone (315 mg/ml versus 7 mg/ml), solvent mixtures of acetone-ethanol (Ac-EtOH) were used. As a consequence of the addition of a poor solvent to PVP (acetone), higher supersaturation levels can be achieved and a higher proportion of the solute precipitates, increasing product recovery. In fact, the addition of acetone into ethanol to produce a 50% v/v mixture allowed a successful precipitation in run #3 and the increase in acetone content to 90% v/v further improved PVP recovery in run #4 from 2.0 to 87.0% (**Table 4-1**). These results demonstrate the significant impact of changing the solute solubility in the fluid phase by the manipulation of the solvent power of the organic solution. Pure acetone was not used to process PVP since PVP solubility in acetone is below 10 mg/ml (approximately 7 mg/ml).

The precipitation of PVP from acetone-ethanol mixtures has been previously investigated. However, contrary to what has been demonstrated here, De Marco et al. [24] reported a process yield of around 90% for experiments with several acetone-ethanol mixture compositions, while Rossmann et al. [52] did not discuss product recovery. **Figure 4-2**a,b shows the comparison between raw and processed PVP obtained from run #4. It is clear that there is a decrease in particle size and a narrowing of the particle size distribution after SAS processing.

Curcumin was then processed at the same conditions used for PVP. The solubility of curcumin in acetone was estimated to be around 58 mg/ml, while in ethanol it was below 5 mg/ml. In the experiment with pure ethanol (run #5), a concentration of 2 mg/ml was used; however no powder could be recovered. When curcumin was processed by a 50-50 Ac-EtOH solution (run #6) and by pure acetone (run #7) at 10 mg/ml, product recovery was 23.4% and 34.8%. Despite the higher initial saturation of the ethanol solution in comparison to the acetone solution, when CO_2 is present in the system a co-solvent effect seems to be taking place with ethanol, as already observed for other systems [54,55]. This explains the lower product recovery when ethanol was used. The lower recovery of curcumin produced by similar processes from alcoholic solutions compared to acetone have also been observed elsewhere [56]. The authors explained that the higher volume expansion and consequently more efficient reduction in solvent power are achieved in the case of acetone possibly leading to higher recovery. In runs #5, #6 and #7, the amount of curcumin retained in the filter decreased from 56.4% to 48.2% and 33.0%, respectively (**Table 4-1**). **Figure 4-2**c shows rod-like crystals of raw curcumin with a wide size distribution, while curcumin processed by a 50% Ac-EtOH (**Figure 4-2**d, run #6) and by pure acetone (**Figure 4-2**e, run #7) has an irregular morphology with smaller dimensions. In **Figure 4-2** it is also possible to see that

PVP and curcumin precipitate in completely different morphologies when processed at the same conditions. This underlines the complexity of the SAS process and its compound-dependent characteristic.

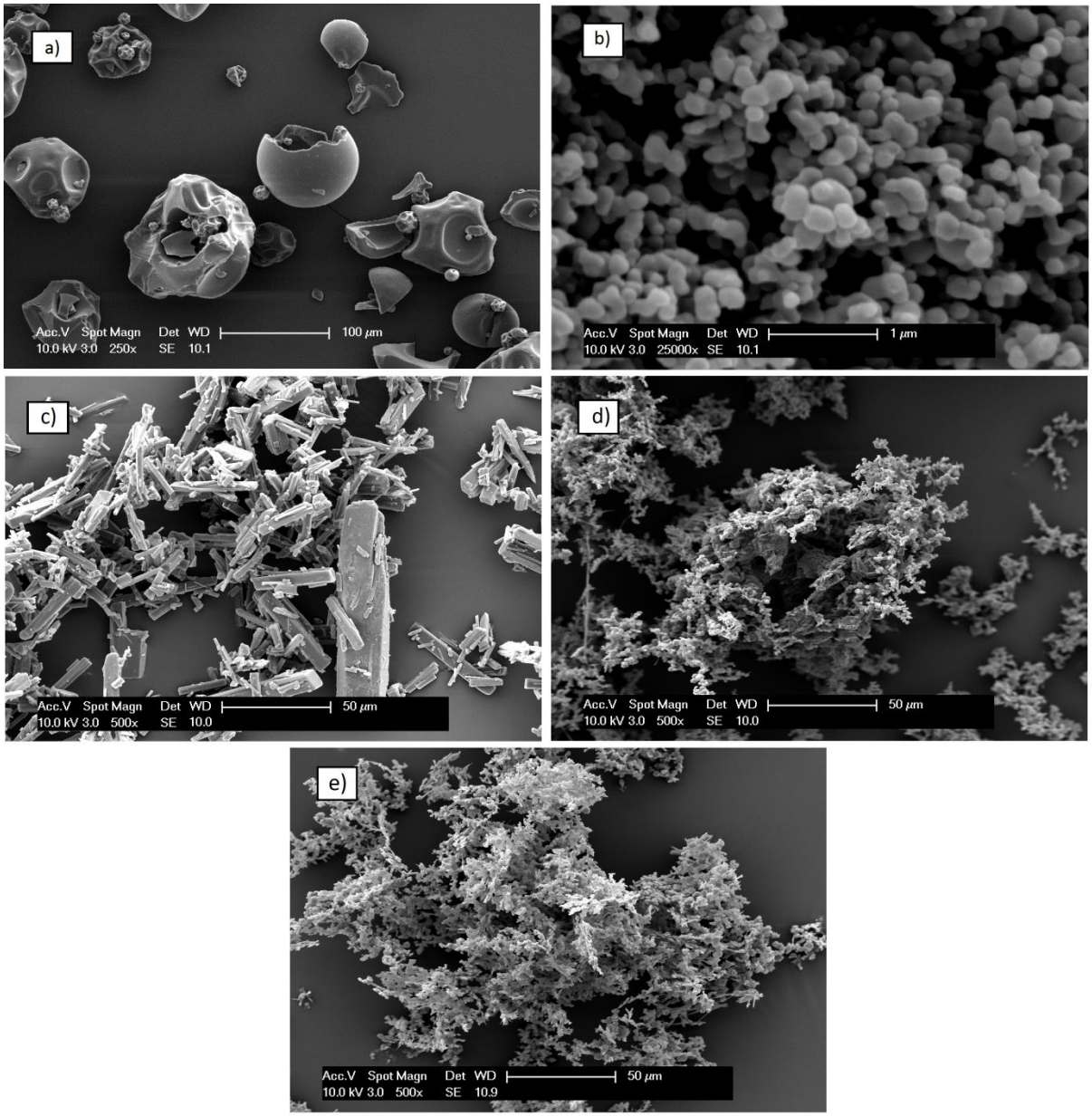

Figure 4-2. SEM images of: a) raw PVP; b) PVP processed by SAS (run #4); c) raw curcumin; d) curcumin processed by SAS from 50% Ac-EtOH (run #6); e) curcumin processed by SAS from acetone (run #7).

Table 4-1. Experimental conditions and results (*p* = pressure; f = solution flow rate; C_{TOT} = total solute concentration; m.d.: mean diameter; s.d.: standard deviation; SMP: sub-microparticles; NP: nanoparticles; CM: coalescing material). Experiments ran at 40°C and CO_2 flow rate of 40 g/min.

#	*p* (MPa)	T (°C)	f (ml/min)	C_{TOT} (mg/ml)	solvent	Solvent volumetric composition Ac-EtOH	Drug/polymer mass ratio	Total product recovery (%)	Curcumin recovery (%)	Curcumin retained in the filter (%)	m.d. (nm)	s.d. (nm)	Morphology
1	9.0	40	1	10	EtOH	0-100	pure PVP	≈ 0	-	-	-	-	-
2	9.0	40	1	20	EtOH	0-100	pure PVP	≈ 0	-	-	-	-	-
3	9.0	40	1	10	Ac-EtOH	50-50	pure PVP	2.0	-	-	-	-	-
4	9.0	40	1	10	Ac-EtOH	90-10	pure PVP	87.0	-	-	123	27	SMP
5	9.0	40	1	2	EtOH	0-100	pure curcumin	≈ 0	≈ 0	56.4	-	-	-
6	9.0	40	1	10	Ac-EtOH	50-50	pure curcumin	23.4	23.4	48.2	-	-	-
7	9.0	40	1	10	Acetone	100-0	pure curcumin	34.8	34.8	33.0	-	-	irregular
8	9.0	40	1	10	EtOH	0-100	1:3	43.1	45.5	41.4	-	-	irregular
9	12.0	40	1	10	EtOH	0-100	1:3	63.1	68.1	25.5	-	-	irregular
10	9.0	40	1	10	Ac-EtOH	10-90	1:3	58.0	65.3	29.3	327	102	SMP
11	9.0	40	1	10	Ac-EtOH	30-70	1:3	74.3	76.6	10.2	177	57	SMP
12	9.0	40	1	10	Ac-EtOH	50-50	1:3	77.6	78.6	6.7	135	36	SMP
13	9.0	40	1	10	Ac-EtOH	70-30	1:3	87.1	89.0	2.5	96	25	NP

#	*p* (MPa)	T (°C)	f (ml/min)	C_{TOT} (mg/ml)	solvent	Solvent volumetric composition Ac-EtOH	Drug/polymer mass ratio	Total product recovery (%)	Curcumin recovery (%)	Curcumin retained in the filter (%)	m.d. (nm)	s.d. (nm)	Morphology
14	9.0	40	1	10	Ac-EtOH	90-10	1:3	90.0	89.2	0.8	51	12	NP
15	8.0	40	1	10	Ac-EtOH	70-30	1:3	56.4	59.6	20.8	181	48	SMP
16	12.0	40	1	10	Ac-EtOH	70-30	1:3	79.1	88.1	6.7	67	17	NP
17	9.0	35	1	10	Ac-EtOH	70-30	1:3	89.5	94.9	5.0	72	20	NP
18	9.0	50	1	10	Ac-EtOH	70-30	1:3	76.9	83.7	9.9	176	56	SMP
19	9.0	40	1	5	Ac-EtOH	70-30	1:3	80.7	88.9	5.6	65	14	NP
20	9.0	40	1	20	Ac-EtOH	70-30	1:3	80.2	90.5	6.2	117	30	SMP
21	9.0	40	1	10	Ac-EtOH	50-50	1:10	60.7	60.2	26.3	-	-	CM
22	9.0	40	1	10	Ac-EtOH	70-30	1:10	79.7	79.9	5.5	173	76	SMP
23	9.0	40	1	10	Ac-EtOH	70-30	1:20	69.2	67.9	9.6	205	49	SMP
24	9.0	40	0.5	10	EtOH	0-100	1:10	34.3	36.1	48.7	-	-	CM
25	9.0	40	0.5	10	Ac-EtOH	10-90	1:10	47.6	50.8	24.9	-	-	CM
26	9.0	40	0.5	10	Ac-EtOH	70-30	1:10	79.7	82.3	4.0	220	85	SMP

4.5.2. Coprecipitation of CURC/PVP

It has been demonstrated elsewhere that PVP can interfere in the crystallisation kinetics of some compounds by inhibiting the association of drug molecules to form crystal nuclei during the solvent removal from a drug-PVP solution [10,12,57,58].

In the second phase of this work, the SAS process was used to produce coprecipitates of curcumin and PVP and the effect of adjusting the solvation power of the organic solvent, pressure, temperature, initial solution concentration, mass ratio between drug and polymer and solution flow rate were explored. Five experiments were run in triplicates and the relative standard deviation of total product recovery and curcumin recovery was typically below 5%, showing that the conditions were well controlled. The results shown correspond to the mean values.

4.5.2.1. Effect of solvent mixture composition

Knowing that the relative composition of acetone in the solvent mixture affects the recovery of PVP particles, mixtures of acetone-ethanol with increasing acetone volume fraction from 0 to 90% were used for the coprecipitation experiments (#8-14). Tests were carried out at the same conditions used for the precipitation of the single compounds (40°C, 9.0 MPa, X_{CO2} = 0.98 and 10 mg/ml overall solution concentration) with drug/polymer mass ratio of 1:3. 100% acetone was not used because a clear solution containing both compounds could not be obtained at the specified concentration. The effect of adjusting the solution supersaturation through the manipulation of the solvent power, while keeping the overall solution concentration constant, is demonstrated in this section. Similarities in the vapour-liquid equilibria of the systems CO_2-ethanol and CO_2-acetone can be seen in the supplementary material.

The first interesting result can be seen by comparing run #1 (PVP alone), run #5 (curcumin alone) and run #8 (coprecipitation) performed at the same conditions with ethanol as solvent. For the single compounds no powder was obtained, while in the coprecipitation the total product recovery was 43.1%. Similarly, in run #3 (PVP alone) and run #6 (curcumin alone) product recovery was 2% and 23.4%, respectively, increasing to 77.6% in run #12 when the materials were coprecipitated from a 50-50 Ac-EtOH solution (**Table 4-1**). These results suggest a synergistic effect in improving the supersaturation of the solution when both compounds are present and how the presence of two different solutes can affect the high pressure equilibrium of the system solvent/antisolvent, leading to different results at the same process conditions. **Figure 4-3**a reveals that two different morphologies, crystals (curcumin) and irregular particles (PVP), were obtained when pure ethanol was used (run #8), indicating that coprecipitation was unsuccessful since the compounds precipitated separately. Particle size could not be measured. It was considered that this behaviour may be indicative of precipitation outside of the supercritical region caused by the solutes elevating the critical pressure of the mixture. To test this, an experiment was performed at 12.0 MPa (run #9), far beyond the critical point of the system CO_2-ethanol (8.16 MPa [51]), to ensure supercritical conditions. Curcumin crystals could still be seen, as shown in **Figure 4-3**b, suggesting that the separate precipitation is related to something other than effects on the CO_2-ethanol vapour-liquid equilibrium. As the solubility in ethanol of curcumin and PVP is approximately 5 mg/ml and 315 mg/ml, respectively, the difference in the supersaturation ratio (initial concentration/solubility) of the two compounds might be so high that simultaneous precipitation would not be achieved. On the other hand, higher pressure increased product recovery from 43.1% (run #8) to 63.1% (run #9), suggesting a decrease in the solute solubility in the fluid phase.

In run #10, the addition of 10% acetone resulted in a successful coprecipitation, as shown in **Figure 4-3**c. Spherical, largely uniform particles were produced and curcumin rod/filament morphology could no longer be detected indicating that curcumin is well dispersed in the polymer matrix. A possible reason for this behaviour may be that addition of acetone to ethanol simultaneously decreases the solubility of PVP and increases the solubility of curcumin (as it does at room temperature), leading to more similar supersaturation ratios of the two solutes when mixed with CO_2. The composite material retained the morphology of the polymer as previously observed in several studies with PVP-drug [33], demonstrating that the precipitation behaviour is now dominated by PVP. In **Figure 4-4**a it is interesting to observe the gradual increase in the total product recovery (from 43.1 to 90.0%) and decrease in the mean particle size of coprecipitates (from 327 to 51 nm) by increasing the acetone content from 0 to 90%. SEM images shown in **Figure 4-3**c,d,e,f,g clearly demonstrates this tendency. The size range changed from sub-microparticles to nanoparticles and the particle size distribution narrowed (**Figure 4-4**b). De Marco et al. [24] explained that the variation of the solvent mixture composition can affect the SAS process in two different ways: by changing the solvation power of the solvent (ability of the solvent to dissolve the solute at fixed conditions) and/or the mixing behaviour of the injected solution with CO_2 (large or sharp pressure transition range from two-phase to one-phase mixing). In terms of mixing regimes, ethanol and acetone have been shown to have similar behaviour (sharp transition pressure range) [24], therefore the decrease in the mean particle size can be explained by the decrease in the solvation power as acetone is added to the solvent mixture. Other authors have suggested that acetone repels the polymer molecules which then tend to be arranged in a more compact configuration, consequently decreasing particle size [24,53]. The amount of curcumin retained in the filter gradually decreased from 41.1 to 0.8% as the acetone content

increased from 0 to 90% (**Table 4-1**). Probably, when more acetone is present in the system, higher supersaturation can be achieved and the material precipitates in the first centimetres of the precipitator. The concentration of the fluid phase decreases and less curcumin is left to nucleate within the thimble walls when passing through it. A decrease in the degree of particle coalescence was also observed with the addition of acetone, explained by the fact that acetone experiences a higher volume expansion than alcohols when in contact with sc-CO_2 [59,60], being more efficiently removed from the precipitating particles.

Figure 4-5a shows the comparison between curcumin content in the processed samples and in the feed solutions. For all experiments, the contents before and after processing are similar; therefore the values of curcumin recovery are close to the respective values of the total product recovery, gradually increasing from 45.5 (run #8) to 89.2% (run #14) with increasing acetone content. This demonstrates that the conditions selected are appropriate to precipitate both compounds in the designed proportion since their proportion was kept almost the same in the feed solution and in the coprecipitated powder. It is also interesting to observe in **Figure 4-5**b that no degradation of curcumin occurred after SAS processing. Curcumin retention time (highest peak) was around 7.6 minutes with impurities being detected slightly before (small peak). By comparing the area of the peaks, curcumin concentration was determined to be around 90% in all samples (raw curcumin, #6 and #13). As it is not the aim of this work, the nature of the impurities was not determined, however curcumin is known to be found with other two curcuminoids (demethoxycurcumin, and bis-demethoxycurcumin) in turmeric extracts which have been analysed in many works elsewhere [40,61–63].

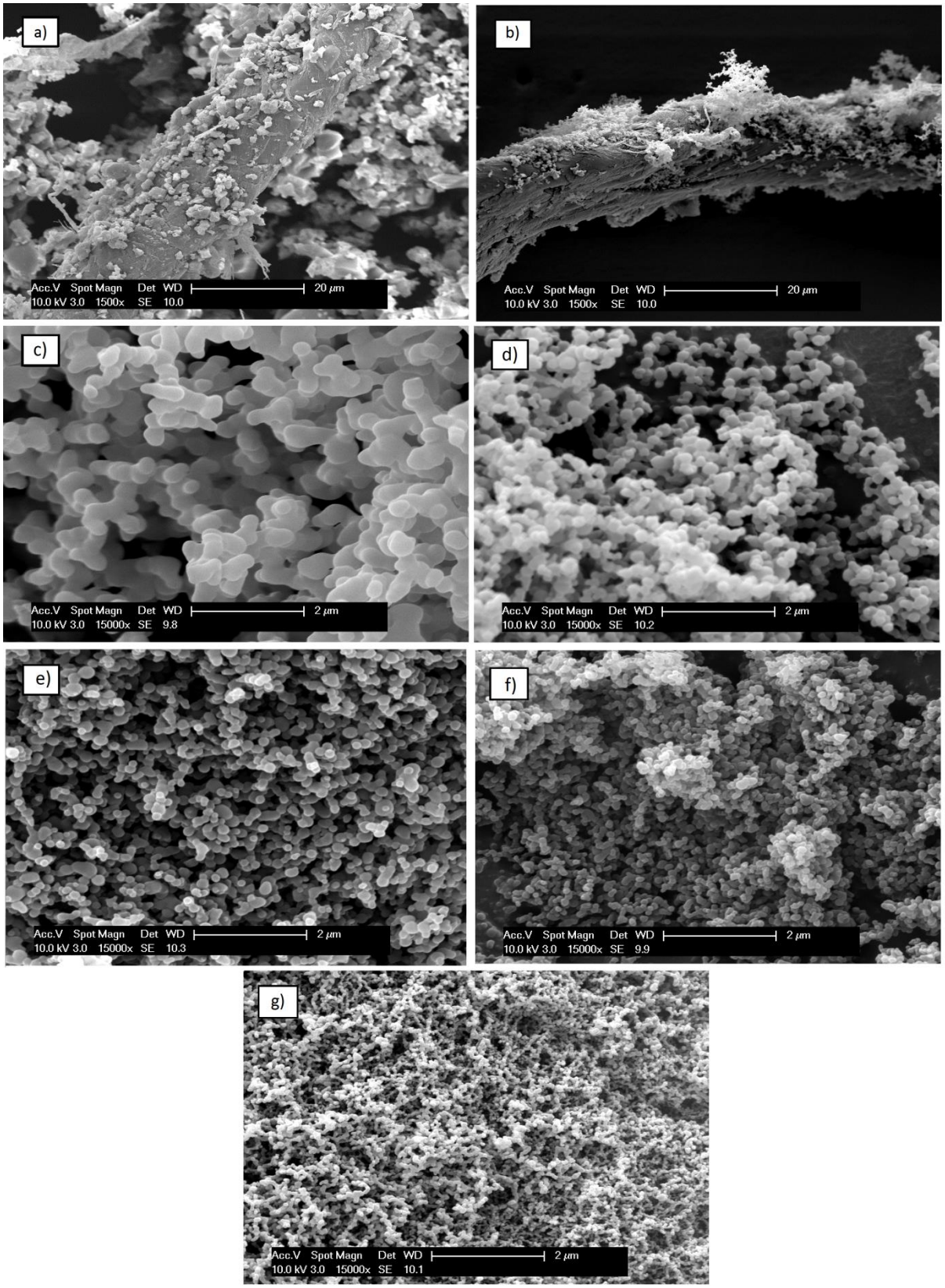

Figure 4-3. SEM images of CURC/PVP processed from pure ethanol at 40°C, 1.0 ml/min, 1:3 CURC/PVP ratio and different pressures: a) 9.0 MPa (run #8); b) 12.0 MPa (run #9); and samples processed at 9.0 MPa, 40°C, 1.0 ml/min, 1:3 CURC/PVP ratio from different Ac-EtOH compositions: c) 10-90 (run #10); d) 30-70 (run #11); e) 50-50 (run #12); f) 70-30 (run #13); g) 90-10 (run #14).

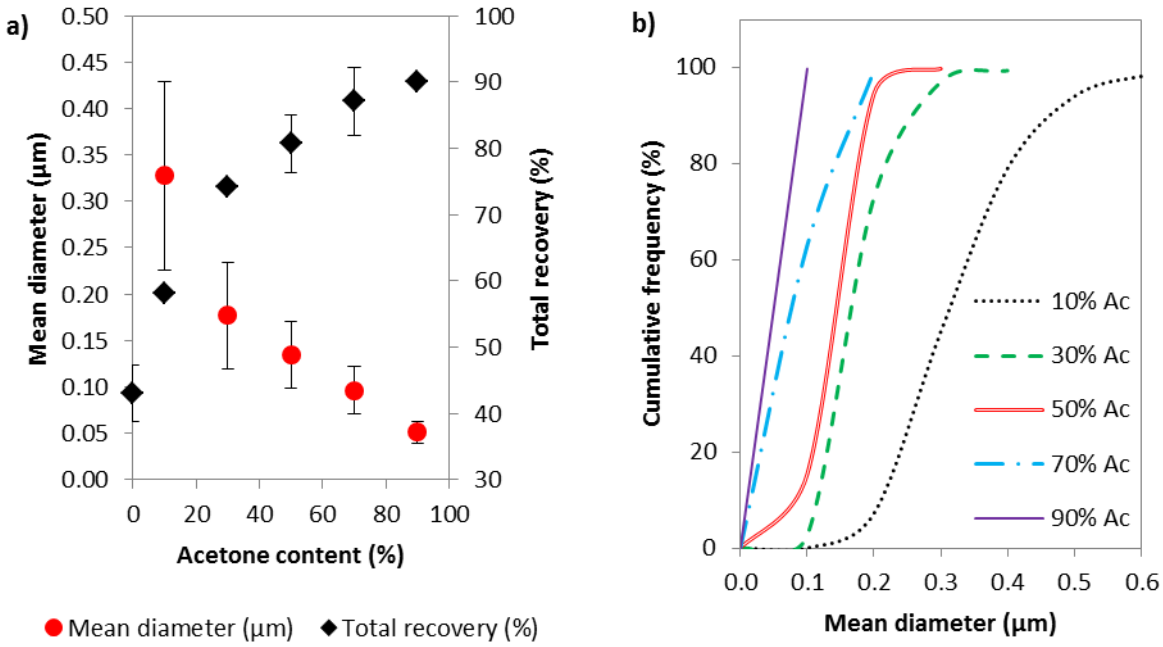

Figure 4-4. Results for coprecipitates obtained from solutions with different acetone (Ac) contents at 9.0 MPa and 40°C (run #8, #10-14, **Table 4-1**): a) mean diameter and total product recovery (error bars show standard deviation); b) particle size distribution.

The effect of solvent can also be analysed in runs #21-22 (**Figure 4-6**a,b) performed at 1:10 CURC/PVP ratio and runs #24-26 (**Figure 4-6**d,e,f) performed at 1:10 CURC/PVP ratio and 0.5 ml/min. Similar trends as runs #10-14 were observed in terms of total product recovery, curcumin recovery (**Table 4-1**) and particle size (**Figure 4-6**), supporting the discussion previously presented. As curcumin recovery did not increase for acetone content higher than 70% (**Table 4-1**), a 70-30 Ac-EtOH solution was selected in order to analyse the effect of other operational parameters on particle size and recovery. Moreover, 30% of ethanol gives flexibility to work with large amounts of PVP. Therefore, the next experiments will be compared with run #13, analysing the effect of pressure, temperature and initial solution concentration.

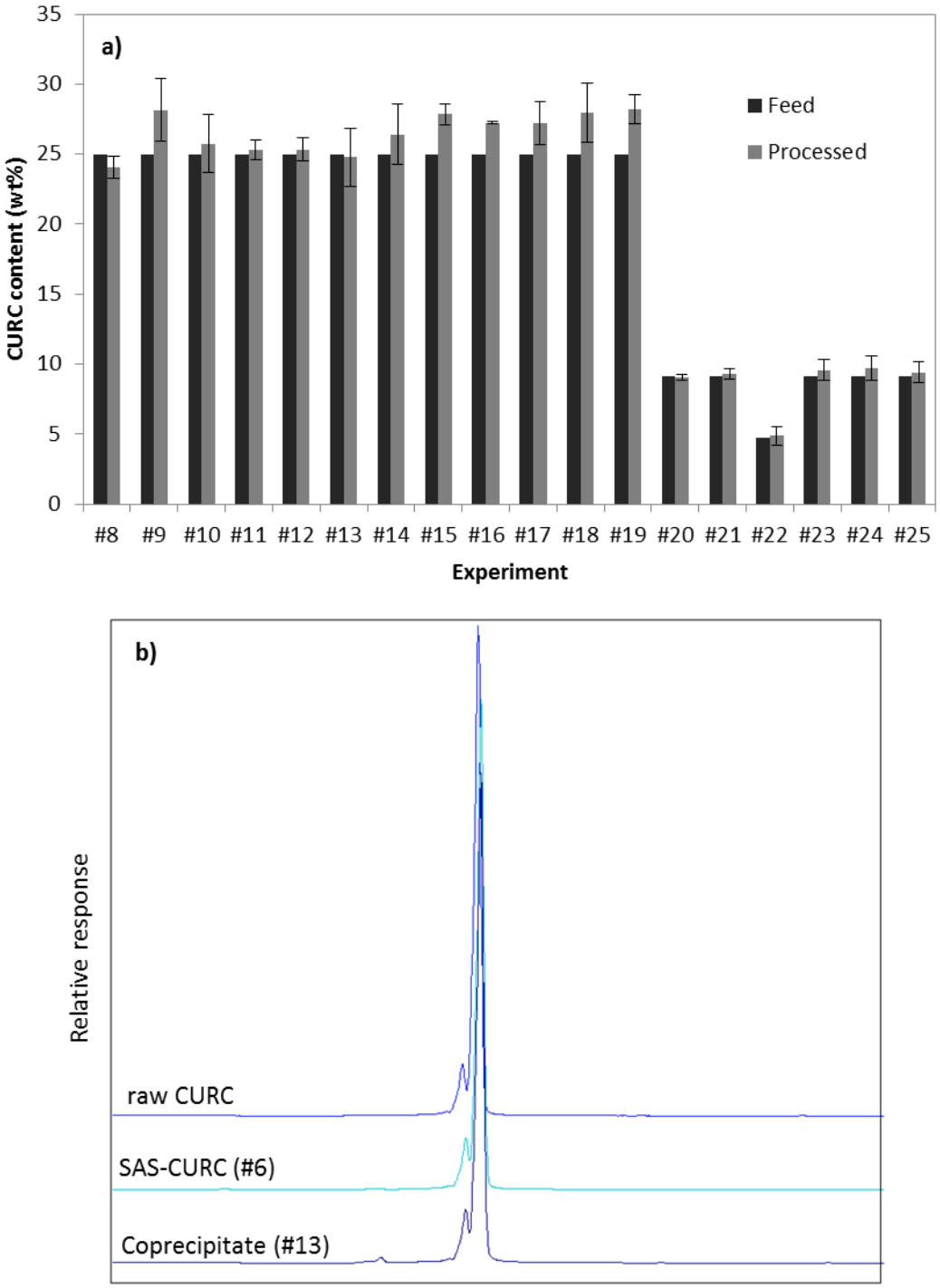

Figure 4-5. a) Curcumin content as fraction of the total solute in the feed solutions and SAS-processed samples analysed by UV-visible spectrophotometer; b) HPLC measurements of raw curcumin and processed samples. Experiment conditions are shown in **Table 4-1**.

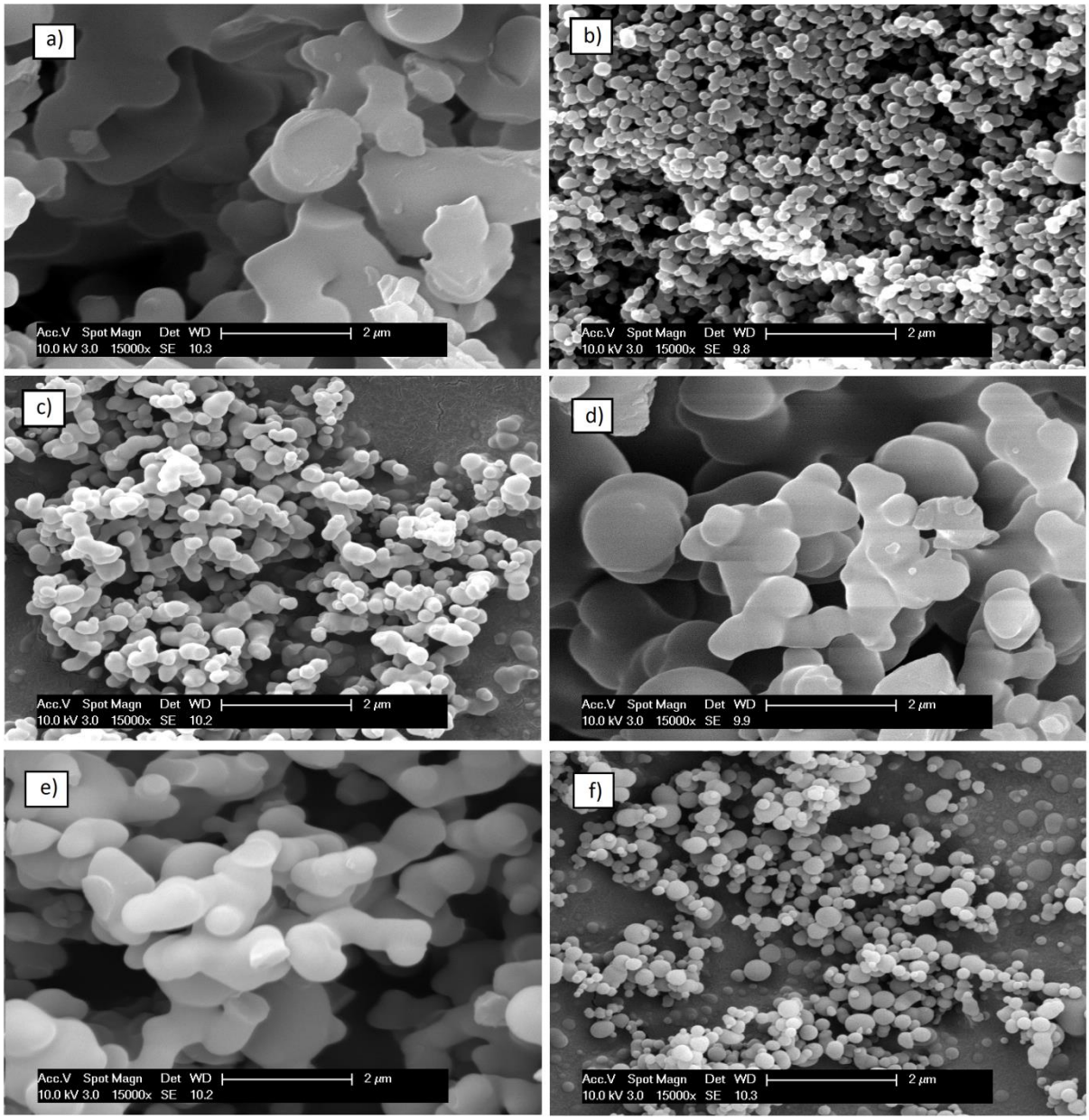

Figure 4-6. SEM images of CURC/PVP processed at 40°C, 9.0 MPa, 1.0 ml/min from different Ac-EtOH compositions and CURC/PVP ratios: a) 50-50, 1:10 (run #21); b) 70-30, 1:10 (run #22); c) 70-30, 1:20 (run #23); and processed at 0.5 ml/min: d) pure EtOH, 1:10 (run #24); e) 10-90, 1:10 (run #25) f) 70-30, 1:10 (run #26).

4.5.2.2. Effect of pressure

The effect of pressure was analysed by keeping the operational conditions the same as in run #13 (40°C, 1 ml/min, X_{CO2} = 0.98, 1:3 CURC/PVP ratio and 10 mg/ml overall solution concentration in a 70-30 Ac-EtOH solution) and changing the pressure from 9.0 MPa to 8.0 MPa (#15) and 12.0 MPa (#16).

As the critical pressures of the CO_2-ethanol and CO_2-acetone systems are approximately 8 MPa at 40°C, the operational point in run #15 might be located in the biphasic region. The density of CO_2 under these conditions (277.9 kg/m^3 [64]) is around 43% lower than at 9.0 MPa (485.5 kg/m^3 [64]). This lowers the power of CO_2 to solubilise the organic solvents and leads to a less effective supersaturation, which might explain the large increase in particle size from 96 nm (#13) to 181 nm (run #15, **Figure 4-7**a) and decrease in curcumin recovery from 89.0 (#13) to 59.6% (#15). A high proportion (around 21%) of the curcumin injected was retained in the cellulose thimble probably due to the presence of liquid in the precipitator (operating point in the biphasic region). When the pressure was increased to 12.0 MPa (#16, **Figure 4-7**b), the CO_2 density increased by 48% and the opposite effect was observed for particle size which decreased to 67 nm. While product recovery (curcumin + PVP, 79.1%) was lower than at 9.0 MPa, curcumin recovery was not much affected, indicating that at higher pressure the precipitation of PVP is less favourable.

Figure 4-8 illustrates how the mean particle diameter of coprecipitates and curcumin recovery varies from the central experiment (#13) as a function of the variation in the CO_2 density with pressure and other operational parameters, which will be discussed in the following sections.

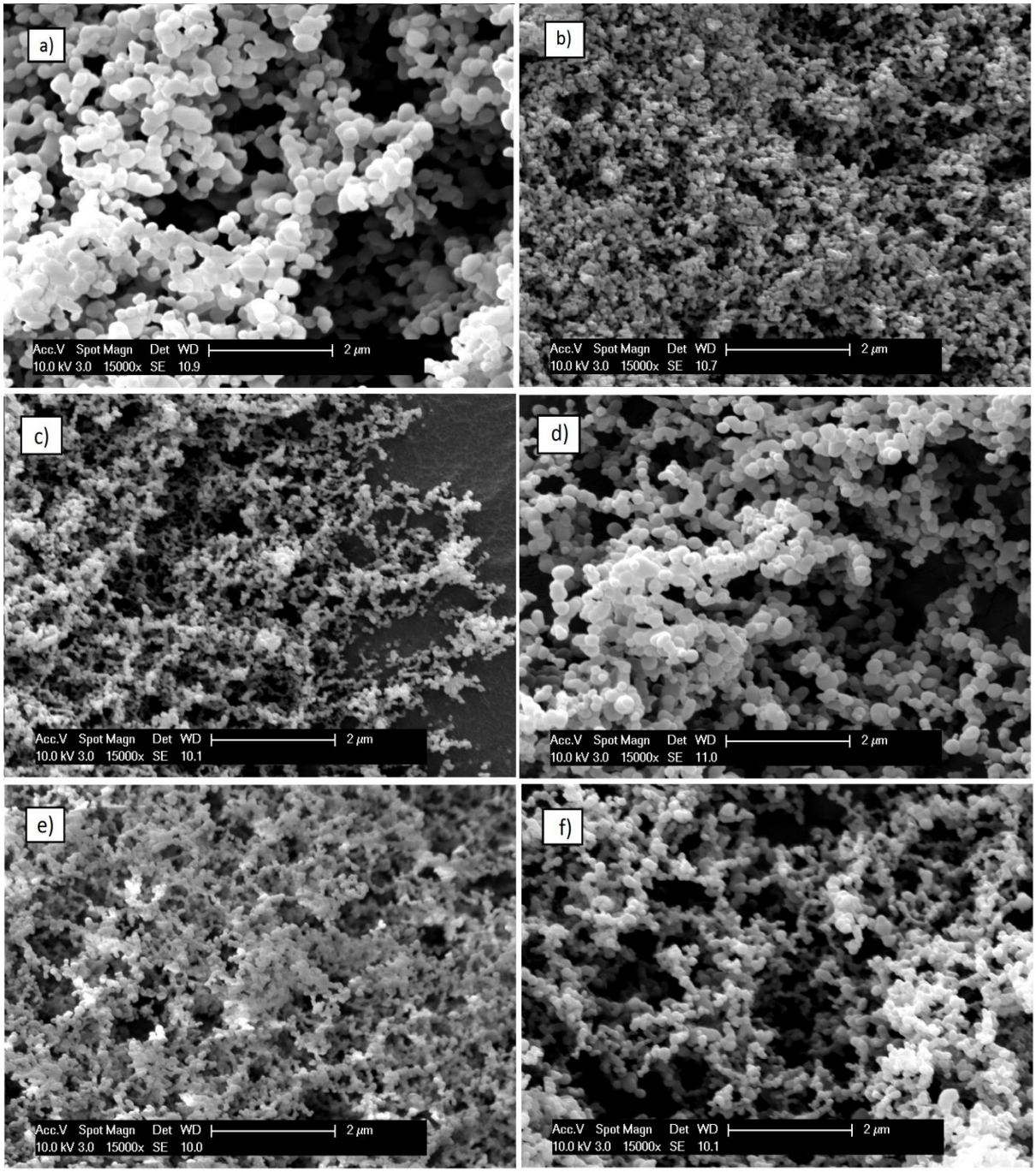

Figure 4-7. SEM images of CURC/PVP processed at different conditions: a) run #15 (8.0 MPa); b) run #16 (12.0 MPa); c) run #17 (35°C); d) run #18 (50°C); e) run #19 (5 mg/ml); f) run #20 (20 mg/ml). The complete set of operational conditions is shown in **Table 4-1**.

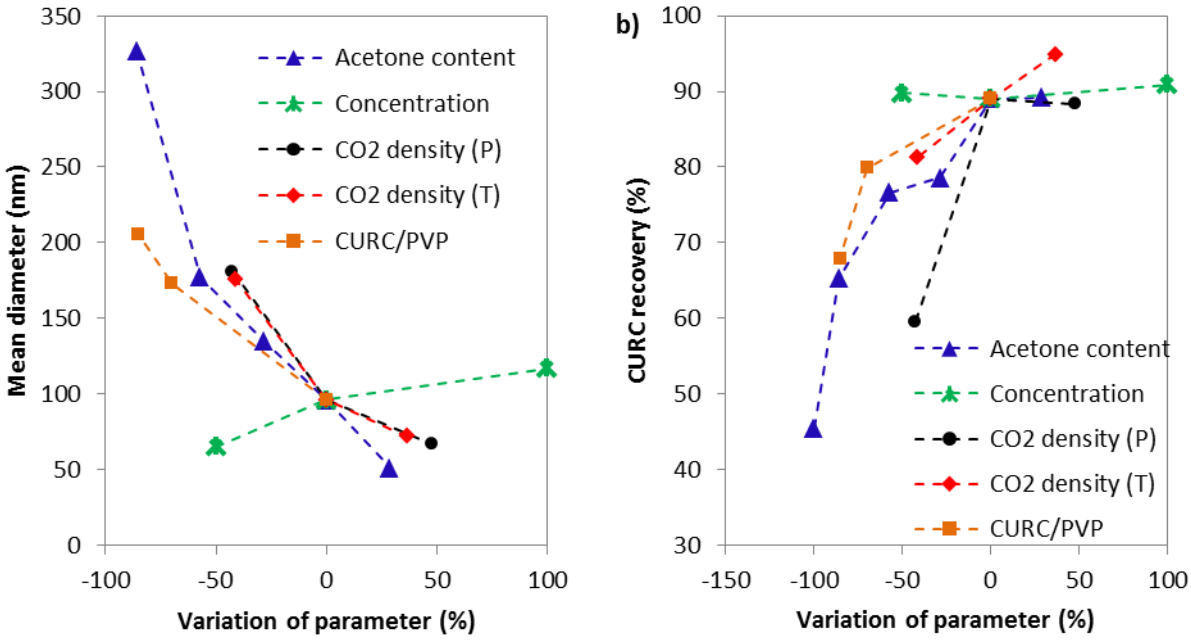

Figure 4-8. Values of a) mean particle diameter and b) curcumin recovery as a function of the variation of different operational parameters in comparison with run #13 (centre point). The standard deviation of curcumin recovery is below 5% and that of the mean diameter is shown in **Table 4-1**.

4.5.2.3. Effect of temperature

The effect of temperature was analysed by keeping the operational conditions the same as in run #13, (9.0 MPa, 1 ml/min, X_{CO2} = 0.98, 1:3 CURC/PVP ratio and 10 mg/ml overall solution concentration in a 70-30 Ac-EtOH solution) which was performed at 40°C, and changing the temperature to 35°C (#17) and 50°C (#18).

Figure 4-7c,d shows the particles obtained at 35°C (#17) and 50°C (#18) measuring 72 and 176 nm, respectively. At 35°C the density of CO_2 is 662.1 kg/m^3 (36% higher than 485.5 kg/m^3 at 40°C[64]) while at 50°C it is equal to 285.0 kg/m^3 (41% lower than at 40°C). It is interesting to observe in **Figure 4-8**a that similar CO_2 density variations from the central experiment (run #13) caused by temperature and pressure lead to the production of coprecipitates with similar particle sizes. Experiments performed at high CO_2 density (low temperature or high pressure) yielded smaller particles due to the improved solvation power of CO_2, while the opposite happened with a decrease in CO_2 density (high temperature or low

pressure). These results demonstrate the relevance of the fluid density in designing SAS experiments but it is also important to be aware that other parameters such as fluid viscosity and solute vapour pressure might play a role in determining particle size as the temperature is changed.

Although similar particle sizes were obtained in runs #15 and #18 (low density) and runs #16 and #17 (high density), both changes in pressure had a negative effect on curcumin recovery (**Figure 4-8**b). In contrast, at 35°C almost all curcumin was recovered, possibly because the vapour pressure and solubility of curcumin in the fluid phase decreased.

4.5.2.4. Effect of solution concentration

The effect of concentration was analysed by keeping the operational conditions the same as in run #13 (9.0 MPa, 40°C, 1 ml/min, X_{CO2} = 0.98, 1:3 CURC/PVP ratio and 70-30 Ac-EtOH solution) and changing the overall concentration from 10 mg/ml (run #13) to 5 mg/ml (run #19) and 20 mg/ml (run #20). The same amount of material was delivered to the precipitator but the solution volume was adjusted (doubled or halved) to obtain the desired concentration.

A low impact on precipitation was observed. In fact, curcumin recovery changed less than 2% as the concentration was increased or decreased (**Figure 4-8**b). Particle size decreased to 65 nm at lower concentration (**Figure 4-7**e) and increased to 117 nm at higher concentration (**Figure 4-7**f), also demonstrating a small influence of concentration (**Figure 4-8**a). Although higher supersaturation occurs in more concentrated solutions, particle growth by condensation is also intensified [50], explaining the results obtained here.

4.5.2.5. Effect of drug/polymer mass ratio

The effect of CURC/PVP mass ratio was studied by decreasing the ratio from 1:3 (run #13) to 1:10 (run #22) and 1:20 (run #23). All other operating conditions were kept the same as run

#13 (9.0 MPa, 40°C, 1 ml/min, X_{CO2} = 0.98, 10 mg/ml overall solution concentration in a 70-30 Ac-EtOH solution). In order to keep the overall concentration constant, the decrease in CURC/PVP ratio was achieved by simultaneously decreasing the concentration of curcumin and increasing the concentration of PVP.

The morphologies of the particles produced at 1:3, 1:10 and 1:20 CURC/PVP ratios are shown in **Figure 4-3**f and **Figure 4-6**b,c, respectively. The results in **Table 4-1** demonstrate a gradual decrease in total product recovery from 87.1% to 79.7% and 69.2% as CURC/PVP ratio decreased. Similarly, curcumin recovery decreased (**Figure 4-8**b) since the curcumin content in the processed sample and feed solution were almost unchanged (**Figure 4-5**a) (the ratio between the drug and polymer remained the same in the precipitated powder). On the other hand, particle size increased from 96 nm to 173 nm and further to 205 nm in these experiments (**Figure 4-8**a). This behaviour has been reported before for the coprecipitation of PVP with other APIs [8,9]. Although the overall concentration was kept constant, the increase in the concentration of the polymer (from 7.5 mg/ml at 1:3 ratio to 9.5 mg/ml at 1:20 ratio) might have increased the viscosity of the solution, which decreases the nucleation rate and lead to the formation of larger and more coalescing particles [48,65,66]. It is also important to highlight that an increase in the concentration of PVP can additionally affect the particle-fluid interfacial tension. This parameter might significantly influence particle size, as demonstrated by Erriguible et al. [67].

Runs #12 (**Figure 4-3**e) and #21 (**Figure 4-6**a) performed with 50% Ac-EtOH solution can also be used to analyse the effect of decreasing the drug/polymer ratio from 1:3 to 1:10. Once again, the same trend was observed: a decrease in total product recovery and curcumin recovery and increase in particle size. It was also noticed that at higher PVP concentration more acetone is needed in the solvent mixture to generate non-coalescing particles. For

coprecipitates with 1:3 CURC/PVP ratio, particles become discrete with 30% acetone (**Figure 4-3**d). However, highly coalescing material is still obtained at 1:10 ratio (**Figure 4-6**a) when the acetone content was 50% (run #21), which prevented the measurement of the particle size. The reason for this behaviour might be that by increasing PVP concentration in the solution, the viscosity of the liquid phase increases, decreasing the supersaturation and nucleation rate and leading to a less efficient mixing and solvent removal from the particles, as previously explained. Therefore, the addition of acetone, which is less viscous and poorer solvent to PVP than ethanol, favours the formation of discrete particles.

4.5.2.6. Effect of solution flow rate

The effect of solution flow rate was analysed by keeping the operational conditions unchanged (40°C, 9.0 MPa and 10 mg/ml overall solute concentration) and decreasing the solution flow rate to 0.5 ml/min (X_{CO2} = 0.99) for a 70-30 Ac-EtOH solution and 1:10 CURC/PVP ratio. This CURC/PVP ratio was selected because the effect of particle coalescence was more pronounce at 1:10 than at 1:3 and therefore we wanted to investigate the possibility of producing discrete particles with higher PVP content. Run #26 (0.5 ml/min) can be compared to run #22 (1.0 ml/min) as all other operating conditions were not changed. The SEM image presented in **Figure 4-6**f (run #26) shows the formation of discrete sub-microparticles compared to the less discrete particles of run #22 (**Figure 4-6**b).

Solution flow rate is supposed to have a minor impact on particle size [50,67,68] since it may cause two opposite effects in relation to the supersaturation. For instance, a decrease in the solution flow rate can lead to a less efficient mixing (which decreases the local supersaturation) and it can also decrease the solvent composition in the fluid phase which decreases the solute solubility and hence increases the maximum attainable supersaturation. Therefore, lower impact is expected comparing to other parameters which affect the vapour-

liquid phase equilibrium (pressure and temperature) [50]. As particle size, morphology and product recovery are affected in different extent by these phenomena, it was observed a small increase in particle size from 173 nm (run #22) to 220 nm (run #26), while product recovery was not significantly affected, with values close to 80% (**Table 4-1**). Particle coalesce was reduced at lower flow rates possibly due to the fact that there is more time for the precipitating particles to dry before they collide with each other, as explained by Gokhale et al. [53]. Similar effects of the solution flow rate on particle size have been reported elsewhere for the precipitation of PVP alone by SAS [53].

4.5.3. X-Ray Diffraction (XRD)

The degree of crystallinity of the samples was analysed by XRD. **Figure 4-9** shows that curcumin alone processed by SAS (SAS-CURC, run #7) is less crystalline than raw curcumin (CURC) as the intensity of the peaks decreased. The physical mixture (PM 1:3) kept all the curcumin characteristic peaks but with lower heights than raw CURC due to the presence of PVP, which is an amorphous polymer. The comparison of the PM (1:3) with the coprecipitates shows that amorphous formulations were formed in all coprecipitates (runs #11, #13, #14).

4.5.4. Differential Scanning Calorimetry (DSC)

Differential Scanning Calorimetry (DSC) was used to access the degree of crystallinity of the samples and possible interactions between curcumin and PVP after processing. **Figure 4-10** shows a sharp endothermic peak corresponding to the melting point of raw curcumin at T_m = 182°C and enthalpy of fusion of ΔH_f = 130.9 J/g, indicating the crystallinity of the compound. Other works have reported similar values for the melting point of unprocessed curcumin but fusion enthalpy varying from 93 – 121 J/g [14,16,56,69,70], which can be explained by

differences in the purity of the sample, not always specified, and differences in the crystal form. PVP, on the other hand, does not show any melting point peak, demonstrating its amorphous structure and glass transition at T_g = 150°C (midpoint of the change in heat capacity). In the physical mixture (PM 1:3) the curcumin characteristic peak was slightly shifted to lower temperature. This behaviour has been observed by other researchers and may be attributable to a solvent effect of PVP [14,16]. For the SAS coprecipitate obtained in run #13, no endothermic peak could be detected in the region of curcumin melting point which indicates that amorphous curcumin was obtained after SAS processing with PVP, confirming the XRD results (section 4.5.3). The presence of a single T_g supports the hypothesis of a single phase and the decrease in T_g compared to the one of PVP is attributed to the plasticizing effect of the drug molecularly dispersed in the polymeric matrix [13,71].

4.5.5. Fourier Transform Infrared Spectroscopy (FTIR)

The infrared spectra of the compounds before and after processing were analysed in order to identify possible interactions between curcumin and PVP. **Figure 4-11** shows the results obtained. Raw curcumin (CURC) presents an absorption band at 3504 cm^{-1} corresponding to O-H stretching vibration. Other peaks can be identified at 1626 cm^{-1} (C=O, C=C), 1601 cm^{-1} (C=C aromatic), 1427 cm^{-1} (C-O phenol), 1025 cm^{-1} (C-O-C), 960 cm^{-1} (benzoate trans-CH) and 855 cm^{-1} (C-H aromatic) [39,72]. The FTIR spectrum of PVP shows a peak at 3466 cm^{-1} assigned to the stretching vibration of O-H and other peaks at 2883, 1651 and 1284 cm^{-1}, corresponding to C-H, C=O and C-N, respectively [10,39].

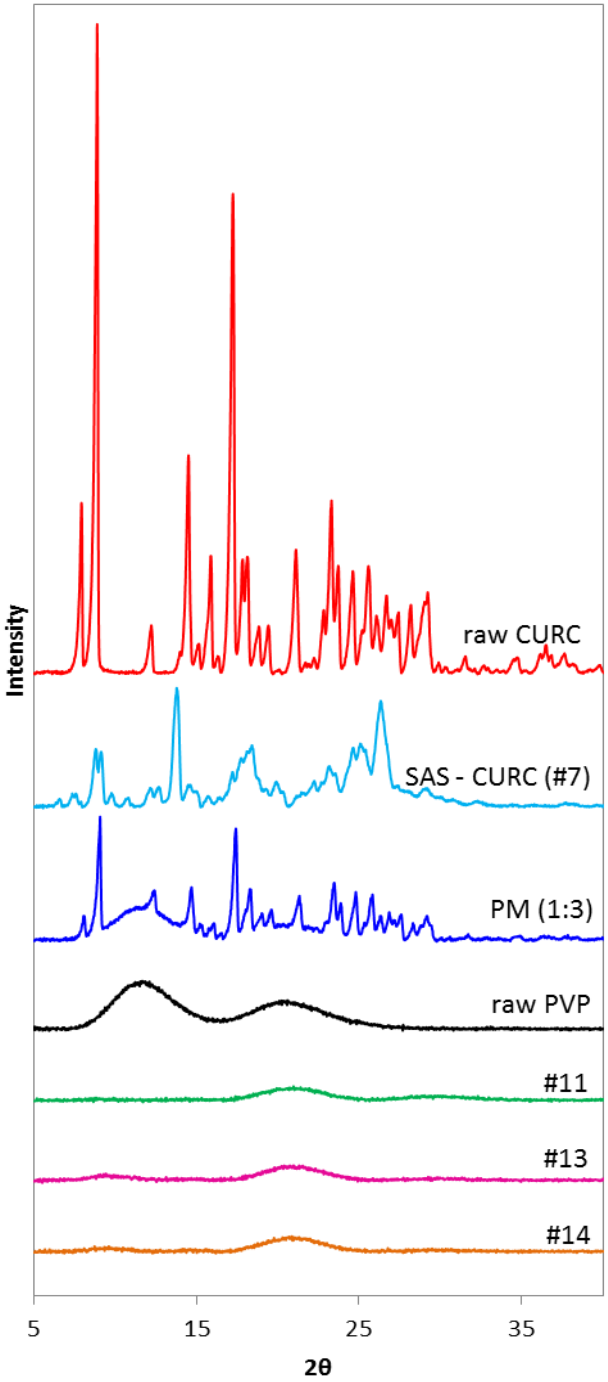

Figure 4-9. XRD patterns of raw curcumin, raw PVP, 1:3 CURC-PVP physical mixture (PM), curcumin processed by SAS (#7) and CURC/PVP coprecipitates (#11, #13 and #14). Experiment conditions are shown in **Table 4-1**.

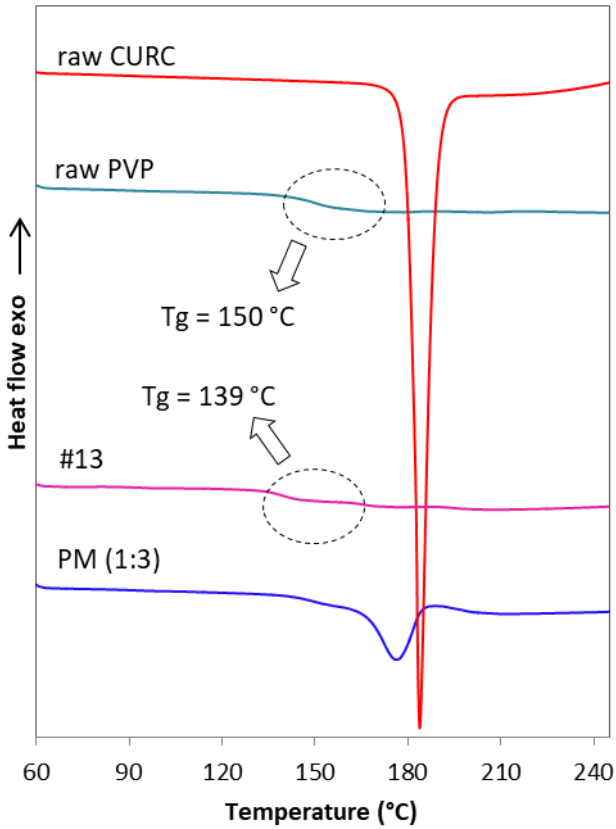

Figure 4-10. DSC thermograms of raw curcumin, raw PVP, 1:3 CURC-PVP physical mixture (PM) and CURC/PVP coprecipitate (#13). Experiment conditions are shown in **Table 4-1**.

The spectrum of the physical mixture (PM 1:3) is similar to the addition of the individual spectra of curcumin and PVP, which indicates that no interaction between them has occurred. On the other hand, for the samples of CURC/PVP processed by SAS (#10, #13, #22, #23), the O-H characteristic peak (3504 cm^{-1}) from curcumin has disappeared. This can be ascribed to an intermolecular interaction, such as hydrogen bonding, between the O-H of curcumin and the C=O of PVP [16]. This behaviour is compatible with the observations of other researchers [16,39,73,74] and might explain the change in the structure of curcumin from crystalline to amorphous (sections 4.5.3 and 4.5.4) and the improvement in the aqueous apparent solubility (section 4.5.6) and dissolution properties of curcumin formulations (section 4.5.7).

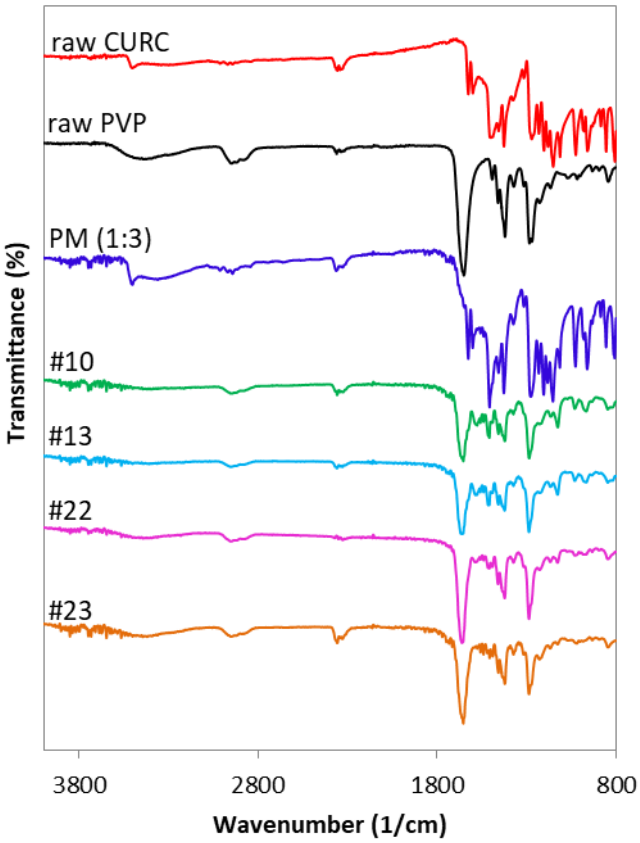

Figure 4-11. IR spectra of raw curcumin, raw PVP, 1:3 CURC-PVP physical mixture (PM) and CURC/PVP coprecipitates (#10, #13, #22 and #23). Experiment conditions are shown in **Table 4-1**.

4.5.6. Drug apparent solubility

The apparent solubility of raw curcumin (CURC), SAS-processed curcumin (SAS-CURC, #7), CURC/PVP physical mixtures (PM) and SAS coprecipitates was determined in water at 25°C. Unprocessed curcumin has not shown any absorbance at these conditions, while other authors have measured 0.006 µg/ml after dissolution for 12h in water [39] and 0.5 µg/ml after dissolved in saline solution and centrifuged at 12,000 rpm for 10 min (25 °C) [36]. The different conditions and method used explain the different results obtained. The low water solubility of curcumin is one of the main causes of its low bioavailability [3].

The apparent solubility of curcumin processed by SAS alone was equal to 0.06 µg/ml, which is still very low. The addition of PVP was found to improve curcumin apparent solubility in

the physical mixtures: 0.3 µg/ml was measured in the mixture at 1:3 CURC/PVP, while 4.4 µg/ml was obtained at 1:10 ratio. This might be explained by a possible decrease in the surface tension of water in the presence of PVP, which enhances the wetting of the curcumin crystal surface [11,65].

CURC/PVP coprecipitates were produced in an attempt to further increase curcumin apparent solubility. The apparent solubility of raw CURC, physical mixtures and curcumin formulations are presented in **Figure 4-12**a. In runs #11 and #13 the apparent solubility increased around 100 times compared with the physical mixture (1:3), while in run #14 an increase of more than 600 times was obtained. By decreasing CURC/PVP ratio, this effect was even more remarkable (**Figure 4-12a)**. In runs #22 and #26 the measured values were 369 µg/ml and 474 µg/ml, respectively. Other authors have also reported an improvement in drug apparent solubility as PVP content increases [74]. This was attributed to the formation of a water-soluble complex between drug and PVP, which was confirmed by FTIR test (section 4.5.5). Chhouk et al. [39] reported a curcumin apparent solubility of 2.34 µg/ml in a formulation with PVP while Kurniawansyah et al. [37] obtained the highest value equal to 77.6 µg/ml for a ternary system containing curcumin, PVP and methyl-β-cyclodextrin in a ratio of 1:4:4 at pH 4.5.

4.5.7. In vitro dissolution studies

The dissolution profile of coprecipitates (#13, #23, #26), raw curcumin (CURC), physical mixture (PM 1:3) and curcumin processed by SAS alone (SAS-CURC, #7) was investigated in water + 0.25% w/v SDS. The surfactant SDS was added to allow for a shorter dissolution study and minimise the impact of curcumin degradation in the results. Moreover, when no SDS was used, there was no discrimination among the release profiles of the raw CURC, PM (1:3) and SAS-CURC (#7) due to their absorbance values being too close to the minimum

detection limit of the UV-visible spectrophotometer used (results not shown; see **Appendix IV**).

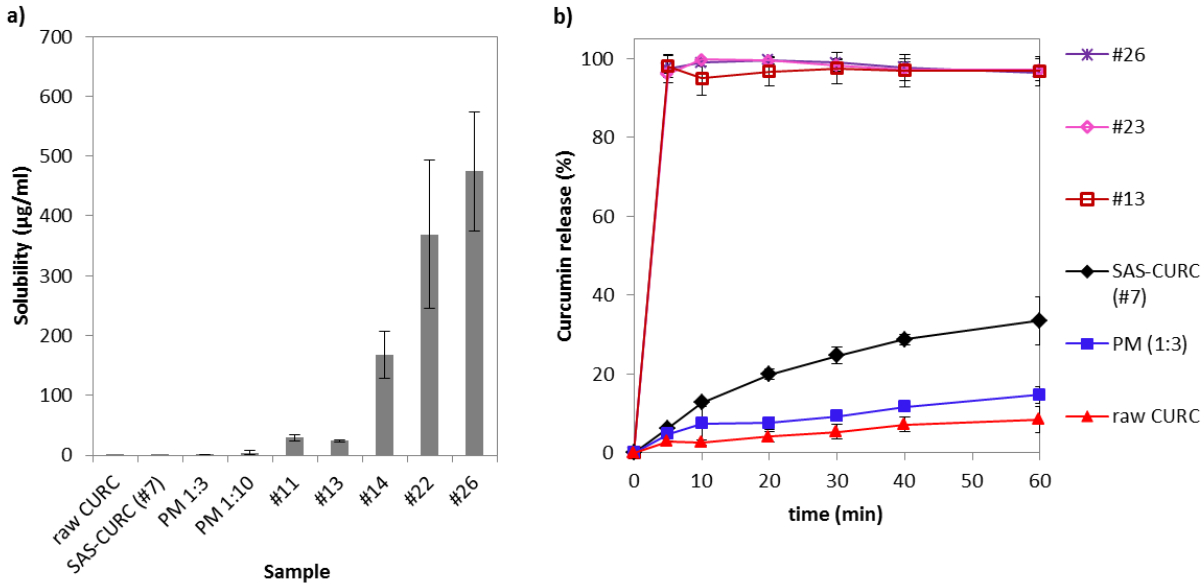

Figure 4-12. a) Apparent solubility and b) dissolution profile of raw curcumin (CURC), physical mixtures (PM) and processed samples. Experiment conditions are shown in **Table 4-1**.

Figure 4-12b shows the dissolution profiles for the various samples in water + 0.25% w/v SDS. PM (1:3) releases faster than raw CURC, which is due to the improvement in curcumin wetting and solubility in the presence of PVP, as discussed in section 4.5.6. The release of SAS-CURC (#7) is faster than the physical mixture (1:3), despite having lower apparent solubility in water (section 4.5.6), as a result of the smaller size of the curcumin crystals (**Figure 4-2**c,d). All the coprecipitates analysed dissolved significantly faster than raw CURC and PM (1:3), with complete release being obtained in the first 10 minutes. In the same period of time, raw CURC, PM (1:3) and SAS-CURC (#7) released only 3.2%, 7.5% and 12.8% of curcumin, respectively. These results, in conjunction with the observations of particle morphology, thermal behaviour and measurements of curcumin recovery, demonstrate that coprecipitates with high curcumin content and improved dissolution properties were successfully produced by SAS. The enhancement in the curcumin dissolution profile can be

attributed to the formation of smaller particles with increased apparent solubility (section 4.5.6) and reduced crystallinity compared to raw CURC (section 4.5.3).

Two mechanisms are suggested to for the precipitation of composite materials: homogeneous nucleation, which produces a solid mixture in which each particle if formed by only one component; and heterogeneous nucleation, which generates particles composed of both materials (coprecipitates) [33]. By the results presented in this work, it is believed that heterogeneous nucleation happened, leading to the formation of composite particles. In any case, the aim of the work was successfully achieved, as the dissolution properties of curcumin were significantly improved.

4.6. Conclusions

In this work, the coprecipitation of curcumin and PVP by SAS was successfully achieved from different solvent mixtures of acetone and ethanol. The results showed that the composition of the solvent mixture plays a major role in determining particle size, particle size distribution and curcumin recovery. Particle size varied from sub-microparticles (327 – 135 nm) to nanoparticles (96 - 51 nm) and the curcumin recovery increased from 45.5 to 89.2% as the relative composition of acetone in the ethanol-acetone mixture was increased. The highest curcumin recovery (95%) was obtained at low temperature (35°C) for a 70-30 Ac-EtOH solution. It was also observed an improvement in curcumin apparent solubility of around 600 times compared with the physical mixture and, consequently, a much faster release. These results are explained by the solid state analyses which have demonstrated the formation of amorphous curcumin-PVP coprecipitates.

4.7. Supplementary material

Detail of the precipitator or high pressure vessel (HPV)

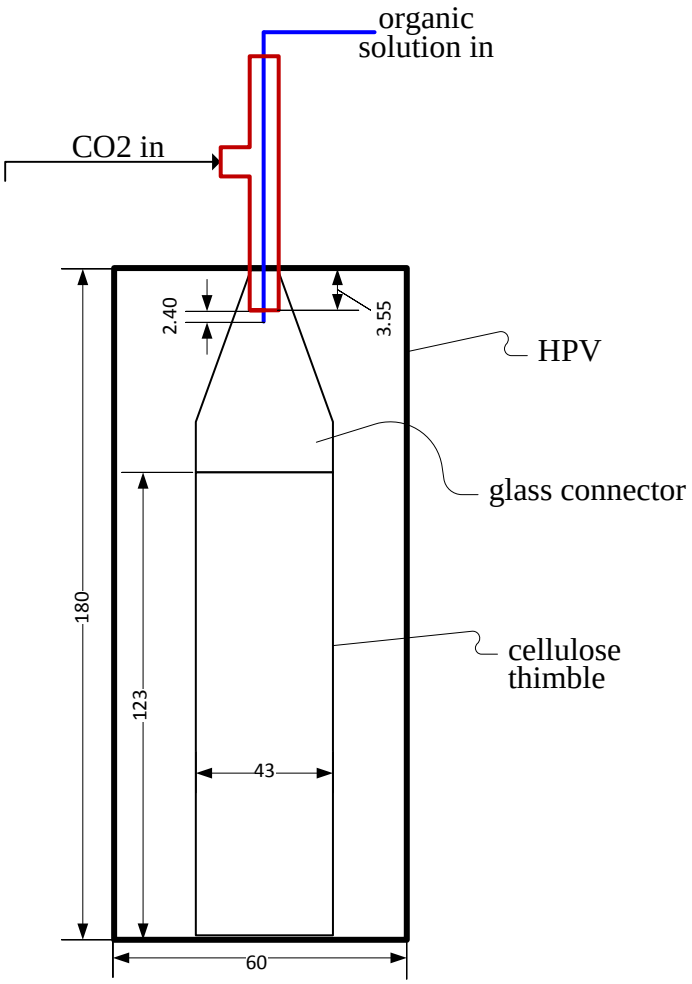

Figure 4-13. Detail of the precipitation vessel (distances in millimetres).

UV spectra of curcumin and PVP

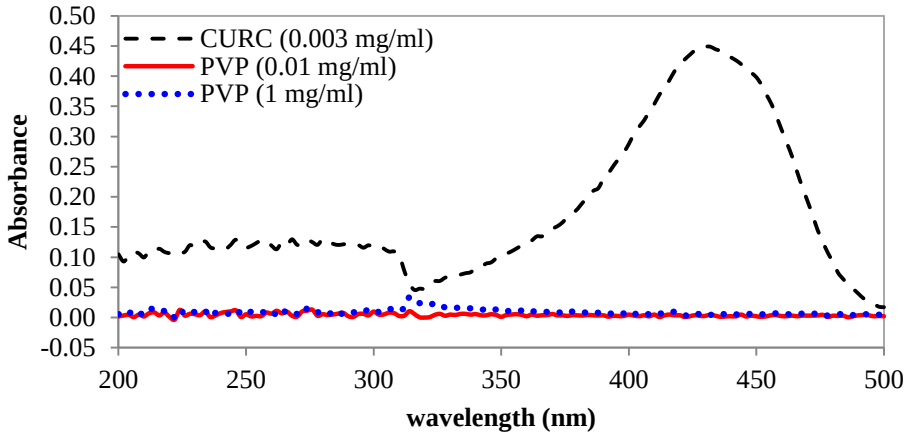

Figure 4-14. UV spectra of curcumin and PVP.

Phase diagram and mixture critical points of the systems CO_2-ethanol and CO_2-acetone

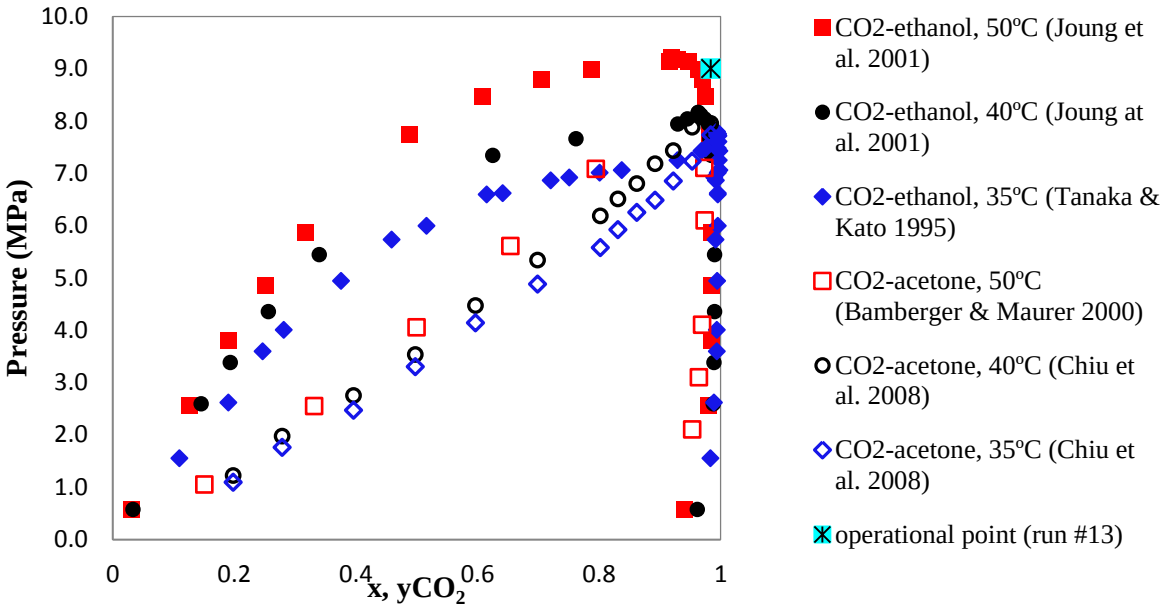

Figure 4-15. Vapour-liquid equilibrium of CO_2-ethanol and CO_2-acetone at 35°C, 40°C and 50°C.

Table 4-2. Mixture critical points of CO_2-ethanol and CO_2-acetone at 40°C.

System	P (Mpa)	X_{CO2}	Reference
CO_2-acetone	7.95	0.984	[75]
CO_2-acetone	8.05	-	[76]
CO_2-ethanol	8.16	0.963	[51]
CO_2-ethanol	7.8	0.985	[75]

4.8. Competing interests

The authors would like to declare that there are no competing interests.

4.9. Acknowledgements

The authors would like to acknowledge the financial support from National Council for Scientific and Technological Development (CNPQ, Brazil) through Science Without Borders Program and Gabor Dravavolgyi for his help in the HPLC.

4.10. References

[1] S.C. Gupta, S. Patchva, B.B. Aggarwal, Therapeutic Roles of Curcumin: Lessons Learned from Clinical Trials, Am. Assoc. Pharm. Sci. J. 15 (2013) 195–218. doi:10.1208/s12248-012-9432-8.

[2] O. Naksuriya, S. Okonogi, R.M. Schiffelers, W.E. Hennink, Curcumin nanoformulations: A review of pharmaceutical properties and preclinical studies and clinical data related to cancer treatment, Biomaterials. 35 (2014) 3365–3383. doi:10.1016/j.biomaterials.2013.12.090.

[3] R.I. Mahran, M.M. Hagras, D. Sun, D.E. Brenner, Bringing Curcumin to the Clinic in Cancer Prevention: a Review of Strategies to Enhance Bioavailability and Efficacy, AAPS J. 19 (2017) 54–81. doi:10.1208/s12248-016-0003-2.

[4] L.P. Cunico, M.C. Acosta, C. Turner, Experimental measurements and modeling of curcumin solubility in CO2-expanded ethanol, J. Supercrit. Fluids. (2017) 1–8. doi:10.1016/j.supflu.2017.06.018.

[5] Z. Hussain, H. Ei, M. Wahab, F. Hussain, T.A. Ahmed, S. Khan, Exploring recent developments to improve antioxidant , anti-inflammatory and antimicrobial efficacy of curcumin : A review of new trends and future perspectives, Mater. Sci. Eng. C. 77 (2017) 1316–1326. doi:10.1016/j.msec.2017.03.226.

[6] A. Sao Pedro, S.D. Villa, P. Caliceti, S.A.B.V. De Melo, E.C. Albuquerque, A. Bertucco, S. Salmaso, Curcumin-loaded solid lipid particles by PGSS technology, J. Supercrit. Fluids. 107 (2016) 534–541. doi:10.1016/j.supflu.2015.07.010.

[7] Z. Hussain, H.E. Thu, S. Ng, S. Khan, H. Katas, Nanoencapsulation , an efficient and promising approach to maximize wound healing efficacy of curcumin : A review of new trends and state-of-the-art, Colloids Surfaces B Biointerfaces. 150 (2017) 223–241. doi:10.1016/j.colsurfb.2016.11.036.

[8] V. Prosapio, E. Reverchon, I. De Marco, Incorporation of liposoluble vitamins within PVP microparticles using supercritical antisolvent precipitation, J. CO2 Util. 19 (2017) 230–237. doi:10.1016/j.jcou.2017.04.004.

[9] V. Prosapio, I. De Marco, M. Scognamiglio, E. Reverchon, Folic acid-PVP

nanostructured composite microparticles by supercritical antisolvent precipitation, Chem. Eng. J. 277 (2015) 286–294. doi:10.1016/j.cej.2015.04.149.

[10] V. Prosapio, I. De Marco, E. Reverchon, PVP/corticosteroid microspheres produced by supercritical antisolvent coprecipitation, Chem. Eng. J. 292 (2016) 264–275. doi:10.1016/j.cej.2016.02.041.

[11] H. Sekikawa, M. Nakano, T. Arita, Dissolution Mechanisms of Drug-Polyvinylpyrrolidone Coprecipitates in Aqueous Solution, Chem. Pharm. Bull. 27 (1979) 1223–1230.

[12] S. Jain, N. Patel, S. Lin, Solubility and dissolution enhancement strategies: current understanding and recent trends, Drug Dev. Indusrial Pharm. 41 (2015) 875–887. doi:10.3109/03639045.2014.971027.

[13] P. Gupta, V.K. Kakumanu, A.K. Bansal, Stability and Solubility of Celecoxib – PVP Amorphous Dispersions : A Molecular Perspective, 21 (2004) 1762–1769.

[14] A. Paradkar, A.A. Ambike, B.K. Jadhav, K.R. Mahadik, Characterization of curcumin-PVP solid dispersion obtained by spray drying, Int. J. Pharm. 271 (2004) 281–286. doi:10.1016/j.ijpharm.2003.11.014.

[15] D. Xu, S. Wang, J. Jin, X. Mei, S. Xu, Dissolution and absorption researches of curcumin in solid dispersions with the polymers PVP, Asian J. Pharmacodyn. Pharmacokinet. 6 (2006) 343–349.

[16] N. Kaewnopparat, S. Kaewnopparat, A. Jangwang, D. Maneenaun, T. Chuchome, P. Panichayupakaranant, Increased solubility, dissolution and physicochemical studies of curcumin-polyvinylpyrrolidone K-30 solid dispersions, Int. J. Medical, Heal. Biomed. Bioeng. Pharm. Eng. 3 (2009) 137–142. http://citeseerx.ist.psu.edu/viewdoc/download?doi=10.1.1.192.9888&rep=rep1&type=pdf.

[17] M.K. Modasiya, V.M. Patel, Studies on solubility of curcumin, Int. J. Pharm. Life Sci. 3 (2012) 2713–2716. doi:10.2330/joralbiosci1965.30.54.

[18] A.S. Silva, M.T. Tavares, A. Aguiar-Ricardo, Sustainable strategies for nano-in-micro particle engineering for pulmonary delivery, J. Nanoparticle Res. 16 (2014) 1–17. doi:10.1007/s11051-014-2602-0.

[19] J.S. Kim, M.S. Kim, H.J. Park, S.J. Jin, S. Lee, S.J. Hwang, Physicochemical properties and oral bioavailability of amorphous atorvastatin hemi-calcium using spray-drying and SAS process, Int. J. Pharm. 359 (2008) 211–219. doi:10.1016/j.ijpharm.2008.04.006.

[20] Y. Li, D.J. Yang, S.L. Chen, S.B. Chen, A.S.C. Chan, Comparative physicochemical characterization of phospholipids complex of puerarin formulated by conventional and supercritical methods, Pharm. Res. 25 (2008) 563–577. doi:10.1007/s11095-007-9418-x.

[21] S.F. Chow, K.Y. Wan, K.K. Cheng, K.W. Wong, C.C. Sun, L. Baum, A.H.L. Chow, Development of highly stabilized curcumin nanoparticles by flash nanoprecipitation and lyophilization, Eur. J. Pharm. Biopharm. 94 (2015) 436–449. doi:10.1016/j.ejpb.2015.06.022.

[22] P. Valeh-e-Sheyda, M. Rahimi, H. Adibi, Z. Razmjou, H. Ghasempour, An insight on reducing the particle size of poorly-water soluble curcumin via LASP in microchannels, Chem. Eng. Process. Process Intensif. 91 (2015) 78–88. doi:10.1016/j.cep.2015.03.018.

[23] F. Sadeghi, M. Ashofteh, A. Homayouni, M. Abbaspour, A. Nokhodchi, H.A. Garekani, Antisolvent precipitation technique: A very promising approach to crystallize curcumin in presence of polyvinyl pyrrolidon for solubility and dissolution enhancement, Colloids Surfaces B Biointerfaces. 147 (2016) 258–264. doi:10.1016/j.colsurfb.2016.08.004.

[24] I. De Marco, M. Rossmann, V. Prosapio, E. Reverchon, A. Braeuer, Control of particle size, at micrometric and nanometric range, using supercritical antisolvent precipitation from solvent mixtures: Application to PVP, Chem. Eng. J. 273 (2015) 344–352. doi:10.1016/j.cej.2015.03.100.

[25] R.L. Matos, T. Lu, C. McConville, G. Leeke, A. Ingram, Analysis of curcumin precipitation and coating on lactose by the integrated supercritical antisolvent-fluidized bed process, J. Supercrit. Fluids. In press. (n.d.). doi:10.1016/j.supflu.2017.12.013.

[26] E. Reverchon, I. De Marco, Mechanisms controlling supercritical antisolvent precipitate morphology, Chem. Eng. J. 169 (2011) 358–370.

doi:10.1016/j.cej.2011.02.064.

[27] E. Badens, Y. Masmoudi, A. Mouahid, C. Crampon, Current situation and perspectives in drug formulation by using supercritical fluid technology, J. Supercrit. Fluids. 134 (2018) 274–283. doi:10.1016/j.supflu.2017.12.038.

[28] E. Reverchon, I. De Marco, R. Adami, G. Caputo, Expanded micro-particles by supercritical antisolvent precipitation: Interpretation of results, J. Supercrit. Fluids. 44 (2008) 98–108. doi:10.1016/j.supflu.2007.08.008.

[29] E. Reverchon, R. Adami, G. Caputo, I. De Marco, Spherical microparticles production by supercritical antisolvent precipitation: Interpretation of results, J. Supercrit. Fluids. 47 (2008) 70–84. doi:10.1016/j.supflu.2008.06.002.

[30] E. Reverchon, I. De Marco, E. Torino, Nanoparticles production by supercritical antisolvent precipitation: A general interpretation, J. Supercrit. Fluids. 43 (2007) 126–138. doi:10.1016/j.supflu.2007.04.013.

[31] I.N. Uzun, O. Sipahigil, S. Dinçer, Coprecipitation of Cefuroxime Axetil-PVP composite microparticles by batch supercritical antisolvent process, J. Supercrit. Fluids. 55 (2011) 1059–1069. doi:10.1016/j.supflu.2010.09.035.

[32] A.Z. Chen, X.M. Pu, Y.Q. Kang, L. Liao, Y.D. Yao, G.F. Yin, Preparation of 5-fluorouracil-poly(L-lactide) microparticles using solution-enhanced dispersion by supercritical CO2, Macromol. Rapid Commun. 27 (2006) 1254–1259. doi:10.1002/marc.200600221.

[33] V. Prosapio, I. De Marco, E. Reverchon, Supercritical antisolvent coprecipitation mechanisms, J. Supercrit. Fluids. 138 (2018) 247–258. doi:10.1016/j.supflu.2018.04.021.

[34] R. Adami, A. Di Capua, E. Reverchon, Supercritical Assisted Atomization for the production of curcumin-biopolymer microspheres, Powder Technol. 305 (2017) 455–461. doi:10.1016/j.powtec.2016.10.020.

[35] D.S. Sogi, S. Sharma, D.P.S. Oberoi, I.A. Wani, Effect of extraction parameters on curcumin yield from turmeric, J. Food Sci. Technol. 47 (2010) 300–304. doi:10.1007/s13197-010-0047-8.

[36] F. Kurniawansyah, R. Mammucari, N.R. Foster, Inhalable curcumin formulations by supercritical technology, Powder Technol. 284 (2015) 289–298. doi:10.1016/j.powtec.2015.04.083.

[37] F. Kurniawansyah, L. Quachie, R. Mammucari, N.R. Foster, Improving the dissolution properties of curcumin using dense gas antisolvent technology, Int. J. Pharm. 521 (2017) 239–248. doi:10.1016/j.ijpharm.2017.02.018.

[38] F. Kurniawansyah, H.T.T. Duong, T.D. Luu, R. Mammucari, O. Vittorio, C. Boyer, N. Foster, Inhalable curcumin formulations: Micronization and bioassay, Chem. Eng. J. 279 (2015) 799–808. doi:10.1016/j.cej.2015.05.087.

[39] K. Chhouk, W. Diono, H. Kanda, S.I. Kawasaki, M. Goto, Micronization of curcumin with biodegradable polymer by supercritical anti-solvent using micro swirl mixer, Front. Chem. Sci. Eng. 12 (2018) 184–193. doi:10.1007/s11705-017-1678-3.

[40] W. Wichitnithad, N. Jongaroonngamsang, S. Pummangura, P. Rojsitthisak, A simple isocratic HPLC method for the simultaneous determination of curcuminoids in commercial turmeric extracts, Phytochem. Anal. 20 (2009) 314–319. doi:10.1002/pca.1129.

[41] B. Li, S. Konecke, L.A. Wegiel, L.S. Taylor, K.J. Edgar, Both solubility and chemical stability of curcumin are enhanced by solid dispersion in cellulose derivative matrices, Carbohydr. Polym. 98 (2013) 1108–1116. doi:10.1016/j.carbpol.2013.07.017.

[42] E. Karavas, G. Ktistis, A. Xenakis, E. Georgarakis, Miscibility behavior and formation mechanism of stabilized felodipine-polyvinylpyrrolidone amorphous solid dispersions, Drug Dev. Ind. Pharm. 31 (2005) 473–489. doi:10.1080/03639040500215958.

[43] A. Bouledjouidja, Y. Masmoudi, M. Sergent, V. Trivedi, A. Meniai, E. Badens, Drug loading of foldable commercial intraocular lenses using supercritical impregnation, Int. J. Pharm. 500 (2016) 85–99. doi:10.1016/j.ijpharm.2016.01.016.

[44] J. Li, I.W. Lee, G.H. Shin, X. Chen, H.J. Park, Curcumin-Eudragit® e PO solid dispersion: A simple and potent method to solve the problems of curcumin, Eur. J. Pharm. Biopharm. 94 (2015) 322–332. doi:10.1016/j.ejpb.2015.06.002.

[45] M. Anwar, I. Ahmad, M.H. Warsi, S. Mohapatra, N. Ahmad, S. Akhter, A. Ali, F.J. Ahmad, Experimental investigation and oral bioavailability enhancement of nano-sized

curcumin by using supercritical anti-solvent process, Eur. J. Pharm. Biopharm. 96 (2015) 162–172. doi:10.1016/j.ejpb.2015.07.021.

[46] V.J. Pereira, R.L. Matos, S.G. Cardoso, R.O. Soares, G.L. Santana, G.M.N. Costa, S.A.B. Vieira De Melo, A new approach to select solvents and operating conditions for supercritical antisolvent precipitation processes by using solubility parameter and group contribution methods, J. Supercrit. Fluids. 81 (2013) 128–146. doi:10.1016/j.supflu.2013.05.010.

[47] I. Kikic, N. De Zordi, M. Moneghini, D. Solinas, Solubility estimation of drugs in ternary systems of interest for the antisolvent precipitation processes, J. Supercrit. Fluids. 55 (2010) 616–622. doi:10.1016/j.supflu.2010.09.034.

[48] M. Kakran, N.G. Sahoo, I.L. Tan, L. Li, Preparation of nanoparticles of poorly water-soluble antioxidant curcumin by antisolvent precipitation methods, J. Nanoparticle Res. 14 (2012). doi:10.1007/s11051-012-0757-0.

[49] S. Bristow, T. Shekunov, B.Y. Shekunov, P. York, Analysis of the supersaturation and precipitation process with supercritical CO2, J. Supercrit. Fluids. 21 (2001) 257–271. doi:10.1016/S0896-8446(01)00100-0.

[50] A. Martín, M.J. Cocero, Numerical modeling of jet hydrodynamics, mass transfer, and crystallization kinetics in the supercritical antisolvent (SAS) process, J. Supercrit. Fluids. 32 (2004) 203–219. doi:10.1016/j.supflu.2004.02.009.

[51] S.N. Joung, C.W. Yoo, H.Y. Shin, S.Y. Kim, K.P. Yoo, C.S. Lee, W.S. Huh, Measurements and correlation of high-pressure VLE of binary CO2-alcohol systems (methanol, ethanol, 2-methoxyethanol and 2-ethoxyethanol), Fluid Phase Equilib. 185 (2001) 219–230. doi:10.1016/S0378-3812(01)00472-1.

[52] M. Rossmann, A. Braeuer, E. Schluecker, Supercritical antisolvent micronization of PVP and ibuprofen sodium towards tailored solid dispersions, J. Supercrit. Fluids. 89 (2014) 16–27. doi:10.1016/j.supflu.2014.02.010.

[53] A. Gokhale, B. Khusid, R.N. Dave, R. Pfeffer, Effect of solvent strength and operating pressure on the formation of submicrometer polymer particles in supercritical microjets, J. Supercrit. Fluids. 43 (2007) 341–356. doi:10.1016/j.supflu.2007.05.012.

[54] M. Muntó, N. Ventosa, S. Sala, J. Veciana, Solubility behaviors of ibuprofen and

naproxen drugs in liquid “CO2-organic solvent” mixtures, J. Supercrit. Fluids. 47 (2008) 147–153. doi:10.1016/j.supflu.2008.07.013.

[55] B. De Gioannis, A. Vega Gonzalez, P. Subra, Anti-solvent and co-solvent effect of CO2 on the solubility of griseofulvin in acetone and ethanol solutions, J. Supercrit. Fluids. 29 (2004) 49–57. doi:10.1016/S0896-8446(03)00035-4.

[56] F. Kurniawansyah, R. Mammucari, N.R. Foster, Polymorphism of curcumin from dense gas antisolvent precipitation, Powder Technol. 305 (2017) 748–756. doi:10.1016/j.powtec.2016.10.067.

[57] H. Sekikawa, M. Nakano, T. Arita, Inhibitory Effect of Polyvinylpyrrolidone on the Crystallization of Drugs, Chem. Pharm. Bull. 26 (1978) 118–126. doi:10.1248/cpb.26.118.

[58] R.T.Y. Lim, W.K. Ng, R.B.H. Tan, Dissolution enhancement of indomethacin via amorphization using co-milling and supercritical co-precipitation processing, Powder Technol. 240 (2013) 79–87. doi:10.1016/j.powtec.2012.07.004.

[59] F.G. Denardin, S.A.B. Vieira De Melo, R. Mammucari, N.R. Foster, Phase transition and volume expansion in CO2-expanded liquid systems, Chem. Eng. Trans. 32 (2013) 529–534. doi:10.3303/CET1332089.

[60] C.J. Chang, C.-Y. Day, C.-M. Ko, K.-L. Chiu, Densities and P-x-y diagrams for carbon dioxide dissolution in methanol, ethanol, and acetone mixtures, Fluid Phase Equilib. 131 (1997) 243–258.

[61] R. Bos, T. Windono, H.J. Woerdenbag, Y.L. Boersma, A. Koulman, O. Kayser, HPLC-photodiode array detection analysis of curcuminoids in Curcuma species indigenous to Indonesia, Phytochem. Anal. 18 (2007) 118–122. doi:10.1002/pca.959.

[62] G.K. Jayaprakasha, L.J.M. Rao, K.K. Sakariah, Improved HPLC method for the determination of curcumin, demethoxycurcumin, and bisdemethoxycurcumin, J. Agric. Food Chem. 50 (2002) 3668–3672. doi:10.1021/jf025506a.

[63] Y. Long, W. Zhang, F. Wang, Z. Chen, Simultaneous determination of three curcuminoids in Curcuma longa L. by high performance liquid chromatography coupled with electrochemical detection, J. Pharm. Anal. 4 (2014) 325–330. doi:10.1016/j.jpha.2013.10.002.

[64] NIST Chemistry WebBook, Thermophysical Properties of Carbon dioxide, SRD 69. (2017). http://webbook.nist.gov/cgi/fluid.cgi?ID=C124389&Action=Page (accessed January 1, 2017).

[65] D. Bolten, M. Türk, Experimental study on the surface tension, density, and viscosity of aqueous poly(vinylpyrrolidone) solutions, J. Chem. Eng. Data. 56 (2011) 582–588. doi:10.1021/je101277c.

[66] S.A.B.V. De Melo, L.T. Danh, R. Mammucari, N.R. Foster, Dense CO2 antisolvent precipitation of levothyroxine sodium: A comparative study of GAS and ARISE techniques based on morphology and particle size distributions, J. Supercrit. Fluids. 93 (2014) 112–120. doi:10.1016/j.supflu.2013.11.019.

[67] A. Erriguible, T. Fadli, P. Subra-Paternault, A complete 3D simulation of a crystallization process induced by supercritical CO2 to predict particle size, Comput. Chem. Eng. 52 (2013) 1–9. doi:10.1016/j.compchemeng.2012.12.002.

[68] C.S. Lengsfeld, J.P. Delplanque, V.H. Barocas, T.W. Randolph, Mechanism Governing Microparticle Morphology during Precipitation by a Compressed Antisolvent: Atomization vs Nucleation and Growth, J. Phys. Chem. B. 104 (2000) 2725–2735. doi:10.1021/jp9931511.

[69] L.A. Wegiel, Y. Zhao, L.J. Mauer, K.J. Edgar, L.S. Taylor, Curcumin amorphous solid dispersions: the influence of intra and intermolecular bonding on physical stability, Pharm. Dev. Technol. 19 (2014) 976–986. doi:10.3109/10837450.2013.846374.

[70] W.M. Giufrida, R. Favareto, V.F. Cabral, M.A. A.Meireles, L. Cardozo-Filho, M.L. Corazza, High-Pressure Vapor-Liquid Equilibrium Data for Ternary Systems CO2 + Organic Solvent + Curcumin, Open Chem. Eng. J. 4 (2010) 3–10. doi:10.2174/1874123101004020003.

[71] F. Zahran, A. Cabañas, J.A.R. Cheda, J.A.R. Renuncio, C. Pando, Dissolution rate enhancement of the anti-inflammatory drug diflunisal by coprecipitation with a biocompatible polymer using carbon dioxide as a supercritical fluid antisolvent, J. Supercrit. Fluids. 88 (2014) 56–65. doi:10.1016/j.supflu.2014.01.015.

[72] P.R.K. Mohan, G. Sreelakshmi, C. V. Muraleedharan, R. Joseph, Water soluble complexes of curcumin with cyclodextrins: Characterization by FT-Raman

spectroscopy, Vib. Spectrosc. 62 (2012) 77–84. doi:10.1016/j.vibspec.2012.05.002.

[73] R.K. Gangwar, V.A. Dhumale, D. Kumari, U.T. Nakate, S.W. Gosavi, R.B. Sharma, S.N. Kale, S. Datar, Conjugation of curcumin with PVP capped gold nanoparticles for improving bioavailability, Mater. Sci. Eng. C. 32 (2012) 2659–2663. doi:10.1016/j.msec.2012.07.022.

[74] H.A. Garekani, F. Sadeghi, A. Ghazi, Increasing the aqueous solubility of acetaminophen in the presence of polyvinylpyrrolidone and investigation of the mechanisms involved, Drug Dev. Ind. Pharm. 29 (2003) 173–179. doi:10.1081/DDC-120016725.

[75] H.-Y. Chiu, R.-F. Jung, M.-J. Lee, H.-M. Lin, Vapor–liquid phase equilibrium behavior of mixtures containing supercritical carbon dioxide near critical region, J. Supercrit. Fluids. 44 (2008) 273–278. doi:10.1016/j.supflu.2007.09.026.

[76] T. Adrian, G. Maurer, Solubility of carbon dioxide in acetone and propionic acid at temperatures between 298 K and 333 K, J. Chem. Eng. Data. 42 (1997) 668–672. doi:10.1021/je970011g.

Chapter 5 -

SINGLE-STEP COPRECIPITATION AND COATING TO PREPARE CURCUMIN FORMULATIONS BY SUPERCRITICAL FLUID TECHNOLOGY

Published article:

The Journal of Supercritical Fluids 159 (2020)

5.1. Abstract

Graphical Abstract

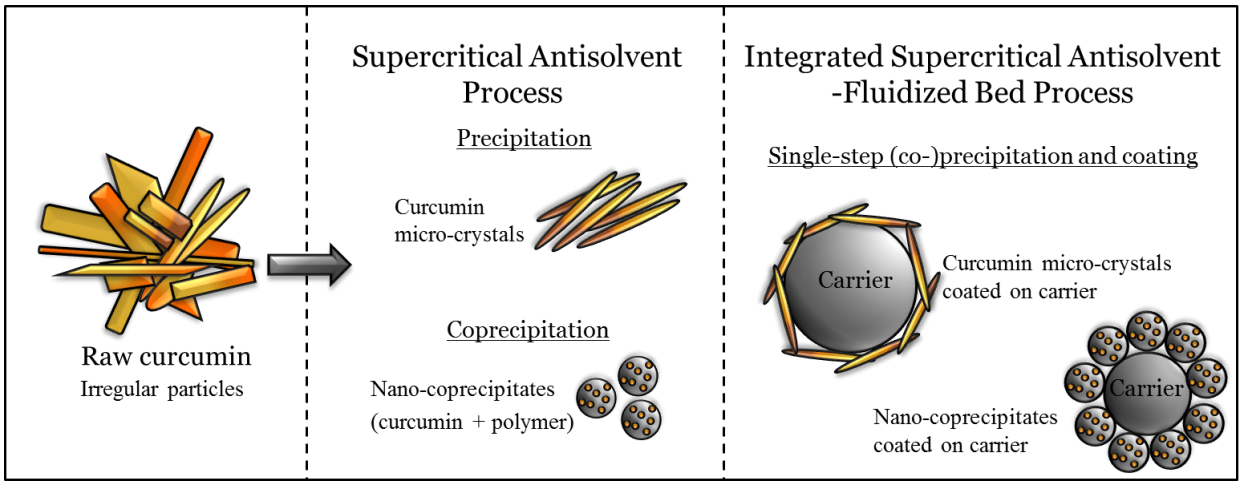

Common strategies to improve the dissolution properties of hydrophobic drug compounds include the preparation of composites with hydrophilic excipients and/or size reduction. However, nanoparticles have poor flowability and difficult handling. Therefore, this work aims to demonstrate the single-step improvement in dissolution and flow properties of pharmaceutical formulations. Coprecipitates of curcumin and poly (vinyl pyrrolidone) (guest particles) are simultaneously produced and coated onto microcrystalline cellulose (MCC, 175 µm), corn starch (15 µm) and lactose (< 5 µm) (host particles), by combining the Supercritical Antisolvent process with two different configurations of fluidized bed (tapered bed and stirred vessel). Experiments were performed at 40°C, 9-12 MPa, 2.5-30.0% guest/host mass ratio and stirrer speed varying from 400 to 1200 rpm. SEM images demonstrated that nanoparticles of coprecipitates were obtained while DSC results showed that they were amorphous, explaining the remarkable improvement in dissolution achieved. Free-flowing powder was obtained when MCC was used as carrier.

Keywords: supercritical antisolvent; coprecipitation; high-pressure fluidization; coating; process integration; curcumin.

5.2. Highlights

- The SAS process was combined with two configurations of fluidized beds
- Properties of fluidization in tapered beds and stirred vessels were discussed
- Curcumin/PVP coprecipitates were produced and coated on different carrier particles
- Curcumin release and flow properties were enhanced in a single-step process

5.3. Introduction

Powder technology has a major impact on the profitability of the pharmaceutical industry as more than 80% of drug products are solids, produced by a number of processing steps [1,2]. In order to improve the efficiency of manufacturing processes and to optimize formulation development, the current trend in the pharmaceutical industry is to develop cost-effective and environmental-friendly processes with fewer steps to gain better understanding and control of the variables [3].

Drug solubility and dissolution rate are some crucial properties investigated in early stages of pharmaceutical formulation development [4]. In fact, more than 49% of drug candidates for oral administration have low water solubility (< 10 μg/ml) [5], which leads to poor bioavailability. As a consequence, the administration of high doses is required to achieve the therapeutic level, usually resulting in undesired side effects. The common approaches to improve the dissolution properties of pharmaceutical compounds are: modifying its crystalline structure; preparing composites with hydrophilic excipients; and/or increasing the surface area of the material by decreasing its size to nano-scale [6].

Particle size reduction (micronization) techniques can be classified into two main categories: top-down and bottom-up. In the former, large drug particles are broken by mechanical means while in the latter, fine particles are precipitated from solution. Conventional top-down

micronization processes, including milling and homogenization, require high energy input, which can damage the crystalline structure of the product and lead to the formation of electrostatically charged and cohesive powders with wide particle size distribution [7–9]. On the other hand, bottom-up processes such as spray drying and solvent evaporation often result in low precipitation yield [10–12], requiring high temperatures to dry the particles, which prevents the processing of thermo-sensitive compounds.

Bottom-up processes based on the use of supercritical fluids (SCFs) are an alternative for these issues. In the proximity of the supercritical region (above critical pressure and critical temperature) a fluid has unique properties, combining liquid-like density (high solvation power) and gas-like compressibility and diffusivity (high mass transfer rates). By the manipulation of the process operating conditions (such as pressure and temperature), the fluid density and solvation power can be adjusted, allowing the control of the solute supersaturation and precipitation [13]. Therefore, particle properties can be tuned and high precipitation yield can be achieved [14–16]. The most used SCF, supercritical carbon dioxide (sc-CO_2), is non-toxic, non-flammable, inexpensive and considered environmental-friendly compared with organic solvents commonly used in the pharmaceutical industry. Its moderate critical pressure (7.39 MPa) and temperature (31.1°C) enable the processing of thermo-sensitive compounds and the production of formulations with low or no residual organic solvent content, avoiding product degradation and the need for further drying. Such processes have been successfully employed to produce uniform micro and nanoparticles and composite materials with high drug loading efficiency [15,17–19].

Although the advantages of nano-particulate systems in drug delivery are well known, the strong Van der Waals attraction force between dry nanoparticles leads to cohesion, aggregation and consequently poor flowability. For this reason, nanoparticles are usually

mixed with or coated onto larger excipients or carrier particles in pharmaceutical formulations to avoid issues when the material flows through the manufacturing line, and also to facilitate the handling and delivery of the formulation to the patient.

SCFs have been combined with fluidized beds to encapsulate particles within a film of the precipitating material, as detailed in a recent review [20]. More recently, particle-on-particle coating has been proposed to simultaneously precipitate and blend particles of active pharmaceutical ingredients (APIs) with larger carrier particles, hence addressing the aforementioned issues of fine powder flowability and handling. These processes work by spraying a solution of the API (in sc-CO_2 or in an organic solvent) into a fluidized bed of carrier/excipient particles, to achieve simultaneous precipitation and coating in a single step. Such process integration reduces the transfer of the product between equipment, lowering the risk of workers' exposure to nanoparticles since they are formed and instantaneously captured onto the surface of carrier particles (referred as host particles in this work). By performing the Supercritical Antisolvent (SAS) process (sc-CO_2 acts as antisolvent) inside a stirred vessel containing fluidized excipient particles, Sanganwar et al. [21] reported the precipitation of nevirapine (18-39 μm) onto the surface of lactose (100 μm) and microcrystalline cellulose (MCC, 50 μm) particles by a process named Supercritical Antisolvent-Drug Excipient Mixing (SAS-DEM). The same group then coated lactose (100 μm) with itraconazole (0.73-1.73 μm) precipitated in the presence of surfactants [22], and fine lactose particles (5 μm) with precipitated rifampicin (~ 5 μm) [23]. Despite the fact that predominantly micro (rather than nano) particles of drug were obtained in these works, improvements in drug release rate were reported, attributed to a reduction in the drug-drug particle aggregation. Powder flowability was also claimed to be improved [21,22], however flow properties were not assessed by the authors. In 2014, our research group adapted the Rapid Expansion of Supercritical Solutions

(RESS) process (sc-CO_2 acts as solvent) in two different setups (Wurster coater - RESS-WTS and fluidized bed - RESS-BFB) to precipitate nanoparticles (< 30 nm) of several APIs onto MCC (300 μm) [24]. Then the combination of the SAS process with a tapered fluidized bed (SAS-FB), in which the upward flow of CO_2 is responsible for promoting the fluidization of the host particles, was proposed. It was employed to simultaneously precipitate and deposit nanoparticles of naringin (100-200 nm) onto the surface of MCC of various sizes (175-295 μm), with great improvements in drug release achieved [25].

In our most recent work using SAS-FB, curcumin (CURC), a hydrophobic material with several therapeutic properties (anticancer, antioxidant, anti-inflammatory, etc.), was selected as a model compound. Formulations potentially suitable for pulmonary delivery were prepared by coating lactose (125 μm) with curcumin crystals (0.4-12.1 μm) [14], however, despite expected improvements in the flowability of the micronized crystals (due to the mixing with free-flowing lactose), the curcumin size reduction achieved was still not sufficient to give desired dissolution enhancement [15]. Our subsequent work focused on improving the dissolution properties of curcumin by producing coprecipitates with poly (vinyl pyrrolidone) (PVP), a hydrophilic polymer, by SAS [15]. Coprecipitation offers advantages over the precipitation of the drug alone: the drug is dispersed in the polymer matrix which can protect the API against degradation while also allowing drug release to be adjusted through polymer selection [26]. The apparent solubility of curcumin from the composite material was much higher (up to 600 times) than from a corresponding physical mixture of as-received components [15] but the nano-coprecipitates produced tended to aggregate due to high surface energy and would not flow.

In order to overcome the issues identified in the previous work, this manuscript reports the production of curcumin formulations combining improved dissolution and flow properties in

a single step. Curcumin and PVP (guest particles) are coprecipitated and simultaneously coated onto the surface of free-flowing host particles (MCC, 175 μm) by using SAS-FB (tapered bed) and SAS-DEM (stirred vessel) processes and the characteristics of the two different configurations of fluidized bed (tapered bed and stirred vessel) are discussed. In addition, formulations potentially suitable for pulmonary delivery are prepared by coating smaller host particles (corn starch, 15 μm and lactose, < 5 μm) by nano CURC/PVP coprecipitates using SAS-DEM. For the first time, the combination of coprecipitation and coating under supercritical conditions is reported and novel curcumin formulations are produced. Since there are few reports in the literature about the use of SAS-FB and SAS-DEM, the composites obtained from both techniques are also analysed and compared, which is another original aspect of this work.

5.4. Experimental

5.4.1. Materials

Curcumin (purity ≥ 90%) was purchased from Cayman Chemical, UK; lactose (Lactohale® 300, < 5 μm) was kindly provided by DFE Pharma, Germany; corn starch (15 μm [27]) was purchased from Argo, USA; microcrystalline cellulose (MCC - Ethispheres 150, 175 μm) was acquired from NP Pharm, France; poly (vinyl pyrrolidone) (PVP, Mw = 10 kg/mol) and sodium dodecyl sulphate (SDS) were purchased from Sigma Aldrich, UK; ethanol (EtOH, purity > 99.8%) and acetone (Ac, purity > 99.8%) were bought from Fisher Scientific, UK; carbon dioxide (CO_2, purity ≥ 99.8%) was purchased from BOC, UK. The materials were used as-received from the suppliers without any additional purification.

5.4.2. SAS equipment and experimental procedure

5.4.2.1. Particles generation by Supercritical Antisolvent (SAS)

A schematic diagram of the SAS process and its variants, SAS-Fluidized Bed (FB) and SAS-Drug Excipient Mixing (DEM), is shown in **Figure 5-1**a. A complete description of the experimental procedure and details of the equipment used in the SAS process has been presented in our previous work [14]. In summary, the precipitator (500 ml water-jacketed vessel) is pressurized with CO_2 up to the operational pressure (9.0 or 12.0 MPa) and then a constant CO_2 flow is set (40 g/min), while keeping pressure and temperature (40 °C) constant. Following this, solvent is pumped into the precipitator through a nozzle (127 μm) to establish a quasi-steady state composition of solvent and CO_2. The pump feed is then switched to deliver the solution (containing curcumin or curcumin + PVP) and produce fine SAS particles. Once the desired volume of solution has been delivered, the liquid feed is switched back to solvent to purge the line (10 ml) and ensure all material has entered the vessel. The flow rate of the liquid was set to 0.5 ml/min in all experiments. A final washing step with CO_2 only is performed to remove any residual solvent from the precipitated powder. Once completed, the system can be slowly depressurized and the sample collected.

The rig and experimental procedures employed in SAS-FB and SAS-DEM are similar to the SAS process, with some adaptations described in the following sections. While in SAS only fine particles are produced, in SAS-FB and SAS-DEM host particles are charged into the vessel before it is pressurized, so the precipitating guest particles are captured onto the host's surface.

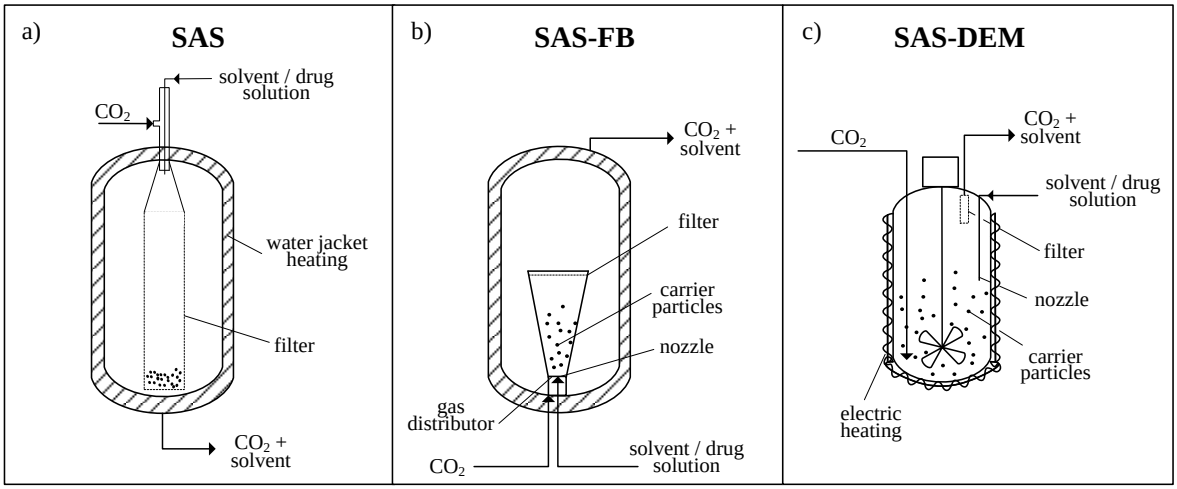

Figure 5-1. Simplified diagram of: a) SAS; b) SAS-FB; c) SAS-DEM.

5.4.2.2. Particles generation and coating by SAS-FB

For the SAS-FB experiments, a glass tapered bed holder with tapered angle (α) of 6.7° and bottom internal diameter of 6.5 mm was used to fluidize the host particles. A sintered stainless steel gas distributor is installed on the bottom of the bed and a 127 µm nozzle is fixed in the middle of it [25], allowing the fluidization of particles and simultaneous delivery of drug solution, as illustrated in **Figure 5-1**b.

In brief, the fluidized bed holder has to be initially loaded with the material to be coated (host particles) and then placed inside the precipitator, which is kept at constant temperature (40°C). After that, the system is closed and CO_2 is initially fed from the top of the vessel (not shown in the figure). Once the operational pressure has been reached (12.0 MPa), the CO_2 inlet is switched to the bottom of the vessel, directly into the base of the bed, and a constant CO_2 flow is then set (40 g/min) by adjusting the outlet micrometric valve. Hence, the upward movement of sc-CO_2 through the gas distributor promotes the fluidization of the host particles. A filter cap on the top of the fluidized bed prevents particles being blown out. Solvent and drug solution are then delivered sequentially into the fluidized bed (0.5 ml/min),

following the SAS procedure previously explained, allowing simultaneous precipitation and coating of guest particles onto host particles.

The minimum fluidization velocity (U_{mf}), that is, the minimum CO_2 velocity to keep particles supported against gravity, was estimated using *Equation 5-1* valid for beds with a tapered angle (α) above 4.5° [28].

$$U_{mf} = \frac{Re_{mf}\ \mu_f}{d_p\ \rho_f} \qquad \textit{Equation 5-1}$$

where μ_f is the kinematic viscosity of the fluid (5.85 x 10^{-5} m^2/s), ρ_f is the density of the fluid (717.8 kg/m^3) and d_p is the particle diameter (1.7 x 10^{-4} m). The Reynolds number at U_{mf} (Re_{mf}) is given by *Equation 5-2*, where *B* is the bottom diameter of tapered bed (6.5 x 10^{-3} m), ε_0 is the voidage of the stagnant bed (0.43), $\emptyset_p$ is the particle sphericity (0.95). The Archimedes number (*Ar*) is given by *Equation 5-3*, where *g* is the gravity acceleration (9.8 m/s^2).

$$Re_{mf} = 10.396\ (Ar)^{0.367}\left(\frac{d_p}{B}\right)^{0.889}\left(\frac{\varepsilon_0}{\emptyset_p}\right)^{-0.731}(\cos\alpha)^{-10.437} \qquad \textit{Equation 5-2}$$

$$Ar = g d_p^3 \frac{(\rho_p - \rho_f)\rho_f}{\mu_f^2} \qquad \textit{Equation 5-3}$$

SAS-FB experiments were performed at U/U_{mf} = 2.8, based on the calculated value from *Equation 5-2*. Two sapphire windows in the precipitator allowed the observation of the behaviour of the fluidized bed during the experiments. However, precise experimental determination of the U_{mf} could not be performed since the CO_2 flow is oscillating (a piston pump is used) and the top of the bed cannot easily be seen.

5.4.2.3. Particles generation and coating by SAS-DEM

In the SAS-DEM configuration, a 300 ml agitated vessel (5500 Compact Mini Bench Top Reactor, Parr Instrument Company) was used to promote particle fluidization. Temperature and stirrer speed can be set by a controller (4836 Reactor Controller, Parr Instrument Company) coupled with the reactor. CO_2 is delivered in the axial direction 2 cm above the bottom of the vessel, helping the impeller to suspend the host particles, while the solvent/solution is delivered in the same direction, 7 cm from the bottom (**Figure 5-1**c).

The experimental procedure begins by loading the host particles into the precipitator, the vessel is closed and the stirrer and heater are switched on. Then the same steps followed in the SAS process are carried out. Similarly to SAS-FB, host particles will be coated by guest particles precipitated from the atomized solution. Particles are maintained in the vessel by a filter placed in the outlet line. In the SAS-DEM experiments, the temperature was kept at 40°C, pressure was 9.0 or 12.0 MPa, liquid solution and CO_2 flow rate were respectively equal to 0.5 ml/min and 40 g/min.

The stirrer speed to keep particles just suspended (N_{js}) depends on the geometry of the system and can be estimated by *Equation 5-4* [29]:

$$N_{JS} = \left(a + b\,\frac{C}{T}\right) \nu_f^{\tau} \left[\frac{g(\rho_p - \rho_f)}{\rho_f}\right]^{\beta} d_p^{\gamma} I^{\delta}\, W^{\theta} \qquad \textit{Equation 5-4}$$

where C is the impeller off bottom clearance (m), T is the inner diameter of stirred tank (m), ν_f is the kinematic viscosity of the fluid (m^2/s), I is the impeller diameter (m), and W is the solid fraction (ratio between solid mass and fluid mass multiplied by 100). For the impeller used here, a 45° pitched 4-blade turbine operating in down-pumping mode (PBT-D), the model parameters are: a = 3.47, b = 1.35, $\tau = 0.1$, $\beta = 0.45$, $\gamma = 0.2$, $\delta = -0.85$; $\theta = 0.22$ ($0.1 < C/T <$

0.35) [29]. In this type of impeller (axial flow in down pumping mode), the material is directed to the periphery of the vessel bottom and then lifted up from the walls [29,30]. The stirrer speed used in the SAS-DEM experiments varied between 1.4 and 4.3 times the N_{js}. As no sapphire window exists in the vessel, the quality of the fluidization could not be assessed during the experiments.

For SAS-FB and SAS-DEM, usually 2 g of host particles were used and different amounts of drug solution were pumped in to achieve the desired guest/host mass ratio. The proportion between the mass of guest particles (m_g) and host particles (m_h) for 100% surface coverage of host particles with a monolayer of guest particles can be calculated by *Equation 5-5* [27], assuming that guest and host particles are spherical with diameters of d_g and d_h and densities ρ_g and ρ_h, respectively.

$$\frac{m_g}{m_h} = \frac{N\, d_g^3\, \rho_g}{d_h^3\, \rho_h} \qquad \textit{Equation 5-5}$$

Where, N is given by *Equation 5-6*:

$$N = 4\, \frac{(d_h + d_g)^2}{d_g^2} \qquad \textit{Equation 5-6}$$

5.4.3. Analyses

5.4.3.1. Scanning electron microscopy (SEM)

Scanning Electron Microscopy (SEM, model Philips XL-30 FEG) was used to access the morphology and size of particles at 10 kV and 10 mA. Samples were deposited on a double-sided adhesive carbon tape and sputter coated (Emscope SC500) with gold for 3 min at 25 mA prior to the analysis.

5.4.3.2. Powder flow properties

Powder flowability before and after coating was accessed by using Carr's compressibility index (CI) and Hausner's ratio (HR), obtained from the tapped and bulk densities of the material, as shown in *Equation 5-7* and *Equation 5-8*, respectively:

$$CI = \frac{\rho_{tap} - \rho_{bulk}}{\rho_{tap}} \times 100\% \qquad \textit{Equation 5-7}$$

$$HR = \frac{\rho_{tap}}{\rho_{bulk}} \qquad \textit{Equation 5-8}$$

Bulk density was estimated by transferring a certain amount of powder to a graduated cylinder (10 ml), weighing the sample and then dividing the mass by the volume occupied. After that, the cylinder was tapped until a constant volume was observed, which was used to obtain the tapped density. The flowability of the samples was then classified according to **Table 5-1** [31].

Table 5-1. Flow behaviour of powders based on their compressibility index (CI) and Hausner's ratio (HI) [31].

CI (%)	HR	Flow character
1-10	1.00-1.11	excellent
11-15	1.12-1.18	good
16-20	1.19-1.25	fair
21-25	1.26-1.34	passable
26-31	1.35-1.45	poor
32-37	1.46-1.59	very poor
>38	>1.6	very, very poor

5.4.3.3. Fourier Transform Infrared Spectroscopy (FTIR)

The chemical structure of raw compounds and processed samples was assessed by Fourier transform infrared spectroscopy (FTIR, Jasco-6300) equipped with an attenuated total

reflectance (ATR) accessory to identify possible molecular interactions among the compounds. Each sample was analysed in triplicate in a range of 800-4000 cm^{-1}. The spectra are composed of 64 scans with a resolution of 4 cm^{-1} [32,33].

5.4.3.4. Differential Scanning Calorimetry (DSC)

Differential Scanning Calorimetry (Discovery DSC 25, TA Instruments) was used to assess the thermal behaviour of unprocessed and processed materials. Each sample was initially deposited in an aluminium pan with a pinhole in the cover and accurately weighed. A heat-cool-heat cycle was used: initial heating from 50°C to 160°C at 20°C/min; quench cool (100°C/min) back to the initial temperature; final heating to 400°C, again at 20°C/min. A nitrogen purge of 50 ml/min was employed during all measurements. This method has shown to be effective in determining the thermal transitions in formulations containing curcumin and PVP [15]. Tests were duplicated and the results presented here correspond to the final heating step.

5.4.3.5. In vitro dissolution studies

A USP 2 dissolution apparatus (rotating paddles) was used to analyse the in vitro dissolution behaviour of the samples. Accurately weighed samples containing equivalent amounts of curcumin (~ 1 mg) were incubated at 37 ± 0.5°C in 200 mL of water with 0.25% w/v sodium dodecyl sulphate (SDS), in accordance with in vitro dissolution procedures for poorly soluble drugs [34–37]. Paddle rotation was kept at 100 rpm and 2 ml of the solution was withdrawn and replaced by the same amount of fresh medium at preselected time intervals. The absorbance of the withdrawn solution was measured by (UV)–visible spectrophotometer (Jenway, Genova Plus) at 425 nm and the corresponding concentration was determined. The percentage of curcumin released at each time (t) was calculated from *Equation 5-9*.

$$Release\ (\%) = \frac{m_t}{m_{100\%}} \times 100\% \qquad \textit{Equation 5-9}$$

where m_t is the mass of curcumin in solution at time t and $m_{100\%}$ is the mass of curcumin after complete dissolution. All tests were carried out in triplicate. The uniformity of the formulations was analysed by the relative standard deviation (RSD) of drug content measured by the (UV)-visible spectrophotometer.

5.5. Results and discussion

5.5.1. Preliminary studies

The combination of particle engineering and coating is an efficient way of preparing drug formulations in a single step. However, due to the number of substances (drug, polymer, carriers, solvents, antisolvent) and phenomena involved, particle precipitation should be initially separated from the fluidization and coating. In other words, first it is necessary to check if particles with the desired properties can be produced by SAS in the selected operating conditions and ensure that the solvents used will not solubilize the host particles. Hence, SAS precipitation and coprecipitation and investigations into solvent suitability were carried out as preliminary studies of this work.

5.5.1.1. SAS precipitation and coprecipitation

Our previous study [15] focused on understanding the coprecipitation of curcumin and PVP by SAS, successfully achieved from different solvent mixtures of acetone (Ac) and ethanol (EtOH) with product recovery as high as 90%. Based on that, the operational parameters for this work were selected. To maximize curcumin recovery, a 70-30 v/v Ac-EtOH solution was used [15], delivered at a flow rate of 0.5 ml/min. The overall (curcumin + PVP) solution concentration was set at 20 mg/ml to intensify the process (decrease the coating time) while

the mass ratio between curcumin and PVP was kept at 1:3 so that the final formulation after coating could have fairly high drug content. The temperature was fixed at 40°C because at lower temperature (35°C), although curcumin recovery increases slightly, particle size decreases [15], leading to a decrease in the guest/host ratio required for full coverage of the host particles surface in the coating experiments performed in the upcoming sections, so a lower drug loading in the formulation would result. The CO_2 flow rate was kept at 40 g/min (X_{CO2} = 0.992), while two different values of pressure were tested, 9.0 and 12.0 MPa. A summary of the materials and operational conditions tested is presented in **Table 5-2**.

Curcumin was initially precipitated alone at 9.0 MPa (run #1, **Table 5-2**) and 12.0 MPa (run #2). For comparison, **Figure 5-2**a,b shows the morphology of unprocessed curcumin and PVP. The rectangular/rod-like shape of raw curcumin crystals with wide size distribution (**Figure 5-2**a) was changed into a combination of needle-like and some spherical particles at the lower pressure (9.0 MPa, **Figure 5-2**c). At the higher pressure (12.0 MPa, **Figure 5-2**d), curcumin precipitated as a needle/filament-like structure with smaller dimensions compared to the raw material.

As the size of curcumin was not significantly reduced and it remained crystalline after SAS precipitation (as will be shown in more detail in section 5.5.8), a significant improvement in its dissolution properties was not be achieved (as demonstrated in section 5.5.9), therefore coprecipitation with PVP was performed by SAS in run #3 at 9.0 MPa (**Table 5-2**). **Figure 5-2**e,f taken at different magnifications show the spherical and uniform nanoparticles of the composite material produced with particle size of 140 ± 63 nm (based on the measurement of 200 particles by Image J analysis software), demonstrating the ability of PVP to inhibit the crystallization of the drug [38].

Table 5-2. Materials, experimental conditions and flow properties of the formulations. Other operational conditions are: temperature = 40°C, X_{CO2} = 0.992, solution concentration = 20 mg/ml, solution flow rate = 0.5 ml/min and CO_2 flow rate = 40 g/min.

Run #	Process	Host particles	Solute	Pressure (Mpa)	m_{guest}/m_{host} (%)	Stirrer speed (rpm)	Carr's index	Hausner's ratio
1	SAS	-	CURC	9	-	-	-	-
2	SAS	-	CURC	12	-	-	-	-
3	SAS	-	CURC/PVP	9	-	-	52%	2.06
4	SAS-DEM	MCC	-	12	-	800	-	-
5	SAS-DEM	corn starch	-	9	-	800	-	-
6	SAS-DEM	lactose	-	9	-	800	-	-
7	SAS-FB	MCC	CURC	12	2.5%	-	10%	1.11
8	SAS-FB	MCC	CURC/PVP	12	2.5%	-	6%	1.07
9	SAS-FB	MCC	CURC/PVP	12	5.0%	-	8%	1.09
10	SAS-DEM	MCC	CURC	12	2.5%	800	5%	1.05
11	SAS-DEM	MCC	CURC/PVP	12	2.5%	800	5%	1.05
12	SAS-DEM	MCC	CURC/PVP	12	5.0%	800	8%	1.08
13	SAS-DEM	corn starch	CURC/PVP	9	5.0%	800	38%	1.61
14	SAS-DEM	corn starch	CURC/PVP	9	10.0%	800	37%	1.58
15	SAS-DEM	corn starch	CURC/PVP	9	20.0%	800	36%	1.55
16	SAS-DEM	lactose	CURC	9	10.0%	800	60%	2.52
17	SAS-DEM	lactose	CURC/PVP	9	10.0%	800	56%	2.29

Run #	Process	Host particles	Solute	Pressure (Mpa)	m_{guest}/m_{host} (%)	Stirrer speed (rpm)	Carr's index	Hausner's ratio
18	SAS-DEM	lactose	CURC/PVP	9	20.0%	800	54%	2.15
19	SAS-DEM	lactose	CURC/PVP	9	30.0%	800	50%	2.00
20	SAS-DEM	lactose	CURC/PVP	9	20.0%	400	58%	2.40
21	SAS-DEM	lactose	CURC/PVP	9	20.0%	1200	57%	2.34

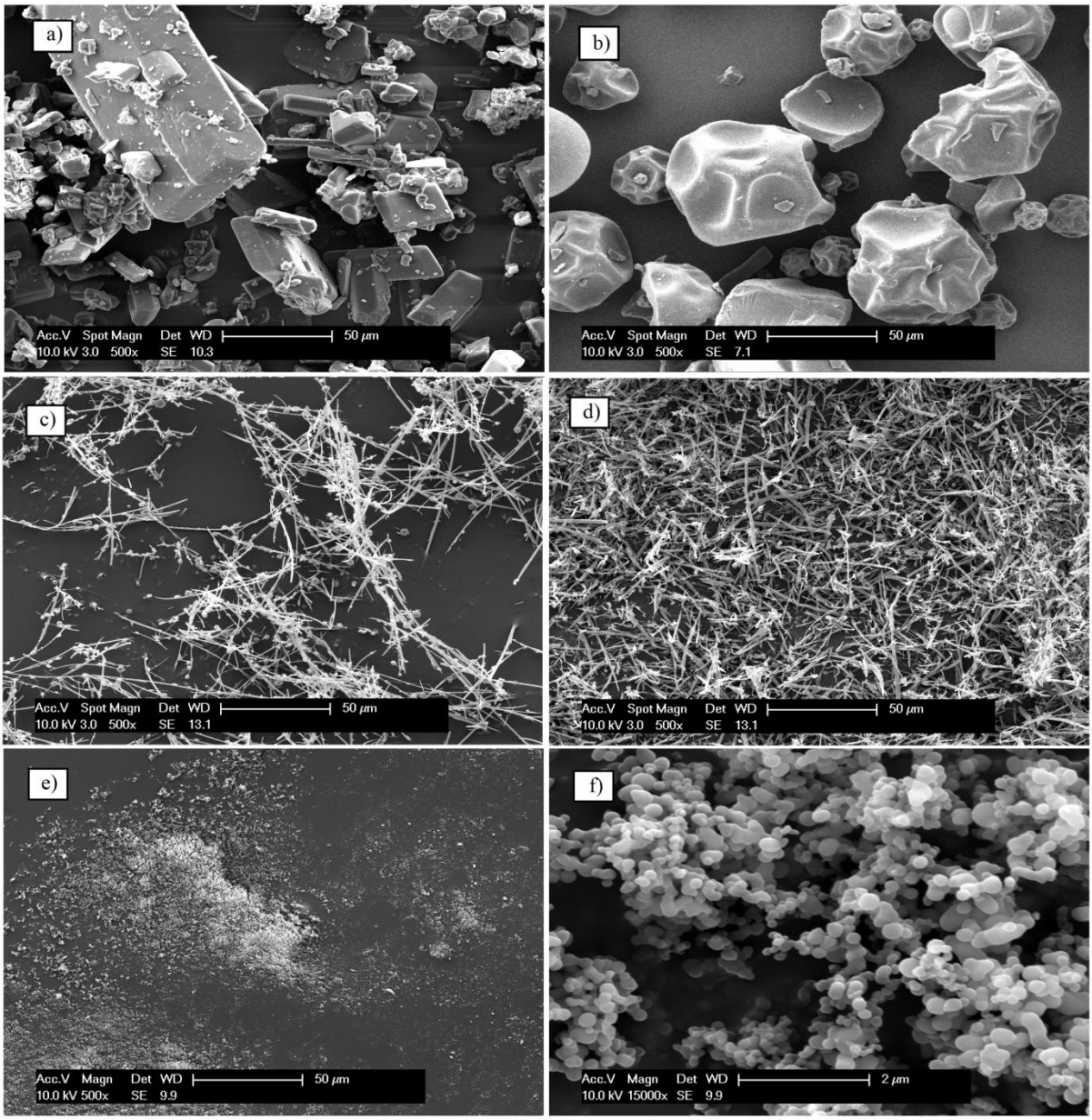

Figure 5-2. SEM images of: a) raw curcumin; b) raw PVP; c) curcumin processed by SAS at 9.0 MPa (run #1); d) curcumin processed by SAS at 12.0 MPa (run #2); e) CURC/PVP coprecipitated by SAS at 9.0 MPa (run #3, Mag. 500X); f) CURC/PVP coprecipitated by SAS at 9.0 MPa (run #3, Mag. 15000X).

Once the SAS coprecipitation of CURC/PVP with the desired features (particle size, morphology and dissolution rate) was demonstrated to be possible at the selected operational conditions, the combination with coating was attempted. As the recovery of CURC/PVP coprecipitates and curcumin loading efficiency have been extensively discussed and optimized in our previous study [15], these properties will not be discussed in the present

work. Here we aim to prove the effectiveness of SAS-FB and SAS-DEM processes in producing formulations with improved release and flow properties in a single step.

5.5.1.2. Compatibility between solvents and host-particles

The first point to be taken into consideration before performing combined coating and coprecipitation is the compatibility between the compounds involved, that is, to ensure that the solvents used to dissolve the drug and the polymer would not dissolve or somehow interact with the host material in the bed. This could change the surface properties of the host particles (for example, surface roughness) and also interfere in the phase behaviour of the precipitating materials.

In this work, the excipients used as host particles are: MCC (175 μm), corn starch (15 μm) and lactose (< 5 μm). Each was treated with solvent only (70-30 v/v Ac-EtOH with no solute dissolved) through SAS-DEM at 800 rpm to investigate possible changes in the surface and morphology of the particles. **Table 5-2** shows the operational conditions used. In runs #4-6, the solvent was delivered for the same duration (and consequently, the same volume) as the solvent and solution delivered in runs #12, #15 and #18, respectively. **Figure 5-3** shows the comparison between the host particles before (left hand side) and after solvent treatment (right hand side), in which no difference in particle surface, shape and size can be seen. This demonstrates that no interactions occurred, and also that the stirrer speed selected was suitable to avoid damaging particles. FT-IR analyses presented later in section 5.5.7 also confirmed that no solvent-excipient interaction took place.

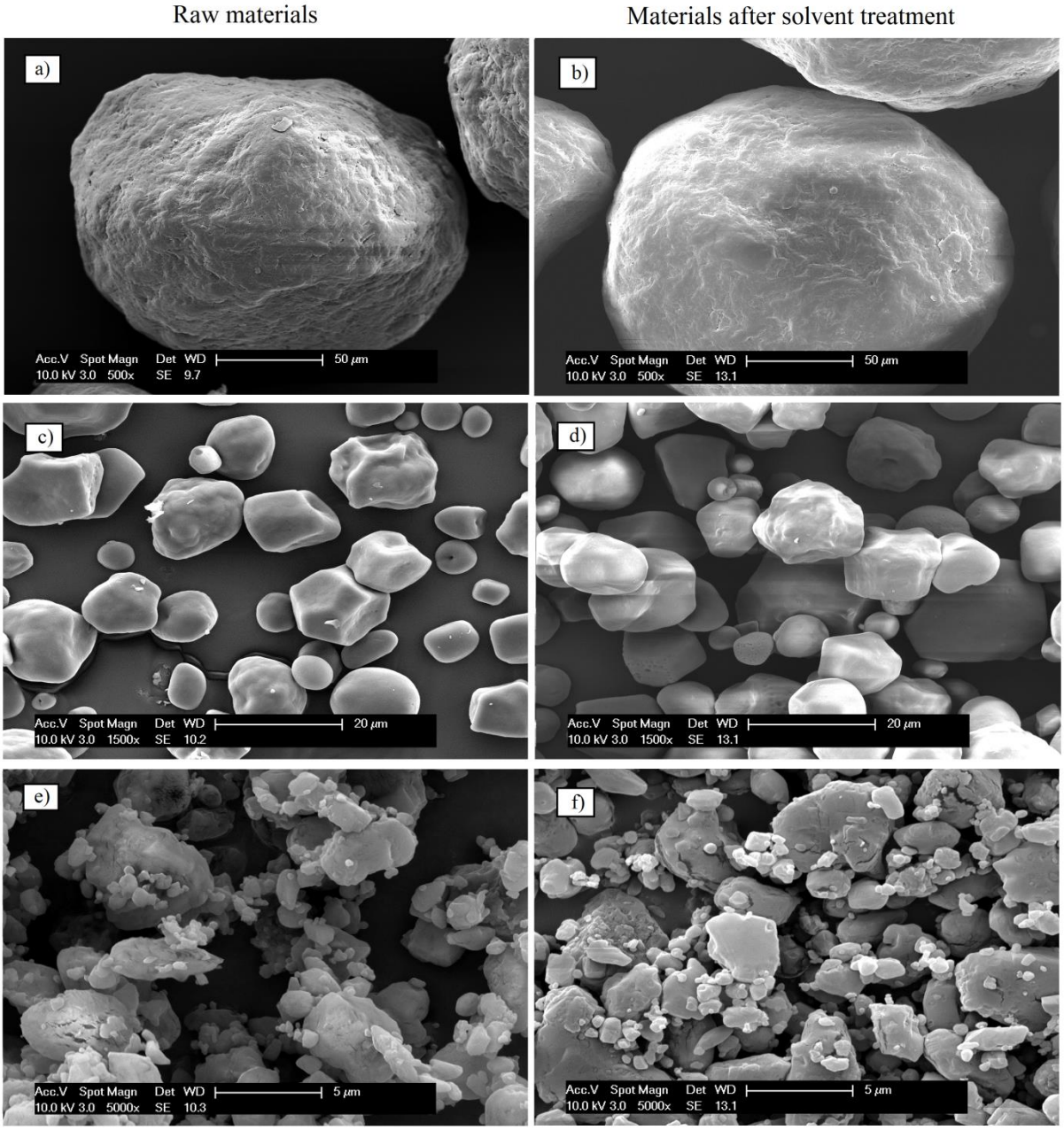

Figure 5-3. SEM images of: a) raw MCC; b) MCC processed by 70-30 acetone/ethanol mixture; c) raw corn starch; d) corn starch processed by 70-30 acetone/ethanol mixture; e) raw lactose; f) lactose processed by 70-30 acetone/ethanol mixture.

5.5.1.3. Guest/host mass ratio for full surface coverage

CURC/PVP coprecipitates were then simultaneously produced and coated on the surface of the host particles. According to *Equation 5-5* (section 5.4.2.3), for a constant mass of host particles (m_h), the smaller its size (d_h), the larger is the surface area available and hence, more

guest particles (m_g) of a certain diameter (d_g) are required for complete coverage of host particles surface. This is illustrated in **Figure 5-4**, calculated for the coating of the host particles by 1:3 CURC/PVP coprecipitates (assuming ρ_g = 1224 kg/m^3, since ρ_{CURC} = 1300 kg/m^3, ρ_{PVP} = 1200 kg/m^3) with diameter (d_g) varying from 10 to 200 nm.

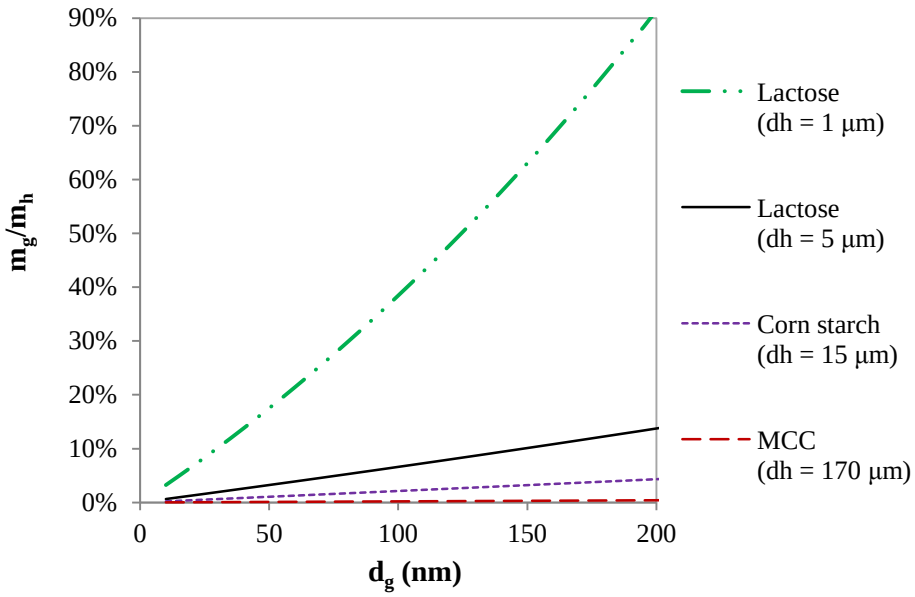

Figure 5-4. Guest/host mass ratio to cover 100% of the surface of host particles (diameter d_h) as a function of the diameter of guest particles (d_g) (*Equation 5-5*).

Table 5-3. Properties of host particles used and guest to host mass ratio.

Material	Role	Density (kg/m^3)	Mean particle size (µm)	m_{guest}/m_{host} (*Equation 5-5*)	m_{guest}/m_{host} tested
CURC/PVP	guest	1224	0.14	-	-
MCC	host	1400	175	0.3%	2.5 - 5.0%
corn starch	host	1550	15	3.0%	5.0 - 20.0%
lactose	host	1540	1 - 5	9.4 - 57.8%	10.0 - 30.0%

For guest particles of 140 nm (representing the coprecipitates obtained in run #3), the calculated mass ratios for complete surface coverage are given in **Table 5-3**, together with the properties of the materials and the range of guest to host mass ratio used in the experiments. As particle sphericity, size distribution and surface roughness are not taken into account in

Equation 5-5, it is possible that the quantity of guest particles required is higher than predicted; therefore, the values calculated were used only as a starting point to select the minimum amount of guest material to be used. Values below 2.5% for guest/host ratio were not used as drug content in the formulations would be too low (< 0.6%).

5.5.1.4. SAS-FB operational conditions

In tapered beds, the inclination of the walls offers unique hydrodynamic properties, resulting in a vigorous circulation of particles [39], which is beneficial in applications that require good mixing and high heat and mass transfer [40]. Although cylindrical beds are more common, the tapered geometry is largely employed in the pharmaceutical, food and chemical industries in processes where a reduction in particle size, due to attrition or chemical reactions, would lead to particle entrainment, channelling and slugging, and hence reduce the efficiency of the fluidization [28]. Since the cross-section area increases with height, the gas velocity is higher in the bottom of the bed, keeping larger particles in movement, while the lower velocity towards the top prevents the elutriation of smaller particles [39,40]. This is advantageous in SAS-FB coating since guest and host particles have very different diameters.

In early exploratory experiments with SAS-FB for MCC coating by CURC/PVP coprecipitates (not shown here), two reasons were identified as the cause of the fluidization to stop: the presence of liquid in the bed and a high proportion of guest/host particles added. In the first case, the operational point (40°C, 9.0 MPa, X_{CO2} = 0.992) was probably below the critical pressure of the mixture 70:30 Ac-EtOH in CO_2, as it has been observed that PVP enlarges the biphasic region of the phase diagram of the CO_2/solvent mixture [41]. In this situation, as the operational point is located within the biphasic region, gas and liquid phases coexist inside the vessel, wetting the host particles. Therefore, they become sticky and lumps are formed in the bottom of the fluidized bed, close to the outlet of the solution jet.

Sometimes the lumps were broken into smaller ones but, still, the top of the bed would usually stop moving. In the second situation, if the ratio guest/host was too high, the strong attraction force between the submicron guest particles also led to the formation of lumps, stopping the fluidization. Taking as reference the reported mixture critical point of the system PVP (with initial concentration of 20 mg/ml) in 50% Ac-EtOH mixture + CO_2 at 40°C (Pc = 9.34, $Xc_{(CO2)}$ = 0.982 [41]), 12.0 MPa was selected to be used in all SAS-FB experiments to make sure that the operating point is located far above the mixture critical point in fully developed supercritical conditions [42], avoiding the presence of liquid in the bed and consequent particle agglomeration.

In SAS-FB, the fluidization of particles is promoted by the upwards flow of CO_2 and the solution jet. Therefore, the CO_2 flow rate selected has to be above the minimum fluidization velocity and at the same time satisfy thermodynamic requirements to favour particle precipitation (molar fraction of CO_2 higher than that of the mixture critical point). The minimum fluidization velocity was calculated according to *Equation 5-1* for MCC particles in a tapered bed (tapered angle α = 6.7° and bottom diameter B = 6.5 mm) at 40°C and 12.0 MPa, resulting in 1.0 cm/s or 14.1 g/min of CO_2. In order to ensure the experiments were performed in the supercritical region, a CO_2 molar fraction above 99% (X_{CO2} = 0.992) was used, based on the delivery of solution at 0.5 ml/min and CO_2 at 40 g/min, which gives U/U_{mf} = 2.8.

Due to the cohesive nature of the finer particles ("Group C" in Geldart's classification [43]), the fluidization of corn starch (d50 = 15 µm) and lactose (d50 < 5 µm) was not possible so only MCC particles (d50 = 175 µm) were coated by SAS-FB. SAS-DEM was then used to coat MCC, corn starch and lactose.

5.5.1.5. SAS-DEM operational conditions

For very small particles, sticky or wet materials, the inter-particle forces are stronger than the hydrodynamic forces exerted by the fluid, leading to channelling, so "normal" fluidization is extremely hard. However, it can be improved by employing stirrers or vibrators [43,44]. In SAS-DEM, the additional energy required to fluidize fine particles is provided by a mechanical stirrer (45° pitched 4-blade turbine). Using an agitated vessel makes the combined coating and coprecipitation process more versatile since the requirement of a minimum CO_2 flow rate to fluidize the particles no longer exists (although the delivery of CO_2 close to the bottom of the vessel helps to keep particles suspended). Moreover, if the operational point falls into the biphasic region, the fluidization should not stop. From the precipitation point of view, the stirrer speed could potentially be adjusted to tune particle size, since it will influence the mass transfer in the system [45]. However, the additional energy requirement and the possibility of damage to the particles need to be taken into account.

The stirrer speed required to have the host particles just suspended (N_{js}) was calculated using *Equation 5-4***,** at the operating conditions shown in **Table 5-2**. In **Table 5-4**, the values obtained are summarized, and the proportion between the stirrer speed used in the experiments (N) and the just suspended speed (N_{Js}) are shown for the different host particles tested.

5.5.2. Coating of MCC by SAS-FB and SAS-DEM

The first coating experiments were performed by precipitating curcumin alone onto MCC particles by SAS-FB (run #7) and SAS-DEM (run #10) with a guest/host mass ratio of 2.5%. The experimental conditions were the same as those used to precipitate curcumin by SAS (run

#2), given in **Table 5-2**. For SAS-DEM, a stirrer speed of 800 rpm (N/Njs = 2.2, **Table 5-4**) was employed.

Table 5-4. Comparison between the just suspended stirrer speed (Njs) and the speed used in the experiments (N) for different host particles and experimental conditions specified in **Table 5-2**.

Host particle	**N_{js} (rpm) (*Equation 5-4*)**	**Speed (N) tested (rpm)**	**N/N_{js}**
MCC	361	800	2.2
corn starch	349	800	2.3
lactose	279	400	1.4
		800	2.9
		1200	4.3

The SEM images in **Figure 5-5**a,c (SAS-FB) and **Figure 5-5**b,d (SAS-DEM) show that the morphology of curcumin crystals obtained by both coating processes was similar (rod/needle-like). However, they are smaller and less aggregated than curcumin produced by SAS, presented in **Figure 5-2**d (for comparison, **Figure 5-5**a,b and **Figure 5-2**d are given in the same magnification). This size decrease following coating has been previously observed, explained by the collection of the precipitating curcumin close to its point of origin on the surface of the host particles, preventing further growth and aggregation [14]. The behaviour of fluidization was observed during the SAS-FB experiment (run #7) through the sapphire windows located in the high-pressure vessel. As predicted by *Equation 5-1* (U_{mf} = 1.0 cm/s, corresponding to 14.1 g/min), the CO_2 flow rate used (40 g/min) was high enough to fluidize the MCC particles but not so high to blow them out of the bed, even when the solution jet was injected. During the entire experiment, a fully fluidized bed was observed, with bubbles being burst at the top [46].

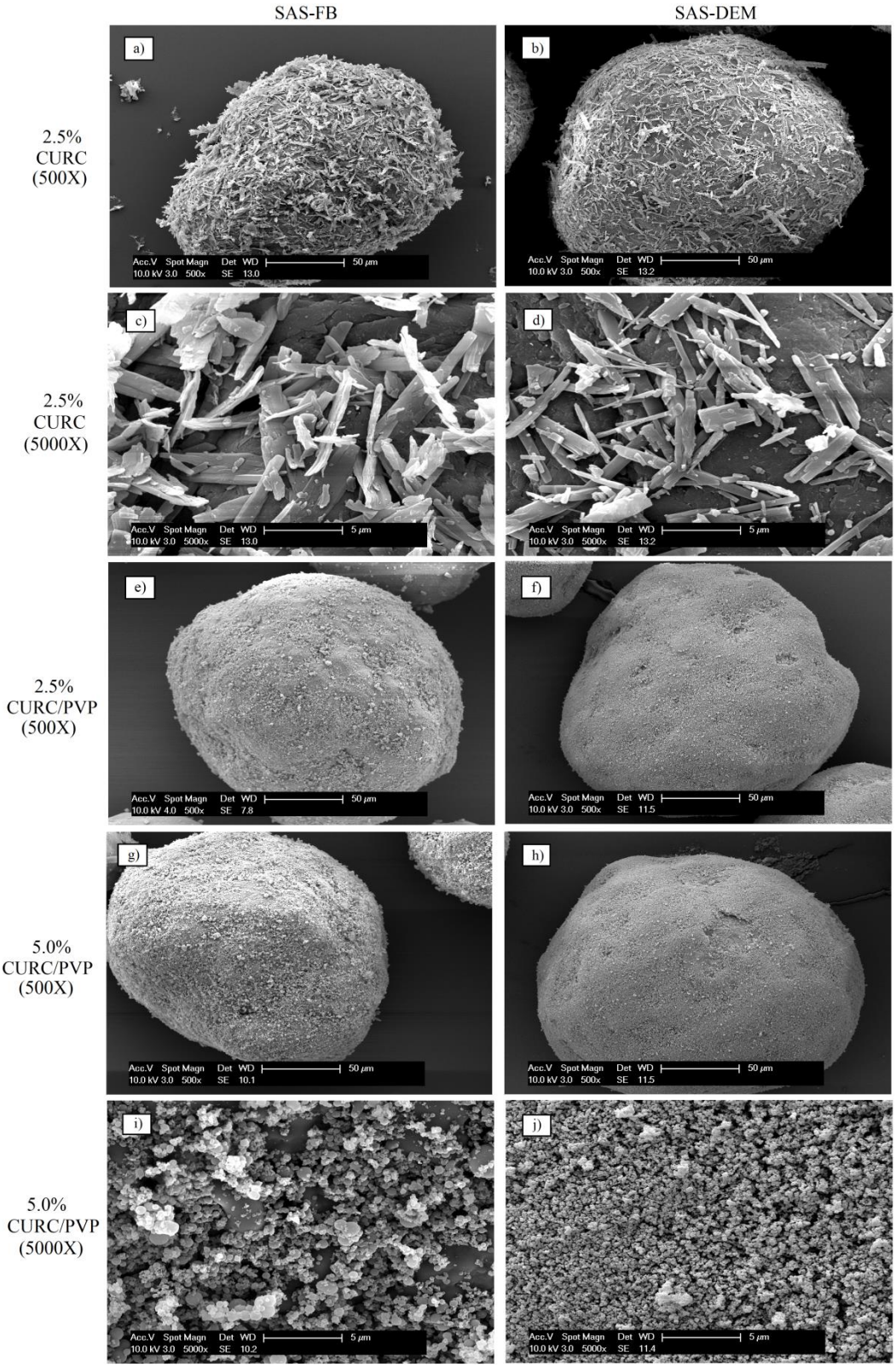

Figure 5-5. SEM images of MCC coated samples using SAS-FB (left-hand side) and SAS-DEM (right-hand side): a) run #7, Mag. 500X; b) run #10, Mag. 500X; c) run #7, Mag. 5000X; d) run #10, Mag. 5000X; e) run #8, Mag. 500X; f) run #11, Mag. 500X; g) run #9, Mag. 500X; h) run #12, Mag. 500X; i) run #9, Mag. 5000X; j) run #12, Mag. 5000X. Experimental conditions are detailed in **Table 5-2**.

In the following tests, curcumin and PVP were coprecipitated and simultaneously coated onto the surface of MCC particles by SAS-FB (runs #8-9) and SAS-DEM (runs #11-12) under the same operational conditions (**Table 5-2**) with two different guest/host mass ratios (2.5% and 5.0%). Samples containing 2.5% guest/host ratio are presented in **Figure 5-5**e (SAS-FB, run #8) and **Figure 5-5**f (SAS-DEM, run #11) while those of 5.0% ratio are shown in **Figure 5-5**g,i (SAS-FB, run #9) and **Figure 5-5**h,j (SAS-DEM, run #12). As the guest/host ratios used were much higher than the calculated value required for full surface coverage of MCC (0.3%, **Table 5-3**), complete surface coverage was achieved in all experiments. Owing to the aggregated nature of the CURC/PVP nanoparticles, a multi-layered coating was obtained (**Figure 5-5**i,j). Pictures taken at higher magnification also reveal that the particle size of the coprecipitates produced by SAS-DEM (**Figure 5-5**j) is considerably smaller than the ones produced by SAS-FB (**Figure 5-5**i) which suggests improved mass transfer.

5.5.3. Coating of corn starch by SAS-DEM

For some pharmaceutical applications, fine excipients are used since they might inhibit the tendency of powder segregation due to differences in particle size between the API and excipient, while also improving compaction properties of tablets [47]. Hence, taking advantage of the additional agitation provided by the stirrer in the SAS-DEM process, fine corn starch particles (15 µm) were fluidized and coated with CURC/PVP coprecipitates using a stirrer speed of 800 rpm (N/N_{js} = 2.3, **Table 5-4**) while keeping the same conditions as in the preliminary studies of SAS coprecipitation (run #3). Three different guest/host ratios were tested: 5% (run #13, **Figure 5-6**a,b), 10% (run #14, **Figure 5-6**c,d) and 20% (run #15, **Figure 5-6**e,f). Although 3% was the calculated guest/host ratio required for full surface coverage of corn starch particles (**Table 5-3**), due to the aggregated nature of the coprecipitates, the coating could not be achieved in a monolayer; hence a much higher proportion of the guest

material was required to cover the surface of the host particles. At 20% mass ratio, the coverage seemed to be almost complete (**Figure 5-6**f), in contrast to the large uncoated areas observed at 5% (**Figure 5-6**b) and 10% ratio (**Figure 5-6**d). Since the attraction force existing between the nanoparticles of coprecipitates is very strong, the stirrer speed used (800 rpm) was not capable of promoting their de-agglomeration.

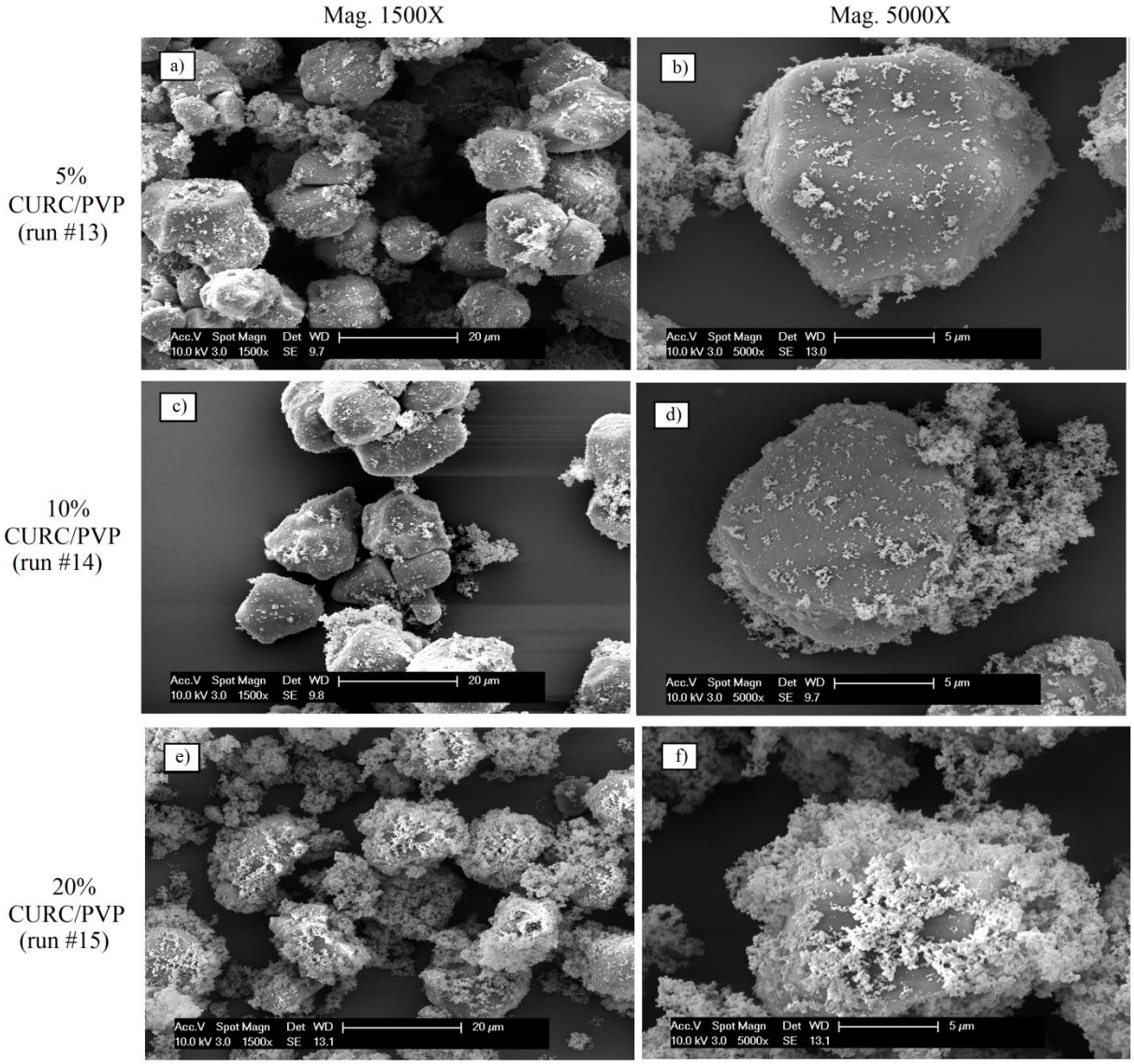

Figure 5-6. SEM images of corn starch coated with CURC/PVP by SAS-DEM at Mag. 1500X (left-hand side) and 5000X (right-hand side) and different guest/host mass ratios: a), b) 5% (run #13); c), d) 10% (run #14); e), f) 20% (run #15). Experimental conditions are detailed in **Table 5-2**.

5.5.4. Coating of lactose by SAS-DEM

Fine lactose particles (d < 5 μm) were also selected to be coated by SAS-DEM in order to produce formulations potentially suitable for pulmonary delivery. Lactose is an excipient approved by most regulatory agencies for such application and its size range (1-5 μm) is appropriate for lung deposition [48,49]. As nanoparticles of coprecipitates would be easily exhaled after inhalation, the combination with carrier particles with the desired properties can be a novel formulation strategy for the delivery of curcumin, which preserves the advantages of delivering nanoparticles to the lungs [50,51].

The coating was performed at a fixed stirrer speed of 800 rpm (N/N_{js} = 2.9, **Table 5-4**) and varying the guest/host ratio in runs #16-19. SEM images showing the formulations obtained are presented in two different magnifications (5000X in the left-hand side and 15000X in the right hand-side) in **Figure 5-7**. In run #16, curcumin alone was used as the guest material, at 10% guest/host ratio. Hence, the typical rod-like crystal morphology of precipitated curcumin, indicated by the red arrows in **Figure 5-7**a,b, can be identified among irregular lactose particles.

In the following experiments, CURC/PVP coprecipitates were used as guest material for the simultaneous coprecipitation and coating of lactose by SAS-DEM. Considering lactose particles with a size range of 1-5 μm (according to the supplier, d_{50} < 5 μm), the guest/host mass ratio required for full lactose surface coverage with a monolayer of CURC/PVP particles would be between 9.4% and 57.8% (**Table 5-3**). The coating experiments were then performed at mass ratios of 10% (run #17, **Figure 5-7**c,d), 20% (run #18, **Figure 5-7**e,f) and 30% (run #19, **Figure 5-7**g,h). Because the size of the coprecipitates is much smaller than the size of the lactose particles, it is possible to clearly see the spherical nano-coprecipitates

coating the irregular lactose particles and aggregates in the SEM images taken at higher magnification (right hand-side of **Figure 5-7**).

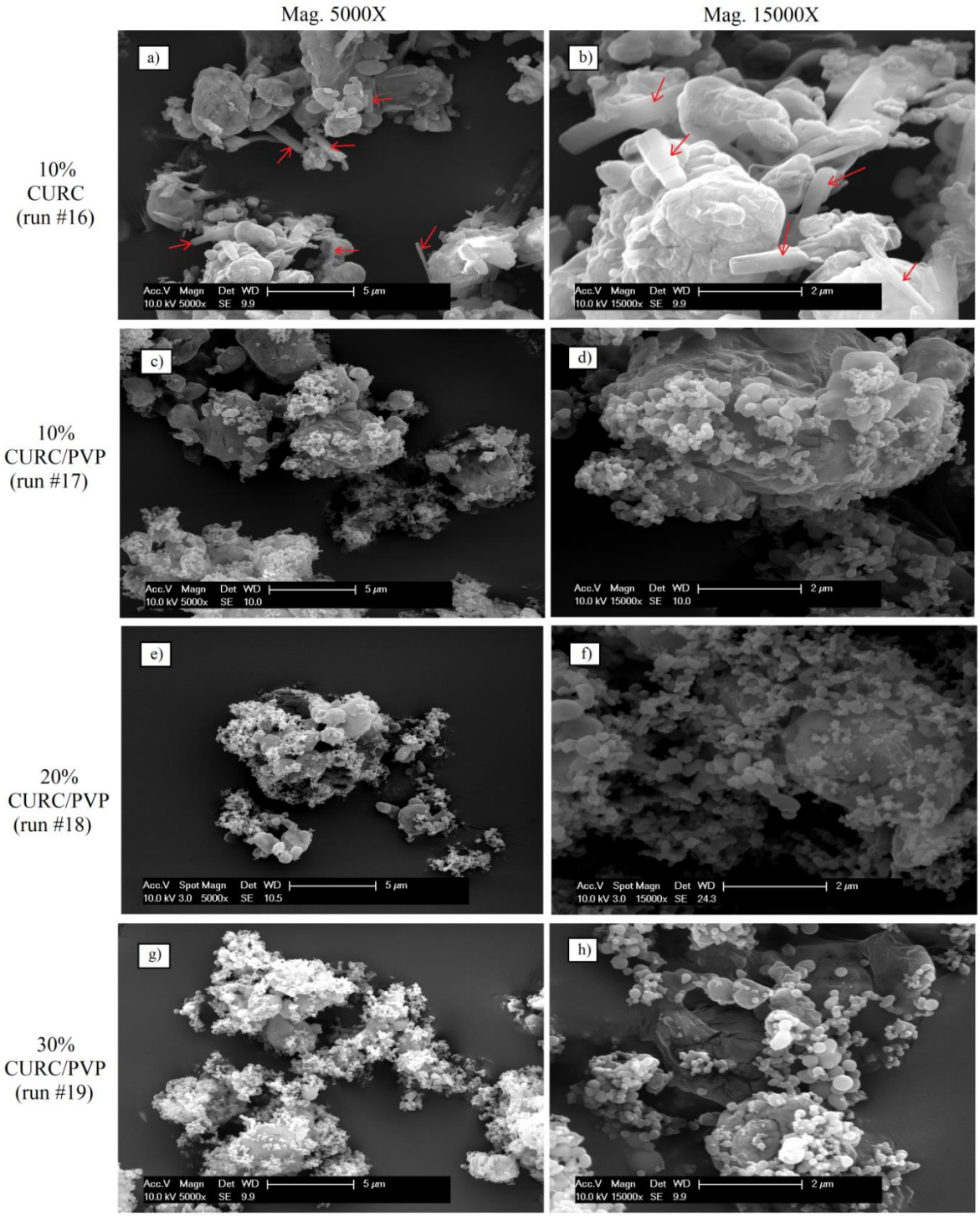

Figure 5-7. SEM images of lactose coated with CURC and CURC/PVP by SAS-DEM at 800 rpm, Mag. 5000X (left-hand side) and 15000X (right-hand side) and different guest/host mass ratios: a) and b) 10% CURC (run #16); c) and d) 10% CURC/PVP (run #17); e) and f) 20% CURC/PVP (run #18); g) and h) 30% CURC/PVP (run #19). Experimental conditions are detailed in **Table 5-2**.

As the size of the carrier/host particles become smaller, it gets more difficult to obtain a uniform surface coating since the host particles also tend to be aggregated. As observed in the SEM images (**Figure 5-7**), the stirrer speed used (800 rpm), was not capable of providing enough energy to break all lactose agglomerates. To investigate the impact of the stirrer speed, two additional experiments were performed: run #20 at 400 rpm (N/N_{js} = 1.4, **Table 5-4**) and run #21 at 1200 rpm (N/N_{js} = 4.3, **Table 5-4**), both at 20% guest/host ratio. As expected, due to the higher energy input, at 1200 rpm (**Figure 5-8**c,d) there seems to be a reduction in the size of the lactose agglomerates in comparison with the sample obtained at 400 rpm (**Figure 5-8**a,b).

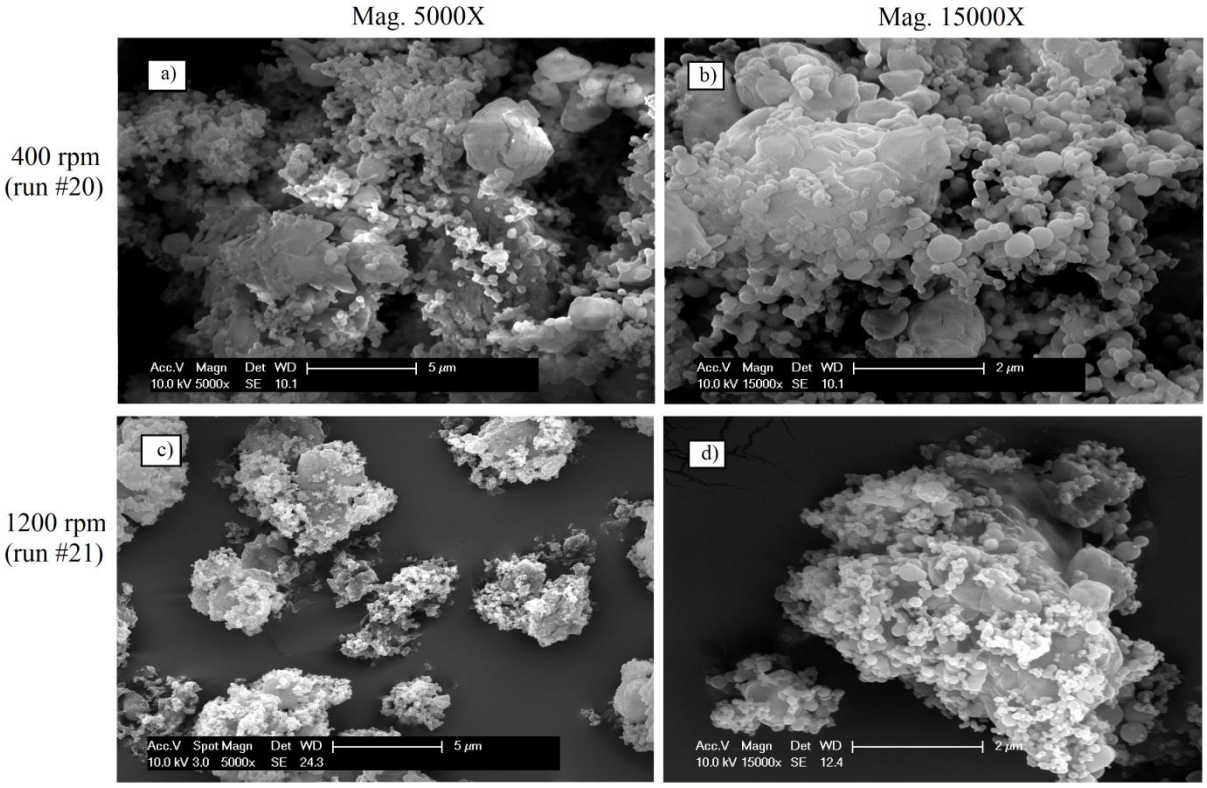

Figure 5-8. SEM images of lactose coated with 20% CURC/PVP by SAS-DEM at Mag. 5000X (left-hand side) and 15000X (right-hand side) and different stirrer speeds: a) and b) 400 rpm (run #20); c) and d) 1200 rpm (run #21). Experimental conditions are detailed in **Table 5-2**.

5.5.5. Product uniformity

Since curcumin is coloured and all host particles are white (**Figure 5-9**), the colour change of host particles after coating can be used as an initial evidence of the success of the process. **Figure 5-9** shows digital pictures of raw materials and some processed samples. As observed, curcumin precipitated by SAS alone (run #2) exhibited an orange colour, but more vivid than that of raw curcumin, probably because of differences in the particle size and in the crystal form produced (section 5.5.8). MCC coated by curcumin (run #7) presents a lighter orange shade, as one would expect from the mixture of orange and white powders. All samples containing CURC/PVP coprecipitates, on the other hand, are yellow due to the change in size and molecular structure of curcumin (section 5.5.8) when dispersed within the matrix of PVP. The colours observed in the coated samples are uniform at this scale, suggesting that the API is uniformly distributed in the formulation. In fact, the relative standard deviation (RSD) of curcumin content varied from 2.2-4.6% for SAS-FB samples and from 1.1-5.7% for SAS-DEM. These values are within the range recommended by FDA (RSD < 6%) [52], demonstrating the ability of both coating processes in producing pharmaceutical formulations in a single-step.

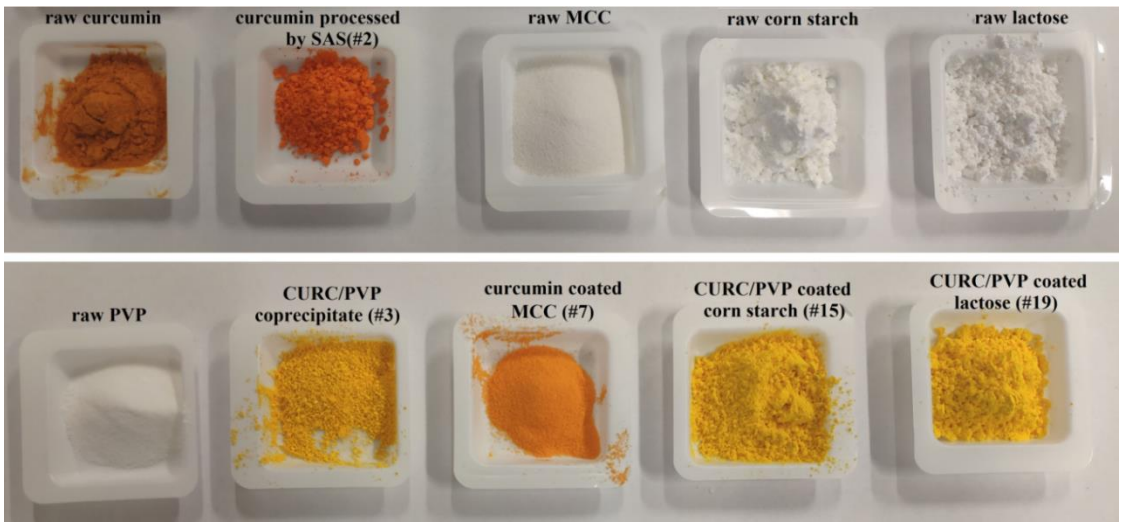

Figure 5-9. Digital pictures of raw materials and processed samples. Experimental conditions are detailed in **Table 5-2**.

5.5.6. Powder flow properties

The flow properties of raw excipients and processed samples were accessed by the measurement of the Carr's compressibility index (CI) and Hausner's ratio (HR) from bulk and tapped density measurements. For raw MCC, corn starch and lactose, the values of CI are, respectively: 7%, 33% and 48%, while the values of HR are: 1.08, 1.48 and 1.90. Therefore, based on **Table 5-1**, these excipients present excellent, very poor and very, very poor flowability, respectively.

The values of CI and HR for the processed samples are shown in **Table 5-2**. As expected, due to the high surface energy of nanoparticles, the coprecipitates produced by SAS (run #3) have even worse flow properties, with CI = 52% and HR = 2.06. By simultaneously precipitating and coating curcumin (run #7, SAS-FB and run #10, SAS-DEM) and CURC/PVP coprecipitates (runs #8-9, SAS-FB and runs #11-12, SAS-DEM) onto the surface of free-flowing MCC particles, the resulting coated materials retained the excellent flowability of the host (5% <CI< 10% and 1.05<HR<1.11) in the range of guest/host ratio tested (up to 5%). This demonstrates the applicability of SAS-FB and SAS-DEM to produce pharmaceutical formulations with improved dissolution (section 5.5.9) and flow properties in a single step by combining fine particles containing the active material with free-flowing host particles.

Formulations with corn starch (36% <CI< 38% and 1.55<HR<1.61) and lactose (50% <CI< 60% and 2.00<HR<2.52) retained the poor flow character of the uncoated carriers. This could be improved by adding very small amounts of flow additives to the formulation, which act as spacers [53] between the host particles, thus reducing inter-particle forces and agglomeration [47,54]. Therefore, future work would aim to explore different mixtures of host particles and additives to optimize the flowability of the powder. By using SAS-DEM, elaborate

formulations with tailored release and flow properties could be produced for direct use in dry powder inhalers [55,56], and to prepare tablets by direct compression [47,57].

5.5.7. Fourier Transform Infrared Spectroscopy (FTIR)

In order to investigate possible interactions between the host particles and solvents, MCC, corn starch and lactose were treated by solvent (70-30 v/v Ac-EtOH mixture) in runs #4-6, for the same duration (same amount delivered) as solvent and solution were pumped in runs #12, #15 and #18, respectively. A qualitative analysis of the IR spectra of compounds before and after solvent treatment (**Figure 5-10**a) revealed that no interactions occurred between solvents and host particles since the same peaks are found comparing the spectra of the materials before and after processing (peak intensity is related to the area of material in contact with the surface of the ATR crystal and the distribution of the sample). Hence, these results confirm that the solvents selected were appropriate for the coating experiments, as previously discussed.

Since the properties of the host particles were unchanged after solvent treatment, the spectra of the coated samples should show a combination of the spectra of raw host particles and guest particles precipitated by SAS (curcumin or CURC/PVP). This can be observed in **Figure 5-10**a, which also shows the chemical similarities between samples produced by SAS-FB (runs #7-8) and SAS-DEM (runs #10-11).

5.5.8. Differential Scanning Calorimetry (DSC)

The thermal behaviour of processed samples and raw materials was analysed by Differential Scanning Calorimetry (DSC). In **Figure 5-10**b it is possible to see that raw curcumin presents an endothermic peak at around 187°C, corresponding to its melting point. After SAS processing (run #2), two peaks were detected (approximately at 178°C and 185°C), which

indicates a change in the crystal form of curcumin [58]. Such crystal modification following supercritical fluid micronization of curcumin has been previously observed [59]. When coprecipitated with PVP, the complete amorphization of curcumin (run #3) is evidenced by the absence of melting point peaks. Only the glass transition temperature of the composite material can be seen at 139°C, close to the glass transition temperature of the pure PVP (150°C), as discussed in more detail elsewhere [15].

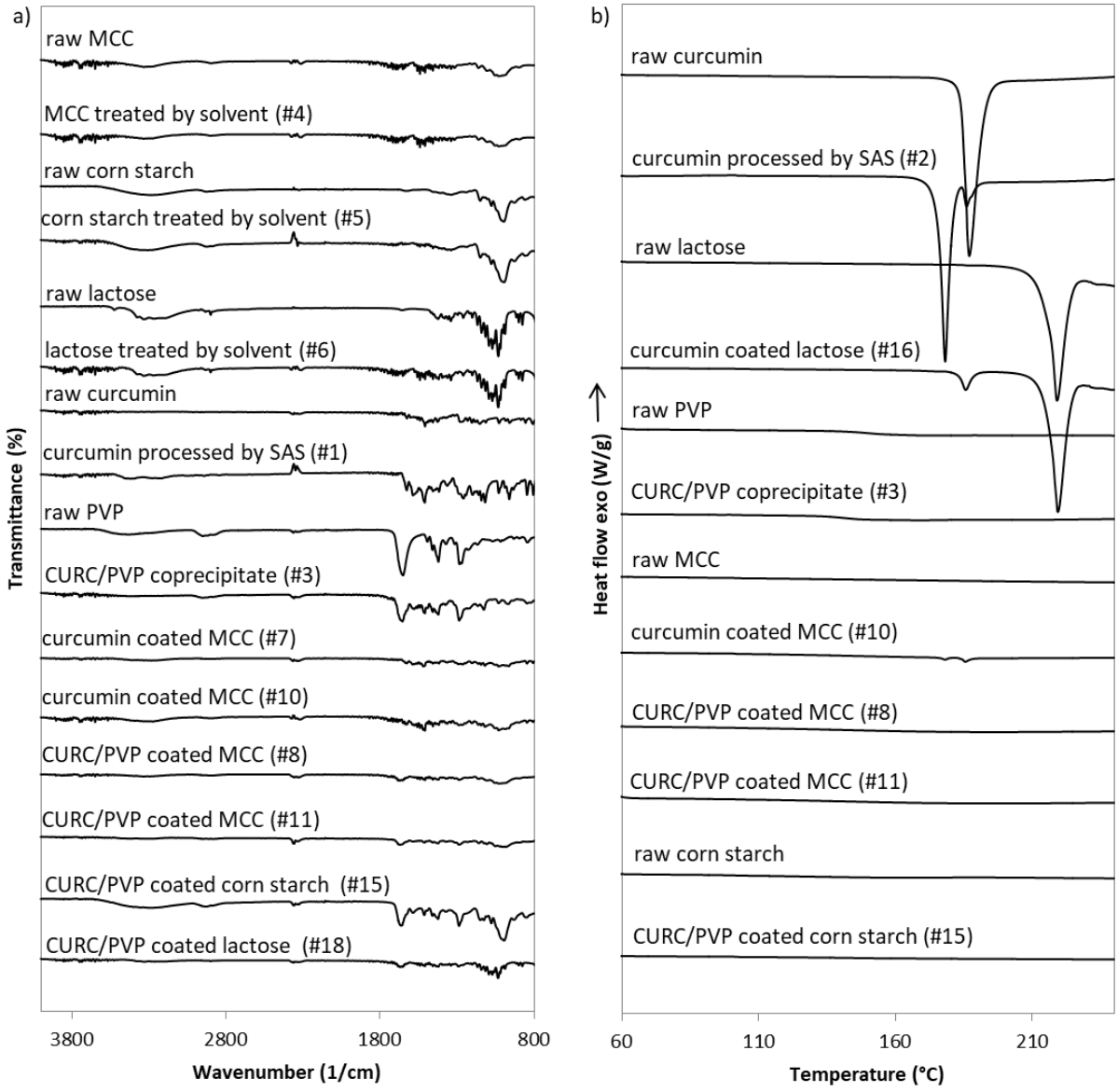

Figure 5-10. a) IR spectra and b) DSC thermograms of raw materials and processed samples. Experimental conditions are detailed in **Table 5-2**.

No thermal transitions for MCC and corn starch could be observed in the temperature range tested, while lactose showed its melting point close to 219°C. In the formulations containing curcumin alone as guest material (runs #10 and #16), one or two melting point peaks were detected, confirming that curcumin maintained a crystalline structure after precipitation and coating. Obviously, formulations with lower curcumin content generated peaks with lower intensity. When CURC/PVP coprecipitates were used as guest material (exemplified by runs #8, #11 and #15 in **Figure 5-10**b), curcumin melting point peaks disappear, showing again the amorphous structure of the coprecipitates.

5.5.9. In vitro dissolution studies

In vitro dissolution studies were performed to analyse the effect of coprecipitation and coating on the release rate of curcumin. **Figure 5-11** shows that the release rate of unprocessed curcumin and 1:3 mass ratio physical mixture (PM) of curcumin and PVP was much slower than the other samples. After 60 minutes of test, only approximately 11% and 15% of curcumin, respectively, was dissolved. This clearly justifies the need of using other approaches to improve curcumin dissolutions properties.

The size reduction accomplished by SAS (run #2) led to a faster release than raw curcumin and physical mixture. However, as SAS-processed curcumin maintained its crystallinity (section 5.5.8), further improvement was prevented and hence the release reached only 60% in 60 minutes. Simultaneous precipitation and coating of curcumin onto host particles in run #7 (SAS-FB) and #10 (SAS-DEM) yields similar behaviour to SAS curcumin (run #2) with no perceived improvement (**Figure 5-11**). In fact, the SAS-processed sample showed an initially faster release probably because thinner crystals (**Figure 5-2**d) were produced compared to the curcumin crystals in the coated samples (**Figure 5-5**a,b).

In contrast, coprecipitation with PVP demonstrated remarkable improvement in the dissolution rate of curcumin. Even though differences in the particle size of coprecipitates produced by SAS-FB (**Figure 5-5**i), and SAS-DEM (**Figure 5-5**j) were observed, the formulations exhibited similar dissolution behaviour. For all samples containing coprecipitates (runs #3, #8, #11, #17 in **Figure 5-11**), a complete release was achieved in the first 5 minutes of the test whereas, at the same time interval, raw curcumin released just 3% and SAS-processed curcumin (run #2) around 20%. The superior dissolution properties of the coprecipitates are explained by the dispersion of curcumin within the matrix of PVP, which lead to the formation of amorphous particles (section 5.5.8) and consequent improvement in curcumin solubility [15].

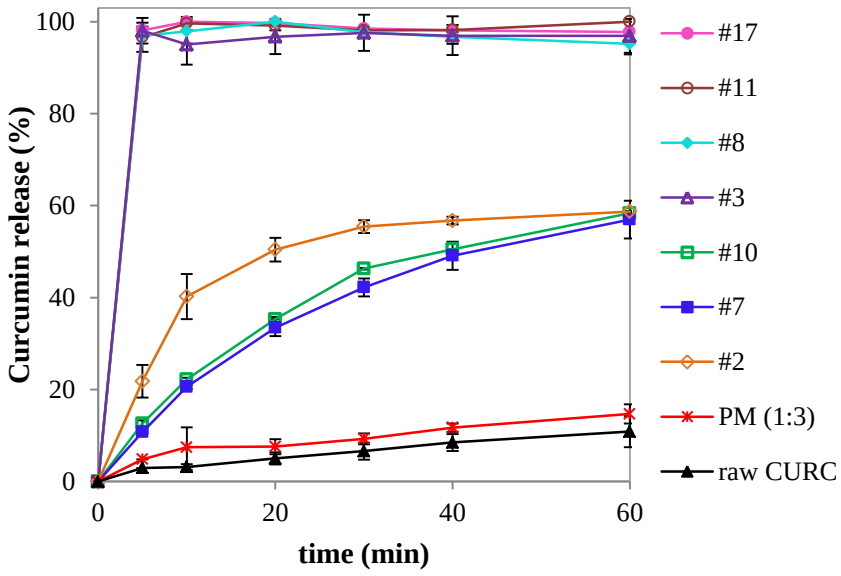

Figure 5-11. In vitro dissolution profile of raw curcumin, curcumin/PVP physical mixture (1:3) and processed samples. Experimental conditions are detailed in **Table 5-2**.

5.6. Conclusions

Curcumin coprecipitation with PVP and simultaneous coating onto host particles was performed in a single step by combining the SAS process with two different configurations of fluidized bed: SAS-FB and SAS-DEM, in which the fluidization was respectively promoted

inside of a tapered bed by the upward CO_2 flow and in a stirred vessel. By employing a systematic exploration of the processes, particle coprecipitation and coating was attempted and successfully achieved for the first time, allowing significant improvement in the release and flow properties of curcumin formulations: the particle size and amorphous nature of the coprecipitated curcumin provided solubility while the size of the host particles contributed flowability.

SAS-FB was demonstrated to be effective for the coating of large MCC (175 μm) particles while fine and cohesive particles of corn starch (15 μm) and lactose (< 5 μm) required the aid of the stirrer in SAS-DEM. As the coated samples retained the flow character of the uncoated host particles, in the range of guest/host ratio tested, excellent flowability was maintained for all MCC formulations which combined the advantages of nano-particulate systems in a free-flowing powder. Fine host particles, on the other hand, would require the addition of flow enhancers, which is the aim of future work.

The integrated SCF-based processes described here benefit from a reduction in the number of processing steps, minimising the requirement to transfer product between process units and lowering the risk of workers' exposure to nanoparticles. They present a great potential for application in other powder processing industries in which the release of the active needs to be controlled.

5.7. Acknowledgements

The authors would like to thank the National Council for Scientific and Technological Development (CNPQ, Brazil) for the financial support through the Science Without Borders Program.

5.8. Competing interests

The authors would like to declare that there are no competing interests.

5.9. References

[1] M. Jivraj, L.G. Martini, C.M. Thomson, C.M. Thomson, An overview of the different excipients useful for the direct compression of tablets, Pharm. Sci. Technolo. Today. 3 (2000) 58–63.

[2] F.J. Muzzio, T. Shinbrot, B.J. Glasser, Powder technology in the pharmaceutical industry : the need to catch up fast, 124 (2002) 1–7.

[3] I. Pasquali, R. Bettini, Are pharmaceutics really going supercritical?, Int. J. Pharm. 364 (2008) 176–187. doi:10.1016/j.ijpharm.2008.05.014.

[4] M. Gibson, Pharmaceutical Preformulation and Formulation: A Practical Guide from Candidate Drug Selection to Commercial Dosage Form, 2005. doi:10.1021/op050157h.

[5] M.S. Ku, W. Dulin, M.S. Ku, W. Dulin, A biopharmaceutical classification-based Right- First-Time formulation approach to reduce human pharmacokinetic variability and project cycle time from First-In-Human to clinical Proof-Of-Concept, Pharm. Dev. Technol. 17 (2012) 285–302. doi:10.3109/10837450.2010.535826.

[6] S. Jain, N. Patel, S. Lin, Solubility and dissolution enhancement strategies: current understanding and recent trends, Drug Dev. Indusrial Pharm. 41 (2015) 875–887. doi:10.3109/03639045.2014.971027.

[7] J. Zhang, L. Wu, H.K. Chan, W. Watanabe, Formation, characterization, and fate of inhaled drug nanoparticles, Adv. Drug Deliv. Rev. 63 (2011) 441–455. doi:10.1016/j.addr.2010.11.002.

[8] M. D. Ticehurst, P. A. Basford, C. I. Dallman, T. M. Lukas, P. V. Marshall, G. Nichols, D. Smith, Characterisation of the influence of micronisation on the crystallinity and physical stability of revatropate hydrobromide, Int. J. Pharm. 193 (2000) 247–259. doi:10.1016/S0378-5173(99)00347-6.

[9] N. Rasenack, B.W. Müller, Micron-Size Drug Particles: Common and Novel Micronization Techniques, Pharm. Dev. Technol. 9 (2004) 1–13. doi:10.1081/PDT-

120027417.

[10] R. Kaur, T. Garg, B. Malik, U.D. Gupta, P. Gupta, G. Rath, A.K. Goyal, Development and characterization of spray-dried porous nanoaggregates for pulmonary delivery of anti-tubercular drugs, Drug Deliv. 23 (2016) 882–887. doi:10.3109/10717544.2014.920428.

[11] D.F. Bain, D.L. Munday, A. Smith, Solvent influence on spray-dried biodegradable microspheres, J. Microencapsul. 16 (1999) 453–474. doi:10.1080/026520499288915.

[12] C. Bosquillon, C. Lombry, V. Préat, R. Vanbever, Influence of formulation excipients and physical characteristics of inhalation dry powders on their aerosolization performance, J. Control. Release. 70 (2001) 329–339. doi:10.1016/S0168-3659(00)00362-X.

[13] R.B. Gupta, Supercritical fluid technology for particle engineering, in: R.B. Gupta, U.B. Kompella (Eds.), Nanoparticle Technol. Drug Deliv., 1st ed., Taylor and Francis Group, New York, 2006: pp. 53–84.

[14] R.L. Matos, T. Lu, C. McConville, G. Leeke, A. Ingram, Analysis of curcumin precipitation and coating on lactose by the integrated supercritical antisolvent-fluidized bed process, J. Supercrit. Fluids. 141 (2018) 143–156. doi:10.1016/j.supflu.2017.12.013.

[15] R.L. Matos, T. Lu, V. Prosapio, C. McConville, G. Leeke, A. Ingram, Coprecipitation of curcumin/PVP with enhanced dissolution properties by the supercritical antisolvent process, J. CO2 Util. 30 (2019) 48–62. doi:10.1016/j.jcou.2019.01.005.

[16] A. Tandya, H.Q. Zhuang, R. Mammucari, N.R. Foster, Supercritical fluid micronization techniques for gastroresistant insulin formulations, J. Supercrit. Fluids. 107 (2016) 9–16. doi:10.1016/j.supflu.2015.08.009.

[17] E. Reverchon, R. Adami, G. Caputo, I. De Marco, Spherical microparticles production by supercritical antisolvent precipitation: Interpretation of results, J. Supercrit. Fluids. 47 (2008) 70–84. doi:10.1016/j.supflu.2008.06.002.

[18] E. Reverchon, I. De Marco, E. Torino, Nanoparticles production by supercritical antisolvent precipitation: A general interpretation, J. Supercrit. Fluids. 43 (2007) 126–138. doi:10.1016/j.supflu.2007.04.013.

[19] V. Prosapio, E. Reverchon, I. De Marco, Formation of PVP/nimesulide microspheres by supercritical antisolvent coprecipitation, J. Supercrit. Fluids. 118 (2016) 19–26. doi:10.1016/j.supflu.2016.07.023.

[20] R.L. Matos, S.A.B. Vieira, D. Melo, E.C.M. Cabral, N.R. Foster, Dense CO2 technology : Overview of recent applications for drug processing / formulation / delivery, Chem. Eng. Process. Process Intensif. 140 (2019) 64–77. doi:10.1016/j.cep.2019.04.009.

[21] G.P. Sanganwar, S. Sathigari, R.J. Babu, R.B. Gupta, Simultaneous production and co-mixing of microparticles of nevirapine with excipients by supercritical antisolvent method for dissolution enhancement, Eur. J. Pharm. Sci. 39 (2010) 164–174. doi:10.1016/j.ejps.2009.11.011.

[22] S.K. Sathigari, C.A. Ober, G.P. Sanganwar, R.B. Gupta, R.J. Babu, Single-Step Preparation and Deagglomeration of Itraconazole Microflakes by Supercritical Antisolvent Method for Dissolution Enhancement, J. Pharm. Sci. 100 (2011) 2952–2965. doi:10.1002/jps.22524.

[23] C.A. Ober, L. Kalombo, H. Swai, R.B. Gupta, Preparation of rifampicin/lactose microparticle composites by a supercritical antisolvent-drug excipient mixing technique for inhalation delivery, Powder Technol. 236 (2013) 132–138. doi:10.1016/j.powtec.2012.04.057.

[24] G.A. Leeke, T. Lu, R.H. Bridson, J.P.K. Seville, Application of nano-particle coatings to carrier particles using an integrated fluidized bed supercritical fluid precipitation process, J. Supercrit. Fluids. 91 (2014) 7–14. doi:10.1016/j.supflu.2014.03.012.

[25] Q. Li, D. Huang, T. Lu, J.P.K. Seville, L. Xing, G.A. Leeke, Supercritical fluid coating of API on excipient enhances drug release, Chem. Eng. J. 313 (2017) 317–327. doi:10.1016/j.cej.2016.12.066.

[26] V. Prosapio, I. De Marco, E. Reverchon, Supercritical antisolvent coprecipitation mechanisms, J. Supercrit. Fluids. 138 (2018) 247–258. doi:10.1016/j.supflu.2018.04.021.

[27] J. Yang, A. Sliva, A. Banerjee, R.N. Dave, R. Pfeffer, Dry particle coating for improving the flowability of cohesive powders, Powder Technol. 158 (2005) 21–33.

doi:10.1016/j.powtec.2005.04.032.

[28] M.H. Khani, Models for prediction of hydrodynamic characteristics of gas-solid tapered and mini-tapered fluidized beds, Powder Technol. 205 (2011) 224–230. doi:10.1016/j.powtec.2010.09.018.

[29] R. Jafari, P.A. Tanguy, J. Chaouki, Characterization of Minimum Impeller Speed for Suspension of Solids in Liquid at High Solid Concentration , Using Gamma-Ray Densitometry, 2012 (2012). doi:10.1155/2012/945314.

[30] M. Schafer, M. Yianneskis, P. Wachter, F. Durst, Trailing Vortices around a 45 " Pitched-Blade Impeller, 44 (1998) 1233–1246.

[31] R. L. Carr, Evaluating flow properties of solids, Chem. Eng. 72 (1965) 163–168.

[32] J. Li, I.W. Lee, G.H. Shin, X. Chen, H.J. Park, Curcumin-Eudragit® e PO solid dispersion: A simple and potent method to solve the problems of curcumin, Eur. J. Pharm. Biopharm. 94 (2015) 322–332. doi:10.1016/j.ejpb.2015.06.002.

[33] M. Anwar, I. Ahmad, M.H. Warsi, S. Mohapatra, N. Ahmad, S. Akhter, A. Ali, F.J. Ahmad, Experimental investigation and oral bioavailability enhancement of nano-sized curcumin by using supercritical anti-solvent process, Eur. J. Pharm. Biopharm. 96 (2015) 162–172. doi:10.1016/j.ejpb.2015.07.021.

[34] V.P. Shah, A. Noory, C. Noory, B. McCullough, S. Clarke, R. Everett, H. Naviasky, B.N. Srinivasan, D. Fortman, J.P. Skelly, In vitro dissolution of sparingly water-soluble drug dosage forms, Int. J. Pharm. 125 (1995) 99–106. doi:10.1016/0378-5173(95)00123-Z.

[35] S.M.H. Rahman, T.C. Telny, T.K. Ravi, S. Kuppusamy, Role of Surfactant and pH in Dissolution of Curcumin., Indian J. Pharm. Sci. 71 (2009) 139–142. doi:10.4103/0250-474X.54280.

[36] K. Gowthamarajan, S.K. Singh, Dissolution testing for poorly soluble drugs: A continuing perspective, Dissolution Technol. 17 (2010) 24–32. doi:10.14227/DT170310P24.

[37] P. Knöös, S. Onder, L. Pedersen, L. Piculell, S. Ulvenlund, M. Wahlgren, Surfactants modify the release from tablets made of hydrophobically modified poly (acrylic acid),

Results Pharma Sci. 3 (2013) 7–14. doi:10.1016/j.rinphs.2013.08.001.

[38] H. Sekikawa, M. Nakano, T. Arita, Inhibitory Effect of Polyvinylpyrrolidone on the Crystallization of Drugs, Chem. Pharm. Bull. 26 (1978) 118–126. doi:10.1248/cpb.26.118.

[39] F. Depypere, J.G. Pieters, K. Dewettinck, PEPT visualisation of particle motion in a tapered fluidised bed coater, J. Food Eng. 93 (2009) 324–336. doi:10.1016/j.jfoodeng.2009.01.042.

[40] M. Rasteh, F. Farhadi, A. Bahramian, Hydrodynamic characteristics of gas-solid tapered fluidized beds: Experimental studies and empirical models, Powder Technol. 283 (2015) 355–367. doi:10.1016/j.powtec.2015.06.002.

[41] R. Campardelli, E. Reverchon, I. De Marco, PVP microparticles precipitation from acetone-ethanol mixtures using SAS process: Effect of phase behavior, J. Supercrit. Fluids. 143 (2019) 321–329. doi:10.1016/j.supflu.2018.09.010.

[42] I. De Marco, M. Rossmann, V. Prosapio, E. Reverchon, A. Braeuer, Control of particle size, at micrometric and nanometric range, using supercritical antisolvent precipitation from solvent mixtures: Application to PVP, Chem. Eng. J. 273 (2015) 344–352. doi:10.1016/j.cej.2015.03.100.

[43] D. Geldart, Types of gas fluidization, Powder Technol. 7 (1973) 285–292. doi:10.1016/0032-5910(73)80037-3.

[44] D. Geldart, N. Harnby, A.C. Wong, Fluidization of cohesive powders, Powder Technol. 37 (1984) 25–37. doi:10.1016/0032-5910(84)80003-0.

[45] A. Martín, M.J. Cocero, Numerical modeling of jet hydrodynamics, mass transfer, and crystallization kinetics in the supercritical antisolvent (SAS) process, J. Supercrit. Fluids. 32 (2004) 203–219. doi:10.1016/j.supflu.2004.02.009.

[46] Y. Peng, L.T. Fan, Hydrodynamic characteristics of fluidization in liquid-solid tapered beds, Chem. Eng. Sci. 52 (1997) 2277–2290. doi:10.1016/S0009-2509(97)00061-4.

[47] Z. Huang, J. V Scicolone, X. Han, R.N. Davé, Improved blend and tablet properties of fine pharmaceutical powders via dry particle coating, Int. J. Pharm. 478 (2015) 447–455. doi:10.1016/j.ijpharm.2014.11.068.

[48] A.S. Silva, M.T. Tavares, A. Aguiar-Ricardo, Sustainable strategies for nano-in-micro particle engineering for pulmonary delivery, J. Nanoparticle Res. 16 (2014) 1–17. doi:10.1007/s11051-014-2602-0.

[49] D.I. Daniher, J. Zhu, Dry powder platform for pulmonary drug delivery, Particuology. 6 (2008) 225–238. doi:10.1016/j.partic.2008.04.004.

[50] C. Loira-Pastoriza, J. Todoroff, Delivery strategies for sustained drug release in the lungs, Adv. Drug Deliv. Rev. 75 (2014) 81–91. doi:10.1016/j.addr.2014.05.017.

[51] I.M. El-sherbiny, N.M. El-baz, M.H. Yacoub, Inhaled nano- and microparticles for drug delivery, Glob. Cardiol. Sci. Pract. (2015) 1–14. doi:10.5339/gcsp.2015.2.

[52] C.J.S. BRIAN R. ROHRS, GREGORY E. AMIDON, RICHARD H. MEURY, PAMELA J. SECREAST, HARRY M. KING, Particle Size Limits to Meet USP Content Uniformity Criteria for Tablets and Capsules, J. Pharm. Sci. 95 (2006) 1049–1059. doi:DOI 10.1002/jps.

[53] C. Bresges, N.A. Urbanetz, Determination of the minimum number of spacer particles ensuring non-contact between host particles - A new approach by numerical modelling, Powder Technol. 187 (2008) 260–272. doi:10.1016/j.powtec.2008.03.002.

[54] L. Qu, Q. Zhou, J.A. Denman, P.J. Stewart, K.P. Hapgood, D.A. V Morton, Influence of coating material on the flowability and dissolution of dry-coated fine ibuprofen powders, Eur. J. Pharm. Sci. 78 (2015) 264–272. doi:10.1016/j.ejps.2015.07.016.

[55] Q.T. Zhou, D. a V Morton, Drug-lactose binding aspects in adhesive mixtures: Controlling performance in dry powder inhaler formulations by altering lactose carrier surfaces, Adv. Drug Deliv. Rev. 64 (2012) 275–284. doi:10.1016/j.addr.2011.07.002.

[56] M. Gera, V. a Saharan, M. Kataria, V. Kukkar, Mechanical methods for dry particle coating processes and their applications in drug delivery and development., Recent Pat. Drug Deliv. Formul. 4 (2010) 58–81. doi:10.2174/187221110789957200.

[57] M.C. Gohel, P.D. Jogani, A review of co-processed directly compressible excipients, J. Pharm. Pharm. Sci. 8 (2005) 76–93.

[58] P. Sanphui, N.R. Goud, U.B.R. Khandavilli, S. Bhanoth, A. Nangia, New polymorphs of curcumin, Chem. Commun. 47 (2011) 5013–5015. doi:10.1039/c1cc10204d.

[59] F. Kurniawansyah, R. Mammucari, N.R. Foster, Polymorphism of curcumin from dense gas antisolvent precipitation, Powder Technol. 305 (2017) 748–756. doi:10.1016/j.powtec.2016.10.067.

Chapter 6 -

GENERAL DISCUSSION AND RECOMMENDATIONS FOR FUTURE WORK

6.1. Main findings and recommendations for future work

This work has demonstrated the steps taken towards the development of curcumin formulations with improved dissolution and flow properties using supercritical fluids. Several formulation strategies and processing methods were reviewed in Chapter 2 and the combination of SAS precipitation and coating in a tapered fluidized bed (SAS-FB) and stirred vessel (SAS-DEM) were found to be suitable means to achieve the aims of the project.

Therefore, in Chapter 3, curcumin was precipitated onto the surface of free-flowing lactose particles (125 μm) by SAS-FB with the aim of improving curcumin dissolution (by size reduction) and flowability (by association with larger carrier particles). The investigation of several operational parameters contributed to a better understanding of the precipitation behaviour of curcumin from two different solvents and, for the first time, in the presence of fluidized particles. It was shown that formulations with uniform curcumin content were obtained, practically free of residual organic solvent while keeping the chemical structure of the raw materials. Moreover, SAS-FB particles were found to be smaller and less aggregated than SAS particles, so the formulation obtained would potentially be suitable for inhalation. Additional tests in a Twin Stage Impinger (TSI) [1,2] and Andersen Cascade Impactor (ACI) [3,4], for example, would have to be performed to check the amount of drug reaching the different regions of the respiratory tract and hence, confirm the suitability of the formulation for the suggested delivery route.

The progress of the research showed that, although a reduction in the size and crystallinity of curcumin was previously achieved, this was insufficient to significantly improve its dissolution properties (dissolution tests only presented in Chapters 4 and 5). Chapter 4 then focused on that issue. Curcumin was coprecipitated with PVP by SAS, exploring again in the experimental design different regions of the VLE phase diagram of the solvent-antisolvent

mixture, which were shown to affect product recovery and particle size. Even greater effect on that properties were observed when different solvent mixtures of ethanol and acetone where employed due to their high impact on the degree of supersaturation achieved (more acetone added in the mixture leads to a decrease in particle size and increase in product recovery). It was found that ethanol alone was not capable of producing coprecipitates of curcumin and PVP at the experimental conditions tested, explained by the great difference in the supersaturation ratio (concentration/solubility [5]) of the two compounds. It would be very interesting in future work to investigate this hypothesis by testing other solvent mixtures and solutes to better understand how the difference in the supersaturation ratio of the solutes affects the coprecipitation results. Other important findings were that low solution flow rate (0.5 ml/min) reduced particle coalescence of coprecipitates and low temperature (35°C) increased curcumin recovery. Testing higher overall concentration of the organic solution would be desirable to intensify the process, so other solvents and solvent mixture could be employed.

The objective of Chapter 4 was achieved, with coprecipitates showing an improvement in water solubility of up to 600 times compared to the physical mixture of the raw materials, due to amorphization and size reduction of curcumin. Dissolution tests were presented in a mixture of water and SDS (0.25%) to demonstrate the differences in the release profile of raw curcumin, curcumin-PVP physical mixture, curcumin processed by SAS alone and CURC/PVP coprecipitates. However, in order to optimize the formulation produced in terms of curcumin release rate, dissolution tests in a medium capable of discriminating among different coprecipitates (using less SDS or other buffer solutions, as exemplified in **Appendix IV**) would be required. Since SDS significantly changes the release rate of curcumin (**Appendix IV**), another recommendation for future work would be the incorporation of SDS

in the formulation (coprecipitation of the three compounds – CURC/PVP/SDS). The analysis of the samples after some storage time could also provide important information about the stability of the formulation to prevent curcumin degradation and recrystallization. Naturally, bioavailability tests would be the next stage on the formulation development process.

Chapter 5 then brings together the enhancement in solubility and flowability in the same formulation and a more comprehensive description of the characteristics of the integrated processes (SAS-FM and SAS-DEM), and requirements for successful coprecipitation and coating were given. It was shown that when MCC (175 μm) was used as carrier, the formulation produced maintained the excellent flow properties of MCC. It would be interesting to identify the maximum guest/host mass ratio possible while keeping the formulation in a flowable form. Smaller carriers (corn starch, 15 μm and lactose, < 5 μm) were employed as an attempt to produce novel nano-on-micro formulations for pulmonary delivery; however the flowability of the powder was very poor. Future work would aim to improve the flow properties of the formulation by adding small amounts of flow additives [6,7] (such as magnesium stearate and silica) in the precipitator to be mixed with the carrier prior to precipitation. After that, lung deposition measurements by TSI and ACI would be necessary for further development of the formulation. The use of a more robust experimental design (based on Response Surface Methodology [8,9], for example) would also be beneficial to evaluate a wider range of conditions and interactions of different process parameters on the dissolution and flow properties of the samples.

In terms of process improvements, some changes in the rig are suggested, such as having CO_2 delivered from a larger tank kept outside the Lab. Besides being safer, this would eliminate the inconvenience of recording the total CO_2 mass used since the last cylinder replacement and planning the next replacement prior to starting an experiment (cylinders were usually

replaced before being completely used). Moreover, it was observed that the check valves of some cylinders were not working properly, creating some kind of resistance to the flow of CO_2. Many times, during experiments, even though the conditions were stable, the pressure would start to decrease and then rapidly increase again after a noise was heard from the cylinder. Such variations in pressure, and consequently in the flow rate, led to the loss of many experiments (stopped before the end), so having a larger tank would be highly beneficial with a well-maintained check valve in the inlet line. The recycling of CO_2 is also desirable; however it is necessary to ensure that the separation system (middle pressure vessel and cyclone) for the mixture that leaves the precipitator is efficient to avoid recycling solvent and solute to the precipitator. Currently, the control of the CO_2 flow rate is done manually by adjusting the opening of a micrometric valve. Having a pump with automatic flow control would definitely increase the reproducibility of the process (less dependent on the experience of the operator). Another desirable improvement in safety is having the rig within an enclosed system (fume cupboard), allowing the processing of more dangerous compounds.

A better understanding of the combined fluidization and precipitation at different conditions could be possible if the window of the high-pressure vessel was bigger to allow the observation/recording of the solution jet entering the vessel. Different nozzle configurations/positions (top and bottom [11]) could also be tested. Moreover, measurements of the pressure drop across the bed are highly desirable to allow a more precise calculation of the minimum fluidization velocity for future scaling up of the equipment.

Despite all advantages of SCF-based processing techniques described throughout this work, the elevated costs of high-pressure equipment, difficulties in scaling up throttling devices and incomplete understanding of all factors and interactions of factors affecting supercritical precipitation (thermodynamics, precipitation kinetics, jet hydrodynamics and mass transfer)

limit the applicability of such techniques in an industrial scale. However, the need of finding more environmentally friendly technologies and preparing highly engineered particulate structures will probably drive pharmaceutical research towards a deeper understanding and improvement of such process for future widespread industrial application [12]. Hopefully, this thesis will have given some contribution towards that.

6.2. References

[1] H. Hamishehkar, J. Emami, A.R. Najafabadi, K. Gilani, M. Minaiyan, H. Mahdavi, A. Nokhodchi, Effect of carrier morphology and surface characteristics on the development of respirable PLGA microcapsules for sustained-release pulmonary delivery of insulin, Int. J. Pharm. 389 (2010) 74–85. doi:10.1016/j.ijpharm.2010.01.021.

[2] O. Kusmartseva, A.S. Kattige, R. Price, P.R. Smith, In-line assessment of pulmonary drug delivery using light obscuration, 20 (2004) 468–474. doi:10.1016/j.bios.2004.03.033.

[3] J.O.-H. Sham, Y. Zhang, W.H. Finlay, W.H. Roa, R. Löbenberg, Formulation and characterization of spray-dried powders containing nanoparticles for aerosol delivery to the lung, Int. J. Pharm. 269 (2004) 457–467. doi:10.1016/j.ijpharm.2003.09.041.

[4] F. Kurniawansyah, R. Mammucari, N.R. Foster, Inhalable curcumin formulations by supercritical technology, Powder Technol. 284 (2015) 289–298. doi:10.1016/j.powtec.2015.04.083.

[5] M. Muntó, N. Ventosa, S. Sala, J. Veciana, Solubility behaviors of ibuprofen and naproxen drugs in liquid “CO2-organic solvent” mixtures, J. Supercrit. Fluids. 47 (2008) 147–153. doi:10.1016/j.supflu.2008.07.013.

[6] L. Qu, Q. Zhou, J.A. Denman, P.J. Stewart, K.P. Hapgood, D.A. V Morton, Influence of coating material on the flowability and dissolution of dry-coated fine ibuprofen powders, Eur. J. Pharm. Sci. 78 (2015) 264–272. doi:10.1016/j.ejps.2015.07.016.

[7] Z. Huang, J. V Scicolone, X. Han, R.N. Davé, Improved blend and tablet properties of fine pharmaceutical powders via dry particle coating, Int. J. Pharm. 478 (2015) 447–

455. doi:10.1016/j.ijpharm.2014.11.068.

[8] M. Mushtaq, B. Sultana, H.N. Bhatti, M. Asghar, RSM based optimized enzyme-assisted extraction of antioxidant phenolics from underutilized watermelon (Citrullus lanatus Thunb.) rind, J. Food Sci. Technol. 52 (2015) 5048–5056. doi:10.1007/s13197-014-1562-9.

[9] F. Paulo, L. Santos, Design of experiments for microencapsulation applications: A review, Mater. Sci. Eng. C. 77 (2017) 1327–1340. doi:10.1016/j.msec.2017.03.219.

[10] S. Rodríguez-Rojo, J. Marienfeld, M.J. Cocero, RESS process in coating applications in a high pressure fluidized bed environment: Bottom and top spray experiments, Chem. Eng. J. 144 (2008) 531–539. doi:10.1016/j.cej.2008.07.054.

[11] E. Badens, Y. Masmoudi, A. Mouahid, C. Crampon, Current situation and perspectives in drug formulation by using supercritical fluid technology, J. Supercrit. Fluids. 134 (2018) 274–283. doi:10.1016/j.supflu.2017.12.038.

APPENDIX I - SAS-FB Detailed Experimental Procedure

A detailed experimental procedure for SAS-FB is presented here, with equipment and instruments shown in **Figure 1-I**.

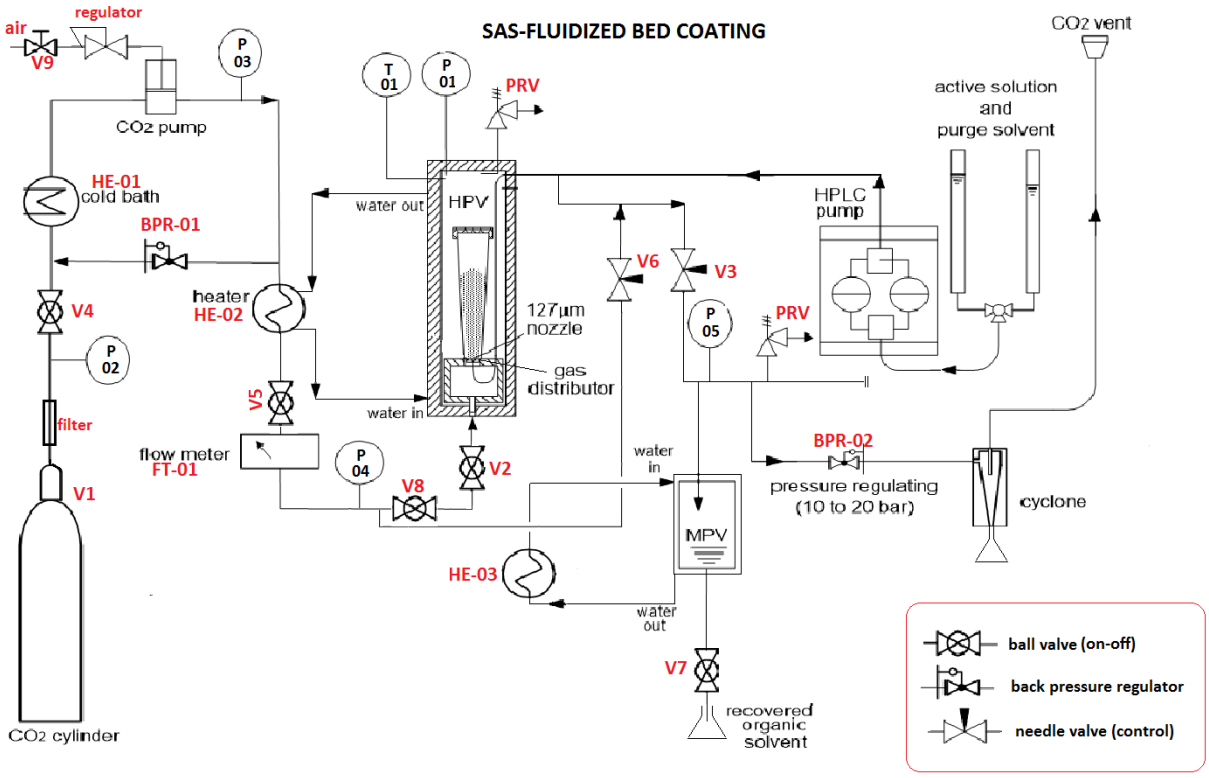

Figure I-1. Diagram of the experimental setup.

ABREVIATIONS

V - valve

HE – heat exchanger

HPV – high pressure vessel

MPV – middle pressure vessel

PRV – pressure relief valve

BPR – back pressure regulator

OPERATIONAL PROCEDURE

1. Turn on all heat exchangers (HE-01, HE-02 and HE-03);
2. Weigh carrier particles and prepare drug/polymer solution;
3. Transfer carrier particles to the bed holder and place them inside the HPV.
4. Fill the pipettes with solvent and drug/polymer solution
5. Close the vessel and connect the pipes (solvent and CO_2).
6. Close V2, V3, V7 and V8;
7. OpenV1, V4, V5 and V6 to pressurize the HPV;
8. Wait until the pressure in PT-01 (inside the HPV) is equal to the pressure in PT-02 (inside the cylinder, approx. 60 bar if the cylinder is full and approx. 40 bar if the cylinder needs replacement);
9. Open V9 (compressed air) to star the CO_2 pump.
10. When the pressure in PT-01 reaches the set point (adjusted in BPR-01), close V6;
11. Open V8 and V2 to start the fluidization;
12. Open V3 to adjust the CO_2 flow rate by watching FT-01;
13. When the flow is stable, turn on the HPLC pump to deliver pure solvent, then drug solution and finally flush the pipe with more pure solvent;
14. Turn off the HPLC pump;
15. Let pure CO_2 running throughout the vessel to remove residual solvent;
16. Close V9 to stop CO_2 pump;
17. Close V1 and wait for the pressure in the HPV to decrease to ambient (check PT-01);
18. Open V7 to collect the recovered organic solvent in the MPV and dispose it in the solvent waste bottle;
19. Disconnect pipes (solvent and CO_2) and open the HPV to remove the bed holder with the coated particles;
20. Collect sample from the bed holder with a spatula.
21. Turn off all heat exchangers.

APPENDIX II - Pictures of the experimental setup

Figure II-1. Rig used in SAS and SAS-FB experiments.

Figure II-2. Lid of high-pressure vessel (500 ml) with detail of solution and CO_2 injection for SAS.

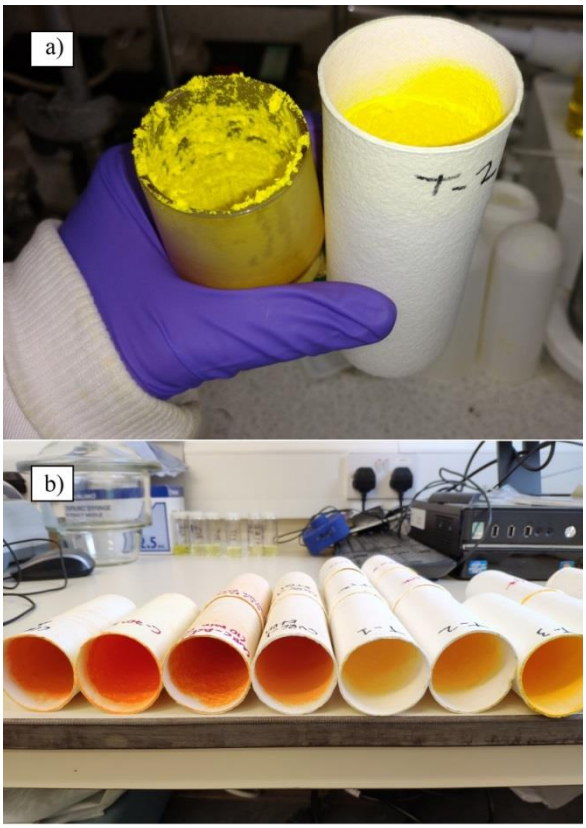

Figure II-3. a) Glass connector and cellulose thimble containg sample of coprecipitate obtained in run #22 (Chapter 4); b) cellulose thimbles obtained from several experiments showing that the amount of curcumin left in the thimble (yellow/orange colour) depends on the experimental conditions.

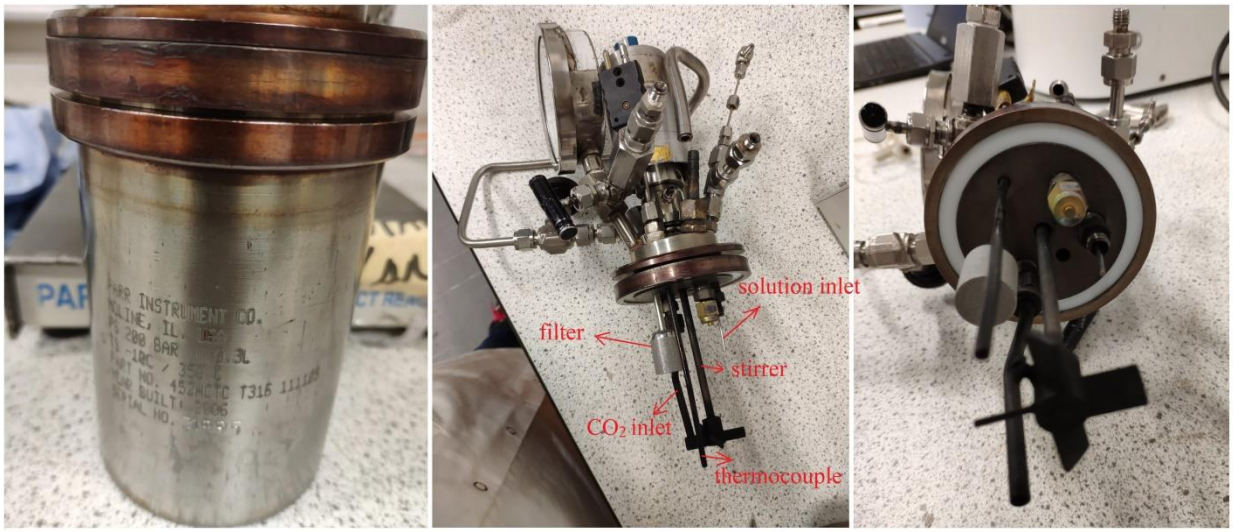

Figure II-4. High-pressure vessel (300 ml) used in SAS-DEM process.

APPENDIX III - Residence Time Calculations

III.1. Residence time in the precipitator

The theoretical mean residence time of the mixture solvent-CO_2 inside precipitator can be calculated according to *Equation 6-1* [1].

$$t_R = \frac{V}{v} \qquad \textit{Equation 6-1}$$

where *V* is the volume of the fluid (volume of cellulose thimble and glass connector, where the precipitation happens) and *v* is the constant volumetric flow rate of the fluid mixture (flow rate of solvent + flow rate of CO_2).

III.1.1. Time to reach quasi-steady state (t_{SS})

It has been demonstrated that in the SAS process the precipitator is self-mixed by the injection of the liquid solution and sc-CO_2, behaving like a well-mixed reactor [2]. Therefore, the mass balance for the organic solvent is given by *Equation 6-2*, where C_{IN} is the constant concentration of solvent in the inlet stream, and *C* represents the concentration of the solvent in the outlet, which varies with time *t* (**Figure III-1**).

$$C_{IN} - C = t_R \frac{dC}{dt} \qquad \textit{Equation 6-2}$$

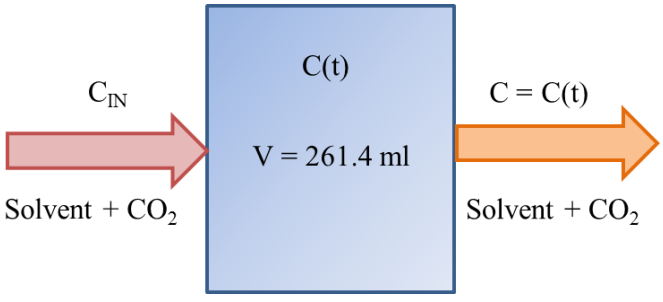

Figure III-1. Representation of the concentration in the inlet and outlet streams in a well-mixed reactor.

In the beginning of the SAS process, pure solvent is pumped inside the precipitator in order to reach a quasi-steady state composition of solvent and CO_2. For a step input, if $t \leq 0 \Rightarrow C = C_{IN} = 0$, and if $t > 0 \Rightarrow C_{IN}$ is constant ($\neq 0$) and $C = C(t)$. Then the integration of *Equation 6-2* gives:

$$t = -t_R \ln\left(1 - \frac{C}{C_{IN}}\right) \qquad \textit{Equation 6-3}$$

Equation 6-3 was then used to calculate the time required to reach quasi steady state composition of organic solvent and CO_2 in the precipitator, assuming $C = 95\%C_{IN}$ and V = 261.4 ml, CO_2 flow rate of 40 g/min (which gives different values of v, depending on the pressure p and temperature T inside the vessel). The calculated values are shown in **Table III-1**.

Table III-1. Mean residence time (t_R), time for reaching quasi-steady state composition of organic solvent in the fluid mixture (t_{SS}) and required flushing time to remove residual solvent from the formulation (t_F) based on different operating pressure (p) and temperature (T).

p (Mpa)	T (°C)	ρ_{CO2} (g/ml)	v_{CO2} (ml/min)	$v_{solvent}$ (ml/min)	v (ml/min)	mean t_R (min)	t_{SS} (min)	t_F (min)
8	40	0.278	143.9	1.0	144.9	1.8	5.4	9.6
9	40	0.486	82.3	1.0	83.3	3.1	9.4	16.6
12	40	0.718	55.7	1.0	56.7	4.6	13.8	24.4
9	35	0.662	60.4	1.0	61.4	4.3	12.7	22.5
9	50	0.285	140.4	1.0	141.4	1.8	5.5	9.8
9	40	0.486	82.3	0.5	82.8	3.2	9.5	16.7
9	40	0.486	82.3	1.5	83.8	3.1	9.3	16.5

III.1.2. Flushing time to remove residual solvent (t_F)

To finish the precipitation process, pure CO_2 is run through the vessel to remove residual organic solvent. It has been shown that the precipitator behaves as a well-mixed reactor if CO_2 is introduced from the bottom, and behaves as a plug flow reactor when introduced from the top, since pure CO_2 is lighter than the CO_2-solvent mixture [2]. During the SAS

experiments, sc-CO_2 was introduced in the vessel from the top, while introduced from the bottom during SAS-FB and SAS-DEM.

As a longer flushing time is required in the case of a well-mixed reactor [2], this was considered for the calculations. In the beginning of the flushing step (t = 0), C_{IN} = 0 (no more solvent enters the vessel). Therefore, the time required to achieve C = 0.5%C_0 was calculated based on the integration of *Equation 6-2*, where C_0 is the concentration of solvent in the outlet stream at the beginning of the flushing step:

$$t = -t_R \ln\left(\frac{C}{C_0}\right) \qquad \textit{Equation 6-4}$$

The calculated values required of CO_2 flushing are shown in **Table III-1** but usually it was run for longer periods (30 minutes).

III.2. References

[1] H.S. Fogler, Distributions of residence times for chemical reactors, in: Elem. Chem. React. Eng., 4th editio, Pearson Education Inc., 2006: pp. 867–944. doi:10.1016/j.memsci.2013.03.029.

[2] E. Carretier, E. Badens, P. Guichardon, O. Boutin, G. Charbit, Hydrodynamics of supercritical antisolvent precipitation: Characterization and influence on particle morphology, Ind. Eng. Chem. Res. 42 (2003) 331–338. doi:10.1021/ie020439v.

APPENDIX IV - Dissolution Method Development

Dissolution of raw and processed samples in different media (samples produced in **Chapter 4**).

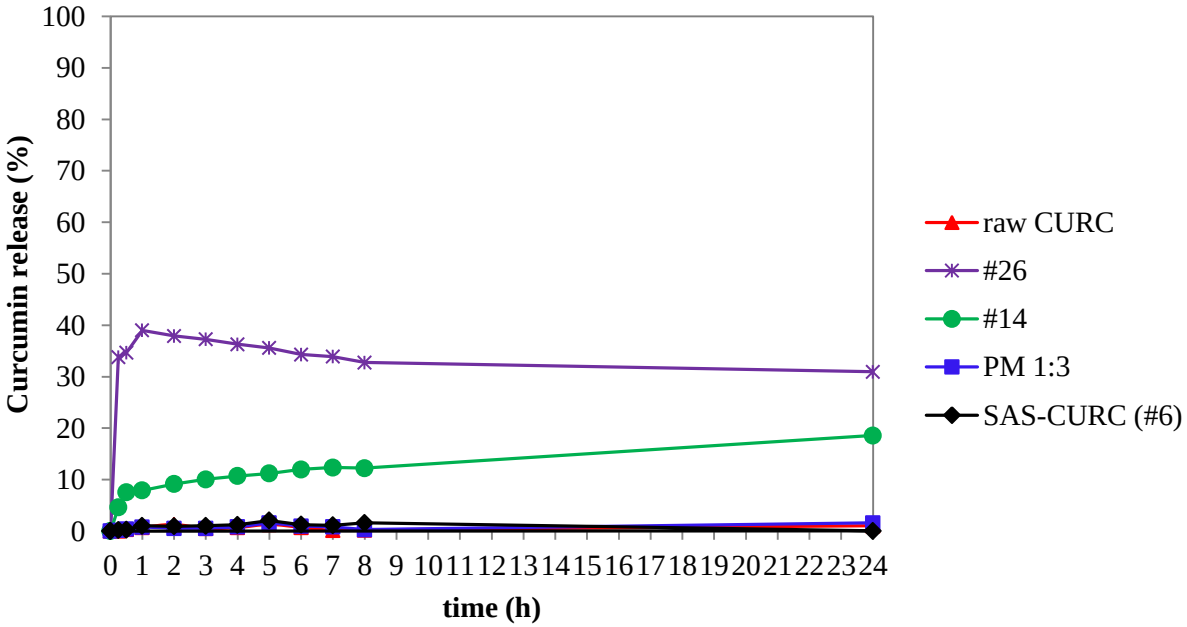

Figure IV-1. Release rate of raw curcumin and formulations in 0.05M phosphate buffer solution (pH 4.5).

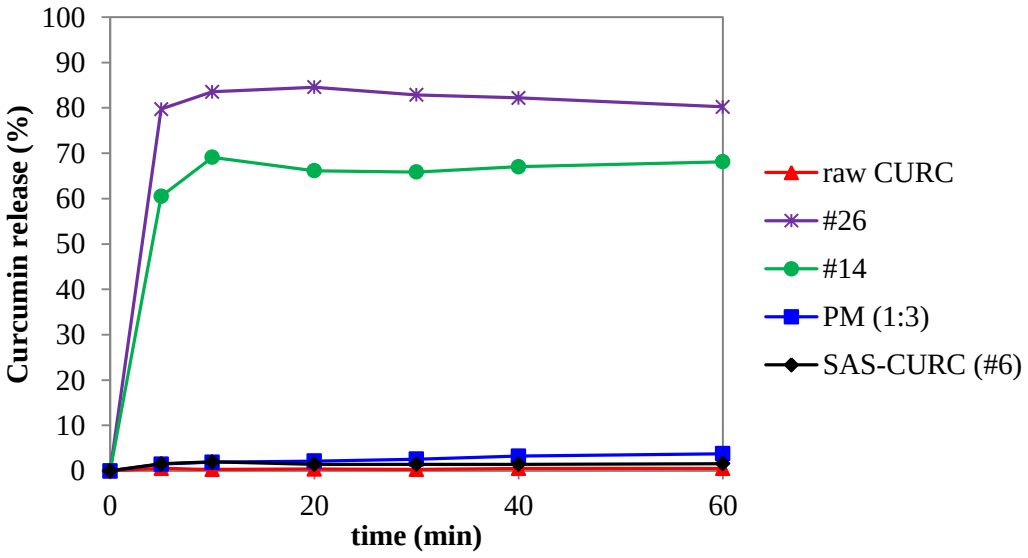

Figure IV-2. Release rate of raw curcumin and formulations in water + 0.1% SDS.

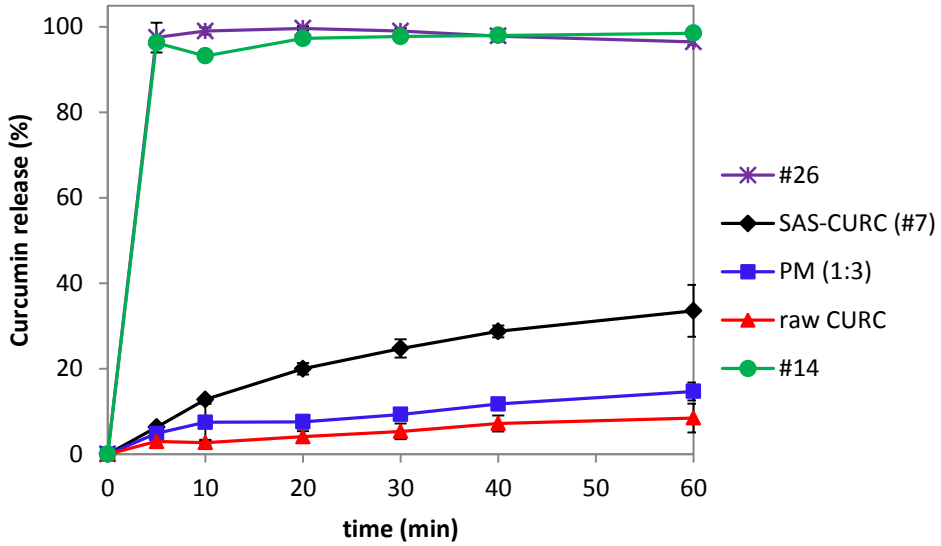

Figure IV-3. Release rate of raw curcumin and formulations in water + 0.25% SDS.